Active control of fluid-borne noise

Wang, Lin

Award date:
2008

Awarding institution:
University of Bath

Active Control of Fluid-Borne Noise

Lin Wang

A thesis submitted for the degree of Doctor of Philosophy

University of Bath

Department of Mechanical Engineering

December 2008

COPYRIGHT

SUMMARY

Fluid-borne noise is one of the main components of hydraulic noise. Its attenuation may have a significant effect on the cost of hydraulic systems. Standard passive silencers and dampers can be useful in reducing it in certain frequency ranges; however, these tend to be heavy, bulky and expensive. Active control algorithms, which are a comparatively recent means of reducing fluid-borne noise, can be applied to overcome this compromise.

The work presented in this thesis is the development of some active control algorithms utilized in a simple hydraulic system to cancel a number of harmonic orders of fluid-borne noise generated by a servo valve or a real pump. To realize cancellation the filtered reference least mean square (FXLMS) adaptive control method is mainly presented. Furthermore, a fast response servo valve is applied as an actuator to generate a proper anti-noise flow signal in real-time. For simplicity, an off-line identification method for the secondary path is applied in the time invariant working condition. Moreover, ripple reflection from both ends of the hydraulic circuit can produce different effects under different working conditions. In order to execute the cancellation without any prior information about the dynamics of hydraulic systems, the on-line secondary path identification method is discussed. However, in this algorithm an auxiliary white-noise signal applied to an on-line method may contribute to residual noise and an extra computation burden may be added to the whole control system.

The performance of these control algorithms is firstly investigated via simulation in a hydraulic pipe model and the real-time application on a test rig using a servo valve as a noise source. Finally, these schemes are realized in a simple hydraulic system with a real pump noise source. The fluid-borne noise can be attenuated by about 20 dB in normal working conditions.

ACKNOWLEDGEMENTS

I would like to give my appreciation to everyone who has contributed to make this thesis a reality.

Particular huge thanks to my supervisor, Dr. Nigel Johnston, for his continued excellent support and expert guidance. It is his encouragement and patience that have helped me through my Ph.D study.

I would like to thank Dr. Andrew Hillis for his suggestions on the work at difficult moments. Thanks to Dr. Sam Akehurst for his selfless help on my experiments.

I would also give thanks to the laboratory staff for their daily assistance in experiments.

Big thanks to my brother XING, Wei for his long time support on my study (非常感谢我的大哥邢伟对我在学习上长期以来的支持).

I would like to thank my wife MENG, Wei for her day-to-day spiritual support and living care during my study (感谢我的妻子孟巍在我的学习期间对我在精神上的支持和生活上的照顾).

I would also give big thanks to my parents and my parents-in-law who always believe me. They are always the ones standing behind to support me (感谢我的父母和岳父母对我长期以来的信任。他们永远都是站在身后支持我的人).

This work is also dedicated to my dearest grandfather and also to my most lovely daughter as a gift for her 1 year old birthday (谨以此献给我最亲爱的爷爷， 同时也献给我最可爱的女儿作为她一周岁的生日礼物).

CONTENTS

NOTATION

SYMBOL	DESCRIPTION
A	Amplitude of input reference signal (Chapter 3, 5)
A	Pipe internal cross-sectional area (Chapter 4)
A_S	Amplitude contribution from secondary path
$\hat{A}_S$	Amplitude contribution from estimation of secondary path
a	Forward path parameter of IIR filter (Chapter 3)
a	Number of delay samples from detecting point to control point (Chapter 4)
B	Bulk modulus
b	Feedback path parameter of IIR filter
C	Arbitrary integer constant
C_{dx}	Coherence between primary noise and reference input
C_{id}	Secondary path identification convergence vector
c	Speed of the sound in liquid
D_c	Delay caused by the control signal route
D_k	Delay from detecting point to control point in Kojima's method
$d(n)/d_n$	Desired signal and signal want to be cancelled
$\overline{E}\_id(k)$	Identification error signal in frequency domain at k^{th} block
$e(n)/e_n$	Error signal
$e(n)$	Residual fluid-borne noise
$e\_id(n)$	Identification error signal
F	Velocity of the fluid pulsation progressive wave in frequency domain (Chapter 4)
$F(z)$	Weighting function of interference controller (Chapter 6)
F_1	Velocity of the fluid pulsation progressive wave
F_{APP}	Fourier transformed approximated friction term

f	Interference in LMS adaptive filter (Chapter 3)
f	Frequency-dependent friction coefficient (Chapter 4)
$f(n)$	Impulse response of interference controller weighting function (Chapter 6)
f_0	Frequency of input reference signal
g	Integer constant in low pass filter (Chapter 4)
$g(n)$	Filtered signal by interference controller (Chapter 6)
H_{APP}	Fourier transform approximate friction function
h	Integer constant in low pass filter (Chapter 4)
$h(n)$	Cancellation signal generated by interference controller
i	Element number of reference input vector
j	Complex factor
k	Discrete time index (Chapter 3)
k	Number of terms in approximated friction series (Chapter 4)
k	Block number (Chapter 6)
k_P	Reflection factor
L	Length of weighting function (Chapter 3, 4)
L	Length of pipe model (Chapter 5)
L	Block length (Chapter 6)
l	Number of cancelled frequencies (Chapter 3)
l	Pipe length (Chapter 4)
M	Length of weighting function
$\overline{M}(k)$	Diagonal form of identification convergence function in frequency domain at k^{th} block
m	Weighting factors in approximated friction series (Chapter 4)
m	Number of sampling time shifts (Chapter 6)
n	Discrete time index (Chapter 3, 6)
n	Weighting factors in approximated friction series (Chapter 4)
n	Number of pipe model node (Chapter 5)
P	Desired-input cross-correlation matrix (Chapter 3)
P	Hydraulic pressure in frequency domain (Chapter 4)
P_0	Power of input signal (Chapter 3)

P_0	Progressive wave (Chapter 5)
P_1	Progressive after one reflection
P_2	Progressive after two reflections
P_3	Progressive after three reflections
$\overline{P}_e(k)$	Power estimation of residual noise signal in frequency domain at k^{th} block
ΔP	Pressure difference
p	Hydraulic pressure
p_1	Pressure at the first pressure transducer in Kojima's method
p_2	Pressure at the second pressure transducer in Kojima's method
p_P	Pressure at point P
p_A	Pressure at point A
p_B	Pressure at point B
p_A^{tn}	Pressure at point A at nth time step
p_B^{tn}	Pressure at point B at nth time step
p_P^{tn}	Pressure at point P at nth time step
Q	Flow rate
q	Flow in hydraulic system
q_A	Flow at point A
q_B	Flow at point B
q_P	Flow at point P
q_A^{tn}	Flow at point A at nth time step
q_B^{tn}	Flow at point B at nth time step
q_{PA}^{tn}	Progressive flow to point P at nth time step
q_{PB}^{tn}	Regressive flow to point P at nth time step
q_S^{tn}	Control flow at nth time step
$q_{progressive}$	Progressive control flow using Kojima's method
$q'_{progressive}$	Progressive control flow using theoretical method
R	Input correlation matrix (Chapter 3)

R	Friction term including frequency dependent and steady state terms (Chapter 4)
$R(z)$	z domain transfer function of interference controller (Chapter 6)
R_0	Regressive wave
R_1	Regressive wave after one reflection
R_2	Regressive wave after two reflections
R_f	Steady state friction term
r	Radius of complex poles (Chapter 3)
r	Pipe internal radius (Chapter 4, 5)
$r(n)$	Impulse response of interference controller (Chapter 6)
r_P	Radius of complex poles
$S(z)$	z domain transfer function of secondary path
S_{dd}	Auto-power of primary noise
S_{dx}	Cross-power of primary noise and reference input
S_{ee}	Auto-power of residual noise
S_{xx}	Auto-power of reference input
$\hat{S}(k)$	Impulse response of secondary path estimation at k^{th} block in frequency domain
$\hat{S}(z)$	z domain transfer function of secondary path estimation
s	Laplace factor
$\hat{s}(n)$	Impulse response of secondary path estimation at n^{th} discrete time
t	Time index
Δt	Sampling time interval
$\overline{U}(k)$	Diagonal form of block white noise signal in frequency domain at k^{th} block
u	Flow velocity (Chapter 4)
$u(n)$	White noise signal (Chapter 6)
$u'(n)$	White noise signal filtered by secondary path
$\hat{u}'(n)$	White noise signal filtered by secondary path estimation

$\bar{u}(k)$	Vector of k^{th} block white noise
$v(n)$	Difference between primary noise and filtered control signal for adaptive filter
$W^* / \bar{w}^*$	Optimum weighting function vector
$w / w_1 / w_2$	Weighting function
w_a	Additional signal added on white noise generated by two-weight adaptive notch filter
$\bar{w}$	Weighting function vector
$\bar{w}^*$	Optimum weighting function vector
X	Weighting factor
x	Distance (Chapter 4)
$x(n) / x_n / x_1(n) / x_2(n)$	Reference input signal
$x_1^{'}(n) / x_2^{'}(n)$	Filtered reference input signal
$\bar{x}(n)$	Vector of input reference signal
Δx	Distance between two pressure transducers in Kojima's method
y	Weighting function (Chapter 4)
$y(n) / y_n$	Control signal from adaptive filter (Chapter 3, 5, 6)
$y^{'}(n)$	Filtered control signal for adaptive filter
Z	Impedance
Z_0	Pipe characteristic impedance
z	z-domain factor
α	Angle of complex poles (Chapter 3, 5)
α	Non-dimensional frequency (Chapter 4)
α	Ratio between pressure difference and flow square (Chapter 6)
β	Ratio of weighting factors in approximated friction series
γ	Smoothing control factor in first-order low pass filter
Δ	Delay
μ	Convergence factor (Chapter 3, 5, 6)
μ	Fluid viscosity (Chapter 4)
ν	Fluid kinematic viscosity
ξ	Mean-square error function (Chapter 3)

ξ	Damping ratio of second order system (Chapter 4)
$\hat{\xi}$	Estimation of mean-square error
ρ	Liquid density
τ	Sound travelling time from detecting point to control point
φ	Arbitrary phase shift of input reference signal
φ_S	Phase contribution from secondary path
$\hat{\varphi}_S$	Phase contribution from secondary path estimation
$\Delta\varphi$	Phase difference between φ_S and $\hat{\varphi}_S$
ω	Angular frequency
ω_0	Normalized frequency of input reference signal
ω_n	Natural frequency of second order system (Chapter 4)
ω_n	Frequency at n^{th} time step (Chapter 8)
∇	Gradient of mean-square error
$\hat{\nabla}$	Estimation of mean-square error gradient

CHAPTER 1

Introduction

The harmful effect caused by unwanted noise is of concern to many people, especially workers in factories. Fluid-borne noise, which is produced by hydraulic transmission equipment, is one of the main sources of the unwanted noise in the working place. Therefore effective methods for the control of fluid-borne noise have been developed to realize comparatively quiet working conditions. Active noise control methods, especially adaptive control algorithms, have their own characteristics, which cannot be achieved using passive noise control methods. This project investigates efficient active control methods for the attenuation of fluid-borne noise on the basis of analysis and evaluation of different noise control methods.

1.1 Background

The best definition of noise is "unwanted sound" [1]. It is obvious that high levels of noise are extremely harmful to people's health, which is the most important reason to control noise. Exposure to a high level of noise could cause immediate and noticeable temporary loss of hearing and permanent hearing loss can be caused to a person exposed to a noise environment above a certain level [2]. Since the Walsh-Healy Act of 1969 was amended by adding restrictions on the workers, most industries and governments are motivated strongly to find some effective and economical methods to reduce the noise produced by machines. Thereby, noise control, which has developed rapidly in the last few years, is a very important subject and is likely to have a promising development in the future [3].

1.1.1 Hydraulic noise

Hydraulic power systems are well known for their high levels of noise. By the 1950s, hydraulic powered machine noise had reached levels that caused frequent complaints [4]. These problems caused by noise cannot only limit the application of fluid power, but also compel the designers to replace it with other methods of power transmission

systems, such as electrical systems [5]. Thereby, the commercial benefit of hydraulic systems is greatly affected.

For hydraulic machinery, more than 95% of the noise comes from the pumps and motors. Valves are another noise source, but they cause fewer problems in industry because of the masking noise from other predominating sources [4].

1.1.2 Types of hydraulic noise

In a hydraulic power transmission system, there are three main forms of noise: air-borne noise, fluid-borne noise and structure-borne noise. Noise energy can be transformed among these different types.

The most obvious form of noise is air-borne noise (ABN), which can be detected by the ears directly and is also known as acoustic noise. The flow and pressure pulsation in hydraulic pipes is called fluid-borne noise, which is the main cause of air-borne noise and vibration of machinery. Fluid-borne noise is primarily caused by the unsteady flow from pumps and motors. Sometimes, valve cavitation and instability are other main factors causing it. The vibration of the machinery on the main bodies and the mounts is called structure-borne noise, which can be quickly transferred among different components of hydraulic structures. Structure-borne noise may not only be caused directly by the mechanical action of pumps and motors, but may also arise as a result of unsteady forces caused by fluid-borne noise [4, 5]. This thesis presents the work that focuses on the investigation of cancelling fluid-borne noise. Figure 1.1 is a power spectrum of fluid-borne noise generated by a three-piston axial pump running at approximately 1000 rev/min (16.5 Hz) at 25 bar. The power is calibrated using $10\log_{10}(power)$ in dB. The fundamental frequency should be $16.5 \times 3 = 49.5\,\text{Hz}$ [6]. This spectrum is obtained using the sampling frequency of 3125 Hz.

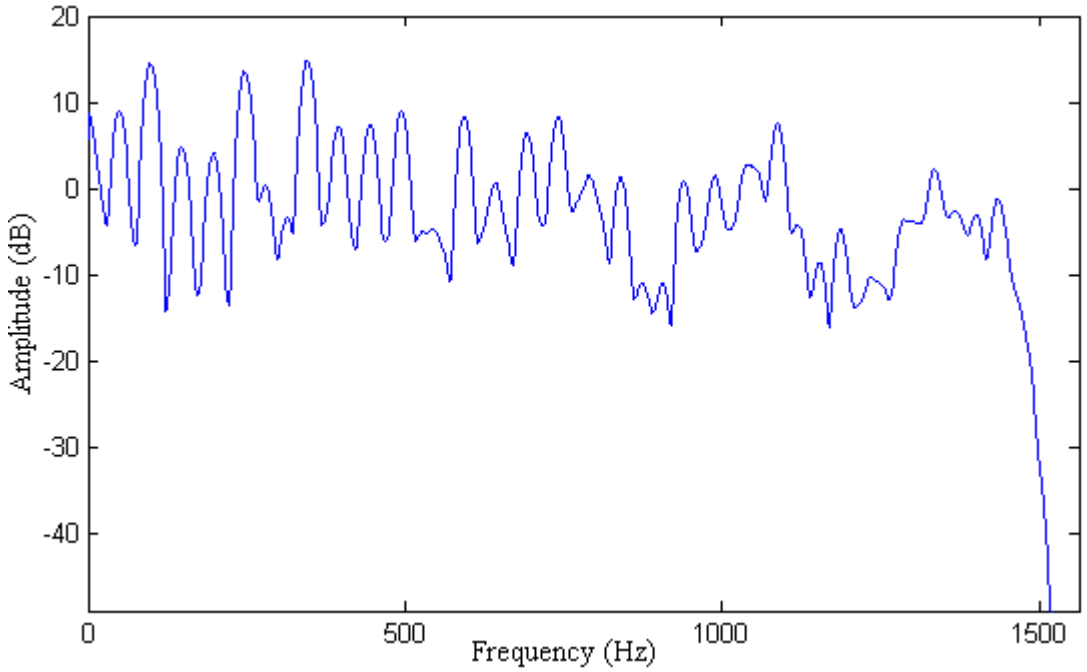

Figure 1.1 Spectrum of fluid-borne noise at 25 bar

From Figure 1.1, the dominant fluid-borne noise occurs at frequencies that are an integer times the fundamental frequency.

1.2 Fluid-borne noise attenuation

Due to the significant impact of fluid-borne noise on both humans and machinery, the attenuation of it has been investigated for some years. Many techniques are available; however, they may be bulky, expensive and difficult to carry out in practice.

1.2.1 Passive method of reducing fluid-borne noise

Sometimes, the unacceptably high levels of fluid-borne noise may cause fluid power transmission systems to be replaced by other methods in applications. Nevertheless, there are several methods that can be used for reducing it in hydraulic systems. These can be divided into three main categories: [6]

- Reduction of pump/motor flow ripples.
- Tuning of the circuit in order to avoid resonant conditions.
- Use of a silencer or pulsation damper.

In the method of reducing the pump /motor flow ripple, the problem can sometimes be solved by changing the operating conditions, which is not practical in most applications. In addition, selecting different pumps with less ripple pulsation may be another solution for the noise problem. However, it is rarely feasible to select a particular pump purely depending on the noise characteristics as other performance characteristics and costs must be considered. With regard to the method of tuning the circuit, varying the length of the pipe is helpful to avoid the resonant peaks of the pressure ripple, but this can also bring restrict the designers. Using fluid-borne noise silencers or pulsation dampers is another effective method. The effect of cancelling the noise is described by the 'transmission loss', which is the ratio of the input noise power to the output noise power under controlled conditions, and is normally expressed in dB. Typically, silencers can provide "transmission loss" of 20 dB to 40 dB (cancelling 90% to 99% noise power) [6]. This method can be separated into two passive types: 1. 'Dissipative' types which use the absorbent materials or orifice to absorb the noise energy. 2. 'Reactive' types, which can reflect the noise energy back to the primary source, like chambers and accumulators. Chambers, which are a typical type of commercial silencer, can give efficient attenuation over a broad frequency range; however, they tend to be bulky and expensive for low frequency operation. The setting of charge pressure and frequent maintenance are the main disadvantages of an accumulator [6].

1.2.2 Active noise control methods

The third type of the silencer is the 'Active' type, which uses an anti-phase signal to attenuate the noise. Active noise control is not a new concept and has aroused more interest in the last 10 to 15 years [7]. There are some applications of this method on the control of air-borne noise and structure-borne noise [8, 9]. This method is at a development stage and is likely to be very expensive for attenuating fluid-borne noise in hydraulic systems. However, it has high potential in flow power transmission systems compared with other methods using bulky and heavy equipment. The physical principle of active noise control, which is the destructive interference of two noise waveforms, has been understood for a long time, but the first application in the form of a patent appeared in 1933 by Lueg in Germany [10]. Although Lueg's application was not very extensive, the methods of cancelling the noise have been widely developed. There are two basic principles for the noise attenuation research [10]:

1. Young's principle is shown in Figure 1.2 from reference [10].

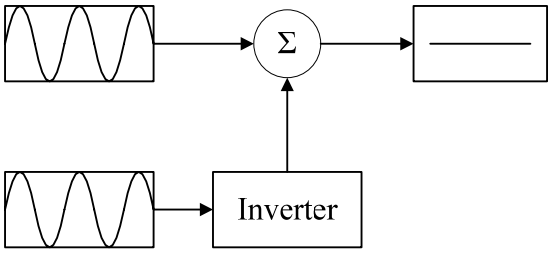

Figure 1.2 Structure concept of Young's principle and Huygens' principle

This principle can be represented simply as: "a pressure wave propagating in the space can be cancelled by the addition of the inverted waveform." However, every waveform has its own "radiation pattern", and the exact matching between the waveform and its inverted waveform is practically impossible to achieve.

2. Huygens' principle, which is based on Young's principle but used for a wide noise attenuation area, is described in Figure 1.3.

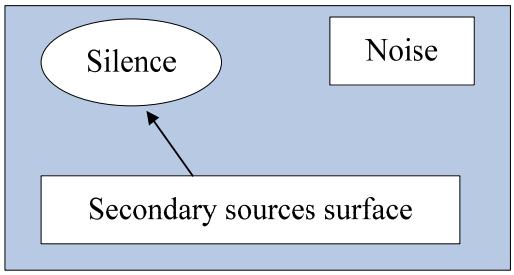

Figure 1.3 Structure concept of Huygens' principle

It can be represented as: the noise field at any point on the surface produced by the primary source outside the surface can be created by the secondary sources continuously distributed along the surface [8, 10].

The main features of the active noise control systems，which has been widely used in a duct system, are shown in Figure 1.4 [11].

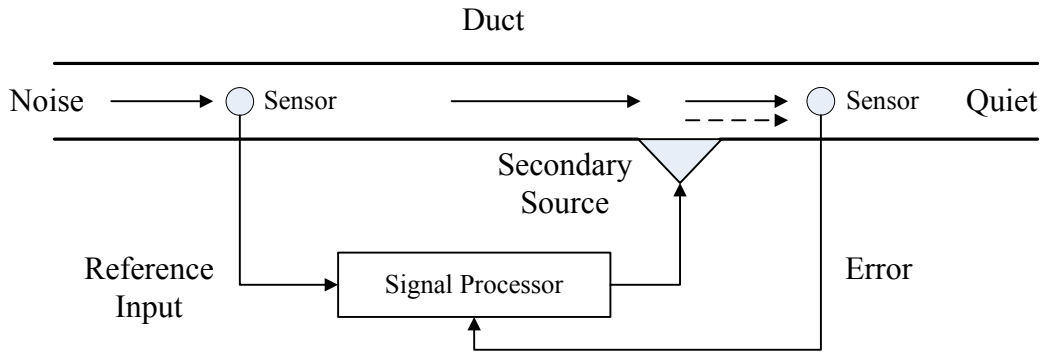

Figure 1.4 Simple structure of active noise control system

The signal processor can drive the secondary source, which is usually an actuator, to produce an "anti-noise" signal to cancel the primary noise downstream by gaining knowledge of the primary noise signal. Both feedback and feedforward control algorithms can be realized and presented using this active noise cancellation structure. Additionally, the use of the reference input sensor and error sensor depends on the control method. The sensors can be accelerometers for structure-borne noise cancellation and pressure transducers can be applied in the applications of fluid-borne noise cancellation.

1.2.3 Introduction to adaptive filtered reference LMS filter

For cancelling the noise in a duct system using active control algorithms, an adaptive least mean square (LMS) filter is a simple and effective method. Figure 1.5 presents a schematic plot of using a LMS filter to cancel the noise from a plant without prior knowledge of its dynamic characteristics in a duct (this duct can be seen as a pipe in a hydraulic system) system [12]. This algorithm is a feedforward control method that detects noise, which goes through the unknown plant, and generates an anti-noise control signal. The LMS algorithm can use the detected signal and residual unconcealed noise to adjust the weighting function until the minimum error is obtained.

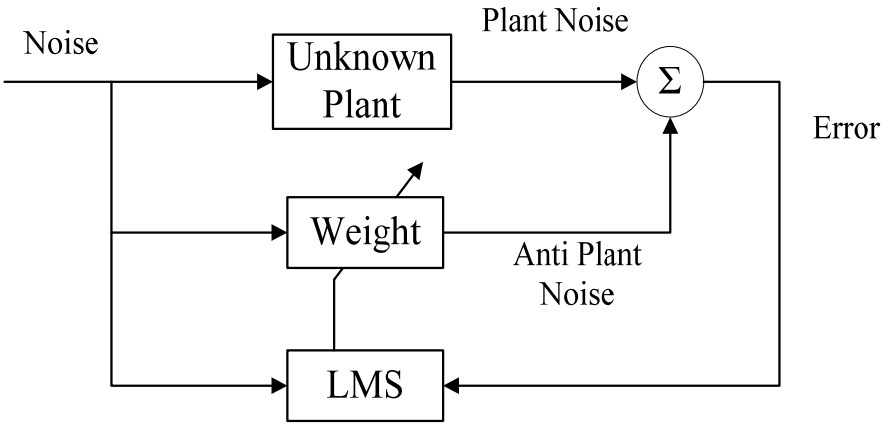

Figure 1.5 Simple structure of noise cancellation using LMS filter

According to this idea, an actuator can be located downstream of a duct to generate an anti-noise signal as shown in Figure 1.6. In this application of cancelling fluid-borne noise, a high frequency response servo valve can be applied as the actuator. Depending on this algorithm the filtered reference LMS (FXLMS) method is widely used in practice to obtain accurate and robust performance. An overview of its structure is illustrated in Figure 1.6 [12].

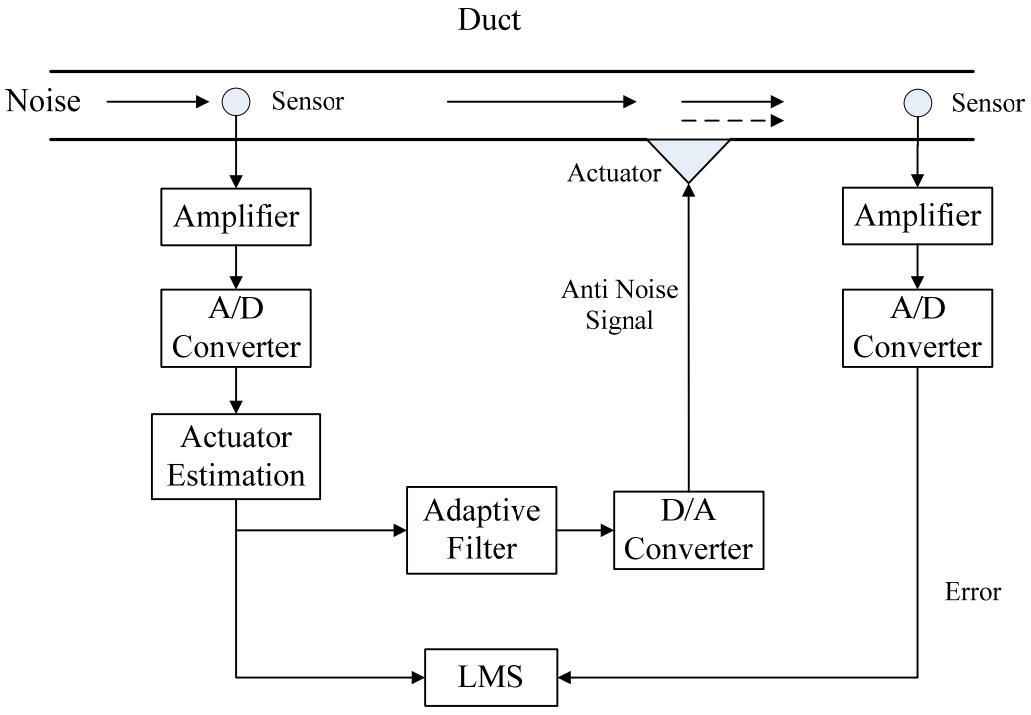

Figure 1.6 Overview of noise cancellation in a duct system using FXLMS method

The actuator in the system can be estimated using off-line or on-line identification to compensate the phase shift of the reference signal.

1.3 Research objectives

The aim of this project is to research and develop active control methods to attenuate fluid-borne noise in a simple hydraulic system under different working conditions. The controller must have simple, robust and rapid performance to changes in different operating conditions, and should be efficient enough to be able to attenuate several harmonic components.

In order to achieve this objective, various active control algorithms need to be investigated and a suitable one chosen. These algorithms then need to be developed and their performance investigated through computer simulation and experimental testing.

1.4 Scope of thesis

Chapter 1 presents an introduction to the research purpose of this subject. An overview of the fluid-borne noise characteristics, methods to attenuate it, especially active control algorithms and the project objective, are provided.

Chapter 2 presents the previous applications in active attenuation of fluid-borne noise and other applications using adaptive control algorithms, especially the FXLMS control method in isolating vibration and similar problems. Finally, relative control methods of on-line system identification in time and frequency domains are also reviewed and discussed depending on their advantages and disadvantages.

Chapter 3 gives the detailed concept and deduction of the adaptive LMS noise cancellation algorithm, which is based on a FIR filter. Investigation works on dynamic characteristics of the LMS adaptive notch filter for narrowband periodic noise cancellation are implemented. The robust and effective two-weight LMS adaptive notch filter is introduced and can be applied in this project. The efficient notch filter form used for multiple frequency noise cancellation is also presented at the end of this chapter.

Chapter 4 describes the modelling of the test rig system applied in this project using the method of characteristics (MOC). This type of finite element algorithm is investigated

in detail. From this model, a more accurate description of pressure and flow ripple dynamic characteristics can be obtained. Furthermore, development, including control flow in the model, is implemented. This developed model algorithm with different accuracy and computing levels is applied on Kojima's method, which is an active feed forward control method for attenuating fluid-borne noise.

Chapter 5 presents the filtered reference LMS controller with off-line identification of the secondary path algorithm on the rig model. The impulse response property of an actuator with different working conditions in a simple hydraulic circuit is analyzed. Two different algorithms, which use series unit delays and an extra LMS adaptive filter before operating fluid-borne noise cancellation depending on the actuator dynamic characteristics, are described.

In Chapter 6 on-line identification that is a more robust, adaptive and simpler strategy is realized on the rig model. Several different on-line system identification methods, which can be divided into time domain and frequency domain series, are investigated. Comparison between these two algorithms is described through typical control methods. Some improvements on these methods are also discussed.

Chapter 7 presents the setting up of experimental hardware and associated equipment. An independent servo valve is applied to generate finite frequency orders of fluid-borne noise as the model of a real pump. Another high response servo valve is applied as the actuator to generate anti-noise. The control algorithms described in Chapter 4 and 5 are realized and analyzed on this rig prior to testing using a real pump. Secondary path identification is obtained under different working conditions. Experiment results are analyzed for each control algorithm.

Chapter 8 describes the investigation work using a real pump, which can generate infinite orders of harmonic frequency theoretically on the same test rig. The frequency of the pump is detected for synchronization of the controller. The control algorithms in Chapters 4 and 5 are utilized under different working conditions and the experiment results are analyzed in order to compare the efficiency of each method.

Chapter 9 presents the conclusion and a discussion of the whole investigation, including advantages and shortcomings. Recommendations on future work and development of this application are also made.

CHAPTER 2

Literature Review

In this chapter, firstly, several applications on the active control of fluid-borne noise are reviewed and evaluated. Secondly, a summary of applications using adaptive filter algorithms for noise cancellation, which are mainly dependent on the LMS adaptive method, are presented. Finally, different algorithms of on-line system identification for the FXLMS method, which is derived from LMS adaptive algorithm, are described both in time and frequency domains.

2.1 Applications of active fluid-borne noise attenuation

During the past few years, many papers have been published on the application of active, especially adaptive, control of acoustic noise (air-borne noise) or structure-borne noise. However, very few papers have been published in the area of cancelling fluid-borne noise. This may be due to limited understanding of the behaviour of fluid-borne noise, limited computational speed of digital signal processing, and most importantly the lack of suitable low-cost, high-speed actuators. In this section applications of active fluid-borne noise attenuation are reviewed from the previous work.

2.1.1 Active accumulator applied in high-frequency band

In the area of cancelling fluid-borne noise, sometimes using passive methods and materials is not effective enough to reduce high frequency pulsations. In 1996 S.Yokota [13] designed and built an active accumulator driven by fast response piezoelectric actuators to cancel the flow rate pulsation in the high frequency band. The active accumulator, which included a piston-cylinder driven by two piezoelectric actuators and two accumulators, was used for generating an inverse-phase flow to attenuate the flow ripple and simultaneously reduce the pulsation pressure downstream. In this application, firstly, a hydraulic piston pump was applied as the pulsation noise source. Secondly, the active accumulator was employed near the outlet of the pump. This active accumulator consisted of a piston cylinder, two multilayered PZT (i.e. a kind of piezoelectric ceramic

made from Lead Zirconate Titanate) actuators located on both sides of the piston to drive it rapidly, and a passive accumulator to reduce the hydraulic impedance and to balance the cylinder. In addition, the piston and the actuator were both pre-compressed by micrometer calliper heads [13]. In experiments there was a hysteresis phenomenon, which was strongly dependent on the amplitude of the input signal, on the piezoelectric actuators when applying a voltage. To avoid the effect brought by the hysteresis, an inverse hysteresis element (IHE) was developed and used [13]. By exchanging the input and output of the hysteresis maps, which were obtained from the experiment prior to the cancellation of flow rate pulsation, the IHE could obtain two different inverse hysteresis maps for extending and retracting processes of the actuator. From the experimental results the IHE could have a good effect on the piezoelectric actuator until 1k Hz. In this system, a cylindrical-choke flow meter was used downstream of the pipe in order to test the instantaneous flow rate there. From the tested instantaneous flow status, the phase shift between fluid-borne noise pulsation and anti-noise pulsation could be obtained and fed back into the computer, which then could give the compatible voltage to drive the piezoelectric actuators. As shown in the experimental results this application performed well at high frequencies (three target frequencies between 500 Hz and 1k Hz) flow pulsation attenuation in the spectrum.

The algorithm used was a type of feedforward control method. The compensation plot of hysteresis effect for piezoelectric actuator and phase shift, which depends on the distance between piston pump and this active accumulator, needed to be obtained in advance. Careful tuning of phase shift between the piston velocity of the active accumulator and the pump rotation was needed in order to obtain the optimal cancellation. Hence this noise cancellation method was strongly linked to the structure of the experimental hydraulic rig. Furthermore, the design of the active accumulator was complex and costly and the volume of the passive accumulator was very high.

2.1.2 Adaptive control method of fluid pressure pulsations

In the above techniques for active control of fluid-borne noise, a feedforward control algorithm was utilized and the control signal was obtained directly from the fluid-borne noise downstream, which sometimes could not reach the optimal control effect. In this application an adaptive algorithm was applied using the knowledge of the error signal, which was the residual noise. A novel active orifice valve, which was driven by two

piezoelectric actuators, was applied as a bypass device to adjust internal leakage to reduce pulsation [14]. The flow ripple could relieve through this orifice valve and the flow rate was proportional to the open area of the orifice. An algorithm named "adaptive-optimum control method" that is similar to the gradient descent method was applied to implement the adaptive control process by adjusting parameters at every iteration against resultant pressure ripple. Since the frequency of the pressure pulsation was the same as that of the flow pulsation, so the frequency spectrum of the flow could be obtained by the fast Fourier transform (FFT). The controlled frequency selected here was close to the natural frequency of the pipeline network in order to cancel the resonance. The signals of the pressure pulsation were obtained from the pressure sensor located downstream. Then, after being processed by the controller, the signals were applied to control the open area of the orifice. As a result the related parameters, which were amplitude and phase shift of the control signals, were modified at every step until the optimum values were obtained. From the experimental results in time domain this method had a beneficial effect on attenuating the fluid-borne noise at a single frequency, which could cause resonance of the pipeline system.

This algorithm was an adaptive control method to find the optimum value to obtain good cancellation and no prior knowledge was needed during the signal processing. Although a piezoelectric actuator was used, no compensation was needed for the hysteresis effect. Regardless of the transient dynamic behaviour, to cancel a single frequency the steady state of the cancellation process could be described using a closed loop transfer function in the frequency domain. According to the feedback control algorithm, the forward part could be viewed as plant and feedback parts were the optimum controller and active orifice valve in parallel. However, the stability of this algorithm was not discussed by the author making it difficult to evaluate the controller performance. Furthermore changing of the active orifice valve transfer function because of ageing of the system, temperature variation and system load variations might also make the whole system unstable. Finally, the power loss due to the internal leakage of the active orifice valve was low when cancelling single frequency at a resonance, but it could be considerably higher at multiple frequency conditions.

2.1.3 Active fluid-borne noise control using progressive wave

In this section an active feed forward fluid-borne noise attenuation algorithm using the progressive wave proposed by Kojima [15] is discussed. The basic concept of this method is that an anti-noise signal generated by a secondary source was applied to cancel the primary noise. Rather than using the detected pressure signal, the progressive wave was applied to control the secondary source in real-time. Flow and pressure at any point along the pipe could be represented using the summation of progressive and regressive waves. Therefore the progressive wave could be described using the flow and pressure. Assumption of laminar flow was made in this algorithm, and according to the equation of motion, the flow could be obtained using the pressure gradient at that point, which could be calculated using the pressure values at two different points. Hence the progressive wave at any point along the pipe can be represented using the pressure values. The control process of Kojima's method is shown in Figure 2.1 [15]. In this method the basic aim was to detect the progressive wave component of the flow pulsation with a delay in the time domain at the 'detecting point' and to generate it in anti-phase by the secondary source at the 'control point'. This control flow splits into two parts, one goes back in the pump direction and the other goes downstream to cancel the pulsation. There were two pressure transducers, which were placed in a suitable distance Δx apart to measure the pressure ripple from the pump. The measured signals passed to the computer to be analysed and then commanded an actuator to generate a suitable 180^0 anti-phase control flow through a servo. Under the effect of this control signal, the downstream pipe was silenced after a momentary delay.

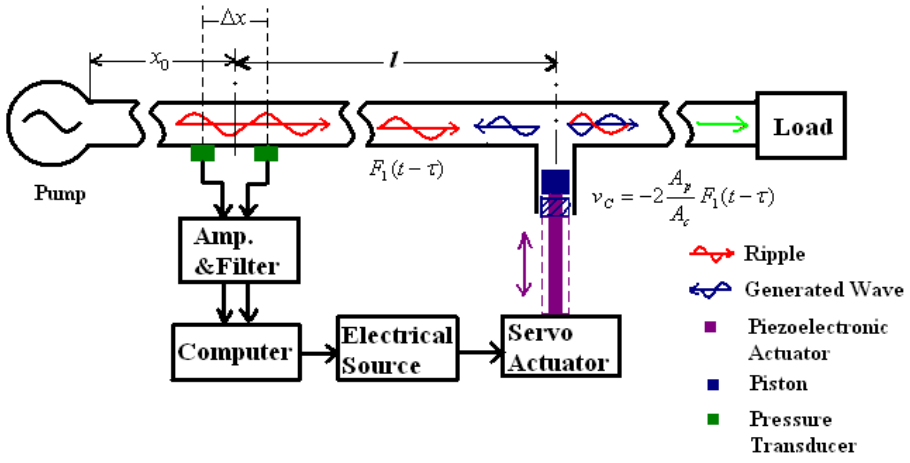

Figure 2.1 Structure and control process of Kojima's active method [15]

From the experimental results done by Kojima good attenuation level of fluid-borne noise could be achieved from 15 Hz to 350 Hz. However, there were some disadvantages to using this attenuation method. Firstly, the friction in a hydraulic system does not only include a steady term but also has an unsteady term, which depends on the frequency of the fluid-borne noise. In Kojima's method only the steady term was considered, which could cause inaccurate control flow. Secondly, as the pressure gradient was obtained using the pressure difference at two points, for high frequency components, close to or bigger than the half of the sampling frequency, inaccurate progressive waves could be obtained and make the system unstable. Thirdly, in real experiments the necessary distance between the two pressure transducers depends on the resolving power of the A/D converter. Since for low frequency fluid-borne noise, when the distance is too small, the A/D converter might not detect the pressure gradient. Fourthly, in real experiments as an actuator was usually applied to generate anti-noise, the amplitude and phase of the control signal might be distorted by this device. Finally, two pressure transducers were applied in this application, which created high costs and a heavy computational burden.

In Chapter 4 Kojima's method is further evaluated during simulation using the pipe model.

2.1.4 Active fluid-borne noise control of a magnetic bearing pump

In this section another application of fluid-borne noise cancellation using an adaptive algorithm is reviewed. An active magnetic bearing system that was applied as an actuator fixed on the pump itself was introduced. Using the same basic principle as the one employed in the last application, an actuator was applied to generate the inverse phase signals to cancel the primary noise. The particular feature was that the actuator was not an independent device in the system but the shaft and the impeller, which were suspended and thrust by magnetic bearings. The impeller was connected directly to the motor and was "overhung" by the shaft [16]. A summed control signal from the active controller and bearing controller was used to drive the magnetic bearing in the motor. The motor contained three bearings: two magnetic radial bearings and a magnetic thrust bearing. The magnetic radial bearing could suspend the rotating shaft by magnetic forces, which were controlled by the electric current through the bearing circuits. Similarly the magnetic thrust bearings could move the shaft and impeller up and down

vertically by varying the electric current. Therefore, the impeller in the pump could be used as an actuator to generate inverse phase pressure signals to cancel the fluid-borne noise in the pump piping system. Two kinds of control algorithms were applied in this application to attenuate the narrowband fluid borne noise: adaptive feedforward control and adaptive feedback control. In the feedforward control method, the filtered-x controller, which was designed to operate on the noise with a frequency of 29.5 Hz, was applied. For the feedback control algorithm, which was the main control method evaluated in this application, there were two different designs [16]. The magnetic bearing actuator and controller could be described using two transfer functions separately. The spectral response of actuator was measured using a signal analyzer to search capable anti-noise frequency range that could be supplied by the actuator. Generally, in a real-time experiment the actuator could affect both amplitude and phase shift to the control signal to make the whole system unstable. In order to overcome this problem, a transfer function, which was the approximate inverse of the actuator, was applied as a compensator in the first feedback control algorithm. Additionally, an extra transfer function was used in series with the inverted actuator transfer function in this controller to increase the bandwidth of noise cancellation. From the experimental results near the pump suction port, a 12 dB reduction could be obtained in narrowband cancellation, and only 6 dB reduction could be measured while increasing the bandwidth of interest. However, at a distance far from the suction port very little contribution could be obtained from this controller. In the second feedback control algorithm a feedback path and a forward path were combined and then again in series with the actuator transfer function. If the feedback term was equal to the approximation of actuator, the controller could be seen as a simple control algrithm. Furthermore, if the feedforward part was equal to negative value of inverse of actuator, the fluid-borne noise could be removed completely. From the results of the experiment up to 5 dB reduction could be obtained in the frequency range 75 Hz to 85 Hz and insufficient attenuation achieved on the ranges of 10 Hz to 75 Hz and 85 Hz to 100 Hz.

In this application a novel actuator using a magnetic bearing combined with a pump could give an efficient frequency range to cancel fluid-borne noise and an acceptable static pressure environment compared with traditional actuators. Two feedback and two adaptive feedforward control algorithms were evaluated and investigated. Good noise cancellation results could be obtained for narrowband frequency using feedforward

methods. In contrast, feedback algorithms could not give sufficient attenuation of fluid-borne noise. For both feedback control methods approximation accuracy of magnetic bearing identification was strongly related to control performance. Insignificant effect was activated for broadband noise attenuation, which was a shortage using feedback algorithm in this application. As the magnetic bearing was mounted on a centrifugal pump, the methods and system mentioned in this application might not work on other types of pump.

As described above, an adaptive control algorithm may be a feasible and promising method of cancelling fluid-borne noise. In the following section, applications using this algorithm are reviewed and evaluated.

2.2 Applications using adaptive control methods

Adaptive filtering algorithms are now used widely in the applications of noise cancellation, which results in potential benefits in weight, volume and cost. However, recently most of these applications are realized in cancelling the acoustic noise (air-borne noise) and machinery noise (structure-borne noise), and very little work is published for fluid-borne noise attenuation. In this section, three applications using broadband, narrowband feedforward and feedback adaptive control algorithms are reviewed and evaluated.

2.2.1 Broadband adaptive feedforward control of acoustic noise

An application using an adaptive broadband algorithm to cancel the acoustic noise was simulated and the related experiment was designed by Morgan and Quinlan in [17]. This application is described and evaluated here firstly to give an elementary understanding of adaptive feedforward LMS adaptive control method. This application was realized in an enclosed room. An acoustic noise source was located on one side of the room and a loudspeaker, which could be described using a transfer function, was employed on the other side of the room as an actuator to generate an anti-noise signal. Two sensors were located not far from the noise source and loudspeaker respectively. The acoustic travelling path from the noise source to the two sensors could be presented using two transfer functions. The existence of the loudspeaker could affect the control performance [12]. In order to compensate for this effect, the filtered reference LMS

(FXLMS) adaptive algorithm was applied. Firstly, the impulse response of the loudspeaker and travelling paths transfer functions were obtained in the same room, and then the actual impulse response of the loudspeaker transfer function was used in the FXLMS controller for the simulation of noise cancellation. The weighting function in the FXLMS adaptive controller should be long enough to cover the combined impulse response of the three transfer functions. A longer weighting function could give a better cancelling result, but a higher calculation burden. Near the loudspeaker a 'silence zone', the volume of which depended on the acoustic wavelength, was obtained [17]. A real experiment was also designed to compare with the simulation results. In the experiment white noise from 100 Hz to 500 Hz was used as acoustic noise. An omnidirectional microphone employed as the error sensor was located in the prospective silence zone to obtain the residual noise signal and another omnidirectional microphone used as a reference sensor, which was near the primary noise, was also applied to derive reference signal. A special controller was also applied, which was able to implement on-line system identification and also avoid the acoustic feedback effect from the loudspeaker.

In this application, elementary understanding of broadband noise cancellation using an LMS adaptive algorithm was presented clearly from the simulation result and experiment design. Two important points, which were actuator compensation and the feedback effect from the actuator, should be considered when using an LMS adaptive filter for broadband noise cancellation. Additionally, in the real experiment after the sensor picked up acoustic noise the controller needed some time to process the signal and send it to the loudspeaker. Two delays should be considered carefully. Electrical delay coming from the controller calculation, A/D and D/A converters and anti-aliasing filter, should be smaller than the acoustic delay, which is caused by sound pressure travelling after picking up time. It was non-causal when electrical delay was longer than acoustic delay, which could lead to significantly degraded performance [12].

2.2.2 Narrowband adaptive feedforward control of active engine mounts

In this section an example using the narrowband adaptive noise control algorithm applied on an active engine mount for attenuating periodical noise signal was implemented by Hillis in [18]. The purpose of this application was to attenuate the engine vibration caused by the rotation of out-of-balance masses in the engine. The only noise frequency of interest here, which was harmonic components of engine rotation

frequency (fundamental frequency), was in the range from 50 Hz to 100 Hz and an electromagnetic moving coil was applied in the engine mounts as an actuator. By contrast with the broadband adaptive noise cancellation algorithm, the reference input signal could be synthesized by synchronizing the transient fundamental frequency using tachometers rather than picked up using error sensors. Additionally, this periodical interference signal was time varying. Therefore an adaptive narrowband control algorithm could be used here. Due to the accumulation of numerical error the 'leaky FXLMS', which was one of the modified FXLMS algorithms [12], to cancel a single frequency noise was applied [18]. For this method prior knowledge of system dynamic characteristics was unnecessary. Unlike the traditional LMS adaptive filter only two weights were applied in the weighting function and the corresponding input reference signals were pure sine and cosine waves respectively. System identification was still applied to compensate for the amplitude and phase shift, which were caused by the secondary path, for implementation of the FXLMS algorithm. In this application a fast block LMS (FBLMS) algorithm, which was realized in the frequency domain, was applied for on-line system identification. The convergence factor in this identification method was updated in different frequency bins using a first order low pass filter form to provide relatively fast convergence speed when interference existed. The real-time experiment was realized in a real vehicle with the engine running at 2700 rpm on the motorway. The tachometer, which could generate a square wave, was applied on the engine to obtain the fundamental frequency of the primary noise. Then a sine wave generator was used to synthesize the reference signals. An accelerometer was placed near the chassis to feed the error signal back to the controller. From the vehicle testing results this leaky FXLMS algorithm could achieve 50%-90% cancellation on a single frequency in the range from 50 Hz to 100 Hz in fewer than 500 sample times.

In this application successful cancellation was achieved using an FXLMS notch filter with on-line identification in the frequency domain by using an FBLMS algorithm. However, time domain identification, which could be corrupted by the uncancelled harmonic components, could make the whole system unstable. The on-line identification in this method could also introduce an extra computation burden to the whole system. Additionally the auxiliary white noise signal, which could not be cancelled, might increase the residual noise level.

2.2.3 Adaptive feedback noise cancellation of headsets

An application using the adaptive feedback control algorithm to design a noise reduction headset for audio and communications was investigated by Gan and Kuo in [19]. Traditional passive headsets were helpful for broadband noise; however, they were comparatively large, costly and ineffective below 500 Hz. In the widely used feedforward LMS active noise control system for a headset the input reference signal was non-stationary and the accurate noise signal was difficult to measure because of feedback effect to the error sensor, so the adaptive feedback control algorithm was applied. For this application the active attenuation method could cancel the undesired noise and allow the desired audio to pass without loss at the same time.

Unlike the normal adaptive feedback algorithm, the notable point in this application was that an estimated noise was obtained through the loudspeaker estimation. This signal was applied as reference input rather than picking it up using an error sensor near the noise source. Hence feedback influence from the loudspeaker could be ignored. Sometimes the large noise level difference could make the feedback system unstable, therefore a normalized LMS filter form was used in which the convergence parameter could be obtained from estimating the noise power in the frequency domain [19, 12]. In the real-time implementation an error sensor was located inside the ear cup. The error sensor not only picked up the residual error but also the desired audio signal: as a result the audio component would affect the adaptation. Assuming the audio signal was uncorrelated with the primary noise signal, a devised method could separate the audio signal, which could be applied as auxiliary input not only to implement identification of the loudspeaker but also to remove itself from the signal picked up inside the ear cup [19]. Assuming the ideal estimation of the loudspeaker could be found, this feedback algorithm structure could be presented using a traditional feedforward LMS adaptive filter to analyze performance and stable conditions. Generally, the spectrum of the loudspeaker was not flat or free of phase shift which can decrease the effective frequency band. Hence the FXLMS algorithm was utilized here to compensate this loudspeaker effect. Both off-line system identification, which could give faster convergence speed, and on-line system identification methods could be used in this application. Therefore the unwanted noise was cancelled without the interference from the audio signal. Two experiments were carried out with siren noise (775 Hz) and

engine noise (61 Hz, 122 Hz and 183 Hz) respectively. From the results 30 dB to 40 dB cancellation were achieved without the loss of the audio signal. In the real experiment, a different sampling frequency was applied for active noise cancellation system and audio processing unit. Hence sampling frequency transforms should be involved in this application [19].

By contrast with traditional LMS adaptive filter, good cancellation results could be obtained without acoustic feedback effect and causality problems. However three disadvantages might decline the control performance. Firstly assumption of the ideal loudspeaker estimation could distort the reference input signal when the on-line system identification was applied. Secondly the audio signal, which could be used as an excitation signal of on-line identification and was uncorrelated with primary noise, might not contain entire frequency components, while primary noise was broadband signal. In this stage accurate loudspeaker identification could not be obtained. Consequently the whole system was unstable. Finally during the noise cancellation process residual noise could lead to very low on-line identification convergence speed or even instability when the power of primary noise was significantly high.

Further study on the headphone noise cancellation was continued by Kuo using the same method [20]. The ideal position of the error sensor in the ear-cup was studied and determined experimentally in [20]. Furthermore, the system might become unstable when the position of the headphone was changed on the head, especially when the headset was taken off, because a large change of working conditions occurred to cause a large secondary path (which was consisted by loudspeaker and amplifiers) fluctuation. To solve this problem, Kuo applied a feedback loop controller in parallel with the secondary path, which might make the system stable during the interested frequency range [21].

2.3 Relative on-line modelling methods for FXLMS adaptive filter

From the applications reviewed, the LMS adaptive algorithm, especially the FXLMS filter, may be a promising method for cancelling fluid-borne noise. Accurate estimation of secondary path applied to compensate for its effect is the key point for this algorithm. There are two methods, with and without an auxiliary signal, which can be applied. In this section the widely used on-line identification algorithms are reviewed.

2.3.1 On-line identification algorithms with auxiliary signal

Generally the on-line identification algorithms using auxiliary signal can be divided into time and frequency domains. Eriksson provided an on-line system identification algorithm in time domain for both broadband and narrowband noise signals described in [22]. Low power random noise, which was uncorrelated with primary noise, was applied as the auxiliary signal to implement the on-line identification and the estimated impulse response of the secondary path could be used for compensation synchronously. Assuming the unwanted primary noise was totally attenuated, the on-line identification could converge to a unique steady solution. However, during the adaptation process strong residual primary noise, which was combined with random noise, might lead the identification process to an inaccurate solution. As a consequence distorted secondary path estimation was used for compensation, making the whole system unstable. A small value of convergence factor might be helpful to improve the stability but very low convergence speed occurred at the same time. To overcome this interference effect during the identification process, Kuo [23] introduced a prediction error filter to remove it. In Kuo's algorithm a delay unit was applied in the prediction filter and zero mean, uniformly distributed white noise was utilized to excite the on-line identification part. Under appropriate selection of a delay number, the effect from residual noise could be eliminated. However, a small distortion could exist on the filtered white noise signal passing through secondary path. Additionally, this algorithm could only be applied for narrowband noise cancellation because of predictability of primary noise. In order to improve the accuracy of the on-line identification and extend this method to the broadband area, Zhang developed a new algorithm described in [24]. Rather than using the error signal in Kuo's method the input signal was applied as a reference for the prediction and hence the number of delays was no longer constrained. A similar method without a delay unit using a prediction filter was proposed by Bao in [25]. By contrast a suitable number of delays in Zhang's method could avoid the causality problem. Although residual noise interference was eliminated, the low level auxiliary white noise could not be removed and might affect the performance of primary noise cancellation and the prediction filter performance. Zhang also developed another algorithm with a more complicated structure to overcome this problem in [26]. All the algorithms described in this section need an extra LMS adaptive filter, which could result in more

calculation time depending on the weighting function length, to cancel the interference effect.

The on-line system identification could also be realized in frequency domain using a fast block LMS adaptive (FBLMS) algorithm, which was discussed by Shynk in [27]. Rather than a constant convergence factor for all frequency components an adaptive vector, in which one element corresponds to one frequency bin, was applied to represent the convergence factor. This vector was adaptively updated in the form of a first order low-pass filter and the initialization could be an arbitrary small positive value. The residual primary noise at a certain frequency could be minimized by a relatively small convergence value at that frequency bin depending on the amplitude of primary noise. Therefore an extra LMS adaptive filter was unnecessary for eliminating the interference effect. However, since in this algorithm the signal needs to be transformed between time domain and frequency domain twice, computation time might be increased for a long weighting function.

All these on-line identification algorithms will be discussed and evaluated during simulation in Chapter 6.

2.3.2 Overall modelling algorithm

The overall modelling algorithm, which was a simple on-line system identification method associated with a FXLMS adaptive filter, was firstly developed by Kuo and Wang in 1992 [12]. The most obvious difference of this method from other on-line identification algorithms was that the primary noise was applied as a reference input signal, rather than using white noise or chirp signals as excitation input. Three different LMS adaptive filters were utilized to implement both system identification and noise cancellation. During the cancellation, firstly an off-line initialization should be accomplished before the noise cancellation [12]. In this stage two LMS adaptive filters were applied to obtain the identification of an unknown system plant and the secondary path. The excitation signals for both identifications were supplied by primary noise. A delay unit consisting of several times unit delay of sampling time was used in front of the actual secondary path. The purpose of this delay unit was to make the excitation signals to the unknown plant and secondary path uncorrelated. Hence both of these weighting functions could converge to optimum solution separately. After initialization

the third LMS adaptive filter was used and its weighting function replaced the delay unit to implement noise cancellation with any change on either unknown plant or secondary path. A switch could be used here to make the transition between the delay unit and the third weighting function when a significant change occurred on both unknown plant and secondary path.

In this algorithm residual noise could be unaffected by auxiliary signal. More accurate cancellation results could be obtained in this way. However some insufficiencies still exist to influence the control performance. Firstly the excitation signals are highly dependent on primary noise, which might be narrowband. Therefore the entire dynamic information of secondary path might not be obtained. The convergence factor might also change with variance of primary noise amplitude. Secondly, in general primary noise might contain many narrowband frequency components from a rotating device that could not be used to excite the secondary path. A significant effect might be to make the system unstable by these signals. Finally the switch between delay unit and the third weighting function could break the noise cancellation process.

2.4 Conclusions

In this chapter, firstly, the previous applications using active control methods on fluid-borne noise are reviewed and evaluated. Equipment applied in these applications were bulky and there were restrictions on other hardware and inefficiency. Effective fluid-borne noise cancellation results were obtained, but were not remarkable. Secondly, other applications using adaptive control algorithms in isolating vibration and similar problems are described and evaluated as well. By comparing all of these applications the most popular, which means the simple and efficient, active control algorithm was LMS adaptive filter; moreover associating with the actuator FXLMS control method was widely applied in practice. Finally, to obtain good control performance relative on-line system identification methods in time domain and frequency domain are also discussed according to their advantages and disadvantages.

For time domain methods:

1. In Kuo's algorithm interference effect from uncancelled noise can be eliminated to produce a fast convergence of on-line system identification. However, a delay unit

of prediction filter, which is applied to cancel the residual error signal, needs to be selected carefully.

2. In Zhang's and Bao's method, as the reference input signal is applied to cancel the interference, a prediction filter is not needed. However, the auxiliary white noise exists in the residual noise, which may affect the noise cancellation performance.
3. In Kuo and Wang's method auxiliary white noise is not used, giving a good cancellation performance. However, the excitation signal from primary noise may affect the identification performance to make the system unstable.

For the frequency domain method, an interference controller is not needed to make the system simple and give a better on-line identification result. However, signal transformation between time and frequency domains is needed, hence more calculation burden is introduced to the processor.

CHAPTER 3

The Adaptive LMS Controller

For the past twenty years the research of the "adaptive system" has been applied in a variety of adaptive automatons. Particularly the least mean square (LMS) adaptive filter has been applied to numerous active noise and vibration control and system identification applications. It has been found that the LMS adaptive filter not only has simple structure and efficient control performance but also can be realized in real-time using digital signal processor. In this chapter the derivation of the LMS adaptive filter, especially the two-weight adaptive notch filter for narrow band noise cancellation, is described. Efficient notch filter form used for multiple frequency noise cancellation is also presented.

3.1 Basic concept and relevant applications

An adaptive system is well known as "a system that can modify its characteristics to achieve certain objectives, and usually accomplish the modification (adaptation) automatically" [12, 29]. In this section, the background and relative knowledge of LMS adaptive filters are described.

The basic and principal property of the adaptive system is its time varying and self-adjusting performance. Their characteristics depend on other things, such as the input signals and the desired signals [28]. In the adaptive system the "adaptation" is realized by using an adaptive digital filter for a short time. A standard form of the adaptive LMS digital filter can be as illustrated in Figure 3.1. In this structure x_n is the reference input signals while d_n is the desired response signals, y_n is the real output from the digital filter given by the input reference signal x_n; and e_n, which is well known as an error, is the difference between the actual response and the desired response; and *n* is the time index [12]. The purpose of the LMS adaptive algorithm is minimizing the mean-square error by adjusting the weighting function of the digital filter.

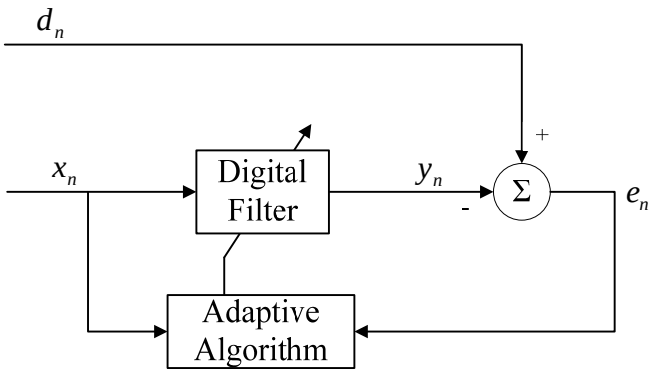

Figure 3.1 Sketch of LMS adaptive filter

3.1.1 IIR and FIR filters

An adaptive filter always consists of two parts: a digital filter, such as the finite impulse response (FIR) filter, and an infinite impulse response (IIR) filter, and an adaptive LMS controller for adjusting the coefficients (i.e. the weights of the input signals) of the filter. The typical structure of an IIR filter is shown in Figure 3.2 [28].

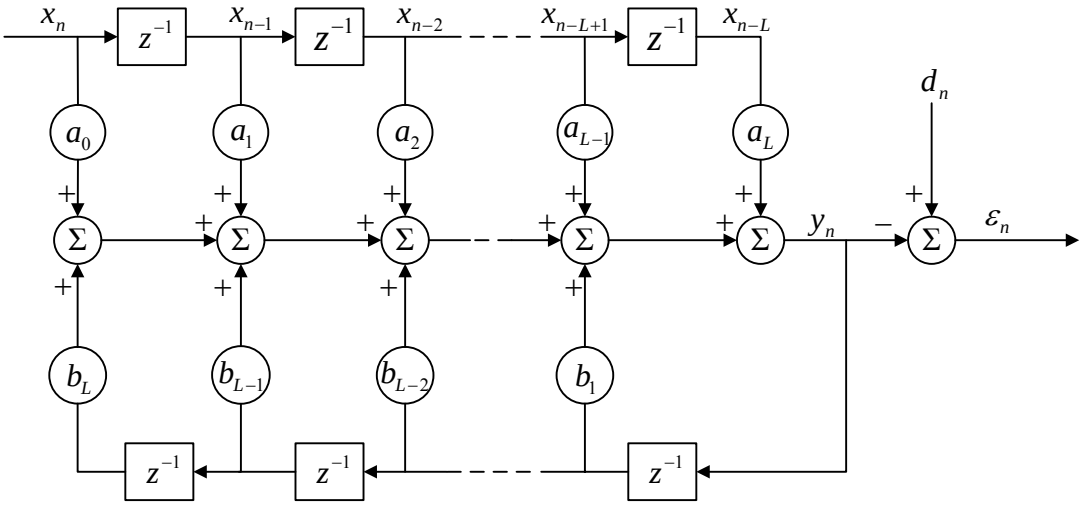

Figure 3.2 Structure of IIR filter

where z^{-1} is the unit delay.

This filter can be efficiently described as lightly damped resonant system by transforming the differential equations from continuous-time form into a discrete-time

one. The relationship between the input and the output signals can be described as follows:

$$y_n = \sum_{k=0}^{L} a_k x_{n-k} + \sum_{k=1}^{L} b_k y_{n-k}$$

This is a recursive adaptive filter and the stable condition is that all the poles should be in the unit cycle. If $b_k = 0$ for all k, the form can be used to describe the FIR filter, which is usually applied with the LMS adaptive filter. The FIR filter has its own advantages compared with the IIR filter. As only x is used in it, the FIR filter is inherently stable.

3.1.2 Deduction of LMS adaptive filter

The weight vector in the FIR filter does not only depend on the input signal but also on the other data such as, "desired response" or "training signal" [28]. In this structure, assume that the desired signals $d(n)$ and input signals $x(n)$ are statistically stationary [12]. $x(n)$ is the reference signal picked up by sensor, $d(n)$ is the noise needing to be cancelled, $\overline{w}(n)$, which is a vector, is the weighting function and $y(n)$ is anti-noise. These parameter relationships can be described in the following equations and the bar on the top of them represents a vector:

$$y(n) = \overline{w}^T(n)\overline{x}(n) \tag{3.1}$$

where,

$$\overline{w}(n) = [w_0(n) \quad w_1(n) \quad \cdots \quad w_{L-1}(n)]^T \tag{3.2}$$

$$\overline{x}(n) = [x(n) \quad x(n-1) \quad \cdots \quad x(n-L+1)]^T \tag{3.3}$$

and

$$e(n) = d(n) - y(n) \tag{3.4}$$

μ is convergence factor and L is the length of the filter.

As the desired signal and the input signal are assumed to be statistically stationary, from equations (3.1) to (3.4) the square of error signal can be obtained and then the expected value of (3.4) taken over a time period:

$$E\left[e_n^2\right] = E\left[d_n^2\right] + \overline{w}_n{}^T E\left[\overline{x}_n \cdot \overline{x}_n^T\right] \cdot \overline{w}_n - 2E\left[d_n \cdot \overline{x}_n^T\right] \cdot \overline{w}_n \tag{3.5}$$

and $E[\cdot]$ denotes the expected value, subscript *n* is still the time index.

It is important to note that the expected value of any sum is the sum of the expected values, and the expected value of a product is the product of expected values if the variables are statistically independent [28]. However, in most applications the input signals and the desired signals are not independent. So the mean-square error (MSE) function is conveniently represented as below:

$$MSE \equiv \xi = E\left[e_n^2\right] = E\left[d_n^2\right] + \overline{w}_n{}^T R \overline{w}_n - 2P^T \overline{w}_n \tag{3.6}$$

where the P is the "desired-input cross-correlation matrix", which is the set of cross-correlation between the desired responses and the input signals, shown as follows:

$$P = E\left[d_n \overline{x}_n\right] = E\left[d_n x_n \quad d_n x_{n-1} \quad \ldots \quad d_n x_{n-L}\right]^T \tag{3.7}$$

and the R is the "input correlation matrix" described in (3.8), in which the main diagonal are the mean-square of the input components and the cross terms are the cross correlation of the input signals. R can be written in the following equation:

$$R = E\left[\overline{x}_n \overline{x}_n^T\right] = E\begin{bmatrix} x_n^2 & x_n x_{n-1} & x_n x_{n-2} & \cdots & x_n x_{n-L} \\ x_{n-1} x_n & x_{n-1}^2 & x_{n-1} x_{n-2} & \cdots & x_{n-1} x_{n-L} \\ x_{n-2} x_n & x_{n-2} x_{n-1} & x_{n-2}^2 & \cdots & x_{n-2} x_{n-L} \\ \vdots & \vdots & \vdots & & \vdots \\ x_{n-L} x_n & x_{n-L} x_{n-1} & x_{n-L} x_{n-2} & \cdots & x_{n-L}^2 \end{bmatrix} \tag{3.8}$$

From equation (3.6), it is clear that the mean-square error performance is a quadratic function of the weight matrix $\overline{w}$, when the input and the desired signals are "stationary stochastic variables" [27]. There is a scalar value of the mean-square error for every

component in the weight vector $\overline{w}(n)$. Therefore the mean-square error value and the corresponding $\overline{w}(n)$ compose a $L+2$ space. Figure 3.3 is a typical three-dimensional MSE function surface when $L=1$ [12].

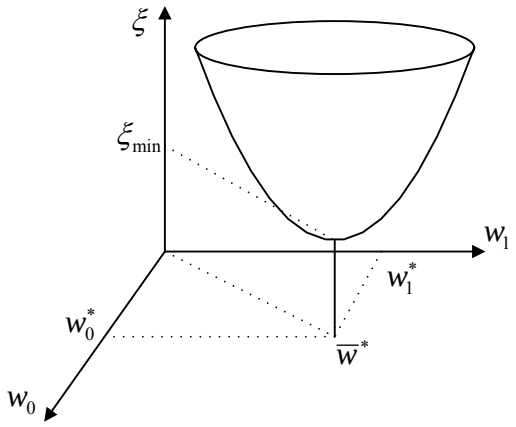

Figure 3.3 Three dimensional performance surface, L=1

The vertical axis represents the MSE while the horizontal axes describe the weight vector. Contours of constant mean-square error are elliptical when setting ξ constant in equation (3.6) [28], here $\overline{w}^* = \begin{bmatrix} w_{0n} & w_{1n} \end{bmatrix}^T$ is the optimal weight value at the bottom of the surface and the mean-square error is the minimum, $\xi_{\min}$, here. With the purpose of finding the $\xi_{\min}$ value, obtaining the gradient of the mean-square error on the performance surface is an efficient way:

$$\nabla_n \equiv \frac{\partial \xi_n}{\partial \overline{w}_n} = \left[\frac{\partial \xi_n}{\partial w_{0n}} \quad \frac{\partial \xi_n}{\partial w_{1n}} \quad \cdots \quad \frac{\partial \xi_n}{\partial w_{Ln}} \right]^T = 2RW - 2P \tag{3.9}$$

where *P* and *R* are described in equations (3.7), (3.8) respectively. In order to obtain the minimum mean-square error, the optimal weight vector $\overline{w}^*$ can be substituted into (3.9), letting $\nabla = 0$:

$$\nabla = 0 = 2RW^* - 2P \tag{3.10}$$

then

$$W^* = R^{-1}P \tag{3.11}$$

which is known as the Wiener-Hopf equation in matrix form [28]. Substituting (3.11) into (3.6):

$$\xi_{\min} = E\left[d_n^2\right] - P^T R^{-1} P = E\left[d_n^2\right] - P^T \overline{w}^* \tag{3.12}$$

which represents the mean-square error performance surface.

In equation (3.11) the optimal weight vector is deduced, however, this solution needs the continuous estimation of the input correlation matrix and the desired-input cross-correlation matrix, which needs a considerable computation over a long period because they are not stationary. There are indeed some methods to calculate them, but they entail excessive work for the signal processor when the dimension of the input correlation matrix is large [30]. Therefore a more efficient algorithm, which is named the "descent method", is obtained by improving the recursive method for computing the weight vector [28, 30]. There are two well-known methods, which are Newton's method and the method of steepest descent, based on this algorithm that make the local gradient estimation in each cycle move the weight vector towards the optimal value. The weighting function update of Newton's method and the method of steepest descent can be described in (3.13) and (3.14) separately:

$$W_{n+1} = W_n - \mu R^{-1} \nabla_n \tag{3.13}$$

$$W_{n+1} = W_n + \mu\left(-\nabla_n\right) \tag{3.14}$$

However, in Newton's method the inverse of the input correlation matrix needs to be estimated, which still requires a lot of time to calculate. Moreover, in the method of steepest descent the largest eigenvalue of input correlation matrix is also needed in order to obtain a stable condition.

Both of these methods add a burden to the computation. Therefore, another widely used method, which is known as the least-mean-square (LMS) algorithm deduced by Widrow and Hoff (1960), is developed in practice. This algorithm is an important member of the "stochastic gradient algorithm" family [31] and inherits the concept of the method of steepest descent, but uses a special gradient estimation [28]. In the previous adaptive algorithms the gradient estimation is obtained from the expected value of the square of

the error signal. In reality, for the LMS algorithm the square of the error signal itself is taken as estimate of ξ_n instead of $E\left[e_n^2\right]$:

$$\hat{\xi}_n = e_n^2 \tag{3.15}$$

Then the instantaneous estimate of the gradient at every iteration is [28, 12]:

$$\hat{\nabla}_n = \begin{bmatrix} \frac{\partial e_n^2}{\partial w_{0n}} \\ . \\ . \\ . \\ \frac{\partial e_n^2}{\partial w_{Ln}} \end{bmatrix} = 2e_n \begin{bmatrix} \frac{\partial e_n}{\partial w_{0n}} \\ . \\ . \\ . \\ \frac{\partial e_n}{\partial w_{Ln}} \end{bmatrix} = -2e_n \bar{x}_n \tag{3.16}$$

According to the concept of the method of steepest gradient (3.14), the definition of LMS can be described as:

$$\bar{w}_{n+1} = \bar{w}_n - \mu \hat{\nabla}_n = \bar{w}_n + 2 \cdot \mu \cdot e_n \cdot \bar{x}_n \tag{3.17}$$

Simply written:

$$\bar{w}_{n+1} = \bar{w}_n - \mu \hat{\nabla}_n = \bar{w}_n + \mu \cdot e_n \cdot \bar{x}_n \tag{3.18}$$

This is the well-known LMS algorithm, which is the same as method of steepest descent, the largest eigenvalue of input correlation matrix is still needed to obtain a stable condition. A simple method has been used to deduce it, which can be written as [12]:

$$0 < \mu < \frac{1}{(L+1)P_0} \tag{3.19}$$

where P_0 is the power of the input signal and equals $E[\bar{x}_n^2]$.

The detailed structure of this algorithm associated with the FIR filter is shown in Figure 3.4.

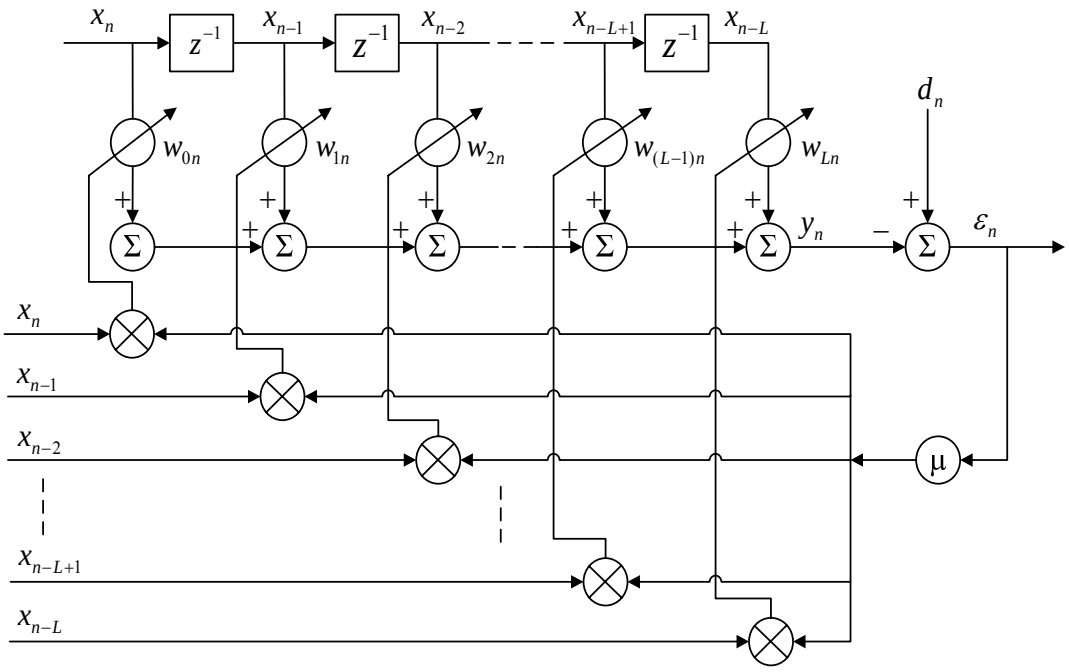

Figure 3.4 Structure of LMS adaptive method using FIR filter

This algorithm can be summarized as follows [12]:

1. Decide the constant convergence factor μ, the number of weights L and its initial value w_{0n}.
2. Calculate the output y_n and then the error e_n using (3.1) and (3.4).
3. Update the weight vector using (3.17).

As for all adaptive algorithms, stability, convergence and the excess mean-square error [27] are important characteristics for the LMS method. Now, looking at the equation (3.16) the gradient estimate of it can be unbiased if the weight vector is constant. Take the expected value on both sides of equation (3.16):

$$E[\hat{\nabla}_n] = -2E[e_n \bar{x}_n] = 2(R \cdot \bar{w} - P) = \nabla_n \tag{3.20}$$

From this description the expected value (mean value) is equal to the real gradient ∇_n, and it also means $\hat{\nabla}_n$ is an unbiased estimate [28]. Therefore the convergence analysis of the LMS algorithm can be taken into the method of steepest gradient by estimating the weight vector at each cycle. In this way, $\hat{\nabla}_n$ can get close to ∇_n and (3.17)

approaches (3.14) after adapting several steps [28]. From equation (3.17) the weight vector is a function only related to the previous values of the input signals. If the weight vectors are independent on the input signals, the expected value of weight vectors $E[\overline{w}_n]$ can converge to the optimal solution in (3.11) after many iterations.

3.1.3 Coherence in LMS adaptive filter

The cancellation effect using the LMS adaptive filter can be evaluated using the coherence function in the frequency domain between measured and reference input signals [12].

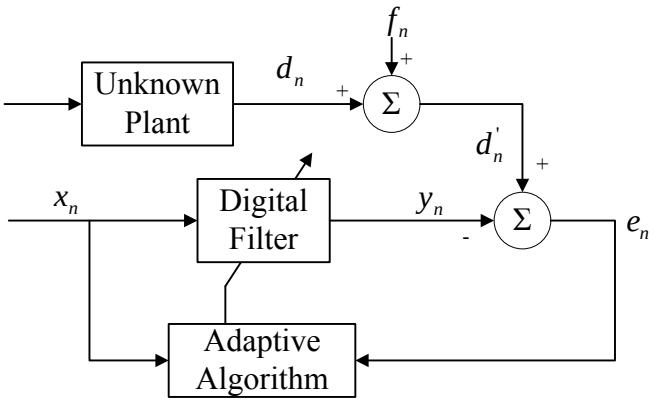

Figure 3.5 Structure of LMS adaptive filter with interference

From the structure in Figure 3.5 the typical form of this coherence function can be presented as:

$$C_{dx}(\omega) = \frac{\left|S_{d'x}(\omega)\right|^2}{S_{d'd'}(\omega) \cdot S_{xx}(\omega)} \tag{3.21}$$

where d_n' is the signal need to be cancelled, f_n is the interference signal, d_n is the signal from unknown plant and the digital filter can be represented using the weighting function in equation (3.2). $S_{d'x}(\omega)$ is the cross-power, which can also be seen as the Fourier transform of cross-correlation function, between primary noise and reference input signal and $S_{d'd}(\omega)$, $S_{xx}(\omega)$ are auto-power of primary noise and reference input signals separately. This coherence function is a measure of the relative linearity of the

two signals $d_n^{'}$ and x_n. When $C_{d^{'}x}(\omega)$ is equal to one, the primary noise and the reference input are highly correlated [32]. In this situation the primary noise can be completely attenuated. However, usually the interference signal f_n is not correlated with x_n. Therefore $C_{d^{'}x}(\omega)$ is significantly smaller than one and the performance of cancellation is degraded. Same result can also be presented using an auto-power equation of residual noise signal [12]:

$$S_{ee}(\omega) = \left[1 - C_{d^{'}x}(\omega)\right] \cdot S_{dd}(\omega) \tag{3.22}$$

where $S_{ee}(\omega)$ is the auto-power spectrum of the error signal, which is desired to be as small as possible in the control process in Figure 3.5. Therefore the control performance is highly related to the interference level f_n.

This interference, which is uncorrelated with primary noise and reference input, can hardly be affected by the control signal. However, if the power of interference is significantly large compared with primary noise the cancellation performance may be degraded and may even be unstable. This effect on relative application will be discussed in the following sections. In real experiments, according to the requirement, small interferences are tolerated during noise cancellation or system identification processes.

3.1.4 Possible applications of the LMS adaptive filter

There are four main purposes for using the adaptive digital filter [31]:

1. System identification: An adaptive filter is used as a linear model and applied to imitate the performance of the unknown plant. The adaptive digital filter and the unknown plant are driven by the same input signal while the actual output from the plant is used as the desired response. If the plant is “dynamic in nature”, the modelling will be time varying [31].
2. Inverse modelling: The adaptive filter is used to provide an inverse model to represent an unknown noisy plant.
3. Prediction: In this application the present values of random signal is used as the desired signal and the past values supply the input signal to the adaptive filter. The

output signal from the filter can be used as the system output depending on the application of interest.

4. Interference cancellation: The adaptive filter is applied to cancel the unknown interference, which is known as the adaptive noise control. As has been described before, the desired signal is the primary noise, which needs to be cancelled. A reference signal either obtained from the primary noise directly or synthesized by the sensors (which will be described in the latter section) is employed as the input signal [12, 31]. The error signal is used to adjust the weighting function by an adaptive algorithm. In this section, only the application of system identification is discussed. Narrowband interference cancellation will be discussed in section 3.2.

The structure of system identification is plotted in Figure 3.6.

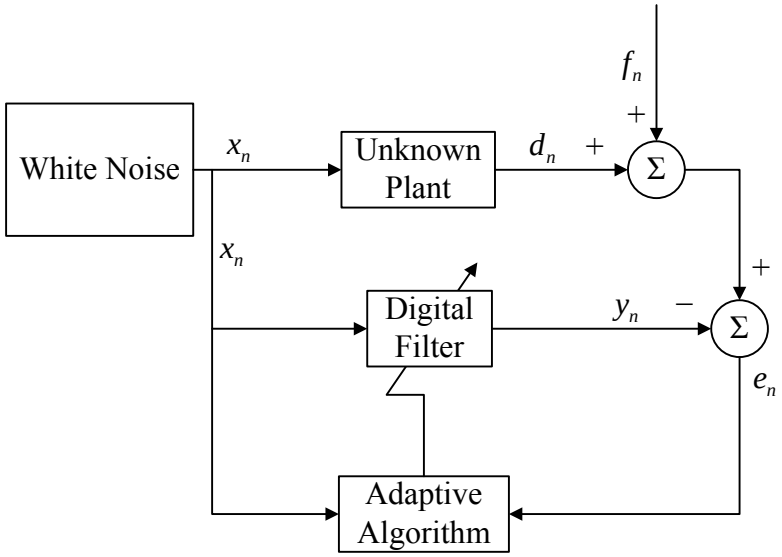

Figure 3.6 Structure of system identification with interference

d_n and x_n are correlated, d_n can be seen as the output from an 'unknown plant' that is excited by x_n. f_n can be seen as the interference, which can affect the identification performance. e_n is the identification error. The value of weighting function is concerned in system identification application. The length of the weighting function should be long enough to catch all the impulse response of this 'unknown plant' to get a good identification result. Inadequacy of the weighting function may lead to a distortion result of an unknown system and a large remnant of noise. In Figure 3.6 an arbitrary second order transfer function with damping ratio 0.05 is applied as

unknown plant. The length of weighting function in the FIR filter is 64 and assuming f_n is zero. The identification process begins at 1s.

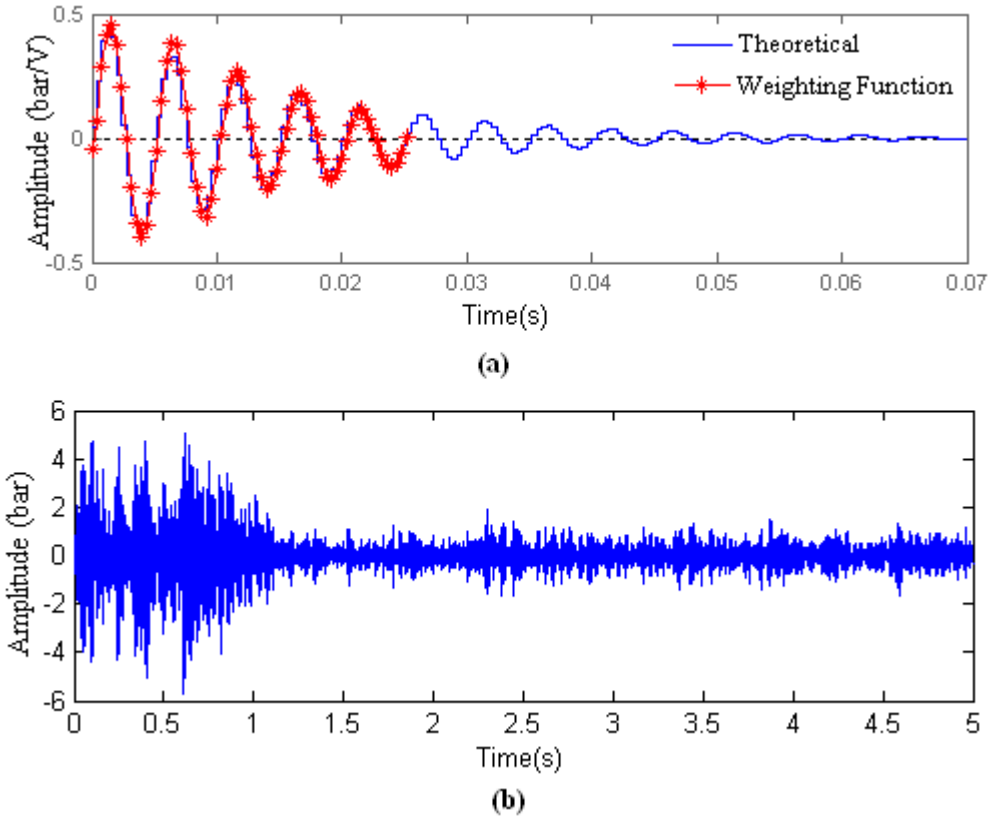

Figure 3.7 (a) Unknown plant impulse response comparing of theoretical value and LMS adaptive filter weighting function with inadequate length

(b) Identification error signal

Comparison of theoretical system impulse response and the LMS adaptive filter weighting function is shown in Figure 3.7 (a). The identification error signal is shown in Figure 3.7 (b). From this figure, the first 1 s is d_n without identification operation, and then after a short period the identification error decreases to a certain level under the effect of y_n. Since an inadequate length of LMS adaptive filter weighting function is used in the system, not all the real information of this second order transfer function can be described. As a consequence a certain residual identification error between unknown plant and weighting function still exists, as shown in Figure 3.7 (b).

On the other hand by changing the damping ratio of the arbitrary second order transfer function to 0.15 the identification weighting function with 64 orders is relatively long enough to catch all information of unknown plant impulse response. Repeat the identification process above. The identification result is shown in Figure 3.8.

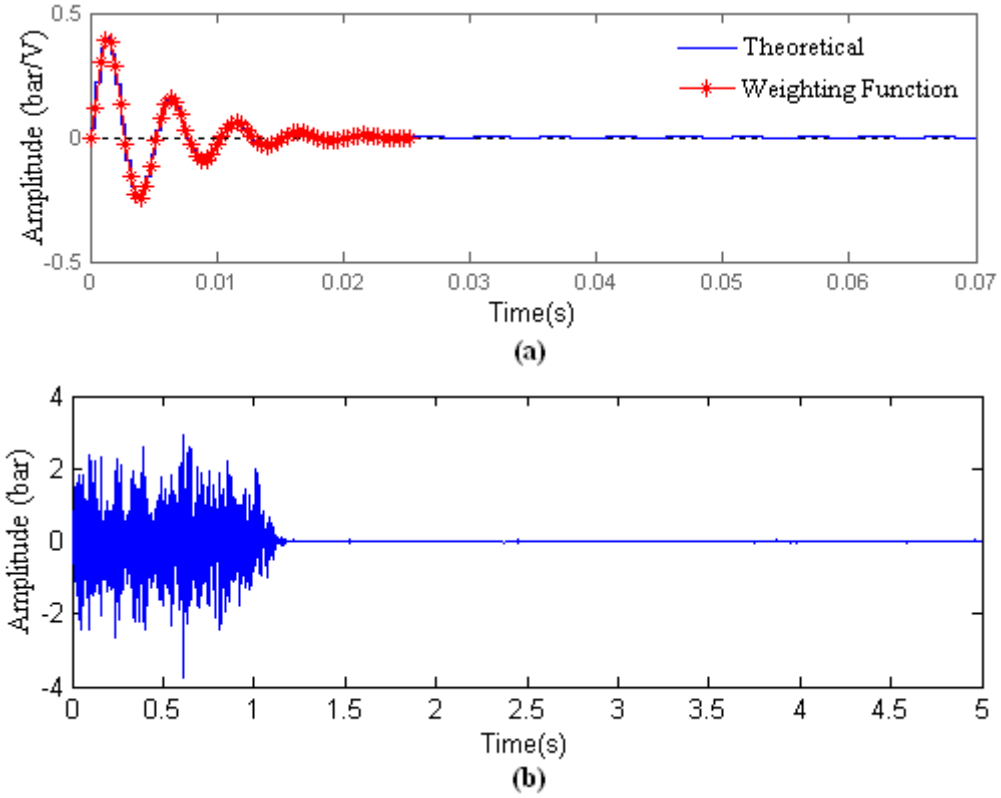

Figure 3.8 (a) Unknown plant impulse response comparing of theoretical value and LMS adaptive filter weighting function with adequate length
(b) Identification error signal

Full characteristics of unknown plant are obtained by comparing with the theoretical value. The error signal is almost zero under this identification. Furthermore identification and results also depend on the sampling frequency of the system. For a constant length a low sampling frequency can let the weighting function cover a relatively long impulse response of unknown plant but can miss high frequency components. However, for a high sampling frequency a compromise is needed between computation time and the weighting function length.

As mentioned, the interference f_n in Figure 3.6 can also affect the identification performance. With higher f_n and higher convergence factor, this effect becomes more significant. Assuming f_n is a 10 Hz pure sine wave with amplitude 1, under this effect

the identification performance can be degraded and even goes unstable using the same convergence factor. However, with adequate small convergence factor the identification can also converge to a good solution and the error signal e_n will ultimately approach f_n. In Figures 3.9 and 3.10 the unknown plant identification results and error signals with different convergence factors are plotted respectively with $f_n = 1$ and compared with the results when $f_n = 0$.

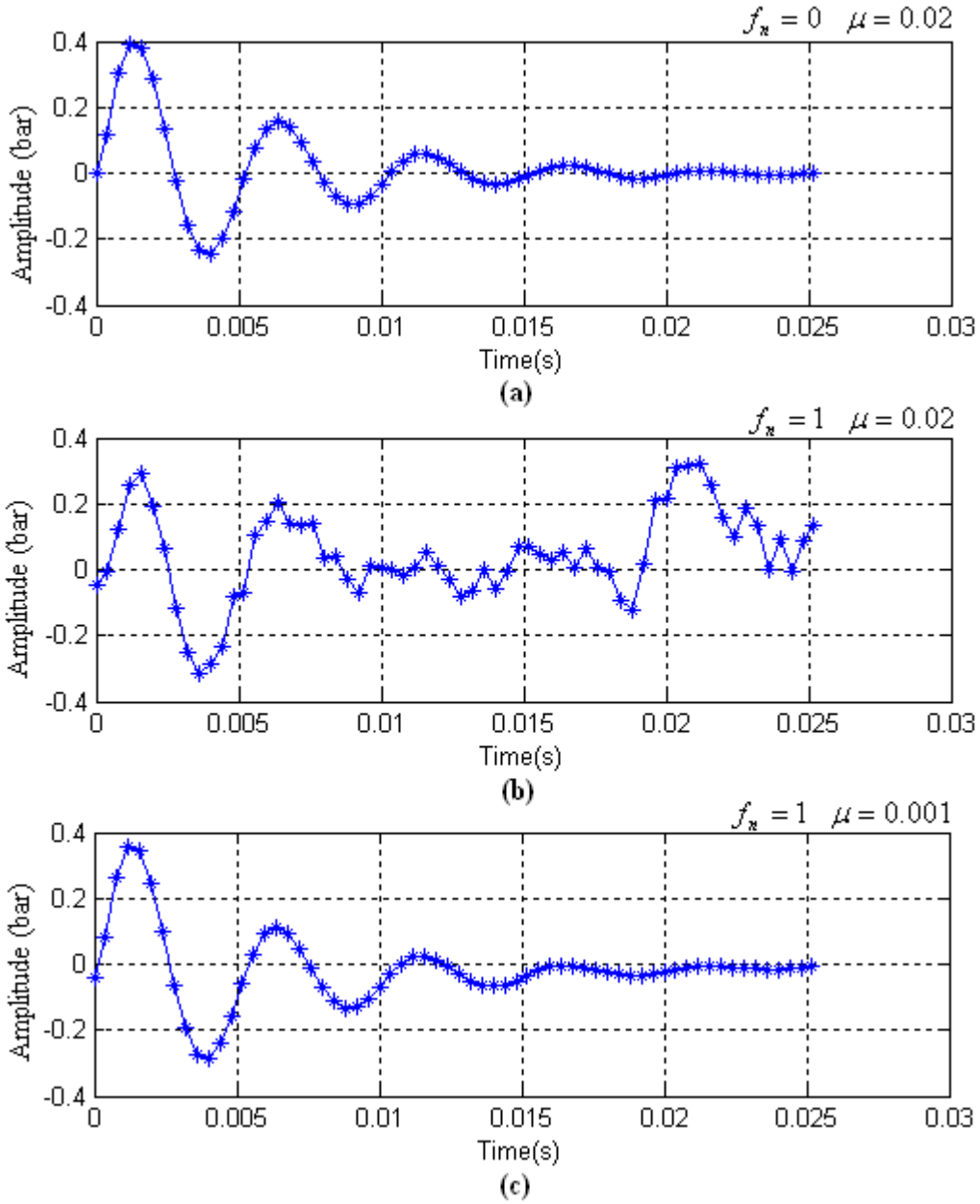

Figure 3.9 Unknown plant identification results with different interferences and different convergence factors. (a): $f_n = 0$ $\mu = 0.02$ (b): $f_n = 1$ $\mu = 0.02$ (c): $f_n = 1$ $\mu = 0.01$

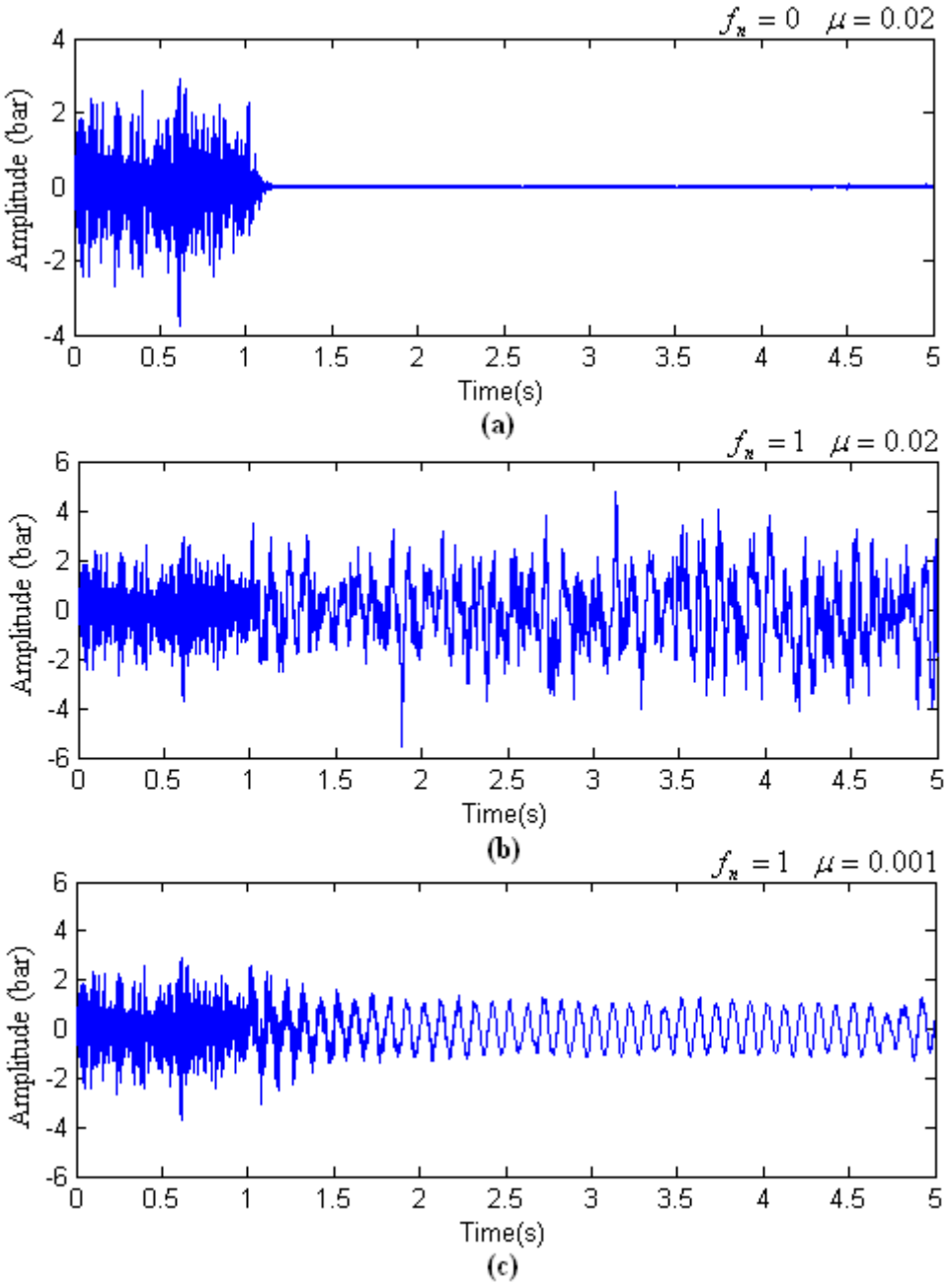

Figure 3.10 Identification error signal with different interferences and different convergence factors. (a): $f_n = 0$ $\mu = 0.02$ (b): $f_n = 1$ $\mu = 0.02$ (c): $f_n = 1$ $\mu = 0.01$

In real experiment some interference may also affect the identification performance. Hence a relatively large white noise signal and small convergence identification factor are necessary for stability.

3.2 Narrowband notch LMS adaptive filter

Basically the applications of noise cancellation using an LMS adaptive filter can be divided into two main parts by frequency: broadband and narrowband. In broadband applications an error sensor is located near the noise source to pick up the signal as a reference, and then inject the anti-noise back to noisy field. However, in this situation the error sensor near the noise source can be affected by this injecting signal to make the system unstable and several limitations can occur. In narrowband applications as the noise signal exists at certain frequencies the reference signal can be synchronized and synthesized by using a sensor such as a tachometer on the rotating machine, from which the noise signal comes [12]. Recently, the adaptive notch filter is the most common algorithm in narrowband noise cancellation. In this section discussion of this method is presented in detail.

3.2.1 General notch LMS adaptive filter

A general structure of the LMS adaptive notch filter is shown in Figure 3.11. Assume only a single frequency component of noise signal to be cancelled. The reference signal in the notch adaptive filter can be described as:

$$x(n) = A \cdot \cos(\omega_0 \cdot n + \varphi) \tag{3.23}$$

where ω_0 is the normalized frequency form that can be extended as:

$$\omega_0 = 2 \cdot \pi \cdot f_0 \cdot \Delta t$$

φ is a arbitrary phase shift of the signal, A is the amplitude and n is the time index.

Combined with equation (3.3), the input signal in (3.23) can be generally written as:

$$x_i(n) = A \cdot \cos(\omega_0 \cdot n + \varphi_i)$$

where φ_i is a arbitrary phase shift at the corresponding input signal. Equations (3.1) to (3.4) can be used to describe the process of using a general notch LMS adaptive filter, and the length of weighting function should be long enough to catch $x(n)$.

The frequency of the noise to be cancelled in $d(n)$ should be the same as that of $x(n)$ and the phase shift between $d(n)$ and $x(n)$ can be adaptively adjusted to zero by the LMS controller. The amplitude of the other signals that do not need to be cancelled may be adjusted slightly and a phase shift also occurs depending on the parameters of the notch filter.

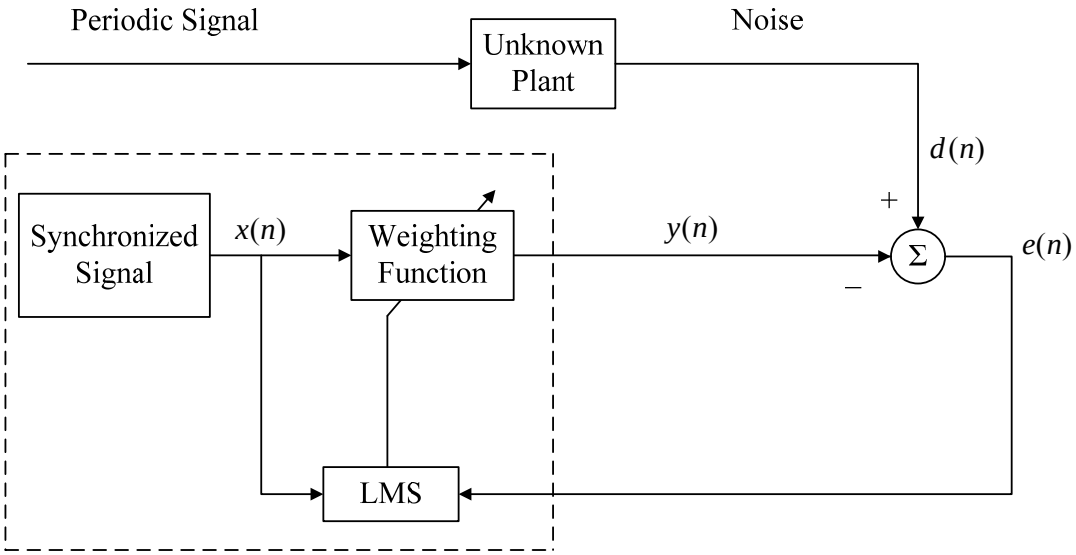

Figure 3.11 Typical structure of general LMS adaptive notch filter

These whole phenomena can be explained by transfer functions as follows. Firstly the dashed line part in Figure 3.11 can be seen as a transfer function $G(z)$ and the structure in Figure 3.11 can be simplified into Figure 3.12 [33]:

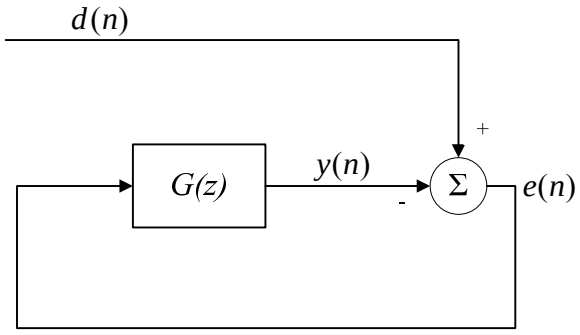

Figure 3.12 Simplification of LMS adaptive notch filter

Analyzing in z domain, $G(z)=\frac{Y(z)}{E(z)}$ $E(z)$ is the z domain representation of $e(n)$ and $Y(z)$ is the z domain description of $y(n)$. However the output signal from $G(z)$ can be presented as [33]:

$$Y(z)=\frac{L\cdot\mu\cdot A^2}{4}\cdot E(z)\cdot\left[U\left(z\cdot e^{-j\omega\cdot\Delta t}\right)+U\left(z\cdot e^{j\omega\cdot\Delta t}\right)\right]+TV \tag{3.24}$$

where TV is the time varying term that can be presented as:

$$TV=\frac{\mu\cdot A^2}{4}\cdot\left[U\left(z\cdot e^{-j\omega\cdot\Delta t}\right)\cdot E\left(z\cdot e^{-j2\omega\cdot\Delta t}\right)\cdot\sum_{i=1}^{L}e^{j2\varphi_i}+U\left(z\cdot e^{j\omega\cdot\Delta t}\right)\cdot E\left(z\cdot e^{j2\omega\cdot\Delta t}\right)\cdot\sum_{i=1}^{L}e^{-j2\varphi_i}\right]$$

and $U(z)=1/(z-1)$, which is the z-domain transfer function between $\mu\cdot\bar{x}(n)\cdot e(n)$ and $\overline{w}(n)$ in the equation (3.18).

A frequency shift component $E\left(z\cdot e^{-j2\omega\cdot\Delta t}\right)$, which is unwanted for deducing $G(z)$, is introduced by this time varying term. A ratio β is applied in the term $\sum_{i=1}^{L}e^{j2\varphi_i}$ and $\sum_{i=1}^{L}e^{-j2\varphi_i}$ to evaluate its effect, which can be written as [33]:

$$\sum_{i=1}^{L}e^{\pm j2\varphi_i}=e^{\pm j[2\varphi_i-\omega_0\cdot(L-1)]}\cdot\beta(\omega_0,L) \tag{3.25}$$

where,

$$\beta(\omega_0,L)=\frac{\sin(L\cdot\omega_0)}{\sin(\omega_0)}$$

β/L as a function against $\omega_0/2\pi$ with different length of L is plotted in [33]. It is found that if $\omega_0/2\pi$ is not too close to 0 or 0.5, $\beta/L=0$ or β/L is closer to zero with more number of weighting function is used [33].

Usually when the effect of β/L is weak, only the time invariant part is considered in $G(z)$, presenting as [33]:

$$G(z) = \mu \cdot A^2 \cdot \left[\frac{\frac{L}{2} \cdot (z \cdot \cos\omega_0 - 1)}{z^2 - 2 \cdot z \cdot \cos\omega_0 + 1} \right] \tag{3.26}$$

From this equation the transfer function between $d(n)$ and $e(n)$ can be obtained as [33, 12]:

$$H(z) = \frac{z^2 - 2 \cdot z \cdot \cos\omega_0 + 1}{z^2 - 2 \cdot \left(1 - \frac{L \cdot \mu \cdot A^2}{4}\right) \cdot z \cdot \cos\omega_0 + \left(1 - \frac{L \cdot \mu \cdot A^2}{2}\right)} \tag{3.27}$$

Therefore the steady state of the LMS adaptive notch filter can be described using a determinate transfer function. However, this conclusion depends on zero assumption of time varying term, which can indeed affect the cancellation result with a small value of L. An improvement of this kind of LMS adaptive notch filter can be realized to overcome the effect from the time varying term.

3.2.2 Two-weight notch LMS adaptive filter

An improved two-weight LMS adaptive filter is proposed [12]. Figure 3.13 shows its simplified structure with interference f_n. Assuming $f_n = 0$, the adaptive process can be described using the following equations for single frequency cancellation.

Reference input signals:

$x_1(n) = A \cdot \sin(\omega_0 \cdot n + \varphi_1)$;

$x_2(n) = A \cdot \sin(\omega_0 \cdot n + \varphi_1 + \pi/2) = \cos(\omega_0 \cdot n + \varphi_1)$

where φ_1 is the arbitrary phase shift. Weighting functions update:

$$w_1(n+1) = w_1(n) + \mu \cdot x_1(n) \cdot e(n);$$

$$w_2(n+1) = w_2(n) + \mu \cdot x_2(n) \cdot e(n)$$

Control signal:

$$y(n) = x_1(n) \cdot w_1(n) + x_2(n) \cdot w_2(n)$$

Error signal:

$$e(n) = d(n) - y(n)$$

In these equations ω_0 is the normalized noise frequency to be cancelled.

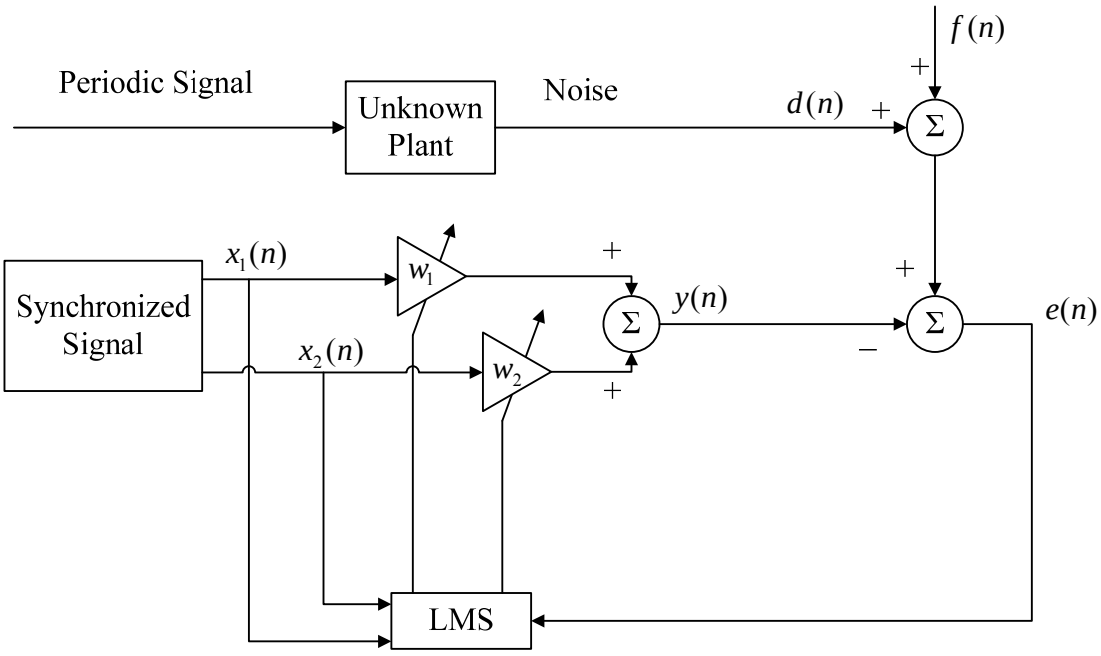

Figure 3.13 Structure of two-weight LMS adaptive notch filter

In this structure rather than applying a series of weights as weighting function only two weights are used here. According to this a sine signal and a cosine signal are

synchronized as references for w_1 and w_2 separately. In this situation $\sum_{i=1}^{L} e^{j2\varphi_i}$ and $\sum_{i=1}^{L} e^{-j2\varphi_i}$ can be written as:

$$\sum_{i=1}^{2} e^{j2\varphi_i} = e^{j2\varphi_1} + e^{j2\left(\varphi_1+\frac{\pi}{2}\right)} = 0$$

$$\sum_{i=1}^{2} e^{-j2\varphi_i} = e^{-j2\varphi_1} + e^{-j2\left(\varphi_1+\frac{\pi}{2}\right)} = 0$$

which means the time varying part in equation (3.24) disappears.

Simulation has been made to compare the cancellation results of the general LMS adaptive filter and the two-weight LMS adaptive filter with a different value of ω_0 in Figure 3.14 with the sampling frequency equal to 10000 Hz. In Figure 3.14 (a) $\omega_0 = 0.001$, which means the time varying part, can contribute to the adaptive process to the interference cancellation result under a fast adaptive setting time. $\omega_0 = 0.01$ is applied in Figure 3.14 (b), good cancellation results can be obtained with little effect from time varying term in equation (3.24).

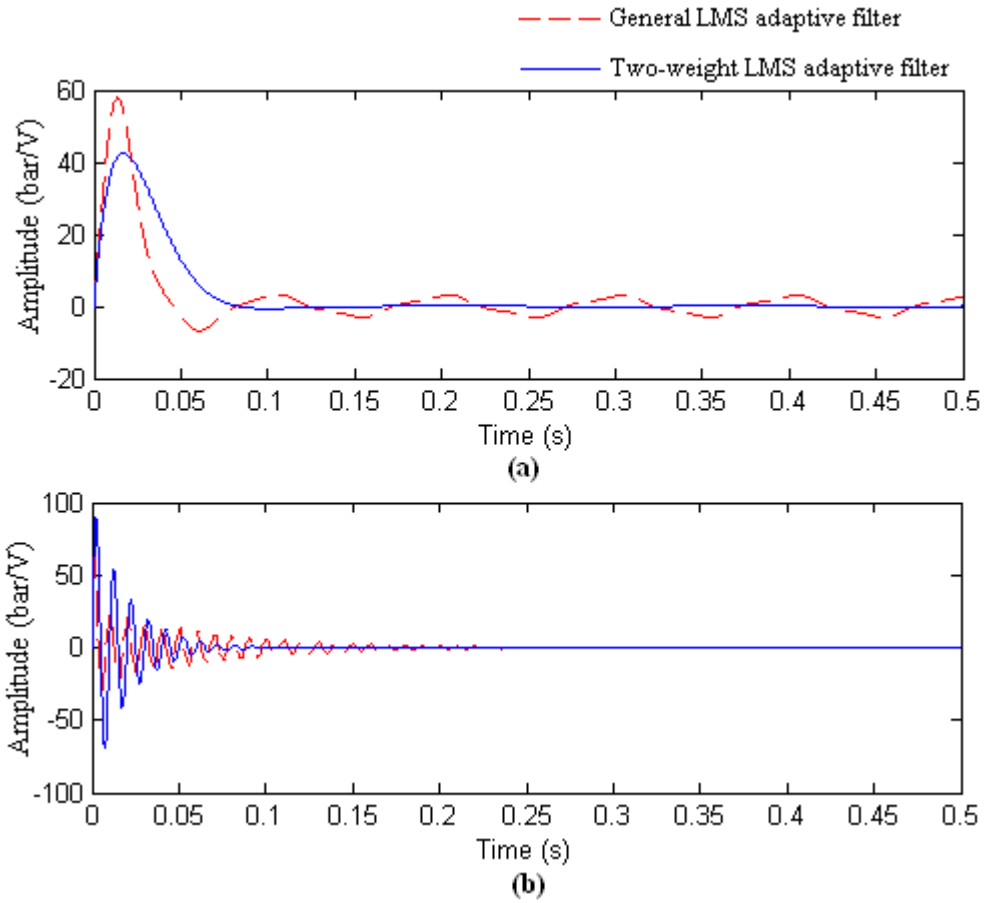

Figure 3.14 Comparison of cancellation results of general and two-weight LMS adaptive filter with different ω_0. (a): $\omega_0 = 0.001$ (b): $\omega_0 = 0.01$

Compared with equation (3.27), the steady state transfer function of the LMS adaptive two-weight notch filter is deduced by Widrow in [28] and can be presented as:

$$H(z) = \frac{z^2 - 2 \cdot z \cdot \cos\omega_0 + 1}{z^2 - 2 \cdot \left(1 - \frac{\mu \cdot A^2}{2}\right) \cdot z \cdot \cos\omega_0 + \left(1 - \mu \cdot A^2\right)} \tag{3.28}$$

The z domain root locus of $H(z)$ can be plotted to discuss the stable conditions in Figure 3.15 and the sampling frequency applied here is 3125 Hz.

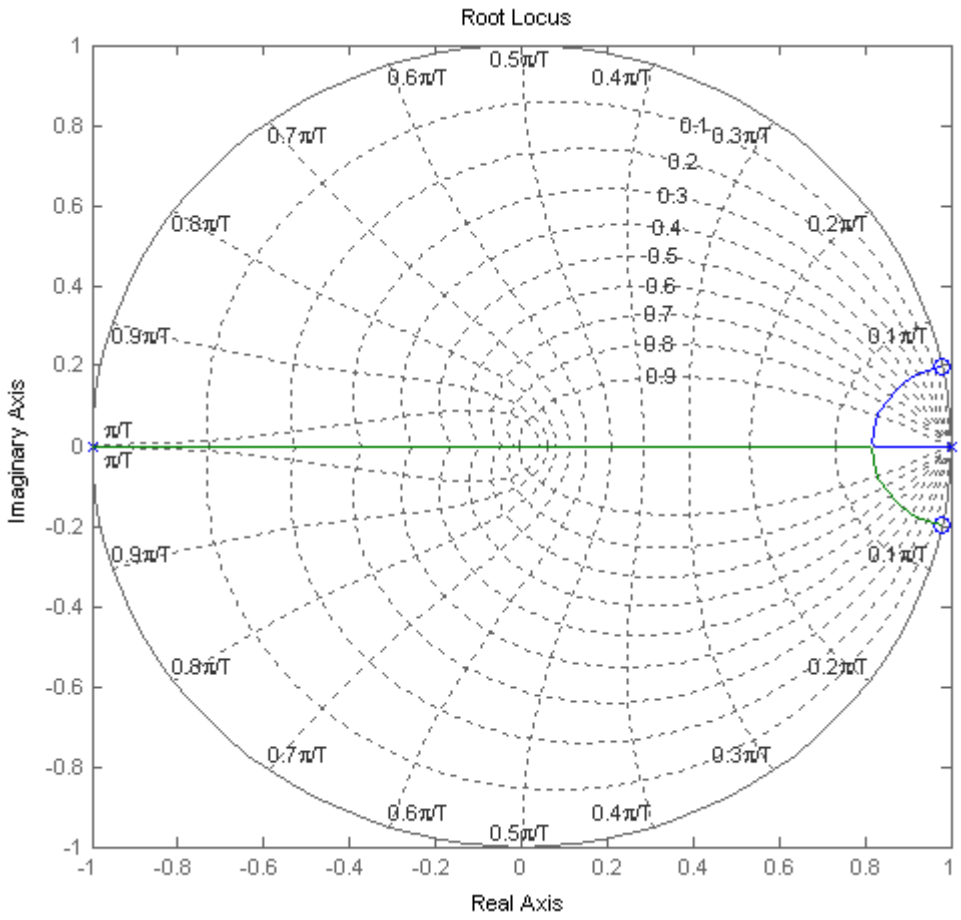

Figure 3.15 z domain root locus of two-weight LMS adaptive filter with f_0 = 100 Hz, $\mu = 2$

From equation (3.28) two complex zeros are obtained: $z = e^{\pm j\omega_0}$, and a real zero is: $z = \dfrac{1}{\cos\omega_0}$.

The poles can be written as:

$$z = \frac{\left(2-\mu\cdot A^2\right)\cdot\cos\omega_0 \pm \sqrt{\left(2-\mu\cdot A^2\right)^2\cdot\cos^2\omega_0 - 4\cdot\left(1-\mu\cdot A^2\right)}}{2}$$

For a small value of $\mu\cdot A^2$ (The range of this value is shown in Appendix 2), complex poles can be obtained. The radius and angle can be presented as:

$$r = \sqrt{1-\mu \cdot A^2}\ ; \qquad \alpha = \pm\cos^{-1}\left[\left(\frac{1-\mu \cdot A^2}{2}\right)\cdot\left(1-\mu \cdot A^2\right)^{-\frac{1}{2}} \cdot \cos(\omega_0)\right]$$

Hence the stable condition of equation (3.28) is: $0 < \mu < \frac{2}{A^2}$.

For a different value of μ, the spectrum of this notch filter is plotted in Figure 3.16, still with sampling frequency 3125 Hz.

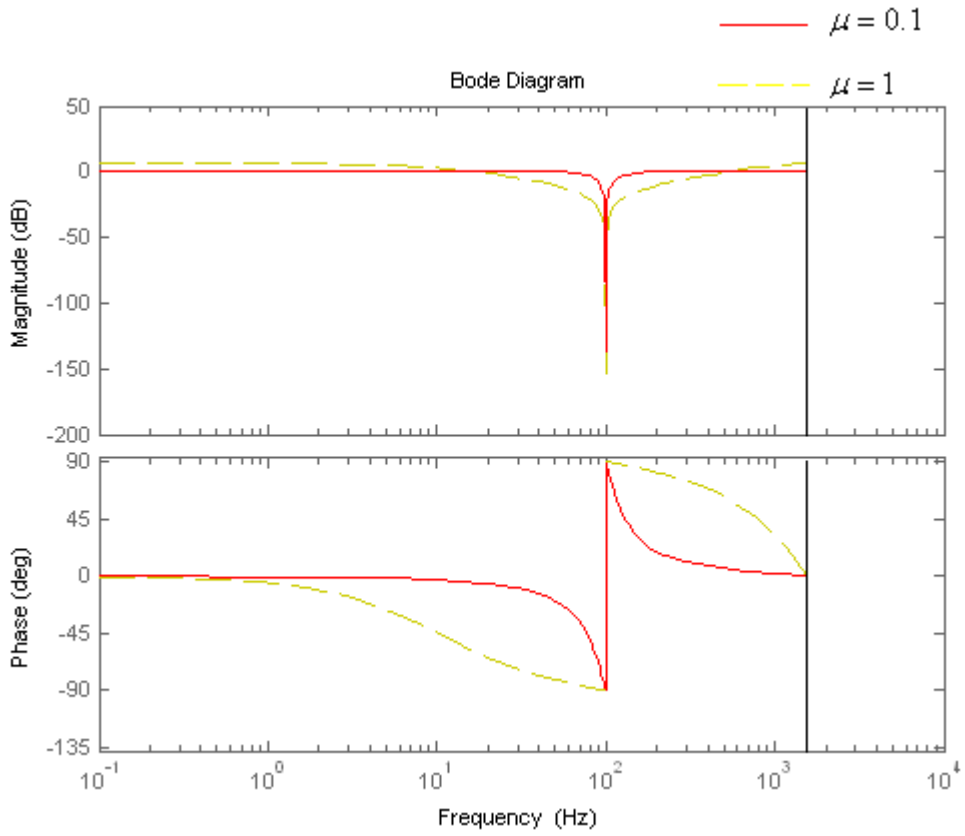

Figure 3.16 Spectrum comparison of two-weight LMS adaptive filter with *f* = 100 Hz and $\mu = 0.1$, $\mu = 1$

An approximation can be made on the radius of the poles [28]:

$$r = \sqrt{1-\mu \cdot A^2} \approx 1 - \frac{\mu}{2} \cdot A^2$$

Hence the amplitude of $H(z)$ can be described using $1-\frac{\mu}{2}\cdot A^2$. For a constant value of A, a higher amplified value and a sharper notch can be obtained by $H(z)$ with a higher value of μ.

Now considering the case where the interference f_n in Figure 3.13 is not zero. As shown in Figure 3.16 the notch filter can have an effect on the frequency components without cancellation. This effect may influence the residual noise and this affected residual can give distortion for online system identification, which will be discussed in Chapter 6. As a result, a tradeoff between fast cancellation settling time and magnification of signals at frequencies without cancellation should be considered when designing a notch filter.

3.2.3 Multiple frequency noise cancellation

Single frequency noise cancellation has been discussed above. Usually $d(n)$ consists of many harmonic frequency orders and most of them need to be cancelled. Typically two types of notch filter, direct form and parallel form, are used [12]. In direct form the reference signal is a summation of a series of sinusoidal waves. When using a general LMS adaptive notch filter, the weighting function should be long enough to catch all frequency components of reference input. In parallel form, which is applied in this work, a series of notch filters is applied in parallel to cancel each corresponding frequency component. For parallel form of two-weight LMS adaptive filter, the reference input and weighting function is presented in vector forms:

$$\bar{x}_1(n) = \begin{bmatrix} x_1^1 & x_1^2 & \cdots & x_1^l \end{bmatrix}$$

$$\bar{x}_2(n) = \begin{bmatrix} x_2^1 & x_2^2 & \cdots & x_2^l \end{bmatrix}$$

$$\bar{w}_1(n) = \begin{bmatrix} w_1^1 & w_1^2 & \cdots & w_1^l \end{bmatrix}$$

$$\bar{w}_2(n) = \begin{bmatrix} w_2^1 & w_2^2 & \cdots & w_2^l \end{bmatrix}$$

where l is the number of harmonic components to be cancelled. Hence control signal y can be presented as:

$$y = \bar{x}_1(n) \cdot \bar{w}_1^T(n) + \bar{x}_2 \cdot \bar{w}_2^T$$

3.3 Conclusions

To summarize, this chapter gives the detailed knowledge including concept and deduction of the adaptive LMS algorithm, which is based on the FIR filter. Applications used in the broadband and narrowband frequency area, especially system identification, are introduced. Robust and effective cancellation and identification results can be obtained through simulations. The dynamic characteristics of LMS adaptive notch filter used in narrowband applications are investigated. To avoid the time varying effect the proposed two-weight LMS adaptive notch filter, which is applied in this project, is evaluated in detail. An efficient notch filter form used for multiple frequency cancellation is also presented at the end of this chapter. It is found that the two-weight adaptive notch filter has a good potential to attenuate the narrowband harmonics of the fluid-borne noise in this work, and the system identification may also be implemented using the broadband LMS adaptive filter.

CHAPTER 4

Modelling of Hydraulic System and Anti-noise System

In this work testing the different researched active control methods on a real rig is the most convincing way to prove the feasibility of these techniques. In this chapter before building up the rig for the real experiment, a model of a simple hydraulic system with control flow was set up using the method of characteristics (MOC) in order to be the basis of researching the efficient active noise control method. Kojima's method, which is an active feedforward control method of fluid-borne noise, is evaluated and improved through simulation using the MOC. Moreover the model with different accuracy and computing levels is also evaluated using Kojima's method.

4.1 Method of characteristic technique

There are many techniques for modelling flow and pressure ripple in a pipe, including distributed parameter wave effects, such as the Method of Characteristics (MOC) and the Transmission-line Method. Johnston proposed an efficient method for numerical modelling of laminar flow ripple status in fluid lines, which is currently one of the most accurate techniques using the MOC [34]. First of all, some basic equations for this method and the previous work are necessary to explain.

The one-dimension motion equation in a pipe can be represented as [34]:

$$\frac{\partial q}{\partial t}+\frac{q}{A}\cdot\frac{\partial q}{\partial x}+\frac{A}{\rho}\cdot\frac{\partial p}{\partial x}+f(q)=0$$

where x is the distance along the pipe, q is the flow at point x, p is the pressure at point x, A is the pipe internal cross-sectional area, ρ is the liquid density and $f(q)$ is the friction term. The second term in the equation can be ignored because $\frac{q}{A}\cdot\frac{\partial q}{\partial x}<<\frac{\partial q}{\partial t}$ [35]. For a steady laminar flow $f(q)$ can be approximated and described as: $f(q)=\frac{8\cdot\nu}{r^2}$ [34], where r is the pipe internal radius and ν is the fluid kinematic viscosity. Therefore, the rearranged and approximated motion equation for the fluid is:

$$\frac{\partial q}{\partial t}+\frac{A}{\rho}\cdot\frac{\partial p}{\partial x}+f(q)=0 \tag{4.1}$$

The continuity equation in one-dimension is:

$$\frac{\partial \rho}{\partial t}+\frac{\rho}{A}\cdot\frac{\partial q}{\partial x}+\frac{q}{A}\cdot\frac{\partial \rho}{\partial x}=0 \tag{4.2}$$

The equation of state for the liquid is:

$$B=\rho\cdot\frac{\partial p}{\partial \rho}=\rho\cdot c^2 \tag{4.3}$$

where c is the sound speed in the liquid. The third term in equation (4.2) can also be ignored because $\left|\frac{\rho}{A}\cdot\frac{\partial p}{\partial x}\right|<<\left|\frac{\partial p}{\partial t}\right|$ [35]. Then by combining (4.2), (4.3), the rearranged continuity equation for the fluid is:

$$\frac{\partial p}{\partial t}+\frac{\rho\cdot c^2}{A}\cdot\frac{\partial q}{\partial x}=0 \tag{4.4}$$

For the liquid in a pipe line, the motion of waves has two directions, given by:

$\frac{dx}{dt}=+c$ and $\frac{dx}{dt}=-c$.

where c is the speed of sound in the liquid.

Therefore equations (4.1) and (4.4) can be combined and transformed into ordinary differential equations [34]:

$$\frac{dq}{dt}+\frac{A}{\rho c}\cdot\frac{dp}{dt}+f(q)=0 \qquad \text{when } \frac{dx}{dt}=+c \tag{4.5}$$

$$\frac{dq}{dt}-\frac{A}{\rho c}\cdot\frac{dp}{dt}+f(q)=0 \qquad \text{when } \frac{dx}{dt}=-c \tag{4.6}$$

These two equations can be approximated using finite difference method. In Figure 4.1, assume the pipe can be divided into four elements for example. At time t_1, the flow and

the pressure at point *A* are q_A and p_A, at point *B* the flow and the pressure are q_B and p_B. At next time step $t_1 + \Delta t$, the flow and pressure at point P, which is on the middle position between *A* and *B*, are q_P and p_P.

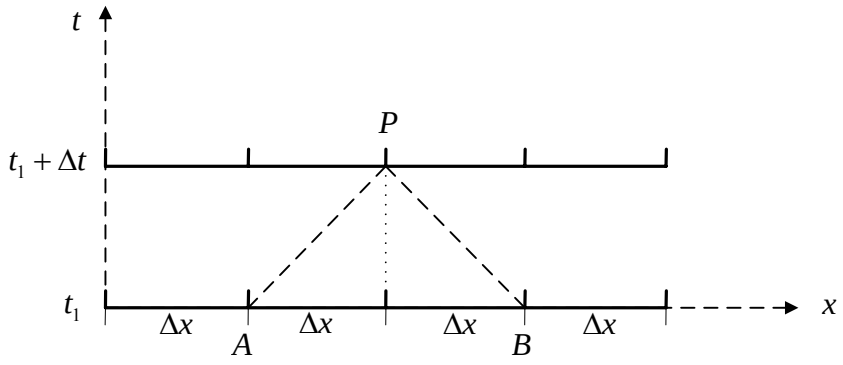

Figure 4.1 Characteristic lines of the MOC

Hence in Figure 4.1, (4.5) can be approximated using difference equation:

$$\frac{q_P - q_A}{\Delta t} + \frac{A}{\rho c} \cdot \frac{p_P - p_A}{\Delta t} + f(q_A) = 0$$

which can be written as:

$$q_P - q_A + \frac{A}{\rho c}(p_P - p_A) + \Delta t \cdot f(q_A) = 0 \tag{4.7}$$

(4.6) can be approximated using difference equation:

$$\frac{q_P - q_B}{\Delta t} + \frac{A}{\rho c} \cdot \frac{p_P - p_B}{\Delta t} + f(q_B) = 0$$

which can be written as:

$$q_P - q_B - \frac{A}{\rho c}(p_P - p_B) + \Delta t \cdot f(q_B) = 0 \tag{4.8}$$

The last term on the left in (4.7) and (4.8) is known as the friction term, and can be represented using f_A and f_B. From equations (4.7) and (4.8) the flow and pressure at *P* point can be written as:

$$q_P = \frac{1}{2}\cdot\left[q_A + q_B + \frac{A}{\rho\cdot c}\cdot(p_A - p_B) - \Delta t\cdot(f_A + f_B)\right] \tag{4.9}$$

$$p_P = \frac{1}{2}\cdot\left[p_A + p_B + \frac{\rho\cdot c}{A}\cdot(q_A - q_B) + \Delta t\cdot\frac{\rho\cdot c}{A}\cdot(f_B - f_A)\right] \tag{4.10}$$

Therefore the flow and the pressure at any point along the pipe can be obtained using the previous value at nearby points.

The friction term f_A and f_B are actually a frequency-dependent value, which includes a steady state and an unsteady or frequency dependent parts [36]. For laminar flow this friction term can be represented approximately in the frequency domain [34]:

$$F_{APP}(Q) = \left[\frac{8\nu}{r^2} + \frac{4\nu}{r^2}\sum_{i=1}^{k}\left(\frac{m_i\, j\alpha}{n_i + j\alpha}\right)\right]\cdot Q = H_{APP}\frac{\nu}{r^2}\cdot Q \qquad \text{where} \qquad \alpha = \frac{r^2\omega}{\nu}$$

where Q is the flow in frequency domain, m_i and n_i are the weighting factors and ω is the frequency of flow ripple. In order to model the transient response in the time domain, the Fourier Transformation is applied to this equation, and a numerical approximation applied:

$$f(t+\Delta t) = \frac{8\nu}{r^2}\cdot q(t+\Delta t) + \frac{4\nu}{r^2}\sum_{i=1}^{k} y_i(t+\Delta t)$$

$$y_i(t+\Delta t) = y_i(t)\cdot e^{-\frac{n_i\nu\Delta t}{r^2}} + m_i\left[q(t+\Delta t) - q(t)\right]\cdot e^{-\frac{n_i\nu\Delta t}{2r^2}}$$

which means at any point along the pipe the friction term can be obtained using the flow values at the current time and previous time. Therefore, f_A and f_B can be obtained.

In the equations above the weighting factors m_i and n_i can be an infinite variety of values. Johnston used an efficient and simple method selecting the weighting factors as geometric series [34].

$m_i = \beta \cdot m_{i-1}$ for $i \geq 3$; $n_i = \beta^2 \cdot n_{i-1}$ for $i \geq 2$

and the term k can be chosen using: $k = ceil\left(\frac{2\log r - \log(n_i \nu \Delta t)}{2\log \beta}\right) + 1$, in this work k is equal to 3.

Therefore, the ripple model of the rig system can be simply represented using Figure 4.1, the horizontal axis can describe all the points along the pipe and the longitudinal axis can describe the time series. In this model the fluid-borne noise can be injected at one end of the pipe and the open area at the other end can be controlled by a loading valve.

In real experiments the reflection from the pipe end, which can be adjusted by the loading valve, can be affected by the flow and pressure in the pipe. Generally, pressure and flow in an orifice for turbulent flow can be presented as [6]:

$$\Delta P = \alpha \cdot Q^2$$

where ΔP is the pressure difference at the orifice and Q is the flow through the orifice. The impedance can be written as:

$$Z = \frac{2 \cdot \Delta P}{Q}$$

The pipe characteristic impedance can be represented as:

$$Z_0 = \frac{\rho \cdot c}{A}$$

A parameter k_P is applied here to describe effect of loading valve reflection factor, which can be written as:

$$k_P = \frac{Z_0}{Z}$$

Its range is from zero to infinity, where k_P equal to zero means the pipe end is fully closed, k_P equal to infinity means fully open, and k_P equal to one means no

reflection coming back from the pipe end. Using (4.9) and (4.10), Figure 4.2 illustrates the flow and pressure ripple against time at points 10 and 13 on the pipe, which is divided using 21 points. The input flow ripple frequency to the pipe is 500 rad/s at a certain power level and $k_P = 0.1$. The related main parameters used in this model are listed in Appendix 1 for this chapter.

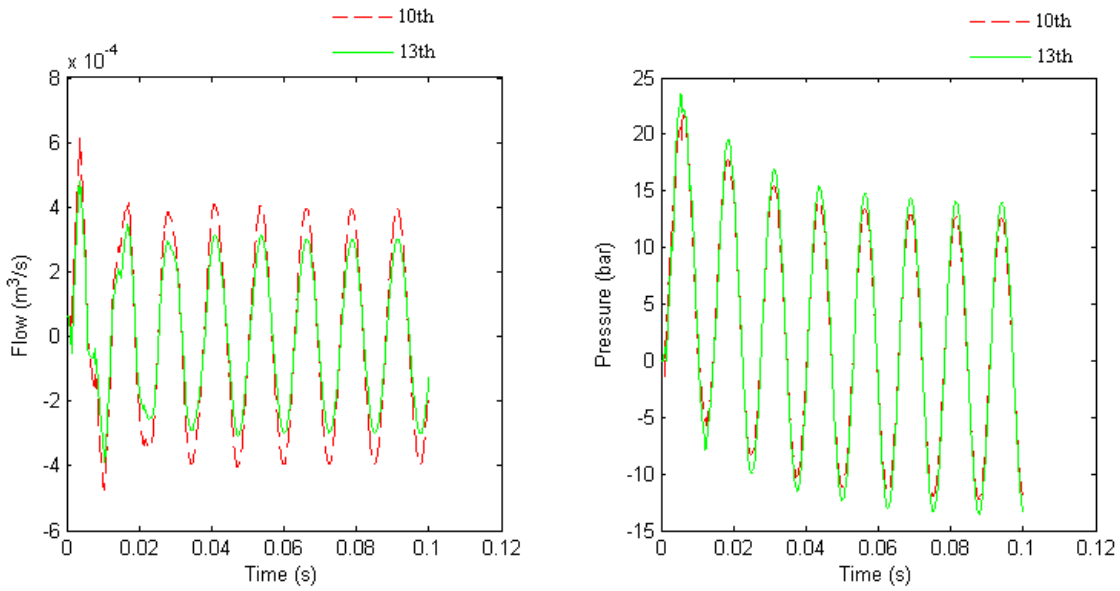

Figure 4.2 Modelling result of flow and pressure ripple in the pipe at 500 rad/s

From Figure 4.2 the accurate dynamic characteristics of flow and pressure ripple at different points on the pipe can be obtained from this model. In the following section this model is developed adding a control flow and is applied on an active control of fluid-borne noise algorithm. The modelling is realized from different parts and the results are analyzed to evaluate this control method and the model.

4.2 Implementation of Kojima's method in MOC

In section 2.1.3 Kojima's method is evaluated. The basic idea is that an anti-noise signal, which could be generated using a secondary source, is applied to cancel the fluid-borne noise. Corresponding to the control process in Figure 2.1 an efficient method to realize this method is represented in the following section. Compared with Johnston's MOC model, in Kojima's method first of all an approximation of the friction was applied in the liquid motion equation:

$$\frac{\partial u}{\partial t} = -\frac{1}{\rho} \cdot \frac{\partial p}{\partial x} - R_f \cdot u \tag{4.11}$$

In this equation the friction term R_f only included the steady part $\frac{8\nu}{r^2}$. Secondly, the pressure gradient term $\frac{\partial p}{\partial x}$ was also approximated using the following difference equation:

$$\frac{\partial p}{\partial x} = \frac{p_2(t) - p_1(t)}{\Delta x} \tag{4.12}$$

p_1 and p_2 could be obtained from the two pressure transducers mentioned previously. Equation (4.12) is substituted into (4.11) and using the Laplace transformation:

$$U(s) = \frac{1}{\rho(s + R_f)} \frac{P_1(s) - P_2(s)}{\Delta x} \tag{4.13}$$

Represented using the convolution integral on (4.13), the fluid velocity pulsation $u(t + \Delta t)$ could be given by the following form [15]:

$$u(t + \Delta t) = e^{-R_f \Delta t} \cdot u(t) + \frac{\Delta t}{2\rho \Delta x} \cdot e^{-R_f \Delta t / 2} \cdot \{p_1(t) - p_2(t) + p_1(t + \Delta t) - p_2(t + \Delta t)\} \tag{4.14}$$

Finally, the velocity of the progressive wave component could be given by:

$$F_1(t) = \frac{1}{2} \cdot \left\{ u(t) + \frac{1}{\rho \cdot c} \cdot \frac{p_1(t) + p_2(t)}{2} \right\} \tag{4.15}$$

However, the friction term was not included in the above equation of progressive wave flow. Therefore the control flow injecting into the pipe could be given by:

$$q(t)_{progressive} = 2 \cdot F_1(t - \tau) \cdot A \tag{4.16}$$

where *A* was the sectional area of the pipe and τ was the time by which the ripple transmitted from detecting point to control point in Figure 2.1.

Theoretically, the flow of progressive wave at a certain point can be deduced using the following equations in frequency domain:

$$F(s) = \frac{1}{2} \cdot \left(Q(s) + \frac{P(s)}{Z(s)} \right) \tag{4.17}$$

where $Z(s) = \frac{\rho \cdot c}{A} \cdot \sqrt{1 + \frac{A \cdot R}{\rho \cdot s}}$ and R is also a frequency dependent term, which is difficult to evaluate [6].

Assume R is a constant, and then the time domain flow of progressive wave is:

$$f(t) = \frac{1}{2} \cdot \left(q(t) + p(t) * z^{-1}(t) \right) \tag{4.18}$$

However, the Laplace transform of $z^{-1}(t)$ is quite difficult to deduce. Therefore the accurate value of progressive wave flow is not obtained from equation (4.18) in this thesis.

A simpler algorithm, in which the flow is assumed frictionless, is usually applied to calculate the progressive flow wave as described in the following part. In equation (4.17) let R, which is the friction term, equal to zero. Equation (4.18) can be written in a more efficient form:

$$f(t) = \frac{1}{2} \cdot \left(q(t) + \frac{p(t)}{z} \right) \tag{4.19}$$

where $z = \frac{\rho \cdot c}{A}$.

Related to this application, the progressive flow can be written as:

$$q(t)'_{progressive} = \frac{1}{2} \cdot \left(q(t)_{\det ect} + \frac{p(t)_{\det ect}}{z} \right) \tag{4.20}$$

$p(t)_{\det ect}$ and $q(t)_{\det ect}$ are the pressure and flow at detecting point at time t.

Comparing equation (4.9) and (4.14) times pipe area, only the steady state friction term R_f is included by Kojima's method. In Figure 4.3 the flows at the detecting point are compared using the method of characteristics (MOC) and Kojima's method simulated in the model described in section 4.1. From this result although the frequency dependent friction term is not involved in Kojima's method, the detecting point flows from these two algorithms are nearly the same. Kojima's method can be realized on a real system in real-time using pressure transducers; however, this method is a kind of recursion algorithm depending on the previous values. In a real-time experiment the initial value is usually unknown; hence a convergence process to steady value occurs at the first stage as can be seen from Figure 4.3.

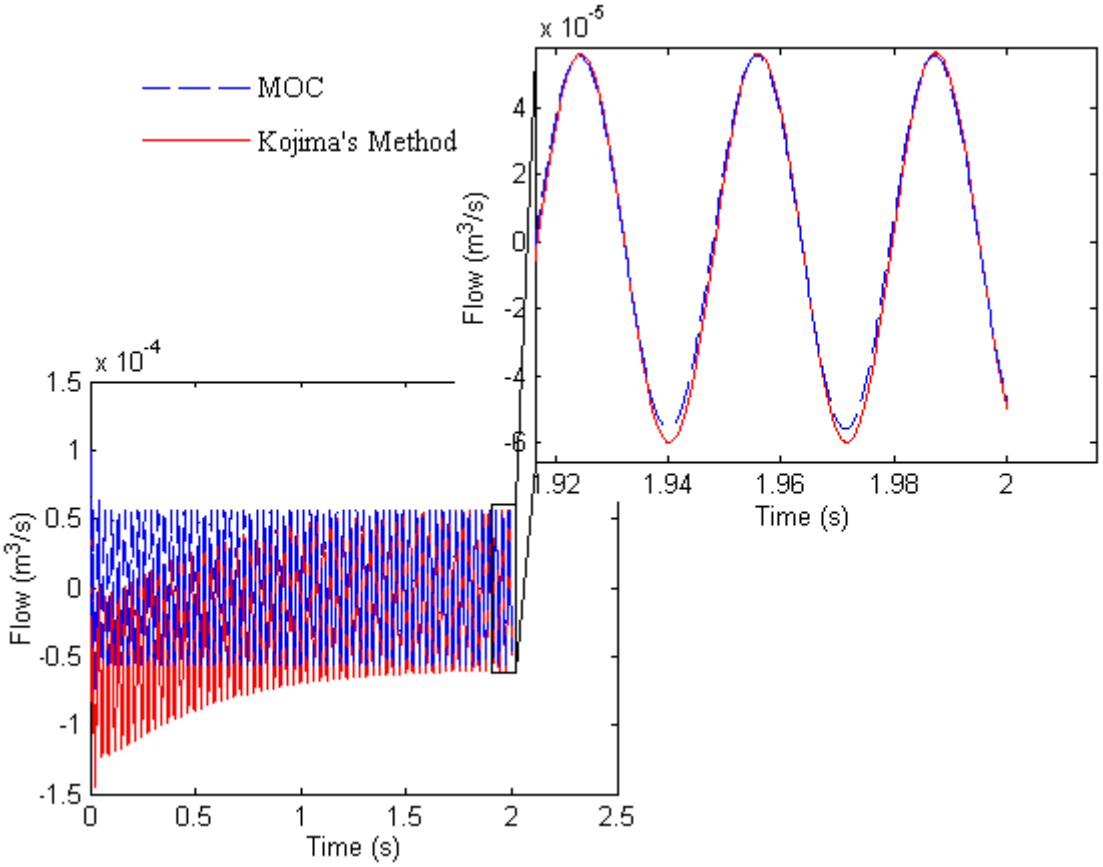

Figure 4.3 Comparison of flow at the detecting point using MOC and Kojima's method

For the flow of progressive wave at the detecting point, equations (4.15) times pipe area and (4.19) can be applied. As for both equations the friction term is ignored a comparable result can be obtained in Figure 4.4, which is similar to that in Figure 4.3. In Kojima's method the pressure used in the progressive wave is an average value from

the nearby two points and for the theoretical method this pressure is the value at the detecting point. Comparing Figure 4.3 and 4.4, this factor has little effect on the accuracy.

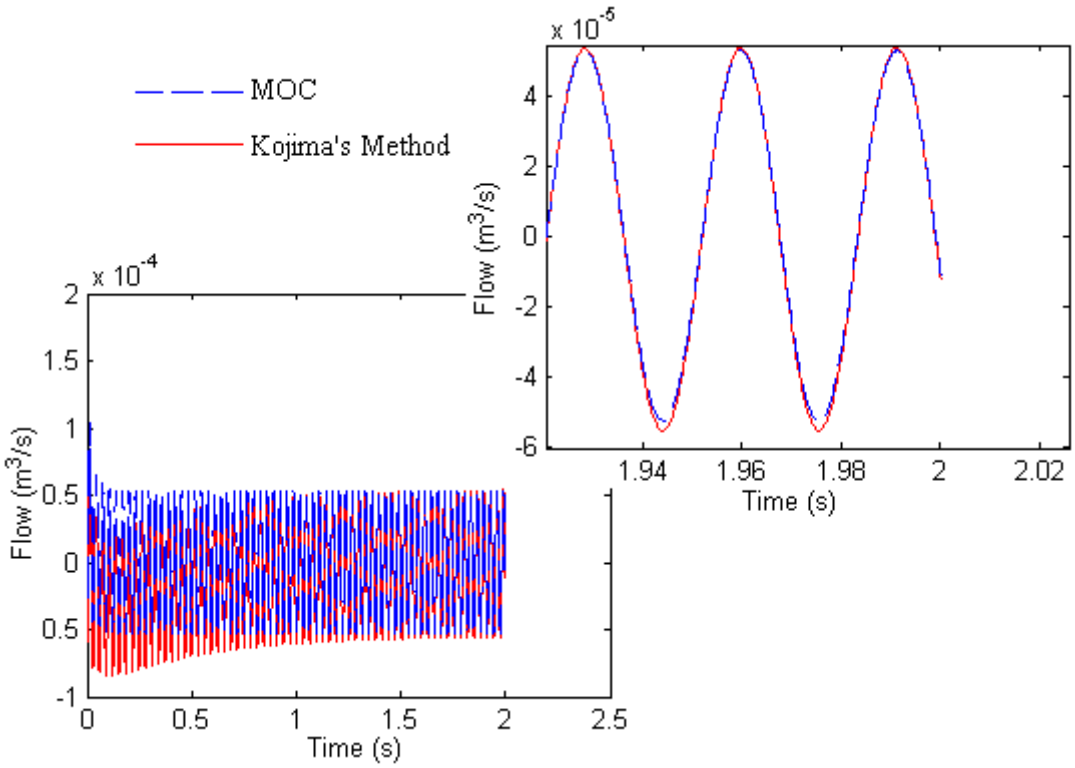

Figure 4.4 Comparison of progressive wave flow at detecting point using MOC and Kojima's method

According to Kojima's technique, Figure 4.5 represents the basic process for adding the control flow using the MOC to realize the modelling of the active control of fluid-borne noise. The vertical axis is the discrete time points and the interval $\Delta t = \Delta x / c$. The horizontal axis represents the pipe, the distance on it depends on the variable of elements selected and the total length when modelling the pipe. In this figure the pipe is divided into four elements.

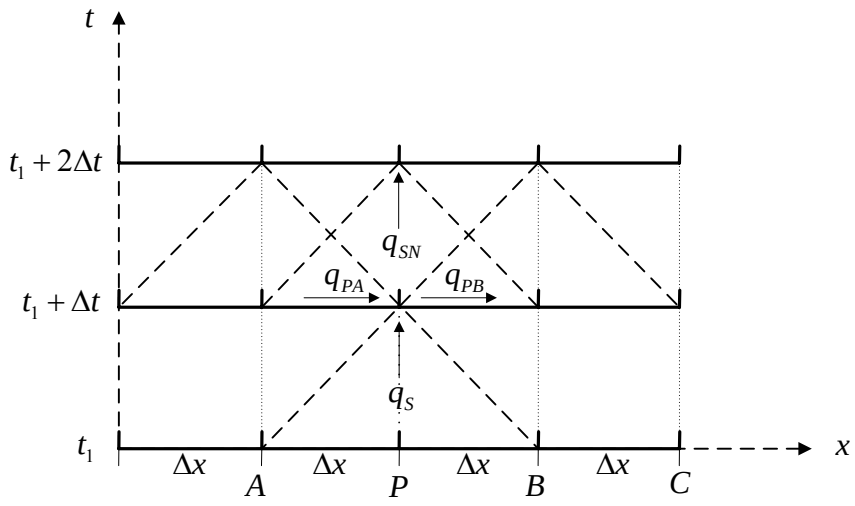

Figure 4.5 Numerical structure model of the fluid filled pipe

In Figure 4.5 as a control q_S is added into the pipe at time $t_1 + \Delta t$, the flow at point *P* to the left of the control flow can be represented using q_{PA} at this time and the flow to the right of the control flow can be described using q_{PB}. Hence an equation can be written as (Note in the following equation upper subscripts denote the time and lower subscript denote points along the pipe.):

$$q_{PA}^{t_1+\Delta t} - q_S^{t_1+\Delta t} = q_{PB}^{t_1+\Delta t} \tag{4.21}$$

When $\frac{dx}{dt} = +c$ similar with (4.7), equation (4.5) can be approximated as:

$$q_{PA}^{t_1+\Delta t} - q_A^{t_1} + \frac{A}{\rho \cdot c} \cdot (p_P^{t_1+\Delta t} - p_A^{t_1}) + \Delta t \cdot f_A^{t_1} = 0 \tag{4.22}$$

and when $\frac{dx}{dt} = -c$ similar with (4.8), equation (4.6) can be approximated as:

$$q_{PB}^{t_1+\Delta t} - q_B^{t_1} - \frac{A}{\rho \cdot c} \cdot (p_P^{t_1+\Delta t} - p_B^{t_1}) + \Delta t \cdot f_B^{t_1} = 0 \tag{4.23}$$

Combining (4.22) and (4.23), the flow and the pressure at point P at time $t_1 + \Delta t$ can be represented as:

$$q_{PA}^{t_1+\Delta t} = \frac{1}{2}\cdot\left[q_A^{t_1} + q_B^{t_1} + q_S^{t_1+\Delta t} - \frac{A}{\rho\cdot c}\cdot\left(p_B^{t_1} - p_A^{t_1}\right) - \Delta t\cdot(f_A^{t_1} + f_B^{t_1})\right] \tag{4.24}$$

$$p_P^{t_1+\Delta t} = \frac{1}{2}\cdot\left[\left(q_A^{t_1} - q_S^{t_1} - q_B^{t_1+\Delta t}\right)\cdot\frac{\rho\cdot c}{A} + p_A^{t_1} + p_B^{t_1} + \frac{\rho\cdot c}{A}\cdot\Delta t\cdot(f_B^{t_1} - f_A^{t_1})\right] \tag{4.25}$$

Then $q_{PA}^{t_1+\Delta t}$ and $p_P^{t_1+\Delta t}$ are stored and used as the previous values when applying the MOC. In the same way, the flow and the pressure at point P at time $t_1 + 2\Delta t$ can be represented:

$$q_{PA}^{t_1+2\Delta t} = \frac{1}{2}\cdot\left[q_A^{t_1+\Delta t} + q_B^{t_1+\Delta t} + q_S^{t_1+2\Delta t} - \frac{A}{\rho\cdot c}\cdot\left(p_B^{t_1+\Delta t} - p_A^{t_1+\Delta t}\right) - \Delta t\cdot(f_A^{t_1+\Delta t} + f_B^{t_1+\Delta t})\right] \tag{4.26}$$

$$p_P^{t_1+2\Delta t} = \frac{1}{2}\cdot\left[\begin{array}{l}\left(q_A^{t_1+\Delta t} - q_S^{t_1+2\Delta t} - q_B^{t_1+\Delta t}\right)\cdot\frac{\rho\cdot c}{A} + p_A^{t_1+\Delta t} + p_B^{t_1+\Delta t} \\ + \frac{\rho\cdot c}{A}\cdot\Delta t\cdot(f_B^{t_1+\Delta t} - f_A^{t_1+\Delta t})\end{array}\right] \tag{4.27}$$

The control flow not only influences the flow status at point P but also affects that at point B. Because q_{PA} is stored as the old value, so (4.21) is applied here. The flow and pressure at point B at time $t_1 + 2\Delta t$ are:

$$q_B^{t_1+2\Delta t} = \frac{1}{2}\cdot\left[q_{PA}^{t_1+\Delta t} - q_S^{t_1+\Delta t} + q_C^{t_1+\Delta t} - \frac{A}{\rho\cdot c}\cdot\left(p_C^{t_1+\Delta t} - p_P^{t_1+\Delta t}\right) - \Delta t\cdot(f_A^{t_1+\Delta t} + f_B^{t_1+\Delta t})\right] \tag{4.28}$$

$$p_B^{t_1+2\Delta t} = \frac{1}{2}\cdot\left[\begin{array}{l}\left(q_{Pa}^{t_1+\Delta t} - q_S^{t_1+\Delta t} - q_C^{t_1+\Delta t}\right)\cdot\frac{\rho\cdot c}{A} + p_C^{t_1+\Delta t} + p_P^{t_1+\Delta t} \\ + \frac{\rho\cdot c}{A}\cdot\Delta t\cdot(f_B^{t_1+\Delta t} - f_A^{t_1+\Delta t})\end{array}\right] \tag{4.29}$$

4.3 Stability of Kojima's method

As the hydraulic system model for fluid-borne noise is built up Kojima's method can be evaluated from this section. Firstly, the pipe in the model is divided into 20 elements and an ideal actuator, which has unit gain and no phase shift for all frequency components, is applied. The control flow signal is obtained from the 3rd point by using point 2 and 4 pressure values, and then is injected back to the pipe at the 13th point. The frequency of noise ripple is 200 rad/s, $k_P = 0.1$ and the time step is 0.00017 s. The

fluid-borne noise downstream after point 13 should be cancelled according to equation (4.15). Firstly, theoretical control flow, which is represented using equation (4.20), is used as control flow. This algorithm can work to get the cancellation result upstream (point 12) and downstream (point 14) in Figure 4.6. It appears very helpful for cancelling the pulsation downstream when switching on the actuator at 1 second. However, the flow at the control point (13^{th}) increases. This is because in equations (4.24) and (4.26) the control flow is added to the control point, but in (4.28) it is subtracted for the downstream ones in the same direction.

Secondly control flow using Kojima's method in equation (4.16) is applied for cancellation and the parameters and control process are the same as those using theoretical control flow. However, the flow and pressure downstream increase and tend to be unstable using Kojima's method in the model. The pressure result at the 14^{th} point is plotted in Figure 4.7.

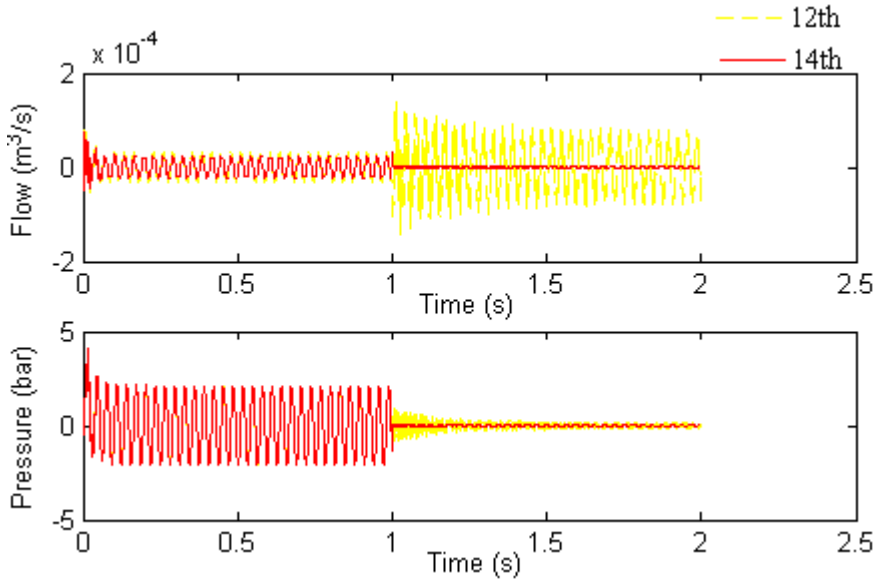

Figure 4.6 Cancellation results using theoretical method of progressive wave upstream and downstream in the pipe

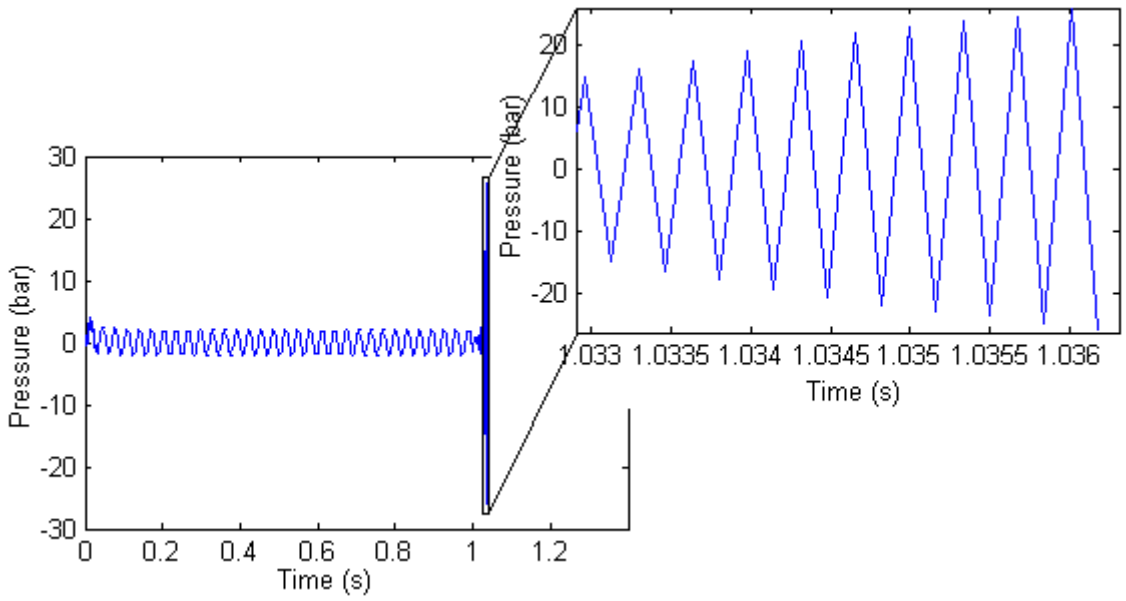

Figure 4.7 Unstable pressure cancellation result obtained using Kojima's method at 14th point

In Figure 4.7 from 0 to 1 s there is only pressure ripple, which is 200 rad/s without cancellation, and then when injecting the control flow the system goes unstable. The main reason of this instability may be overshoot caused by the approximation of the pressure gradient at the detecting point as shown in equation (4.12). During simulation the data is processed every time step, hence from the zoomed figure in Figure 4.7 the frequency of the unstable signal is equal to half of the sampling frequency.

4.4 Low pass filter to improve stability

In order to avoid the high frequency instability in Kojima's method, a zero phase shift low pass FIR filter is applied after the flow of progressive wave in the model to realize the cancellation. This simple filter is of the 'symmetrical triangular form', which is plotted in Figure 4.8.

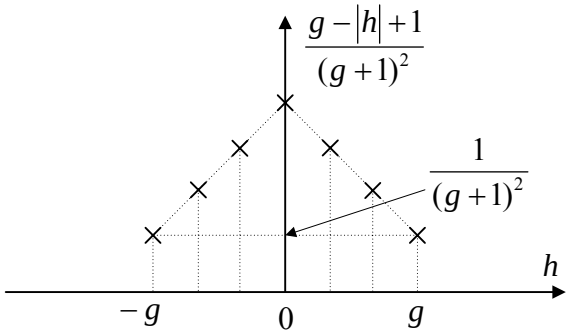

Figure 4.8 Structure of zero phase shift FIR filter

The control flow after this filter can be described using the equation below:

$$q_{control}(t) = \sum_{h=-g}^{g} \frac{q_{progressive}[t + \Delta t \cdot h] \cdot (g - |h| + 1)}{(g+1)^2} \tag{4.30}$$

It is important to notice that this filter itself is zero phase shift, however the future value cannot be used because of causality. Therefore a delay unit should be added on this filter to make the system causal. To realize it (4.30) can be written as:

$$q_{control}(t) = \sum_{h=-g}^{g} \frac{q_{progressive}[t - a \cdot \Delta t + \Delta t \cdot h] \cdot (g - |h| + 1)}{(g+1)^2} \tag{4.31}$$

where a is the number of delay samples from the detecting point to the control point using Kojima's method. For causality, $g \le a$ should be satisfied.

With this filter in the model the cancellation can be implemented by Kojima's method and the results are plotted in Figure 4.9. Note that the '12th' represents a point upstream of the cancellation device, and '14th' is a point downstream.

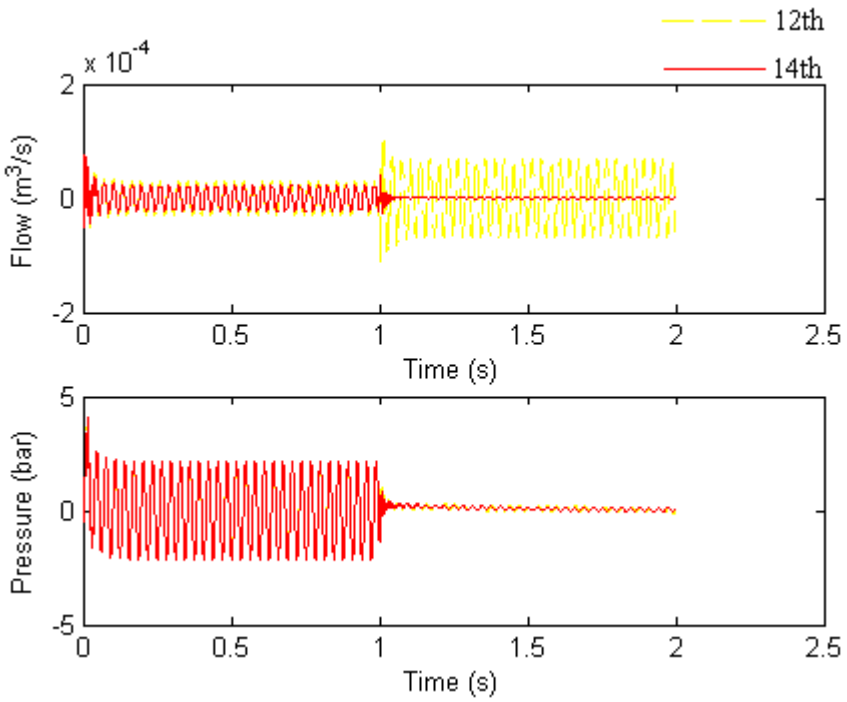

Figure 4.9 Cancellation results using theoretical method of progressive wave upstream and downstream with low pass filter

In this simulation the wave is still 200 rad/s at a certain power level, $k_p = 0.1$, and g is equal to 8 for the low pass filter. A good cancellation result is obtained in this stage and only a little fluid-borne noise left downstream after the control point for both flow and pressure. It seems that this kind of low pass filter can give a satisfactory modification for Kojima's method in simulation.

4.5 Effect of frequency

From the analysis in section 4.2, Kojima's method is a feasible but an inaccurate algorithm in real-time and the instability may not only come from Kojima's method but also from the hydraulic system model used in simulation. In this section effects coming from the hydraulic system model are investigated.

In Figure 4.10, the flow responses with the same modelling conditions used in section 4.4 but different frequencies are plotted, and the sampling rate is 0.00017 s.

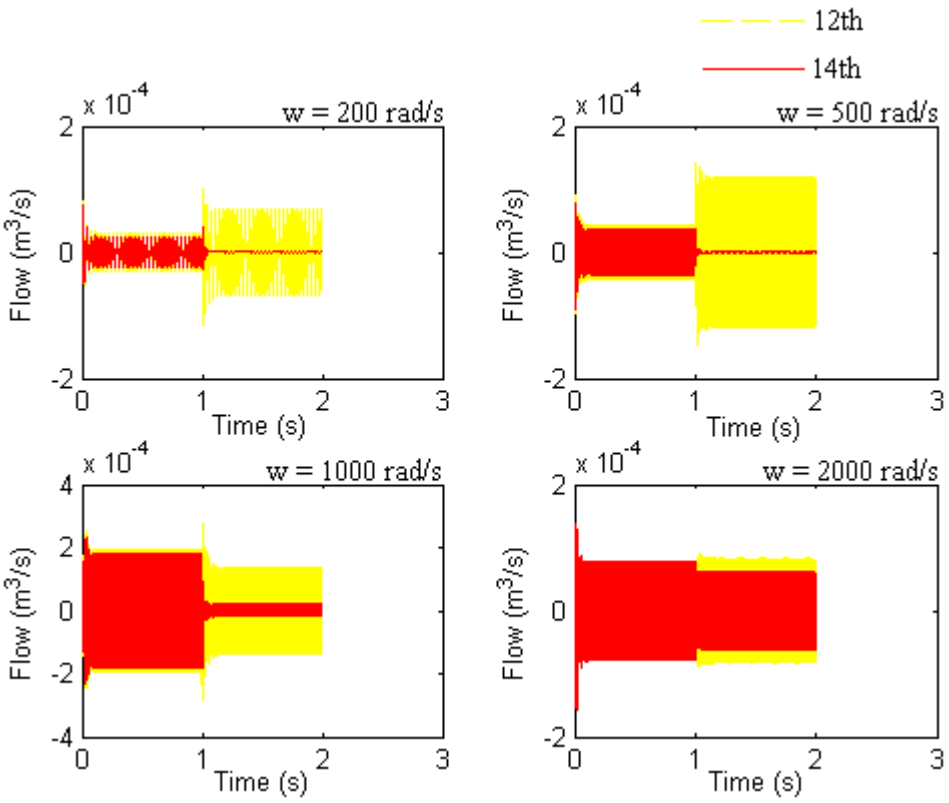

Figure 4.10 Comparison of flow cancellation results from different points on pipe with frequency at ω = 200, 500, 1000 and 2000 rad/s

From the results, the effect of this method becomes smaller along with the increasing frequency as the inaccurate control flow is obtained. The essential reason for this is that the low pass filter applied in Kojima's method reduces the amplitude of the cancellation signal. In order to solve this problem, the fluid pipe is divided into more elements (40 and 80) to achieve better results. Figure 4.11 plots the flow responses with different elements (20, 40 and 80, and sampling rates are 0.00017 s, 0.000085 s and 0.000043 s) with the same simulation condition in Figure 4.10. The input ripple frequency is 2000 rad/s.

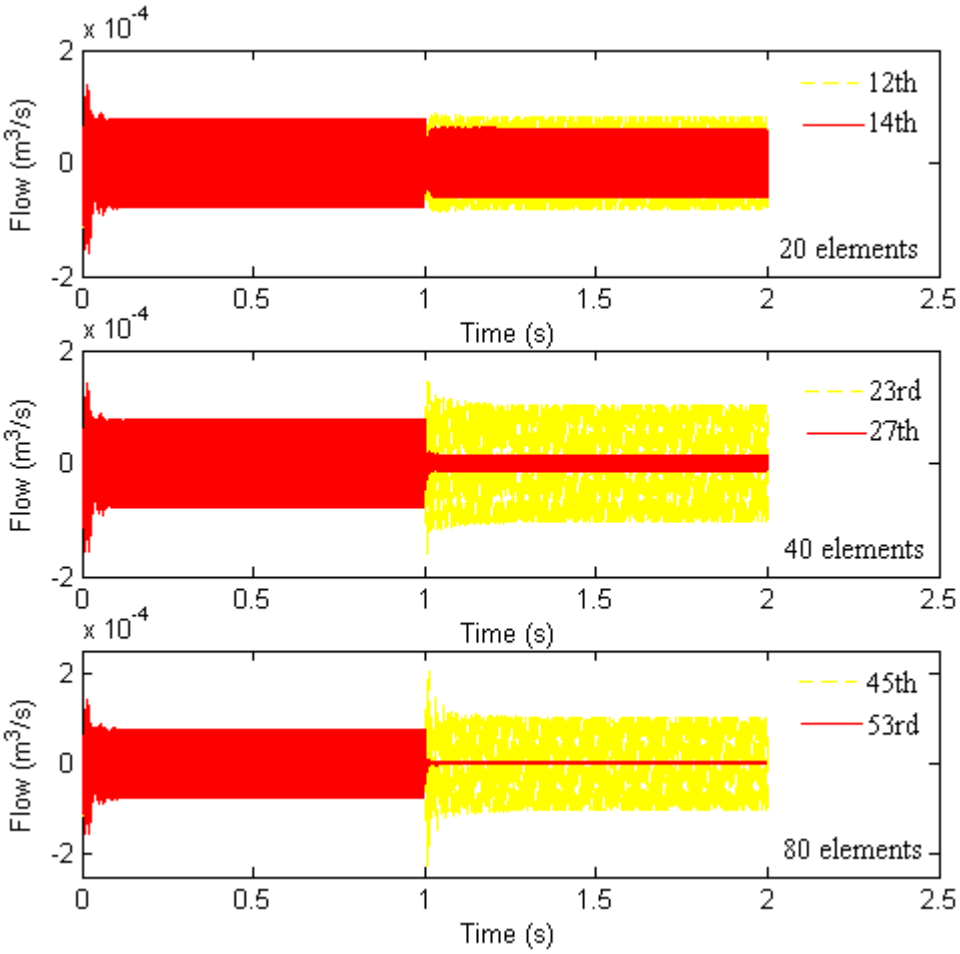

Figure 4.11 Comparison of flow cancellation results from different points on pipe with 20, 40 and 80 elements at 2000 rad/s

A more accurate control flow can be obtained when increasing the number of elements in the pipe. It means that if other conditions are the same, sampling frequency is increased while increasing element numbers and more accurate values can be used by the low pass filter. However, the more elements pipe model needs a long time to run, which is not efficient in the simulation. It can be seen that for this modelling method a compromise should be considered between computation burden and accuracy.

4.6 Effect of actuator dynamics

In the previous sections Kojima's method is evaluated and simulated; however, the control progressive wave flow is directly injected into the control point perfectly without any contribution of actuator dynamics. In an enhanced model an actuator is excited by a control signal to generate anti-noise flow. The actuator is modelled as a

second or high order system. Figure 4.12 is the spectrum of a second order system with $\omega_n = 600$ rad/s and $\xi = 2$, which can be represented using the equation: $\frac{600^2}{s^2 + 2400 \cdot s + 600^2}$.

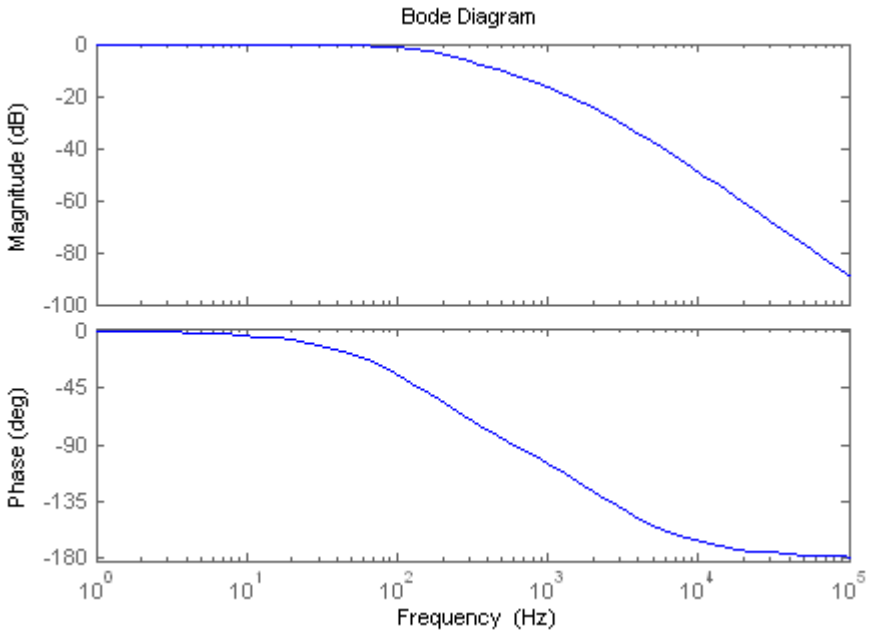

Figure 4.12 Unit step response and spectrum of actuator

Obviously this actuator may affect the amplitude and phase shift of control flow for different frequencies. In this section cancellation of 100 Hz fluid-borne noise using Kojima's method is simulated with this actuator. With the pipe model, the red line in Figure 4.13 is the output when the 100 Hz sine wave passing through this actuator compared with the output with an ideal actuator using blue line in this figure. Both amplitude and phase shift are changed under the effect of the modelled actuator. Hence, the system goes unstable. The flow cancellation results at the 14th point with modelled actuator and ideal actuator are plotted in Figure 4.14.

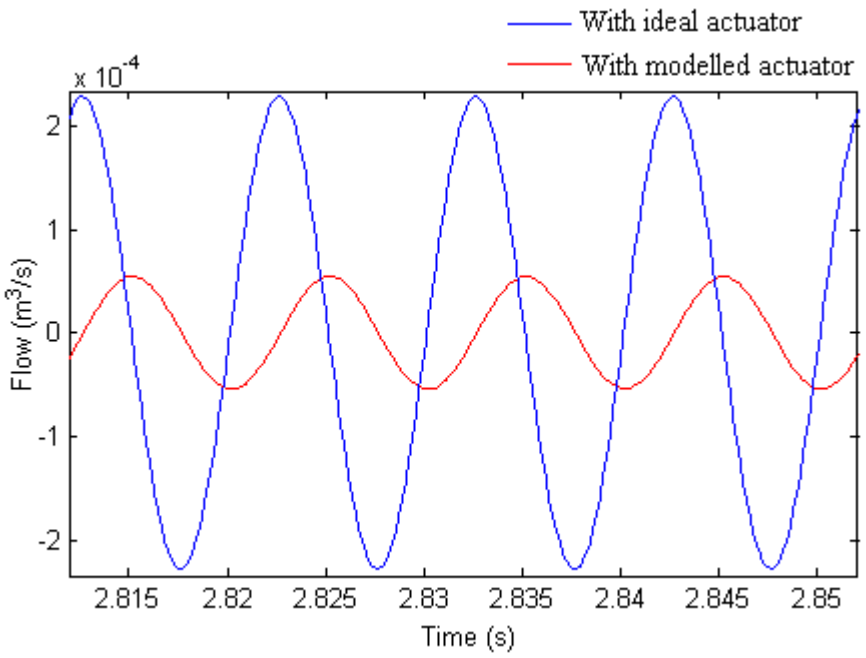

Figure 4.13 Effect of actuator

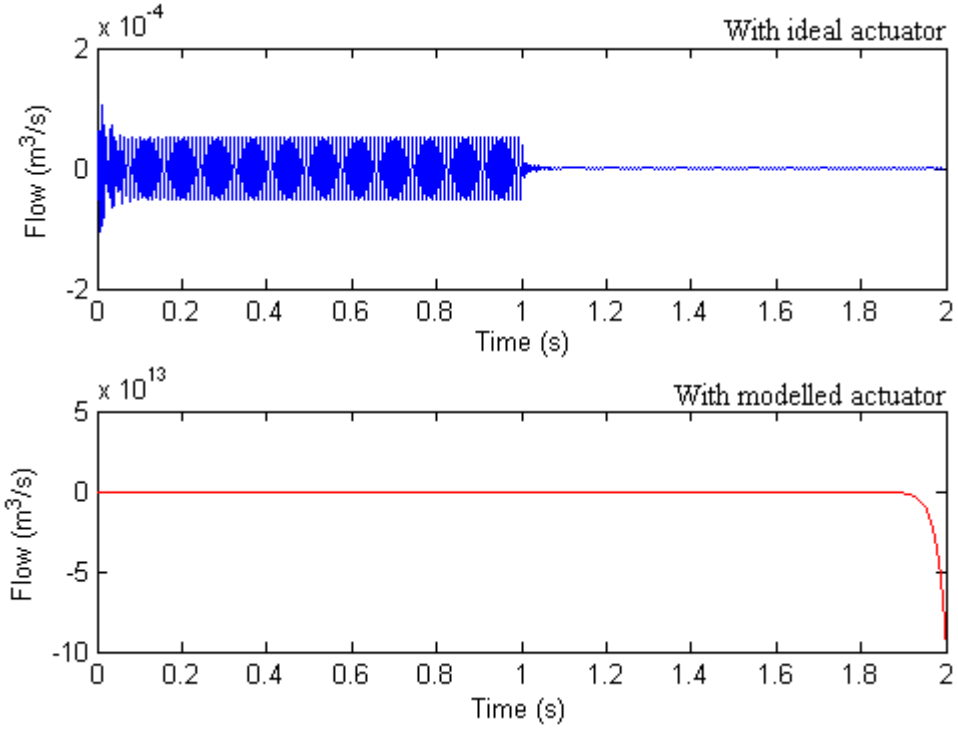

Figure 4.14 Comparison of flow cancellation results at 14th point with ideal actuator and with modelled actuator

In the real experiment a possible way to overcome this problem is by adding an inverse actuator filter in front of the real actuator to compensate for its effect. This proposed Kojima's method is shown in Figure 4.15.

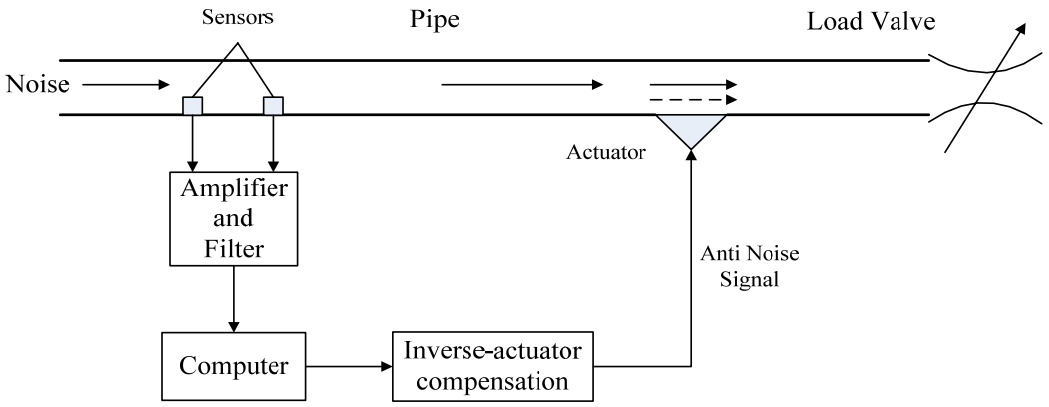

Figure 4.15 Proposed modification to Kojima's method

The compensation can be done by placing the inverse actuator in series with the actuator on the control signal route. In this work the inverse form of the actuator used for compensation is: $\frac{s^2 + 2400 \cdot s + 600^2}{600^2}$. To realize the compensation, the inverse form of actuator is transformed to its difference equation in discrete time. The compensation effect is plotted in Figure 4.16 compared with the signal without actuator.

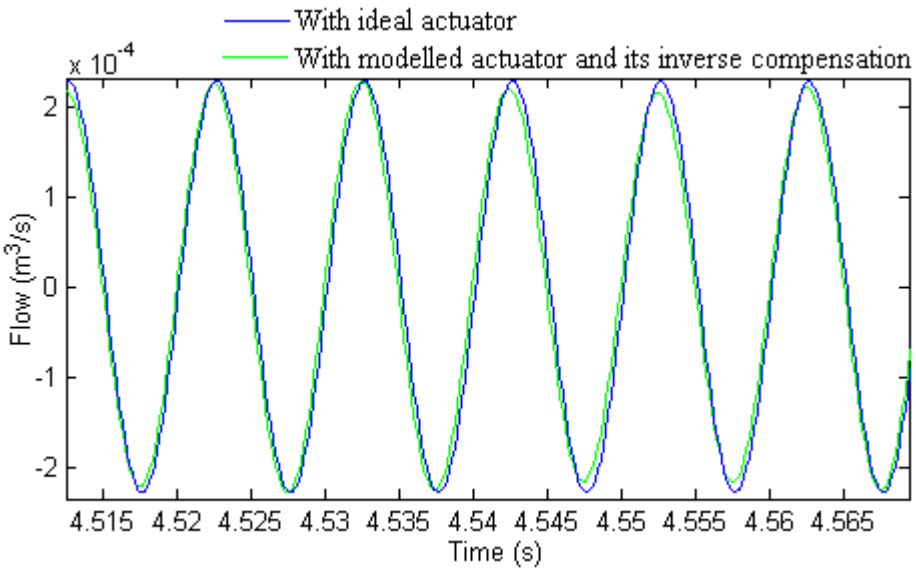

Figure 4.16 Effect of actuator with its compensation

As the compensation is realized using its difference equation, numerical error occurs on the control flow as plotted in Figure 4.16, and this numerical error also exists in the cancellation result as shown in Figure 4.17.

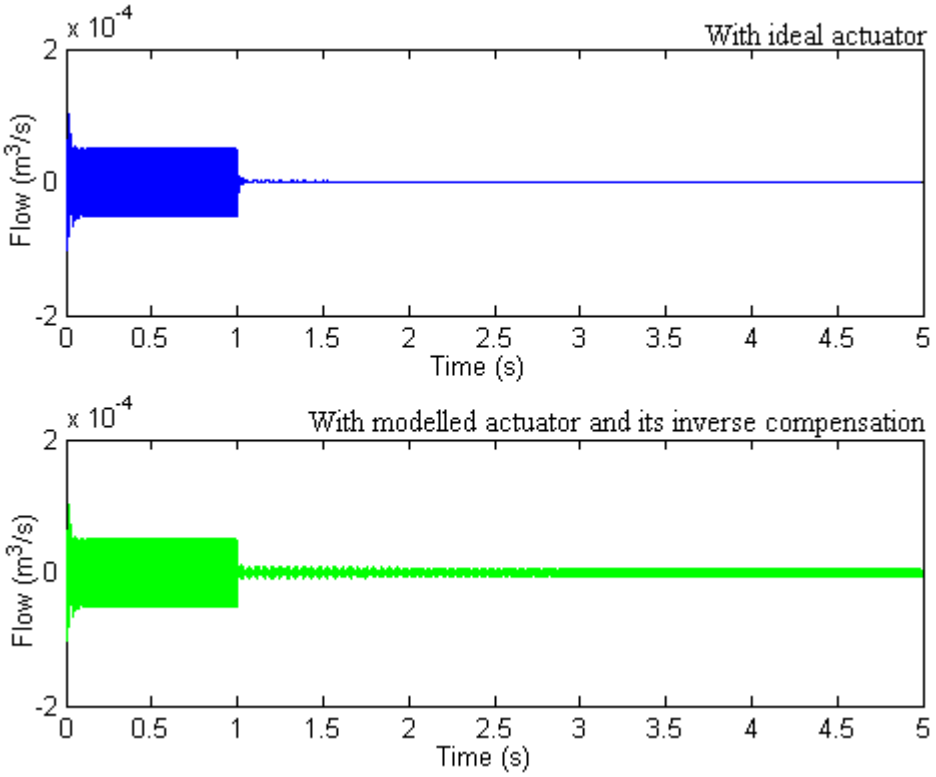

Figure 4.17 Comparison of flow cancellation results at 14th point with ideal actuator, and with the modelled actuator and its inverse compensation

It is necessary to note that in the control signal route, which includes actuator and its compensation, some unwanted delays named as D_c exist. In Kojima's method a number of delays, named as D_k, is also needed from the detecting point to the control point. Hence, the unwanted delay D_c should not be bigger than D_k to make the system stable.

4.3 Conclusions

To summarise, in this chapter a model of the simple hydraulic system which will be used for real-time experiment is built up applying the method of characteristics (MOC). This modelling method is a kind of finite element algorithm with very high accuracy.

From this model accurate dynamic characteristics of flow and pressure value at different points along the pipe can be obtained. In order to inject control flow into this hydraulic system, a development is made on the model still based on the MOC. Kojima's method, an active feedforward control algorithm of fluid-borne noise is described and evaluated. The inherent instability of Kojima's method comes from the estimated pressure gradient. To improve stability, a zero phase shift low pass filter is applied. Furthermore the hydraulic system model is also not accurate enough because of finite elements assumption, and more element number, which can give a high sampling frequency, can improve the simulation accuracy. Finally, in order to realize Kojima's method in real-time a proposed modification to Kojima's method is created. During simulation results it was found that the simple hydraulic system model with control flow, which is built up using MOC, is an efficient and accurate base to test and evaluate the active fluid-borne noise cancellation methods before doing real experiments.

CHAPTER 5

Development and Simulation of Off-line System Identification Algorithm

In real experiment the control signal supplied by the LMS adaptive filter is generated by an actuator, which can affect the control performance and even make the system unstable. The filtered reference LMS (FXLMS) algorithm can be used to solve this problem. In this chapter based on the two-weight adaptive notch filter for narrowband fluid-borne noise cancellation, the derivation of FXLMS algorithm is described. The off-line secondary path identification is applied with the FXLMS algorithm using the simple hydraulic system model. According to the particular dynamic characteristics of the secondary path, a delay unit used as secondary path compensation is proposed. Fluid-borne noise cancellation results are also obtained through simulation for both single frequency and multiple frequency cases. Additionally, the effect on the secondary path caused by the ripple reflection from the pipe end is also evaluated during simulation.

5.1 Filtered reference LMS adaptive filter

Applied in this project, the structure of narrowband fluid-borne noise cancellation process using the FXLMS adaptive filter in a hydraulic pipeline practically is shown in Figure 5.1. A/D and D/A converter, pressure sensors, anti-aliasing filter and actuator can be seen as the secondary path, which can affect the control performance. In the experiment variety of ripple reflection level can be obtained by turning a load valve at the pipe end. During simulation with the pipe model this effect can be represented using reflection coefficient k_P.

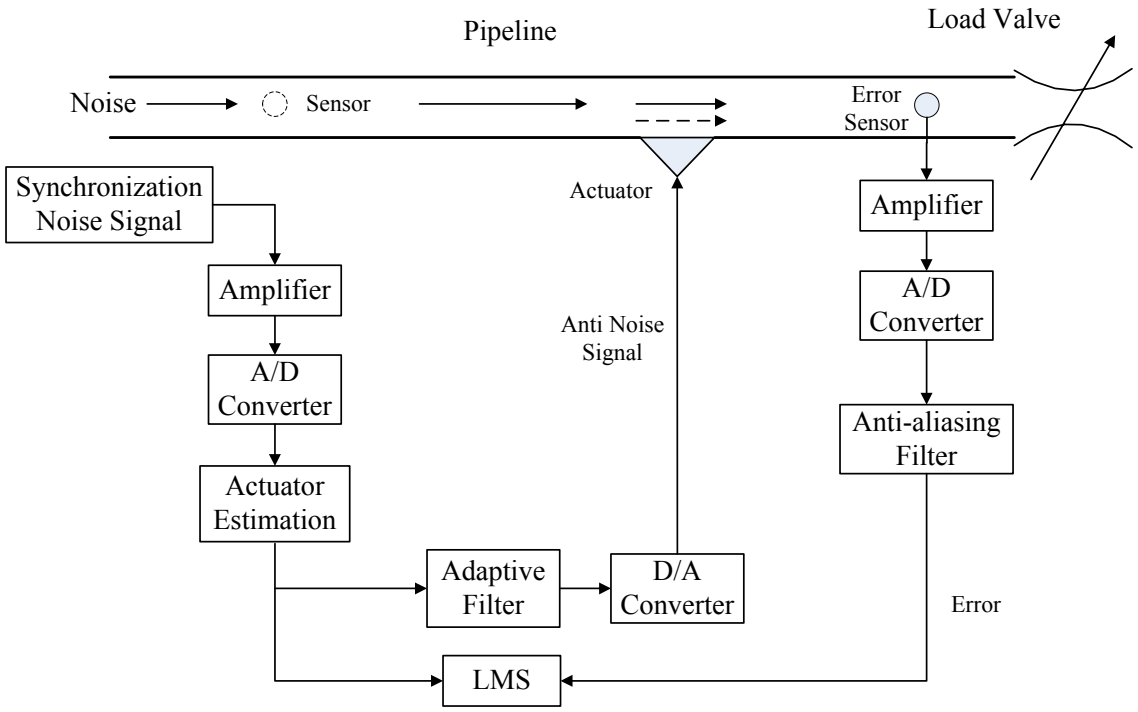

Figure 5.1 Practical structure of using narrowband FXLMS adaptive filter in a hydraulic pipeline

The FXLMS adaptive control process using a two-weight notch filter for single frequency narrowband fluid-borne noise cancellation is simply shown in Figure 5.2.

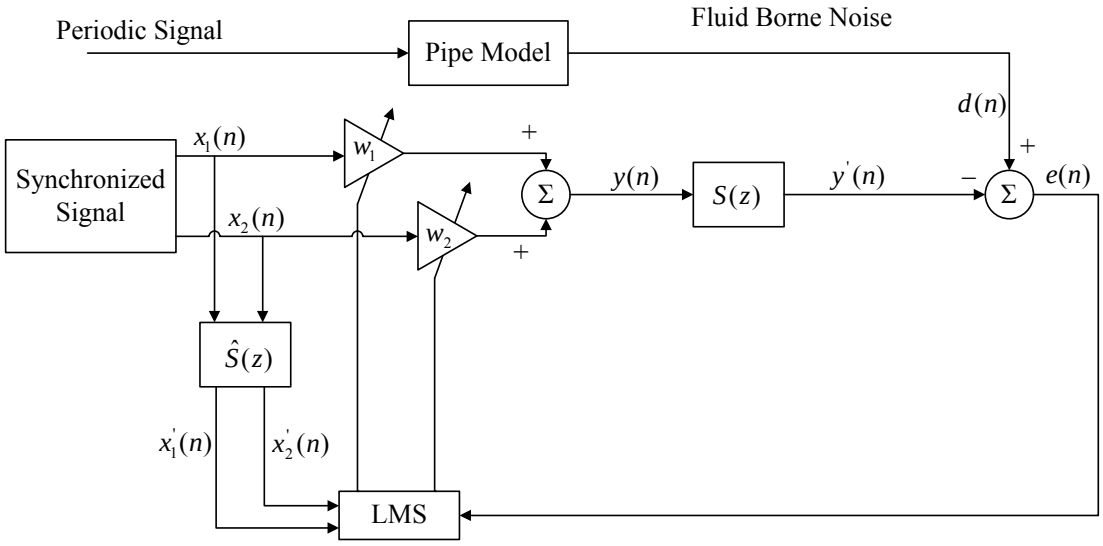

Figure 5.2 Control process of narrowband fluid-borne noise using FXLMS algorithm in the pipe model

By adding the secondary path and its estimation into the two-weight notch adaptive filter, the steady state transfer function in equation (3.28) can be written as:

$$H(z)=\frac{z^2-2\cdot z\cdot\cos\omega_0+1}{z^2-2\cdot\left(1-\frac{a}{2}\right)\cdot z\cdot\cos(\omega_0-\Delta\varphi)+(1-a\cdot\cos\Delta\varphi)} \tag{5.1}$$

where $a=\mu\cdot A^2\cdot A_S\cdot\hat{A}_S$, and $\Delta\varphi=\hat{\varphi}_S-\varphi_S$.

A_S, φ_S are the amplitude and phase shift of the secondary path transfer function; $\hat{A}_S$, $\hat{\varphi}_S$ are the amplitude and phase shift of estimated secondary path transfer function.

The derivation of equation (5.1) is described in Appendix 3. The same result is also presented in [12]. Therefore the radius of complex poles can be written as: $r_P=\sqrt{1-a\cdot\cos\Delta\varphi}$. As a is positive, hence to let the radius to be smaller than one in z domain the condition that $\cos\Delta\varphi>0$, which means $-90^\circ<\Delta\varphi<+90^\circ$, should be satisfied. According to this stable condition accurate compensation should be obtained.

The off-line method is used to determine the compensation function $\hat{S}(z)$. 'off-line' means the identification process is operated before the noise cancellation and before the primary noise starts. Relative to this the on-line method, which is discussed in Chapter 6, means the identification is operated at the same time as the noise cancellation process. As discussed earlier in this section the accuracy of this may not to be too critical on the stability criteria, only requiring the phase shift difference between secondary path and its estimation in the range of $\pm 90^\circ$.

Basically, the off-line compensation for secondary effect can be realized in two ways. Firstly, off-line delay unit compensation using a constant delay unit, which should be determined in advance, can be applied simultaneously with the noise cancellation process. Secondly, off-line impulse response compensation using a LMS adaptive filter to obtain the impulse response of secondary path prior to noise cancellation process and then this constant impulse response can be applied for compensation. In the following sections these two algorithms are presented during simulation work using a rig model.

5.2 Delay compensation of actuator algorithm

Usually the actuator used for fluid-borne noise cancellation has a high damping ratio. Figure 5.3 is the spectrum comparison between a second order transfer function and a suitable delay unit. The sampling frequency is 1000 Hz. The phase of the second order system can be seen to be similar to that of a simple delay over this frequency range. For the effect from the secondary path, only the phase is important for system stability.

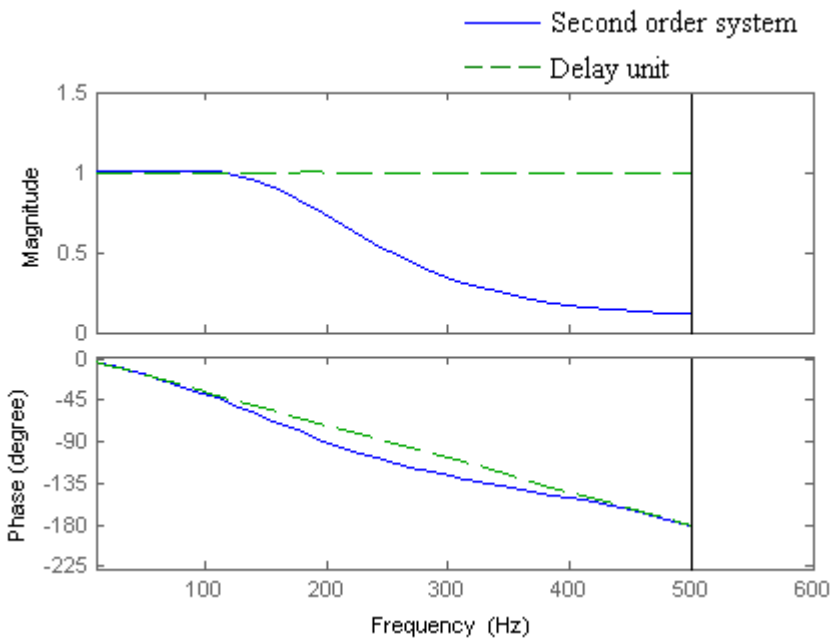

Figure 5.3 Spectrum comparison between a second order system and a suitable delay unit

Additionally, the A/D and D/A converters can also be seen as delay units. Therefore, the spectrum characteristic of the actuator can be tested using the spectrum analyzer and it can be determined whether this delay unit compensation algorithm can be used and how many delays are needed. In this part, assume that the actuator can be roughly seen as a delay unit.

5.2.1 Actuator dynamic characteristics

During simulation the 21-element pipe model is applied in this section and a diagram is shown in Figure 5.4. At point 1 fluid-borne noise is applied to the pipe, point 21 is the end of the pipe. The control flow is injected at point 3 and a pressure sensor is assumed

to be located at point 5 to measure the residual noise signal. As the flow in the pipe has progressive and regressive waves, two reflections from both ends should be considered.

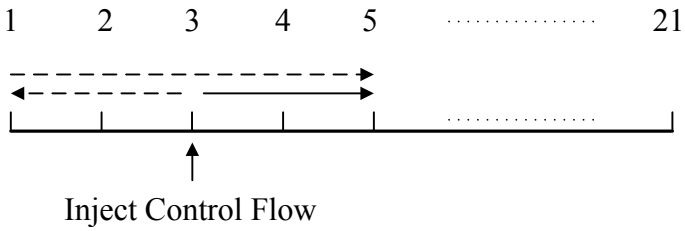

Figure 5.4 Demonstration plot of 21-element pipe model reflection effect with control flow

In order to obtain the compensation impulse response firstly assuming the control flow from the delay unit, which can be seen as the secondary path, is injected into the pipe near the left end. Here the actuator is modelled as 3 sample delay for simplicity and $k_P = 1$, which means no reflection from right end. Its impulse response comparison with and without the pipe is simulated and shown in Figure 5.5. The main parameters used in simulation for sections 5.2 and 5.3 are presented in Appendix 4.

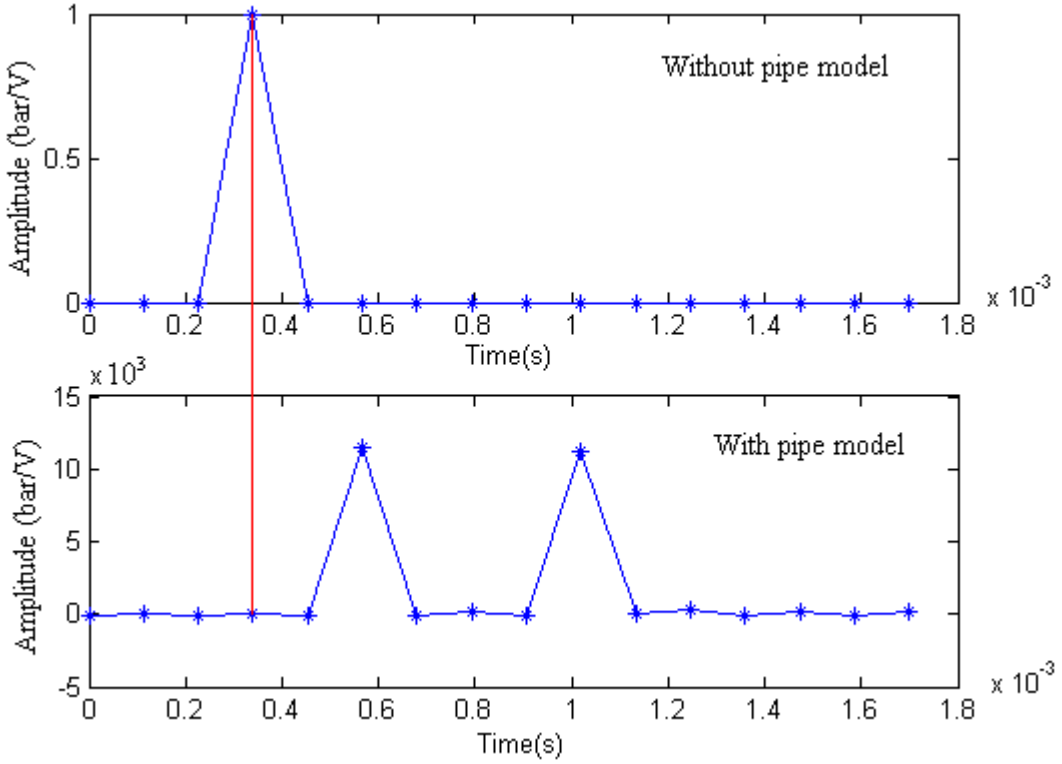

Figure 5.5 Comparison of 3-delay unit impulse response with and without pipe model

From the upper graph in Figure 5.5 three samples delay can be identified. 16 orders of weighting function, for example, is applied for a LMS adaptive filter with and excited using zero mean white noise. The secondary path impulse response with reflection effect from the pipe end is shown in the lower graph in Figure 5.5. As shown in Figure 5.4 the control flow injected at point 3 splits into two parts, which can be named as *R0* and *P0*. *P0* is picked up at point 5, and two sample delays occurred for this progressive wave. Moreover, as reflection from the left end the regressive wave *R1* can be reflected and goes back from left to right as *P0* picked up at point 5, which is plotted by the dashed line in Figure 5.4. Hence six sample delays occur for this flow. As there is no reflection from the right end, there are only two peaks here. Compared with the identification without the pipe model, a small fluctuation exits because of the dynamics effect from the hydraulic pipe, not only the phase shift. The error signals in identification processes with and without the pipe model are compared in Figure 5.6.

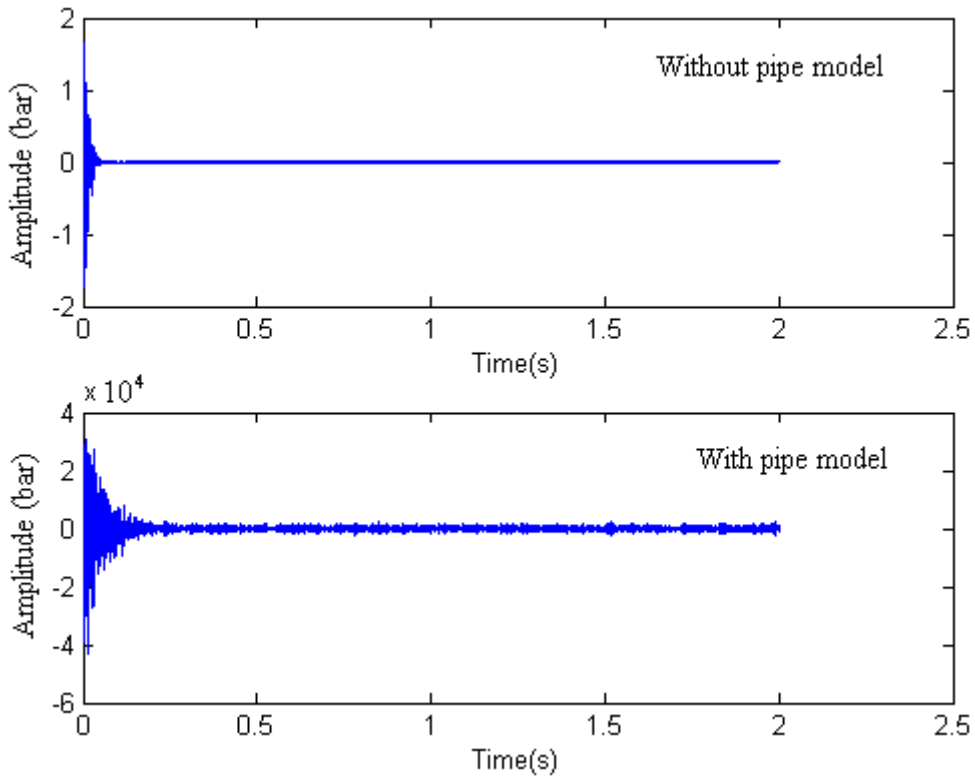

Figure 5.6 Comparison of 3-delay identification error with and without pipe model

From the above error results, more residual fluid-borne noise exists when implementing identification in the pipe model, which may be caused by other dynamic changes, not only the delays from the pipe. To overcome this problem a longer length of weighting

function can be used in the LMS adaptive filter. The compared results are shown in Figure 5.7.

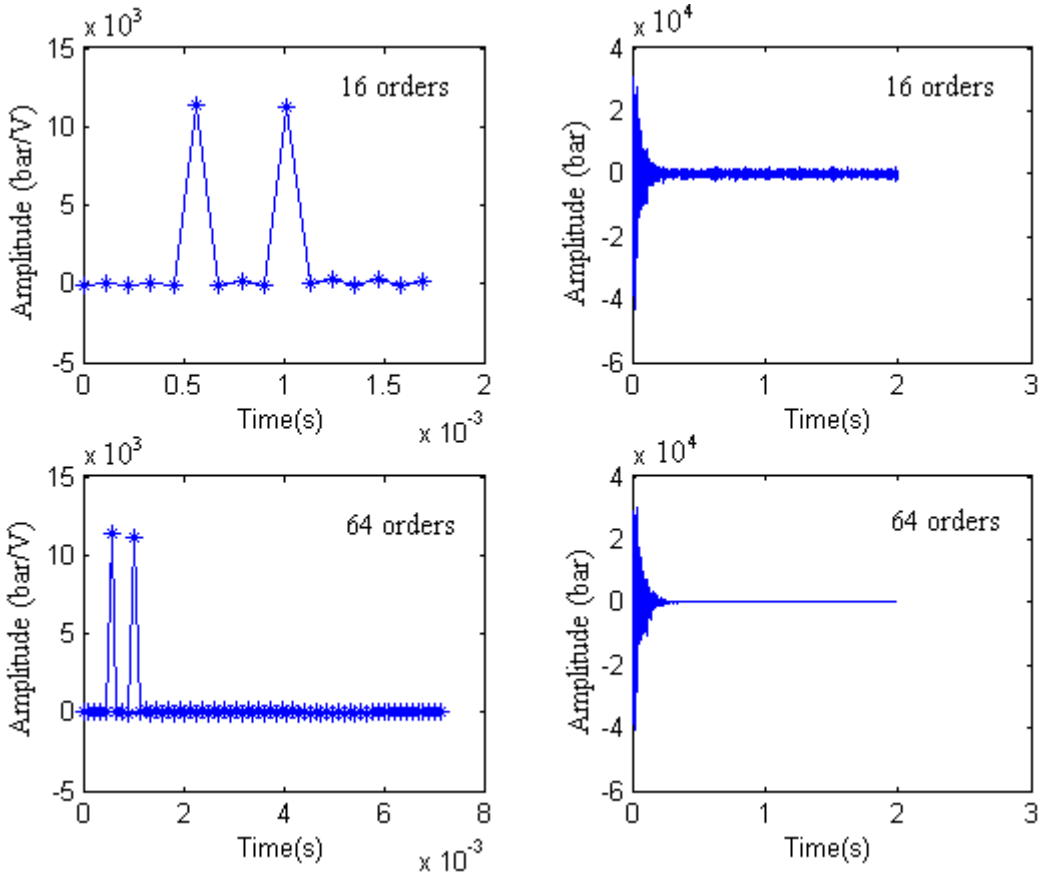

Figure 5.7 Identification impulse and error comparison using 16 orders and 64 orders weighting functions in LMS adaptive filter

In order to get good comparison results, the length of weighting function is selected as 64 samples. Under this identification nearly zero error result is obtained.

Considering the reflection effect from the right end of the pipe, now let $k_P = 0.5$. The progressive wave can be reflected from the right end and becomes a regressive wave back to point 5. However as $k_P > 0$, the power of this regressive part becomes smaller. As shown in the upper graph in Figure 5.8 the length of weighting function is still 64 orders. As mentioned above *P0* and *P1* are reflected to *R1* and *R2*, and then picked up at point 5 near the left end. After this *R1* and *R2* are reflected by the left end again, signed as *P2* and *P3*. Until here one cycle is finished and the whole process will cycle until the responded signal vanishes.

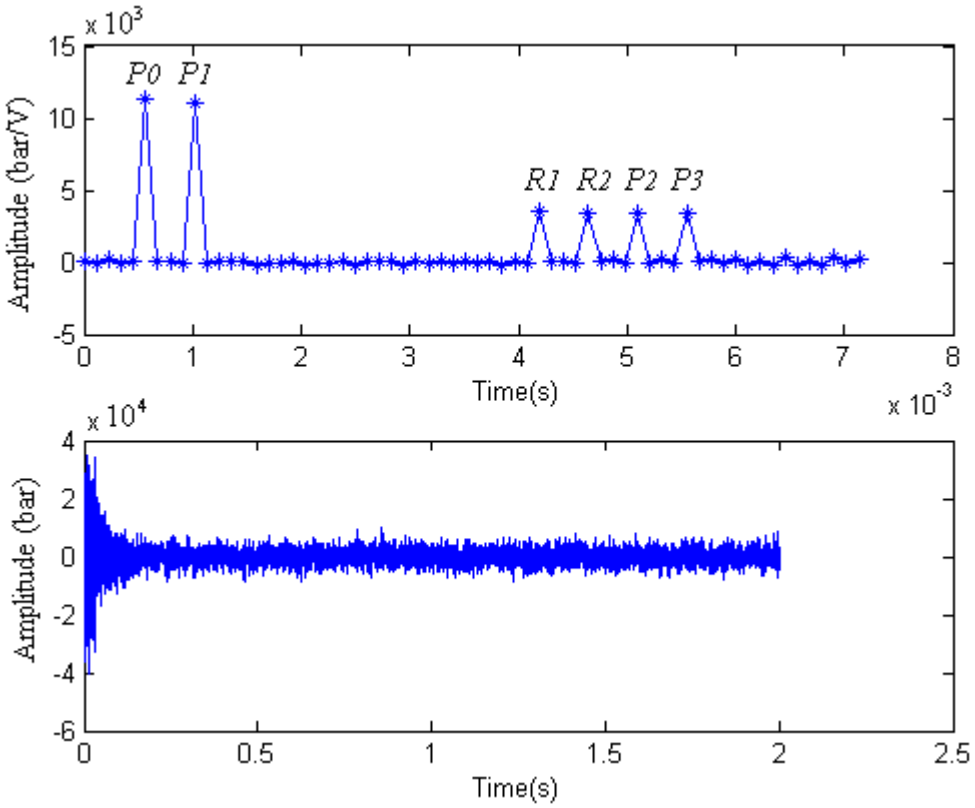

Figure 5.8 Identification impulse and error results using 64 orders weighting functions with $k_P = 0.5$ in LMS adaptive filter

The identification error result is plotted in the lower part of Figure 5.8. Because 64 orders of weighting function is not long enough to catch all the dynamic information of the secondary path response some residual error still exists.

5.2.2 Fluid-borne noise cancellation result using delay compensation

In this part, the fluid-borne noise cancellation process using FXLMS algorithm with delay unit compensation for single frequency input signal is discussed and results are presented during simulation. As mentioned above, the spectrum of the secondary path can be obtained firstly to see whether it can be seen as a delay unit before implementing fluid-borne noise cancellation. There are two ways that can be used. The first one is to deduce ratio between input signal to actuator and output signal from error sensor in frequency domain using Hanning windows, and the second one is to implement the Fourier Transform on the secondary path's identified impulse response. By researching the spectrum of the secondary path as shown in Figure 5.9 using these two methods the number of delays can be determined. In this figure the green line is the 7 samples delay

phase shift, and the frequency domain identification and impulse response identification are matched with each other.

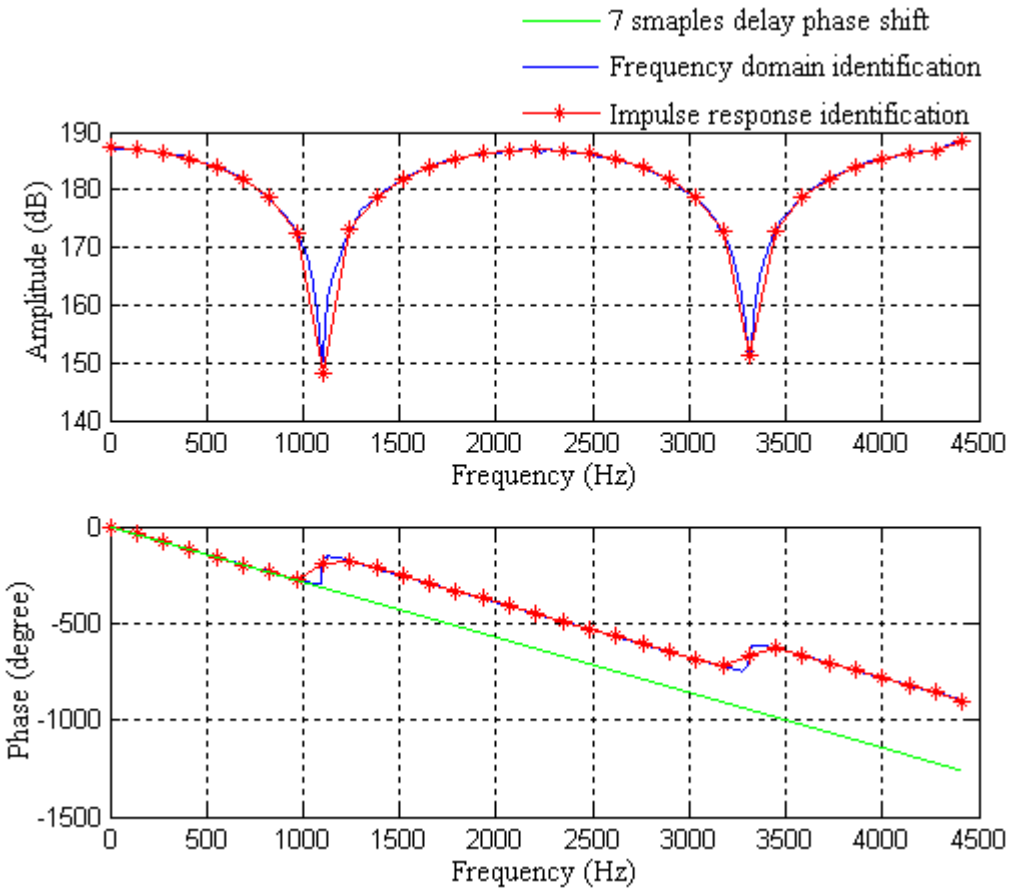

Figure 5.9 Spectrum of the secondary path using frequency domain identification and impulse response identification with $k_P = 1$

Then, this secondary path is directly applied in Figure 5.2 as $\hat{S}(z)$ rather than implementing the convolution using its impulse response. With the delay unit compensation the process of the FXLMS adaptive algorithm with the two-weight notch filter applied to cancel the fluid-borne noise as described in Figure 5.2 is simulated. The attenuation results with and without compensation of $\hat{S}(z)$ are compared in Figure 5.10 with the same simulation conditions.

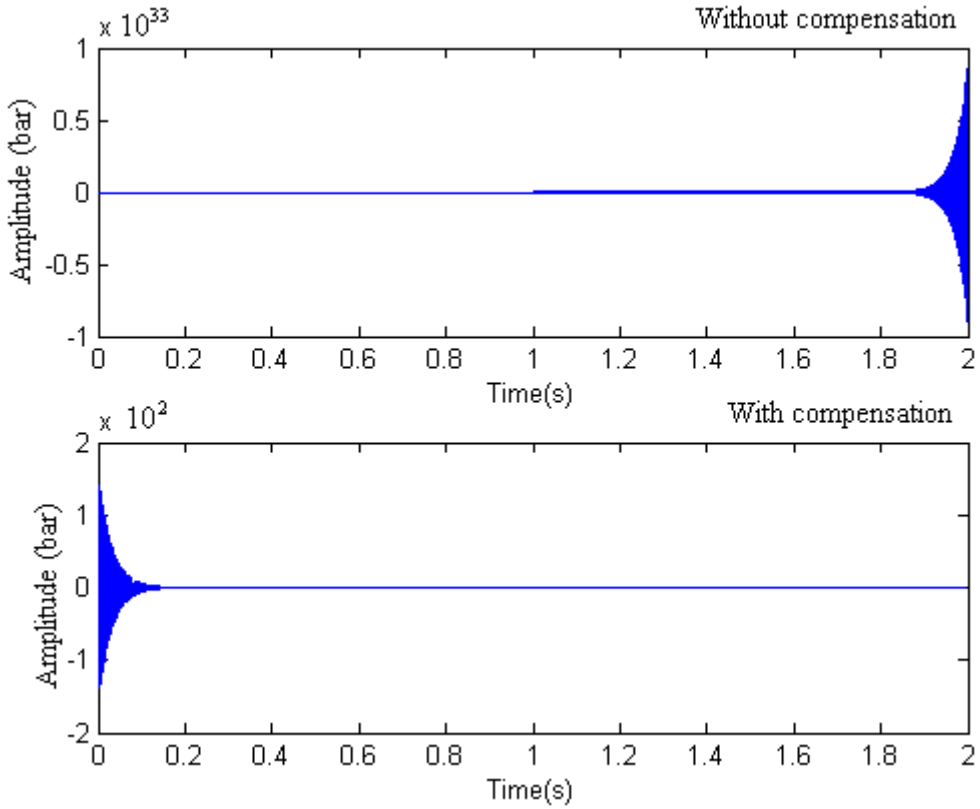

Figure 5.10 Comparison of fluid-borne noise cancellation results with and without delay unit compensation using 3-delay unit actuator in pipe model with $k_P = 1$

In this simulation, frequency of fluid-borne noise is 500 Hz and the actuator is a delay unit with three sample delays and $k_P = 1$. The good cancellation result is obtained in the lower section of Figure 5.10 using the algorithm discussed in this section. Additionally two weights changing with time are plotted in Figure 5.11. A steady solution of optimum weighting function vector $\overline{w}^* = \begin{bmatrix} w_1^* & w_2^* \end{bmatrix}$ is obtained after a short period of adaptive tracking process and the adaptive time depends on the convergence factor. Therefore a tradeoff between stability and fast adaptation should be considered in the real experiment.

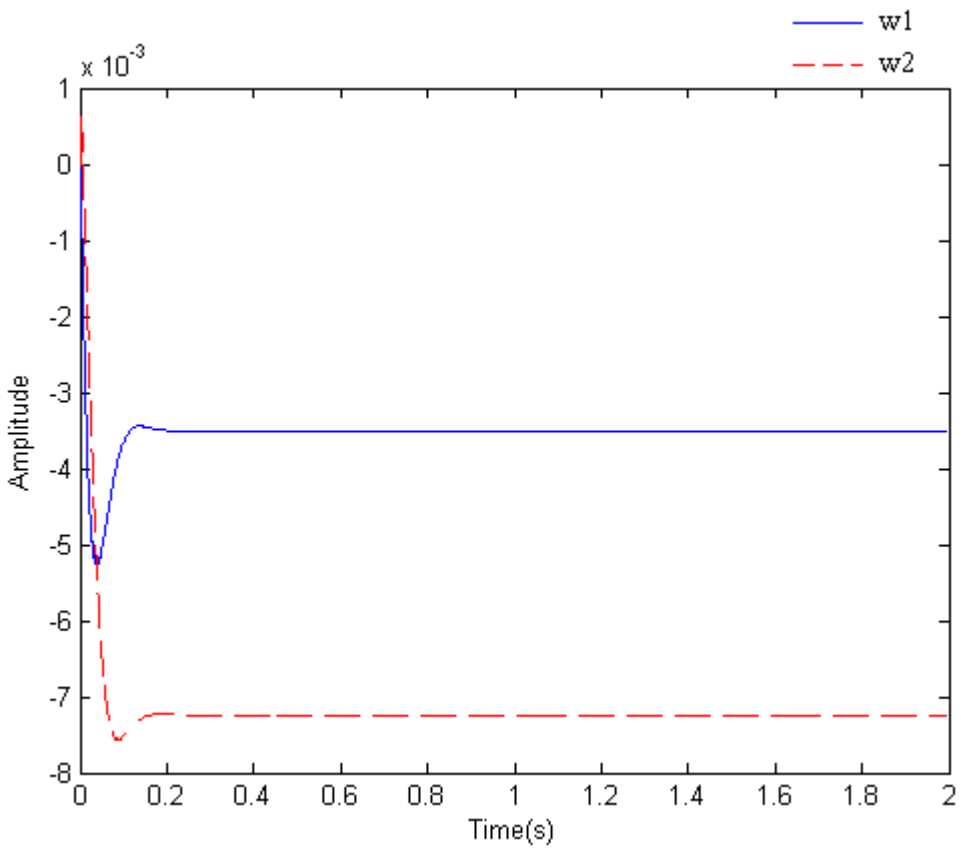

Figure 5.11 Plot of two weights changing with time using FXLMS adaptive filter with delay unit compensation

Now let $k_P = 0.5$, which means reflection from the right pipe end is considered. Under this condition the spectrum of the secondary path, including a 3-delay unit actuator is shown in Figure 5.12. As the slope for both the red and blue lines is not linear, the delay unit for different frequency input is not constant. Hence the system using the FXLMS adaptive filter may be unstable for some frequencies.

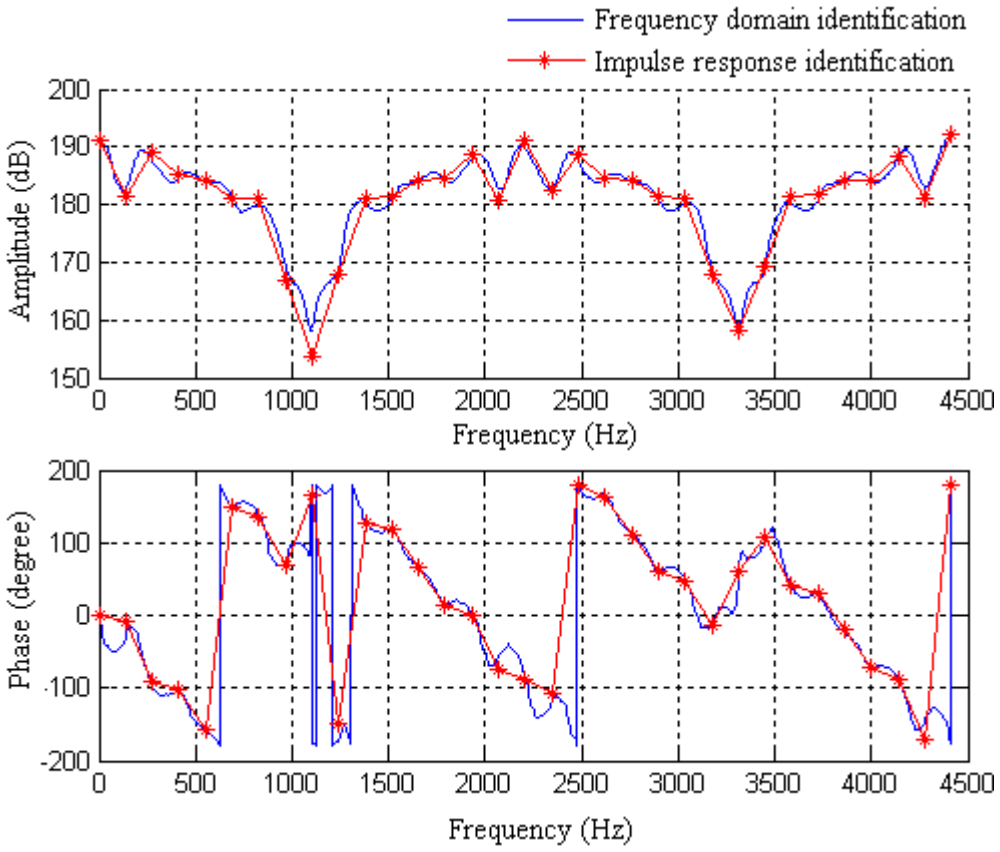

Figure 5.12 Spectrum of the secondary path using frequency domain identification and impulse response identification with $k_P = 0.5$

For multiple frequency fluid-borne noise, different noise controllers are applied in parallel to generate anti-noise for corresponding frequencies as shown in Figure 5.13. The summation of different anti-noise signals is given to the secondary path. Same with the single frequency noise cancellation, the 3-delay unit actuator is also applied. The cancellation result is shown in Figure 5.14 with fluid-borne noise at frequency 300 Hz, 600 Hz and 900 Hz.

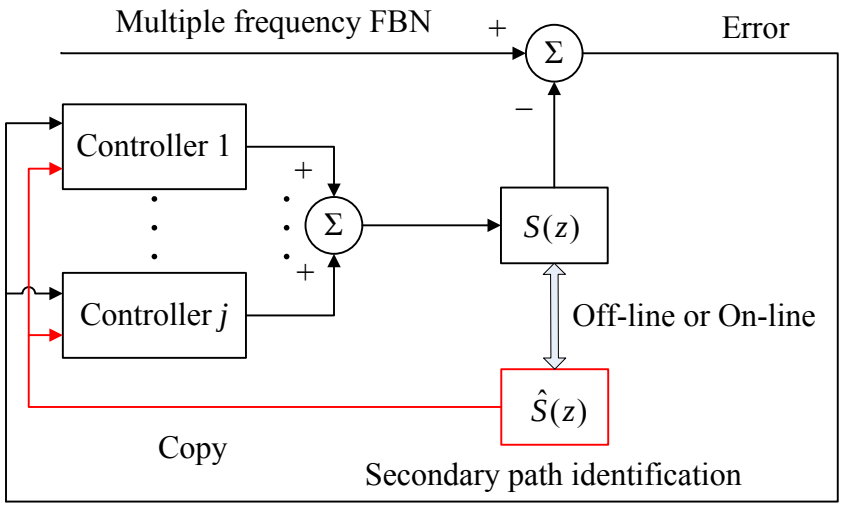

Figure 5.13 Simple structure of multiple frequency noise cancellation

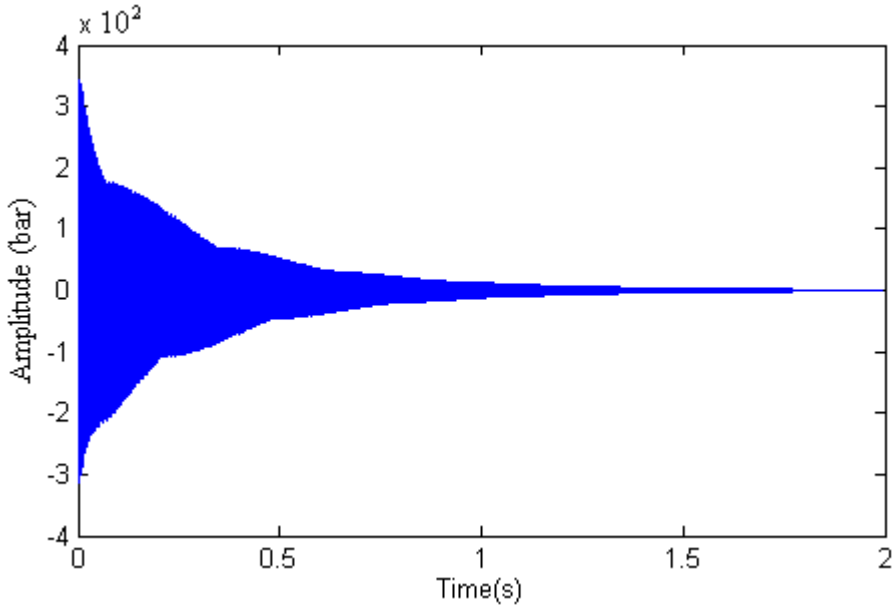

Figure 5.14 Multiple frequency fluid-borne noise cancellation with delay unit compensation using 3-delay unit actuator in pipe model with $k_P = 1$

To summarize, the stable condition for the phase difference between the secondary path and its estimation, which is $-90^\circ < \Delta\varphi < +90^\circ$, is not strict. Sometimes by investigating the spectrum of the secondary path before implementation of fluid-borne noise cancellation the constant delay unit compensation algorithm can be applied during

the whole noise cancellation process for its simple structure and fast calculation. However, usually the actuator is time varying and its dynamic characteristics may change with different working conditions in hydraulic system. Therefore, compared with the delay unit compensation a more accurate way for secondary path identification is discussed in the following section.

5.3 Actuator identification algorithm

In this part, the off-line secondary path identification is implemented using an extra LMS adaptive filter to obtain the correct impulse response of the secondary path. The system identification process is plotted in Figure 3.6 with $f_n = 0$, which means the primary noise is not active during identification. As mentioned in Chapter 3, for the identification application the length of weighting function should be long enough to catch all the information of the secondary path especially the actuator dynamic characteristics under the determined sampling frequency.

Simulation work of this off-line identification algorithm for fluid-borne noise cancellation was realized. An arbitrary second order transfer function was applied as actuator with natural frequency 200 Hz and damping ratio equal to 0.8. Firstly the impulse response of the secondary path was obtained using weighting function with 128 orders in the pipe model with $k_P = 0.5$ as shown in middle graph of Figure 5.15.

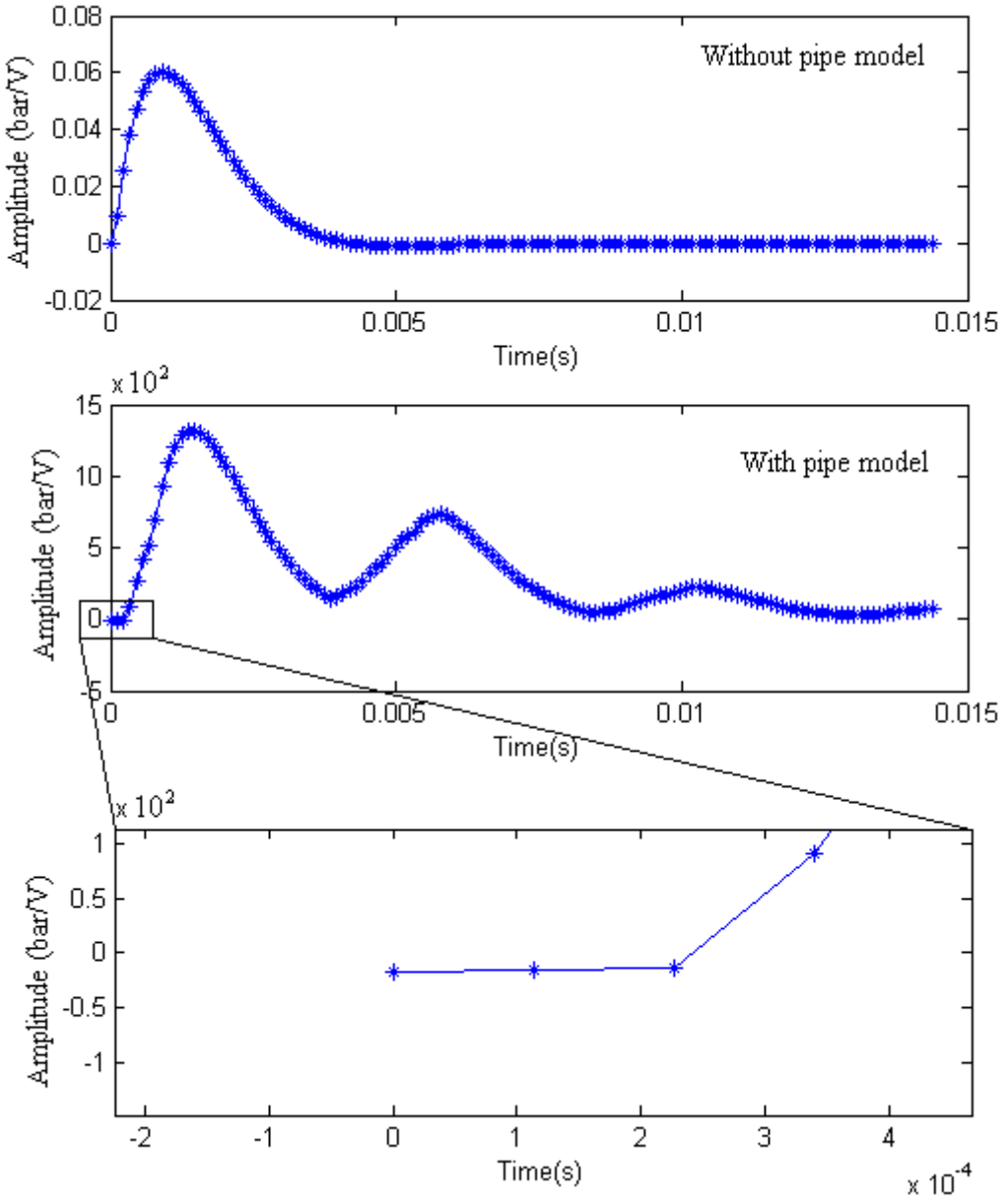

Figure 5.15 Comparison of second order actuator's 128-order impulse response with and without pipe model

For simplicity only the dynamic response of the actuator and pipe model is considered in the secondary path. The actuator's second order impulse response with and without the pipe model were obtained and compared in Figure 5.15. As reflection exists from the right end of the pipe the delayed responses are added together on the original one. Furthermore from the zoomed lowest graph, two sample delays still occur because of the distance between point 3 and 5 in Figure 5.4. The identification errors are plotted in Figure 5.16. A longer length of weighting function used for identification with the pipe model may be helpful in reducing the error.

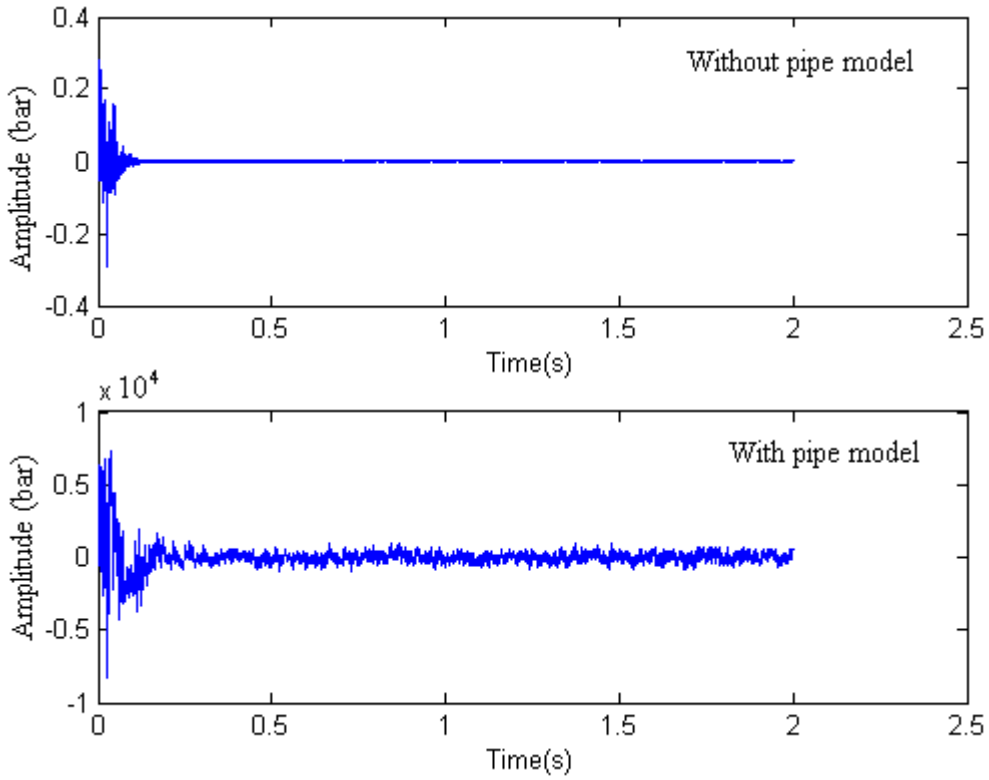

Figure 5.16 Identification error comparison using LMS adaptive filter with 128-order weighting function with and without pipe model

In order to obtain a good fluid-borne noise cancellation result, the length of weighting function for secondary path identification is chosen as 256. The spectrum obtained using frequency domain identification and impulse response identification is plotted in Figure 5.17. Then this obtained impulse response with the pipe model is applied as $\hat{S}(z)$ in Figure 5.2. To implement compensation convolution is realized between impulse response and input reference signals. Single frequency fluid-borne noise cancellation residual errors with and without this compensation are compared in Figure 5.18. With a suitable convergence factor an efficient cancellation result is obtained.

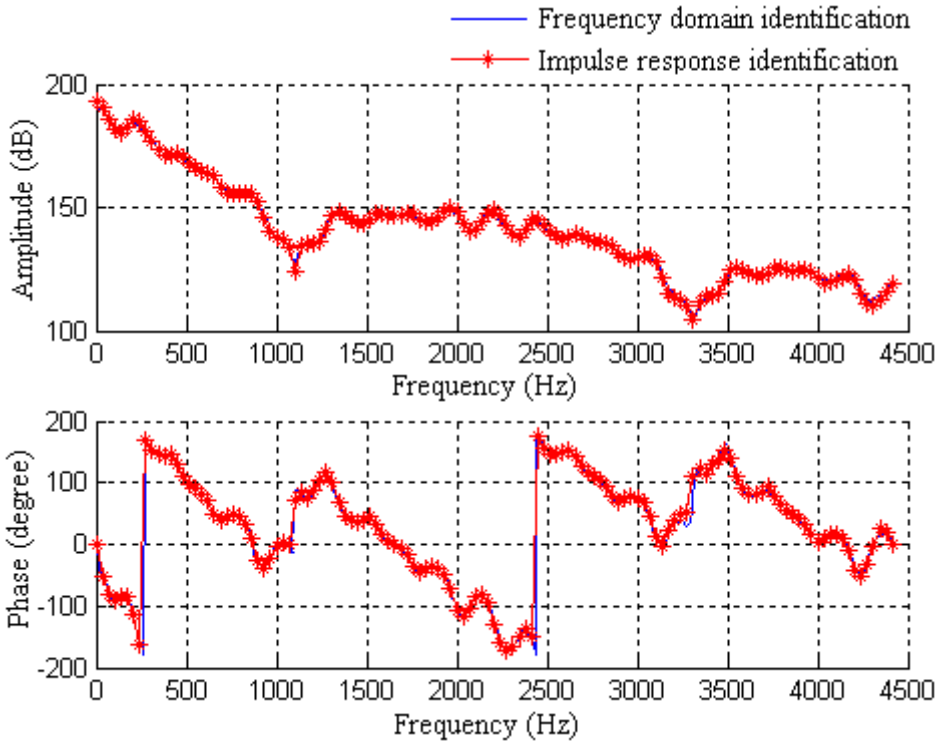

Figure 5.17 Spectrum of secondary path using frequency domain identification and impulse response identification with $k_P = 0.5$

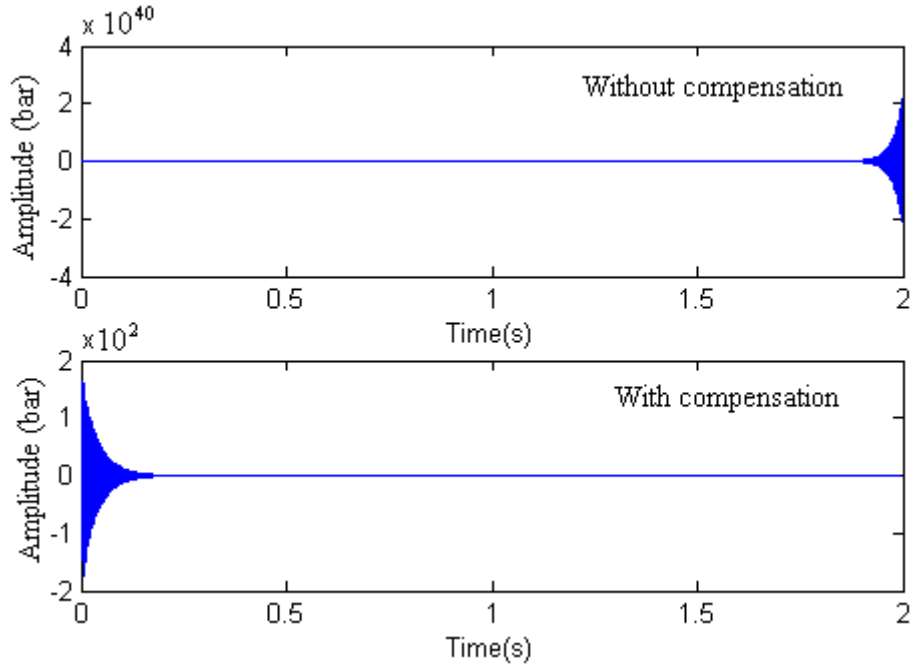

Figure 5.18 Comparison of fluid-borne noise cancellation results with and without off-line impulse response compensation using the second order actuator in the pipe model with $k_P = 0.5$

During the cancellation process the weighting function consisting of two weights changing with time is plotted in Figure 5.19 and a fast adaptive process is obtained.

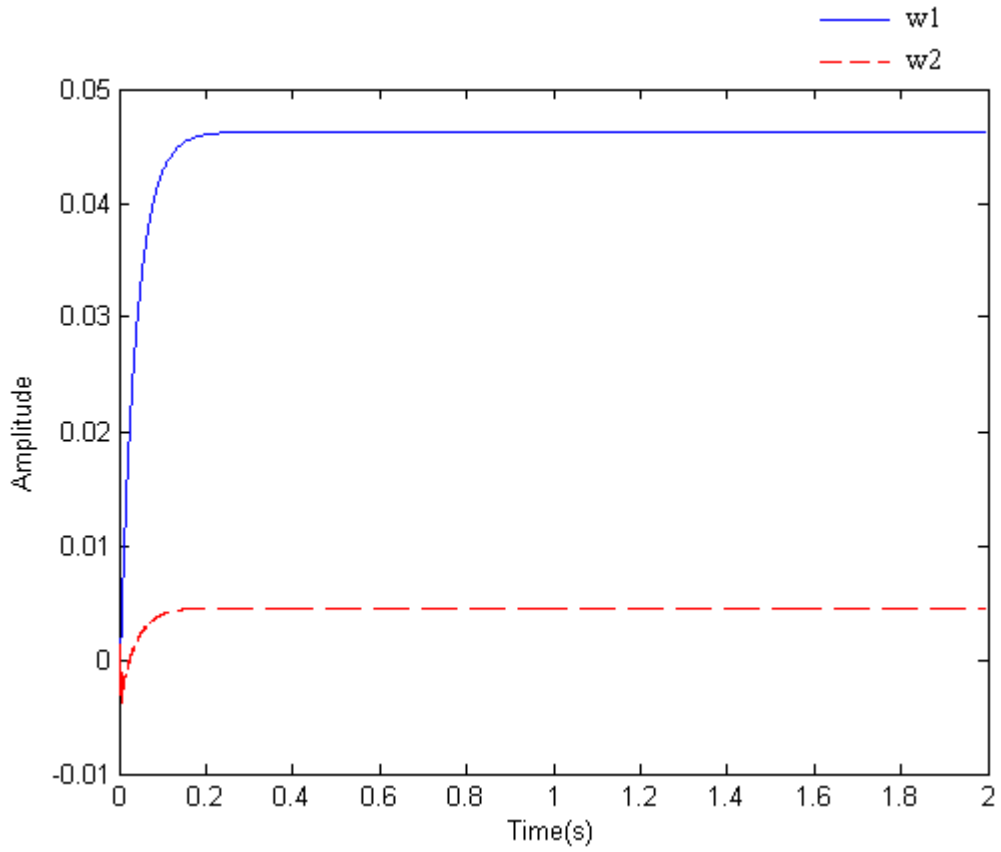

Figure 5.19 Plot of two weights changing with time using FXLMS adaptive filter with off-line impulse response compensation

This off-line identification algorithm associated with the FXLMS adaptive filter is still efficient for multiple frequency fluid-borne noise cancellation. During simulation, the cancellation result is shown in Figure 5.20 with fluid-borne noise at frequency 300 Hz, 600 Hz and 900 Hz in the pipe model using $k_P = 0.5$ under a suitable convergence factor.

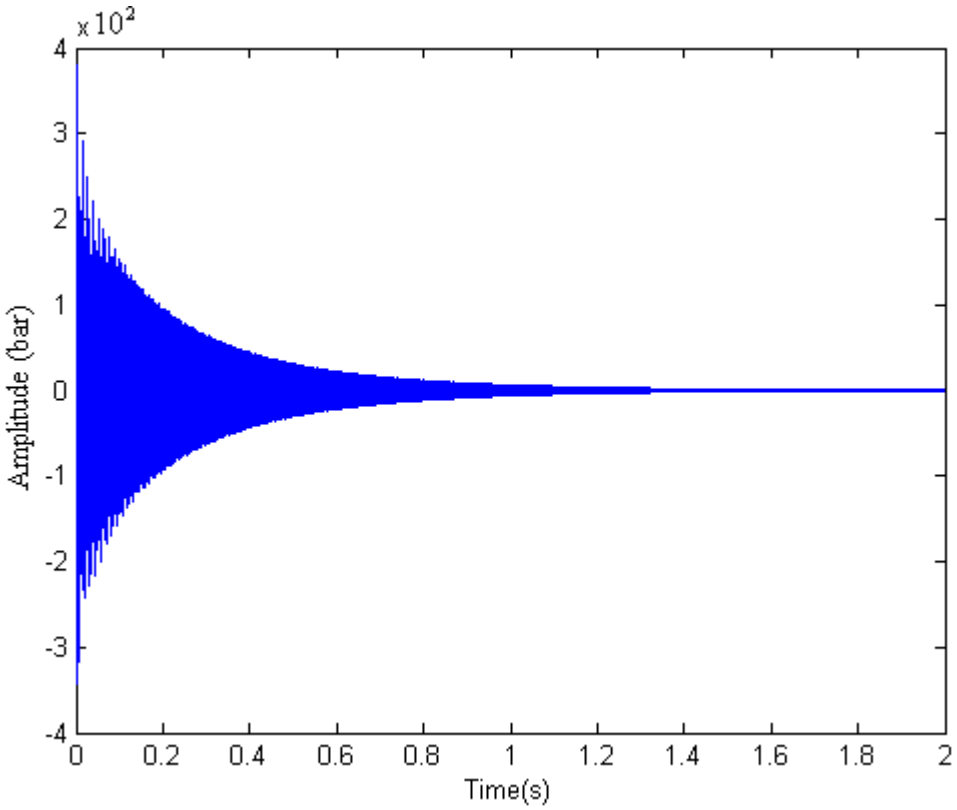

Figure 5.20 Simulated multiple frequency fluid-borne noise cancellation with off-line impulse response compensation using second order actuator in the pipe model with $k_P = 0.5$

From the discussion in this section the off-line impulse response secondary path identification is a more general and accurate algorithm with enough length of weighting function for both single frequency and multi-frequency fluid-borne noise cancellation.

5.4 Conclusions

To conclude, considering the effect of the actuator in the control system, the FXLMS adaptive filter was applied to cancel the fluid-borne noise. Off-line secondary path identification algorithms have been presented. Simulation work was implemented to test the impulse response property of the secondary path with different working conditions in a simple hydraulic circuit model. Depending on the dynamic characteristics of the secondary path, sometimes the secondary path can be roughly seen as a delay unit. As the stability condition is not too critical, a delay unit used as the secondary path compensation was proposed and a good cancellation result was obtained during simulation. Additionally, estimation of the secondary path impulse response using the

LMS adaptive filter could also be applied as the compensation, and a good cancellation result was also obtained using this algorithm during simulation. Moreover, the multi-frequency fluid-borne noise cancellation using these two methods was also simulated. However, without compensation of the secondary path amplitude, the convergence factor of cancellation controller needs to be selected carefully. Furthermore, using the off-line system identification the secondary path identification needs to be re-estimated every time when working condition is changed, which cannot give a wide use for different situations.

CHAPTER 6

Development and Simulation of On-line System Identification Algorithm

In this chapter to track the dynamic variation of secondary path during noise cancellation process, more independent on-line adaptive secondary path identification algorithms are described. This kind of method associated with FXLMS adaptive filter is realized and evaluated by simulation using the simple hydraulic system model with different working conditions. Especially, Bao's method is improved to obtain better secondary path estimation. In the same way as for off-line control algorithms, variation of load valve can be represented using a reflection factor. Two manipulation strategies are proposed to realize fluid-borne noise cancellation during simulation and in real experiments.

6.1 Time domain on-line identification algorithms

For fluid-borne noise cancellation the filtered reference LMS adaptive filter is a robust and efficient algorithm to deal with the secondary path effect. As discussed in Chapter 5 off-line identification methods can be applied with prior knowledge of dynamic characteristics of the secondary path and considerable cancellation results are obtained for both single and multiple frequency input signals. However, most of the time the secondary path, especially the actuator, is time varying and working conditions in the hydraulic system are changing with time, which can also affect the impulse response of the secondary path, to make the control performance degrade and even become unstable. In this section two previous on-line secondary path identification algorithms are evaluated and applied for the fluid-borne noise cancellation through simulation with a pipe model. Main parameters used in the model are shown in Appendix 5.

6.1.1 Eriksson's method

One important on-line identification algorithm with an auxiliary signal was proposed by Eriksson as described in [22]. The structure of its control process with a two-weight

adaptive notch filter is shown in Figure 6.1. The part enclosed by the dashed line is time domain identification. A zero mean white noise, which is uncorrelated with primary noise $d(n)$, is applied here as an auxiliary signal. A second LMS adaptive filter is used to obtain the secondary path impulse response synchronized with the noise cancellation process and this estimation is used directly for compensation.

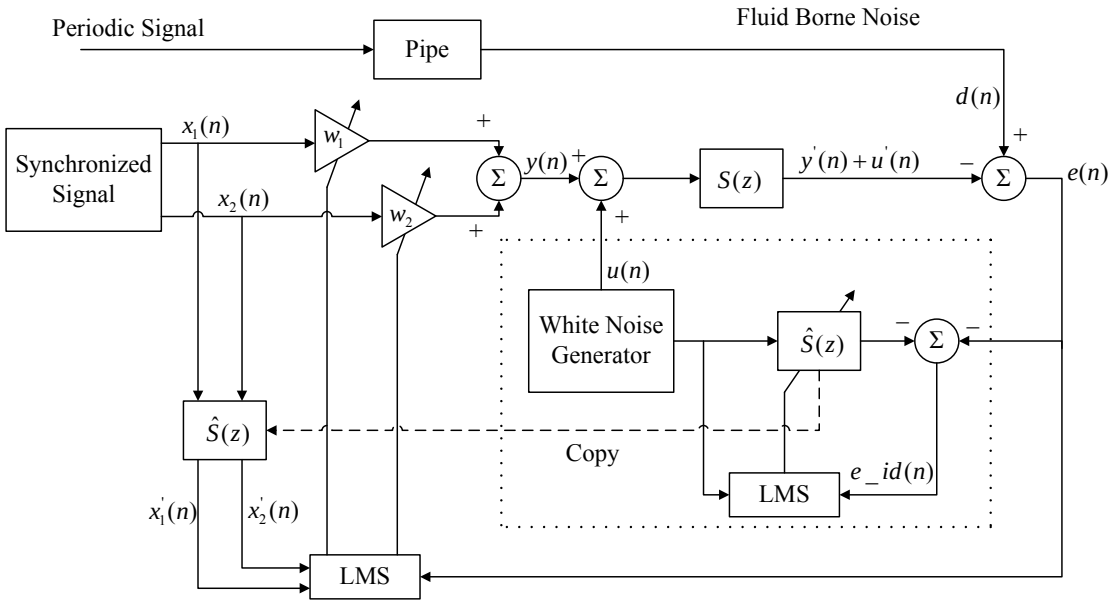

Figure 6.1 Eriksson's on-line identification method using auxiliary white noise

To evaluate this algorithm an additional parameter $v(n) = d(n) - y'(n)$ ($s(n)$ is the impulse response of $S(z)$, and $\hat{s}(n)$ is the impulse response of $\hat{S}(z)$) is introduced. From the identification point of view $v(n)$ can be seen as the interference signal for identification caused by residual noise. According to this, the identification part in Figure 6.1 can be described using Figure 6.2 to represent interference effect [12].

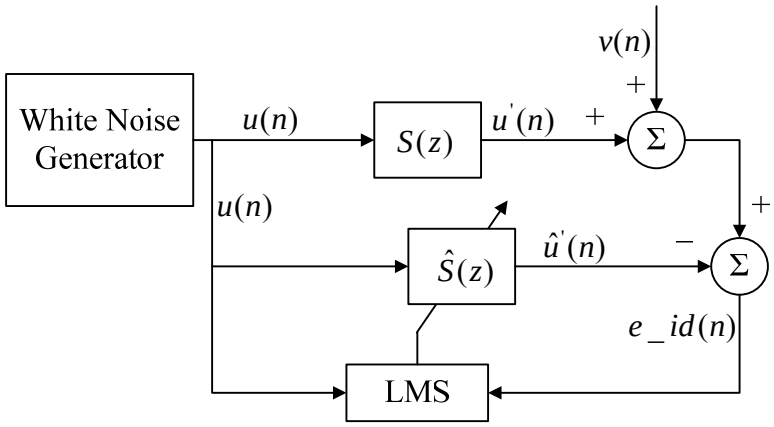

Figure 6.2 Plot of interference effect on on-line identification

Applying equations (3.21) and (3.22) here, $u(n)$ can be seen as the input reference signal $x(n)$ and $u'(n)-v(n)$ is the primary noise signal $d(n)$. S_{dx} can be written as:

$$S_{dx} = E\left[d(n-m)\cdot x(n)\right]$$

$$= E\left[u'(n-m)\cdot u(n)+v(n-m)\cdot u(n)\right]$$

$$= E\left[u'(n-m)\cdot u(n)\right]+E\left[v(n-m)\cdot u(n)\right]$$

Since $v(n)$ and $u(n)$ are uncorrelated, hence $S_{dx} = E\left[u'(n-m)\cdot u(n)\right]$, which means interference v cannot theoretically affect the final solution in equation (3.22) with a significant small convergence factor and quite long running time, and e_id will finally converge to $v(n)$. However, in real simulation or experiment with suitable convergence factor and finite time the theoretical solution mentioned above cannot be realized, and this interference can have a significant effect on the transient behaviour of weighting function updating, which can be shown in the following equation [12]:

$$\hat{s}(n+1) = \hat{s}(n)+\mu\cdot u(n)\cdot\left[u'(n)-\hat{u}'(n)+v(n)\right]$$

$$= \hat{s}(n)+\mu\cdot u(n)\cdot\left[u'(n)-\hat{u}'(n)\right]+\mu\cdot u(n)\cdot v(n)$$

The last term from the above equation is the unwanted part, which can affect the adaptive process by large residual noise. Secondary path impulse response of Eriksson's

algorithm was obtained during simulation using a pipe model and compared with the theoretical value in Figure 6.3 with suitable small convergence factor, and $v(n)$ is a powerful single frequency sine wave with 300 Hz. As the interference noise $v(n)$ with high power is not attenuated, a distorted impulse response result is obtained and the identification error is not zero but converges to $v(n)$.

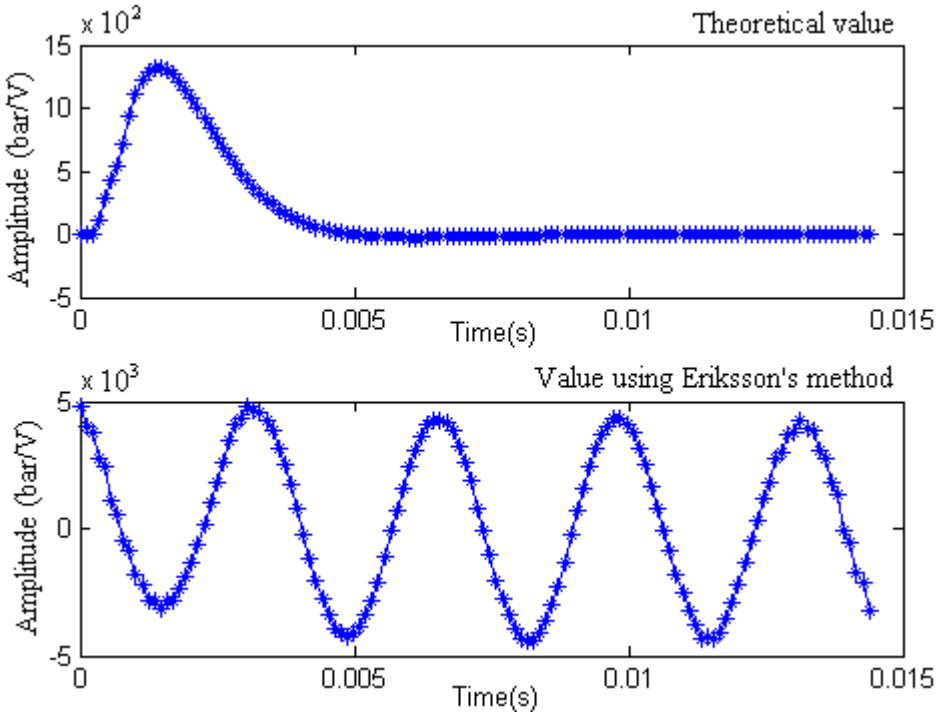

Figure 6.3 Secondary path impulse response using Eriksson's method

6.1.2 Kuo's method

In order to overcome this problem Kuo [23] deduced a prediction filter to remove the interference effect in narrowband noise cancellation as shown in Figure 6.4.

The prediction with an extra LMS adaptive filter is shown in the dashed line block, in which a delay unit is applied. This LMS filter can be a two-weight notch filter for narrowband fluid-borne noise cancellation. Assume the secondary path $S(z)$ can be represented by finite impulse response with length of M. As the auxiliary white noise signal is zero mean and uniformly distributed, $u'(n)$ in $e(n)$ and $u'(n-\Delta)$ in $e(n-\Delta)$ are uncorrelated when the number of delays in the delay block is not smaller than M [23]. Therefore the correlated signal $d(n)-y'(n)$ and $d(n-\Delta)-y'(n-\Delta)$ can

be cancelled by this prediction filter. Rather than using $e(n)$ as identification, the desired signal $g(n)$ is applied, which can be represented as:

$$g(n) = d(n) - y'(n) - \left[d(n-\Delta) - y'(n-\Delta)\right] * f(n) + u'(n) + u'(n-\Delta) * f(n)$$

where $f(n)$ is the impulse response of $F(z)$

After cancelling the interference $v(n)$,

$$g(n) = u'(n) - u'(n-\Delta) * f(n)$$

However, the second term on the right side in the above equation can give a distortion effect to the secondary path identification process.

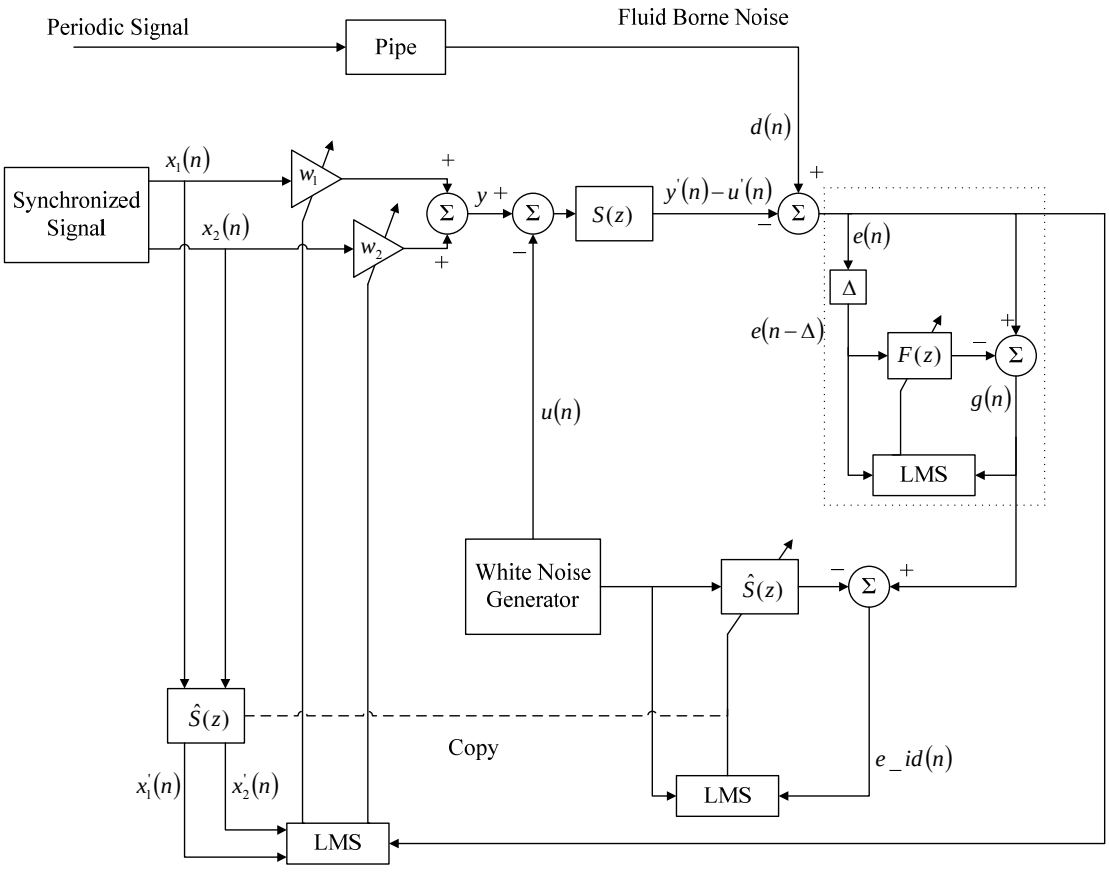

Figure 6.4 Kuo's on-line identification method in time domain [23]

6.1.3 Bao's method and its improvement

Bao introduced an algorithm to solve this problem [25]. As shown in Figure 6.5, the structure in the dashed box can be used to replace that in Figure 6.4. The reference input signal $x_1(n)$ and $x_2(n)$ or $x(n)$, which has the same frequency with $d(n)$, is directly applied to cancel the interference. As with the structure of Kuo's method, $F(z)$ can be a general LMS filter with reference input $x(n)$ or a two-weight adaptive notch filter with reference inputs $x_1(n)$ and $x_2(n)$.

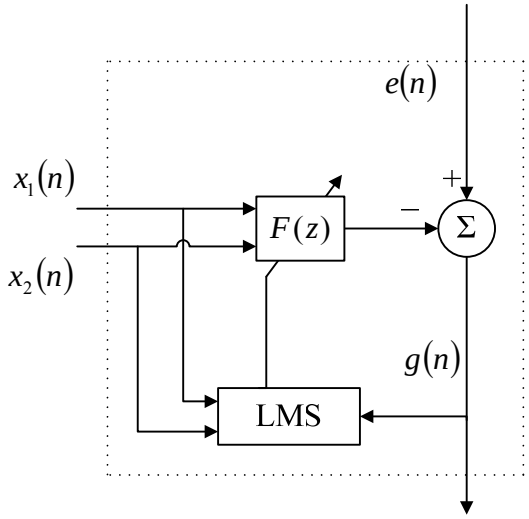

Figure 6.5 Structure of Bao's interference cancellation part

Unlike Kuo's method, signal $g(n)$ used for identification can be written as:

$$g(n) = d(n) - y'(n) - x(n) * f(n) + u'(n)$$

After cancelling the interference $v(n)$,

$$g(n) = u'(n)$$

The unwanted term $-u'(n-\Delta) * f(n)$ is eliminated and the residual primary noise can be attenuated by a two-weight notch filter using the reference input signal. An efficient effect of Bao's method is implemented during simulation with a pipe model using the structure in Figure 6.6. As mentioned in Chapter 3 the dashed line part in Figure 6.5,

which is a two-weight adaptive notch filter, can be seen as a transfer function notated using $R(z)$.

Similarly with the structure in Figure 6.2, in this simulation $v(n)$, which is the residual primary fluid-borne noise, is a 300 Hz single frequency sine wave with considerable amplitude compared with the power of white noise. The length of weighting function is 128. Reflection factor $k_P = 1$.

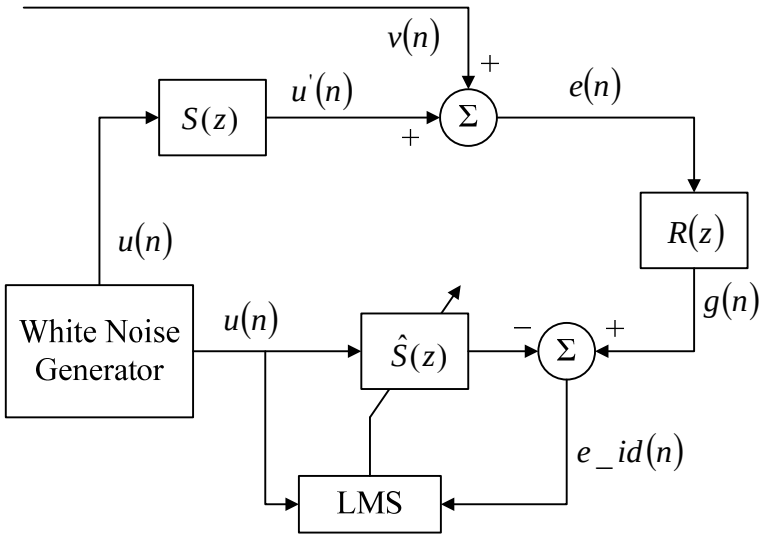

Figure 6.6 Equivalent on-line identification structure of Bao's method

Using this algorithm the interference $v(n)$ is cancelled and the signal $g(n)$, which is used for identification, is quite close to $u'(n)$. Their power is compared in Figure 6.7.

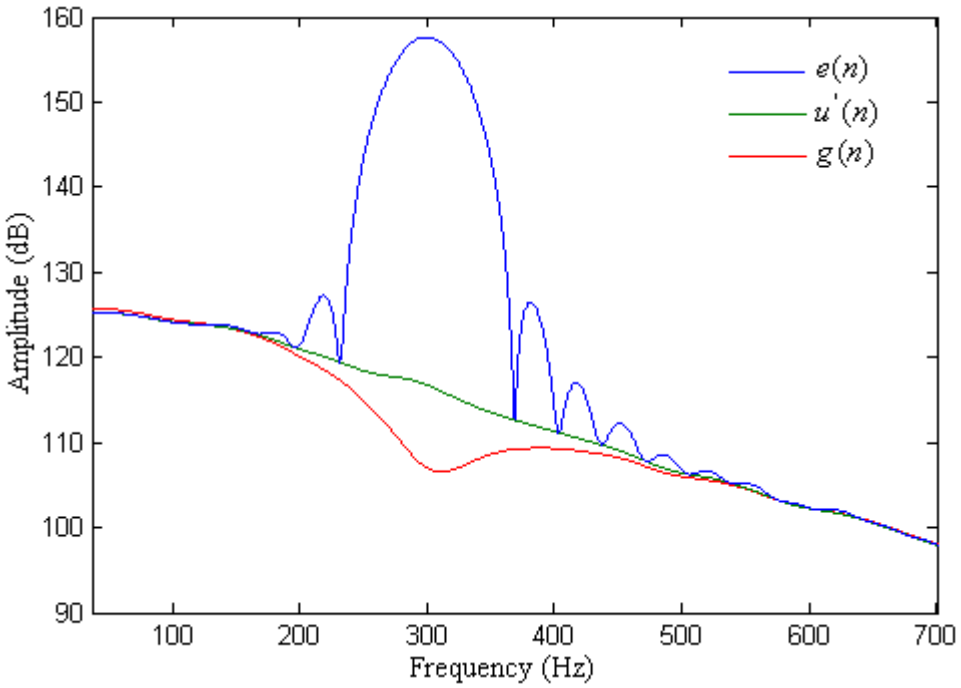

Figure 6.7 Plot of signal *g*(*n*) in the control process in figure 6.6

The effective identification impulse response result is plotted in Figure 6.8.

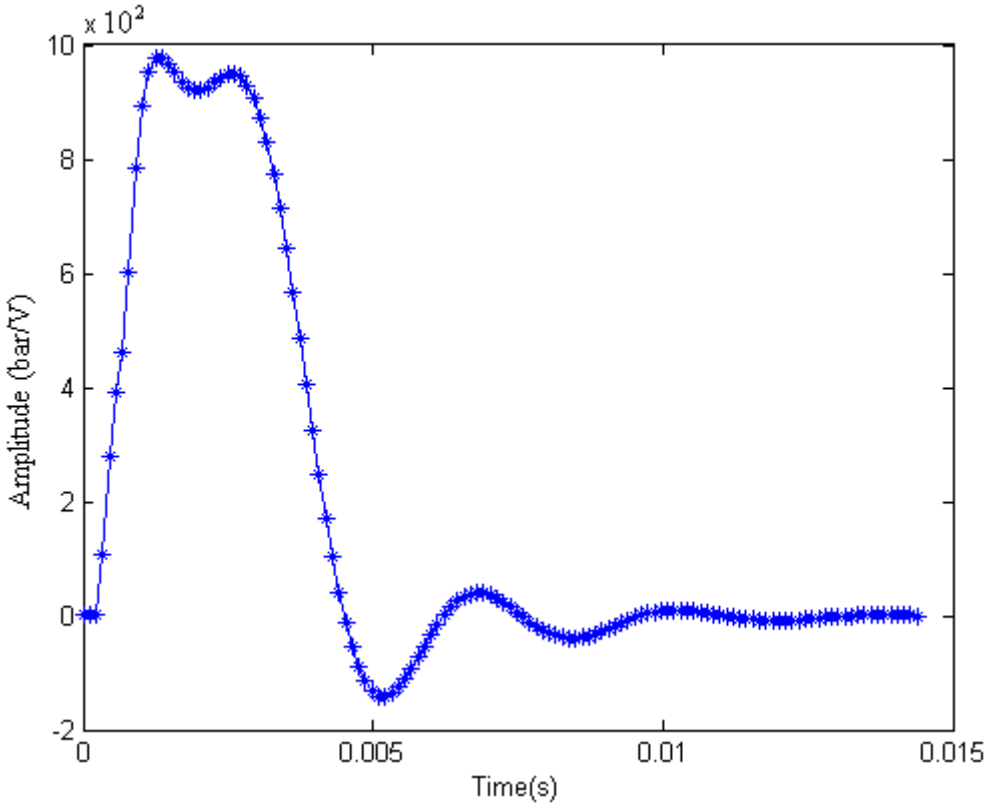

Figure 6.8 Secondary path impulse response using Bao's method with constant single frequency interference

Compared with the result using Errisson's method and the theoretical value plotted in Figure 6.3, a more accurate result is obtained. However, oscillatory distortion exists in the result. From Figure 6.6, identification error signal $e\_id(n)$ can be represented as:

$$e\_id(n) = u(n) * s(n) * r(n) - u(n) * \hat{s}(n)$$

which means an extra transfer function $R(z)$ is involved in the secondary path. Under this effect, the component in white noise that has the same frequency as $v(n)$ is attenuated by notch filter $R(z)$, and with big convergence factor more notch curve occurs to introduce more distortion.

To overcome this problem the same transfer function $R(z)$ is applied to compensate for this effect as shown in Figure 6.9.

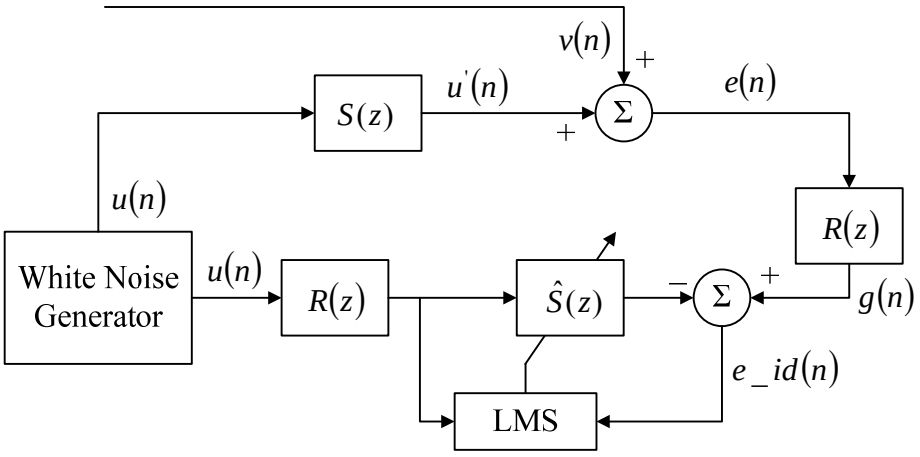

Figure 6.9 Improved equivalent on-line identification structure of Bao's method

Hence, the identification error signal can be written as:

$$\begin{aligned} e\_id(n) &= u(n) * s(n) * r(n) - u(n) * \hat{s}(n) * r(n) \\ &= u(n) * [s(n) * r(n) - \hat{s}(n) * r(n)] \\ &= u(n) * [s_{new}(n) - \hat{s}_{new}(n)] \end{aligned}$$

which means the $R(z)$ can be seen as a part of the secondary path, whose impulse response is represented using $s_{new}(n)$. To be convenient, in the following parts the secondary path impulse response is still represented using $s(n)$.

The detailed structure of improved Bao's method can be shown in Figure 6.10.

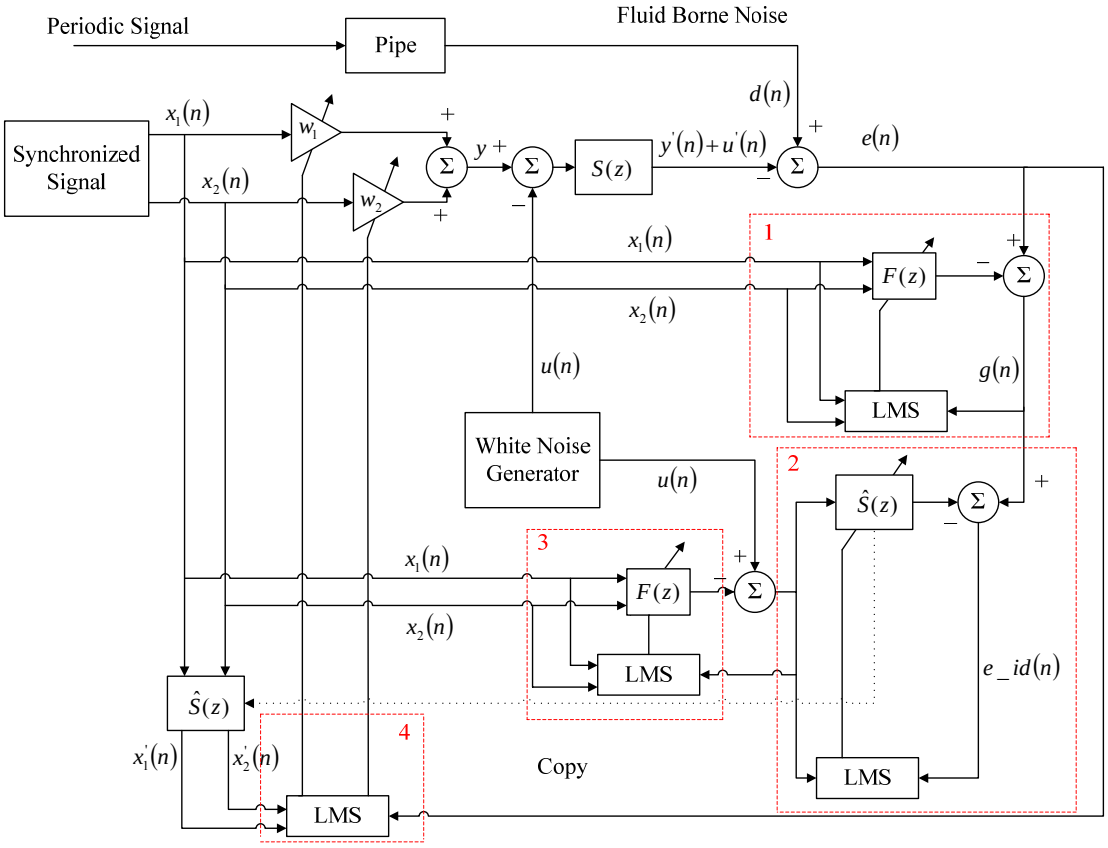

Figure 6.10 Improved Bao's on-line identification method with two-weight notch filter

In Figure 6.10, block 1 in red dashed line is the interference controller, block 2 is the on-line identification controller, block 3 is the compensation for interference controller and block 4 is the two-weight adaptive notch filter for noise cancellation. Under the compensation in block 2, the impulse response of the secondary path is plotted in Figure 6.11 and a satisfactory identification result is obtained.

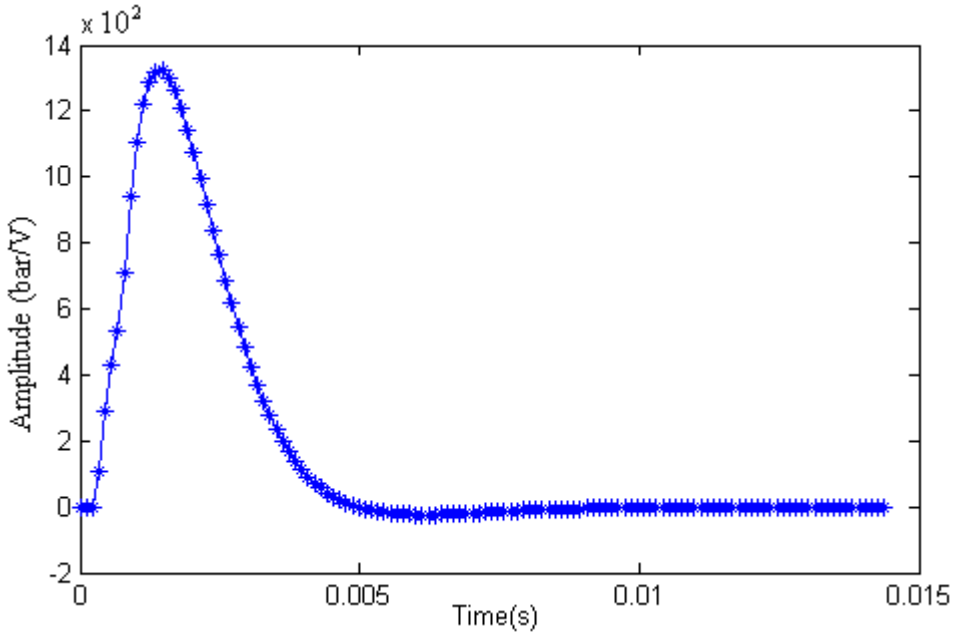

Figure 6.11 Secondary path impulse response using improved Bao's method with constant single frequency interference under compensation

However, the auxiliary white noise, which is uncorrelated with primary noise and reference input signals, still exists in error signal $e(n)$. The control performance of $F(z)$ and w_1, w_2 can be affected, although this white noise has small power.

6.1.4 Zhang's method

For further improvement a more accurate algorithm was proposed by Zhang [26]. Its structure with a two-weight adaptive notch filter is shown in Figure 6.12. In this method three individual LMS adaptive filters are applied. The first LMS filter in block 1 is used to cancel the interference from the primary noise; the second one in block 2 is used for on-line identification; and the third one in block 3 is applied for cancelling the fluid-borne noise. Additionally, filters in blocks 1 and 2 are cross-updated [26]: firstly $u'(n)$ is used to eliminate the white noise effect in $e(n)$, and the obtained signal $e'(n)$ is then applied to update the interference controller in block 1 to obtain the inverse interference signal $h(n)$. Secondly $h(n)$ is used to eliminate the residual primary noise interference signal in $e(n)$, and the obtained signal $g(n)$ is applied to update the on-line identification in block 2. Hence when $\hat{S}(z) = S(z)$, $e(n) = d(n) - y'(n)$ and $g(n) = u'(n)$. Using this method extra perturbation effects to all LMS adaptive filters are eliminated. Especially component in the white noise that has same frequency as

primary is not affected and the compensation filter $R(z)$ in Bao's method is eliminated to make the system simple. Secondary path impulse response is obtained in Figure 6.13 during simulation with pipe model.

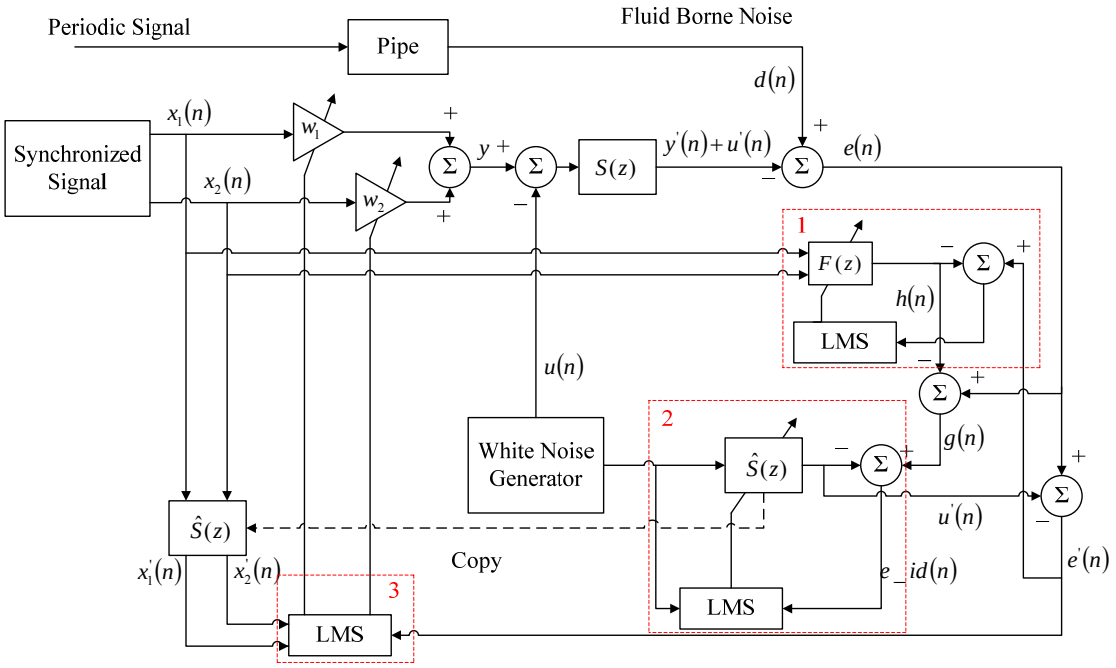

Figure 6.12 Zhang's on-line identification method with two-weight adaptive notch filter

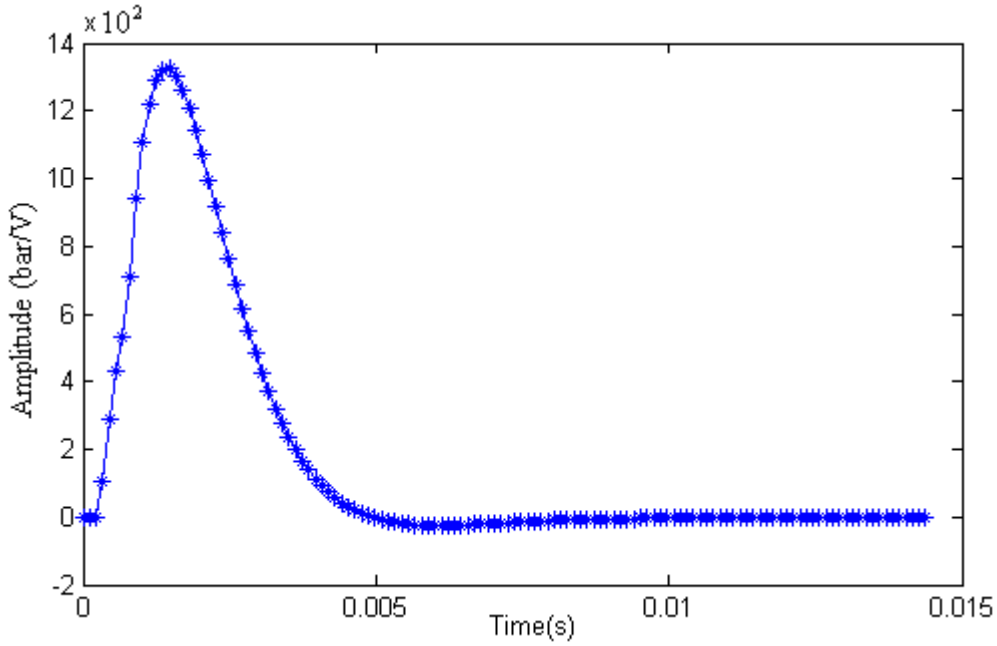

Figure 6.13 Secondary path impulse response using Zhang's method with constant single frequency interference

6.2 Two manipulation strategies

During the simulation process, since a short period of adaptation is needed for secondary path identification and fluid-borne noise cancellation, an inaccurate secondary path impulse response may push the control process to instability in the first running stage. Therefore in simulation, the secondary path identification can start before running noise cancellation. There are two strategies that can realize this implementation in the beginning stage.

6.2.1 First strategy

In the first strategy the control process can be realized in two stages. Firstly the primary fluid-borne noise source and the LMS filter used for the noise controller are switched off while running the secondary path identification. This process is the same as that of the off-line secondary path identification. Secondly the primary noise and the controller are switched on when the comparatively accurate impulse response of the secondary path is obtained. Therefore the effect from the secondary path identification process is eliminated. In this section both the improved Bao's method as shown in Figure 6.10 and Zhang's on-line identification method in Figure 6.12 associated with two-weight adaptive notch filter are simulated in the pipe model to cancel single and multi-frequency noise.

In the first strategy as the primary fluid-borne noise comes into the pipe along with flow and pressure supplied by the pump, the reflection will change while running the pump. Hence secondary path dynamic characteristics may change. Because the convergence condition for phase difference between $\hat{S}(z)$ and $S(z)$ is in the range of $\pm 90^{\circ}$, moderate variation of secondary path dynamic characteristics is tolerable. Then the secondary path impulse response is converged to another solution with reduction of the primary noise when noise cancellation controller is switched on. To represent this condition in the simulation, the reflection factor k_P is set to a relatively large value between 0 and 1 when only operating secondary path identification in the first stage, and then k_P is set to a smaller value between 1 and 0 when the noise controller and its relative parts are switched on in the second stage. As a result the estimated secondary path impulse response will converge to another steady solution.

Firstly, the improved Bao's method and Zhang's method, which are discussed in section 6.1, are compared during simulation with the same parameters. Primary noise is a 300 Hz sine wave, and the length of weighting function in the on-line identification controller is 128. To give a clear comparison, a relatively large convergence factor for a two-weight adaptive notch filter is selected for these two methods and the amplitude of fluid-borne noise is six times bigger than that of the white noise. In the first stage $k_P = 1$ and in the second stage $k_P = 0.6$. In the improved Bao's method as shown in Figure 6.10, the white noise exists in $e(n)$ and is given to the two-weight adaptive notch filter. As shown in the bode graph of the two-weight adaptive notch filter plotted in Figure 3.16 the uncancelled frequency components can be affected by this filter, especially for big convergence factor. As a result, not only the anti-noise signal exists in the control signal $y(n)$ but also the additional signal, which can be named as w_a, caused by the white noise in $e(n)$. w_a, which has adequate frequency range, passes through the interference controller and is used for secondary path identification. Under this effect the on-line identification can be distorted when the convergence factor of two-weight adaptive notch filter is big and this makes the system unstable. However, in Zhang's method as shown in Figure 6.12, when the on-line secondary path estimation converges to a steady solution the white noise is eliminated in $e'(n)$. Therefore, w_a is eliminated and accurate on-line secondary path estimation can be obtained. In this comparison the same relatively large convergence factor of two-weight adaptive notch filter is selected for improved Bao's method and Zhang's method. The same convergence factors of on-line identification and interference controller are also used for these two methods. Secondary path identification results, obtained using the improved Bao's method and Zhang's method, when switching on the fluid-borne noise controller in the second stage compared with the theoretical value are plotted in Figure 6.14.

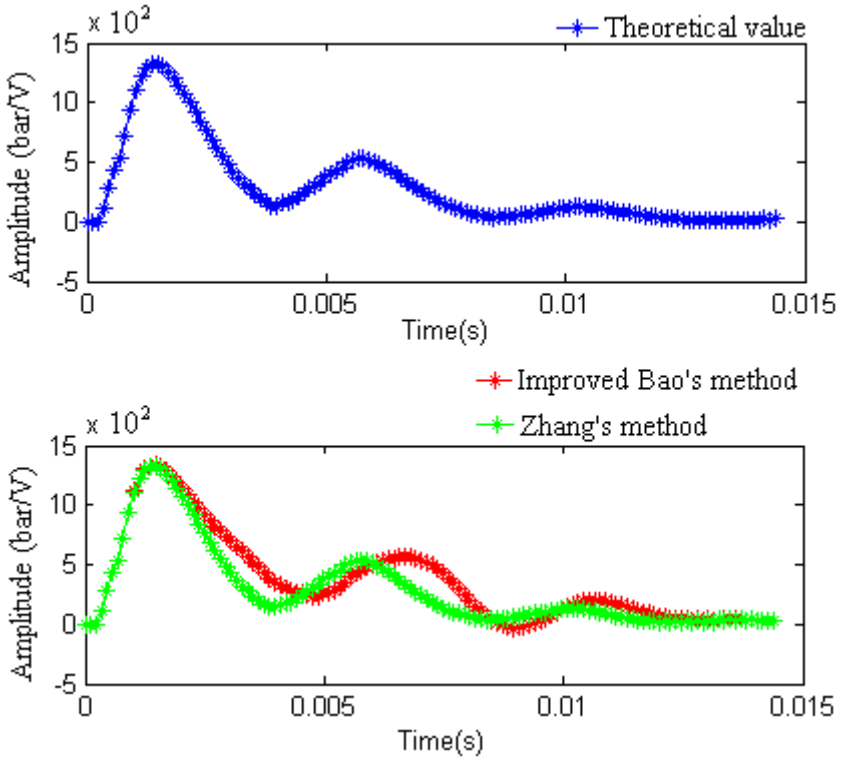

Figure 6.14 Comparison of 128-order secondary path impulse response with $k_P = 0.6$

The distorted identification result obtained using improved Bao's method can make the system unstable, especially for the system which has complicated secondary path dynamic response.

Secondly, the improved Bao's method is simulated with a more suitable convergence factor. In this simulation the frequency of primary fluid-borne noise is 300 Hz and the length of identification weighting function is 512. The amplitude of fluid-borne noise is six times bigger than that of the white noise. To avoid the distorted identification response, a suitable convergence factor for two-weight adaptive notch filter is selected. The first stage runs for 2 seconds when the identification result goes to a steady solution with $k_P = 1$. To evaluate the control ability when switching on the pump of this method, in the second stage $k_P = 0.2$ to give a big reflection change. It is found that at the beginning of the second stage a short adaptive period is needed for primary noise cancellation and interference cancellation. As the secondary path impulse response is converged to another optimum solution in this secondary stage, during this period big variation of primary noise and interference can affect the identification process. Hence,

in this period a relatively small value can be used for on-line identification convergence factor in the second stage. However, after a short period the relatively large value can be applied again for fast convergence. In this simulation, 2×10^3 is applied as identification convergence factor in the first stage and 2×10^2 is used for the first second in the second stage, and then 2×10^3 is applied again in the second stage to give a fast convergence speed. Estimated secondary path impulse response in the first stage can be represented using Figure 6.11 and the accurate impulse response in the secondary stage is plotted in Figure 6.15 compared with the theoretical value.

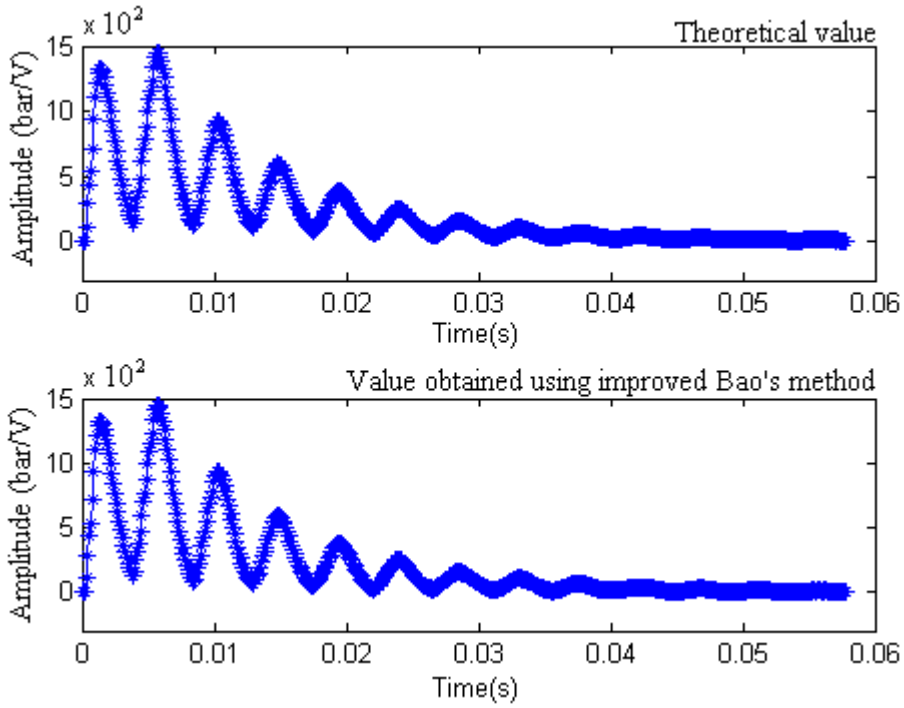

Figure 6.15 Comparison of 512-order estimated secondary path impulse response with $k_p = 0.2$

The adaptive process of the 50th point, which has a big variation on the estimated secondary path impulse response, is plotted in Figure 6.16.

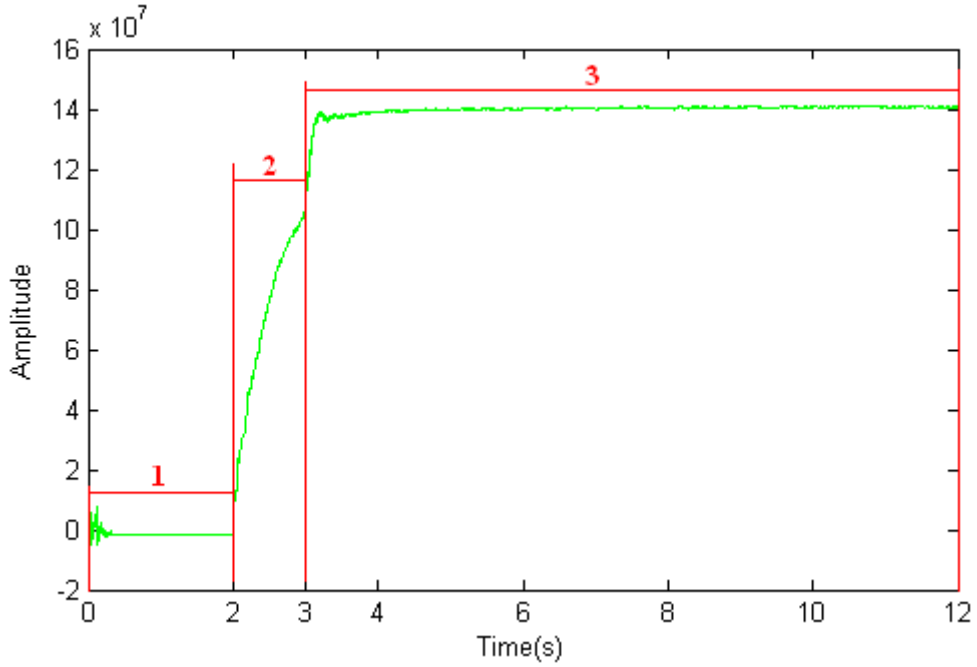

Figure 6.16 Adaptive process of the 50th point on estimated secondary path impulse response with k_P changing from 1 to 0.2 using improved Bao's method

In the above plot period 1 is the first stage from 0 s to 2 s with $k_P = 1$ and the identification convergence factor is 2×10^3, period 2 is the beginning of the second stage from 2 s to 3 s with $k_P = 0.2$ and identification factor is 2×10^2; and period 3 is from 3 s to the end with $k_P = 0.2$ and identification factor is 2×10^3.

The fluid-borne noise cancellation result is plotted in Figure 6.17. The error signal is shown using the blue line. During the first stage from 0 s to 2 s only the auxiliary white noise exists in the error signal as plotted using the blue line. The signal plotted by the green line, which is the noise which would occur with the primary source running without cancellation, which does not exist in the first stage, is used to describe the cancellation effect. The second stage starts from 2 s and a considerable cancellation result is obtained. However, auxiliary white noise that cannot be cancelled still remains.

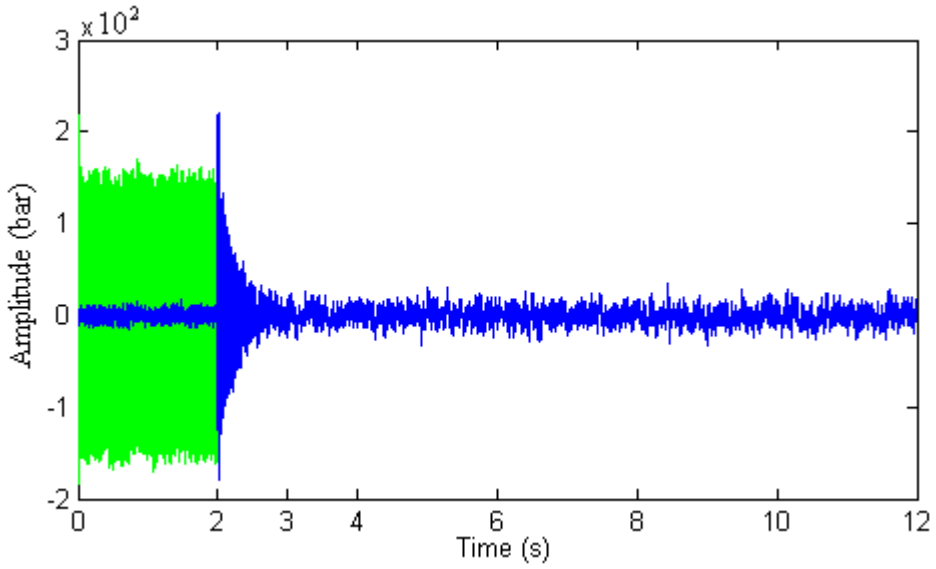

Figure 6.17 Single frequency cancellation result using improved Bao's method

For multiple frequency fluid-borne noise cancellation, several noise cancellation controllers corresponding to every target frequency are in parallel and control flow is the summation of outputs from these controllers as presented in section 3.2.3. In the simulation of the improved Bao's method 300 Hz, 600 Hz and 900 Hz are the target frequencies to be cancelled and three cancellation controllers are used. As more frequency cancellations exist, the identification convergence factor in the second period plotted in Figure 6.18 is 1×10^{2}, which is smaller than that for single frequency cancellation in Figure 6.16. Amplitude of the three different frequencies signal summation is about eight times bigger than that of the white noise. The whole operation process and other parameters (except the convergence factors of two-weight adaptive notch filters for 600 Hz and 900 Hz noise) are the same as with single frequency cancellation. Steady secondary path impulse response with $k_p = 0.2$ in the second stage is almost the same as the one plotted in Figure 6.15. An accurate estimated secondary path impulse response is obtained for this multiple frequency fluid-borne noise cancellation. The fluid-borne noise cancellation result is also compared with uncancelled noise in Figure 6.19.

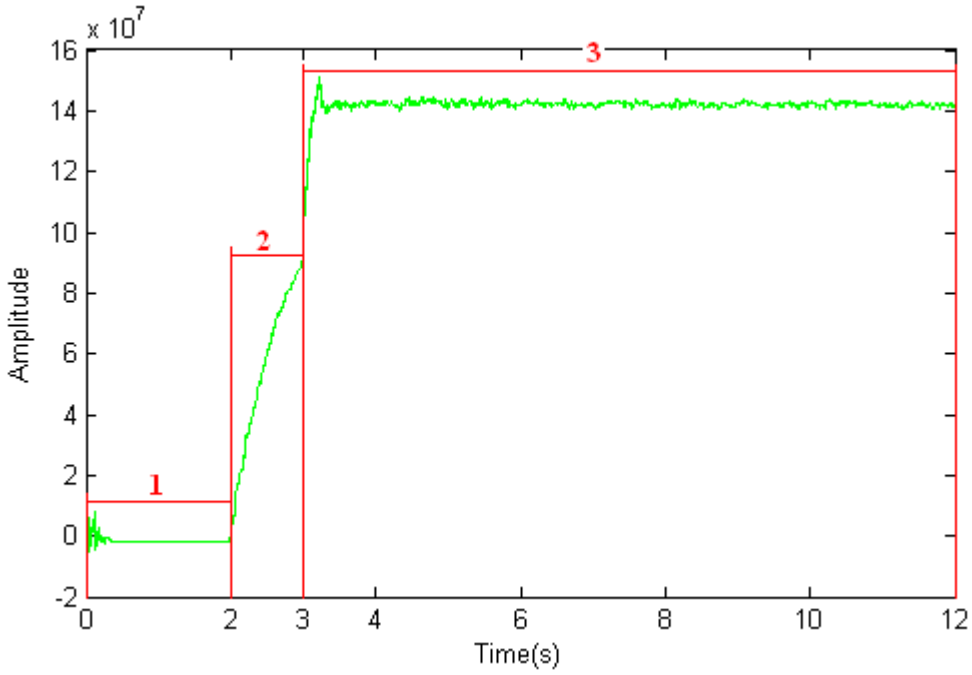

Figure 6.18 Adaptive process of the 50th point on estimated secondary path impulse response with k_P changing from 1 to 0.2 for multiple frequency using improved Bao's method

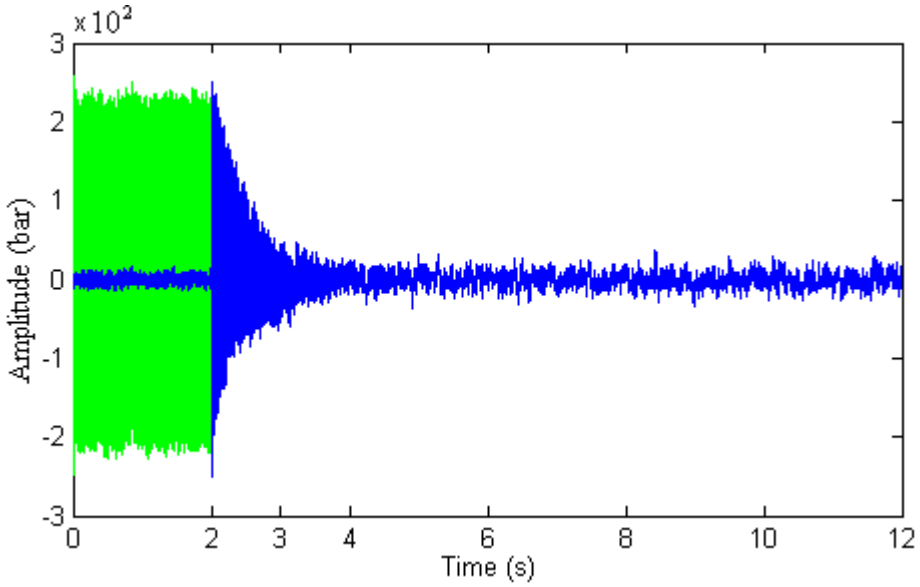

Figure 6.19 Multiple frequency cancellation result using improved Bao's method

As with the improved Bao's method, Zhang's method, which is presented in Figure 6.12, is also simulated for both single frequency and multiple frequency fluid-borne noise

cancellation. In the simulation of Zhang's method, identification is implemented with $k_P = 1$ and the same identification convergence coefficient as the one used in the improved Bao's method is applied in the first stage for 2 s. The length of identification weighting function is 512. The shape of the secondary path impulse response is similar to the one in Figure 6.13. In the second stage, primary fluid-borne noise is applied with 300 Hz frequency, and its amplitude is about six times bigger than that of the white noise. A faster convergence factor of two-weight adaptive notch filter than that used in the improved Bao's method is applied. As in Zhang's method, the assumption $\hat{S}(z) = S(z)$ is made to eliminate white noise effect on noise cancellation controller and white noise distortion at certain frequencies, and the weighting functions of secondary path identification and interference cancellation are cross-updated. Hence inaccurate secondary path identification and distortion of white noise may restrict each other on convergence at the beginning of the second stage. To ensure stability a small convergence factor for on-line identification is applied for 3 s at the beginning of the second stage, as shown in Figure 6.20. As a result it can be seen that more running time is needed to obtain accurate estimated secondary path impulse response.

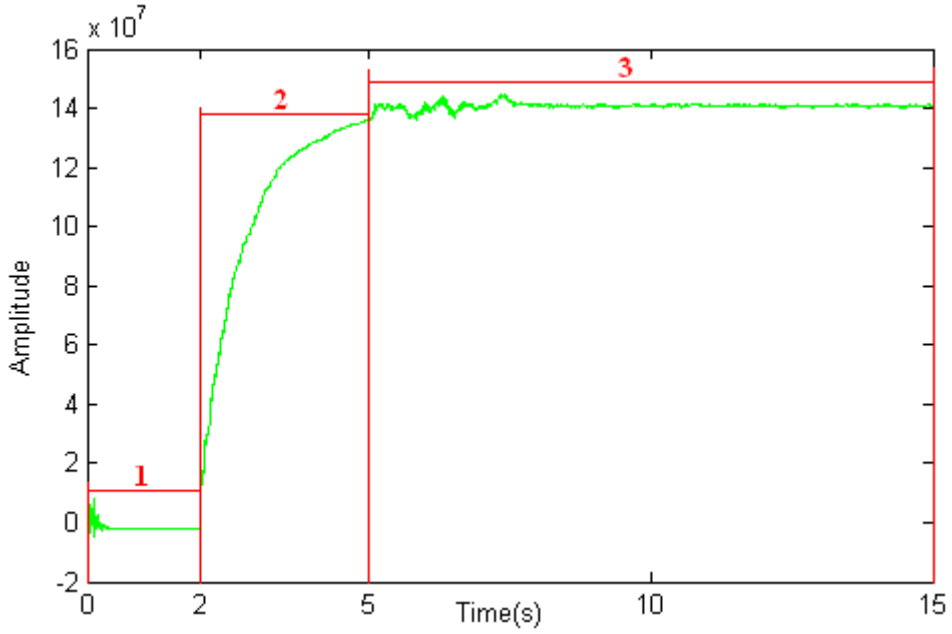

Figure 6.20 Adaptive process of the 50th point on estimated secondary path impulse response with k_P changing from 1 to 0.2 using Zhang's method

Estimated accurate secondary path identification in the second stage and a good cancellation result with fast convergence factor are shown in Figure 6.21 and Figure 6.22. In the cancellation result there is only white noise in the error signal plotted using the blue line. The green line is the noise that would occur without cancellation, for comparison.

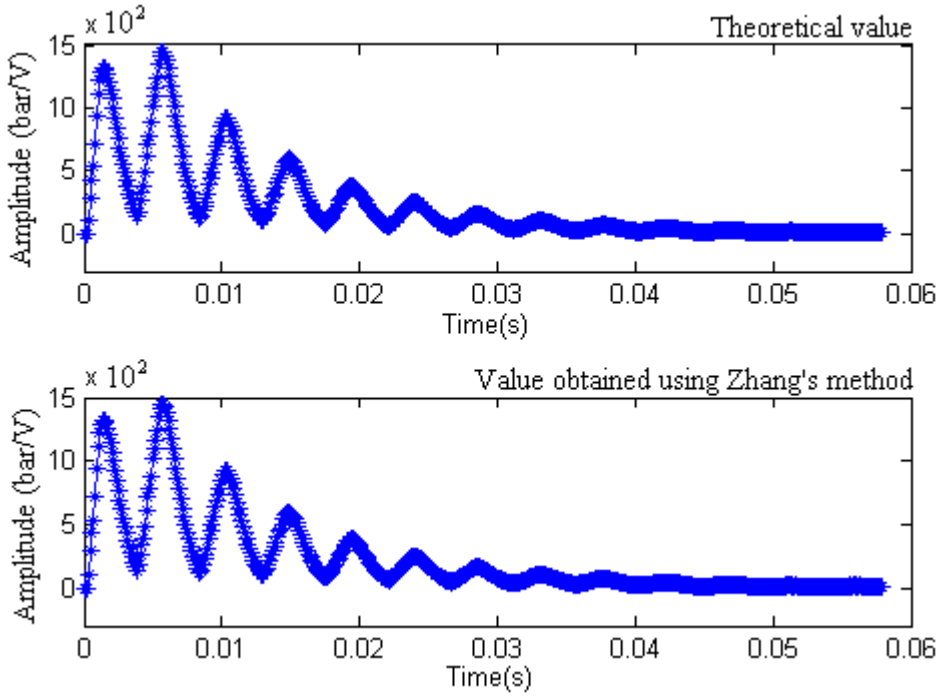

Figure 6.21 Comparison of 512-order estimated secondary path impulse response with $k_p = 0.2$

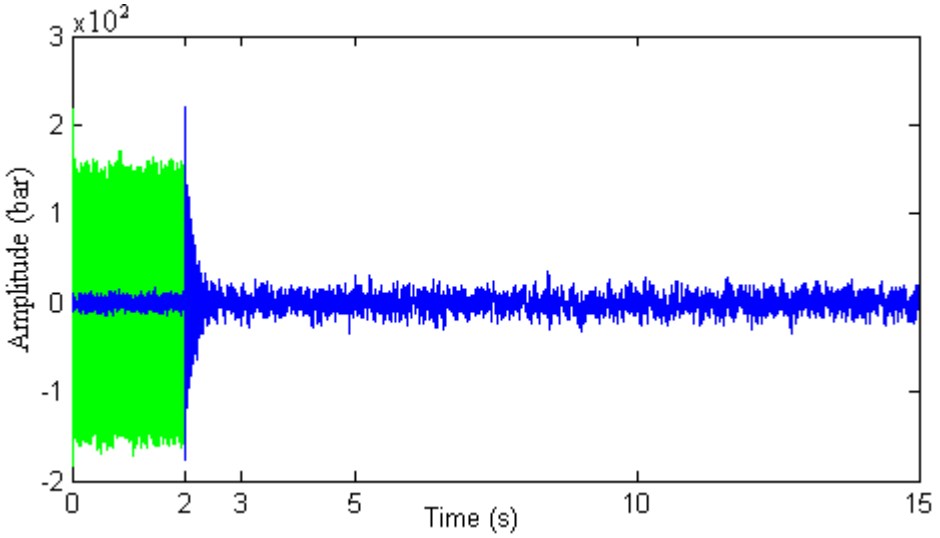

Figure 6.22 Single frequency cancellation result using Zhang's method

Multiple frequency 300 Hz, 600 Hz and 900 Hz fluid-borne noise is also applied in Zhang's method. Simulation conditions are the same as those for single frequency cancellation. The amplitude of the three different frequencies signal summation is about eight times bigger than that of the white noise. 2 s is needed for first stage with $k_P = 1$ and in the second stage $k_P = 0.2$. As three different frequency cancellations operate at the same time, a smaller identification convergence factor 1×10^2 is applied at the beginning of the second stage. The whole adaptive process of the 50th point on the estimated impulse response is plotted in Figure 6.23. The accurate secondary path identification result is nearly the same as the one shown in Figure 6.21. The effective noise cancellation result is shown in Figure 6.24. Although white noise turbulence on noise cancellation and secondary path estimation is eliminated, in experiment this auxiliary cannot be cancelled, as shown in Figure 6.24.

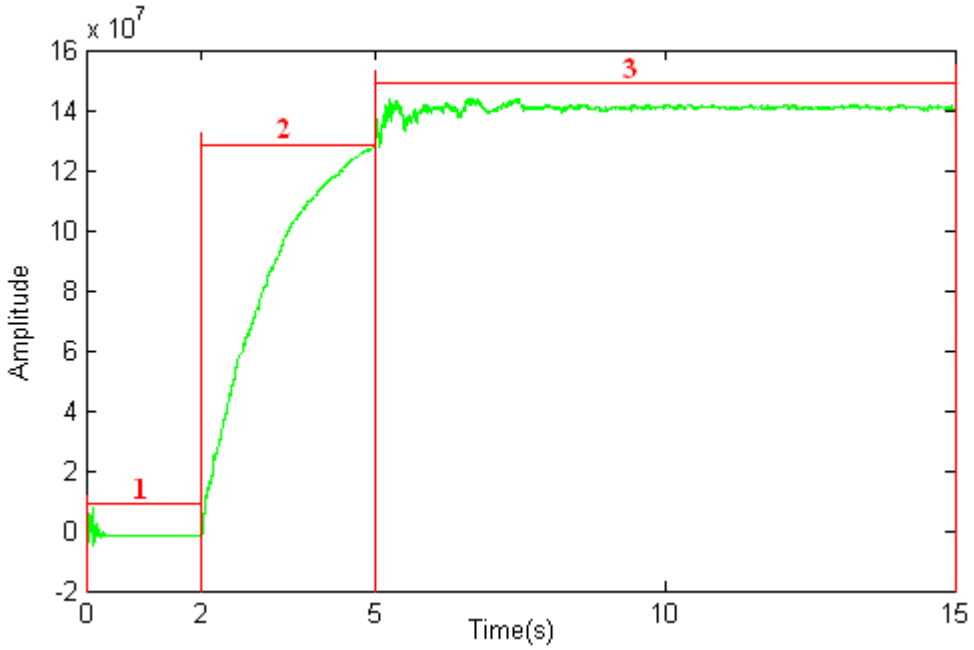

Figure 6.23 Adaptive process of the 50th point on estimated secondary path impulse response with k_P changing from 1 to 0.2 for multiple frequency using Zhang's method

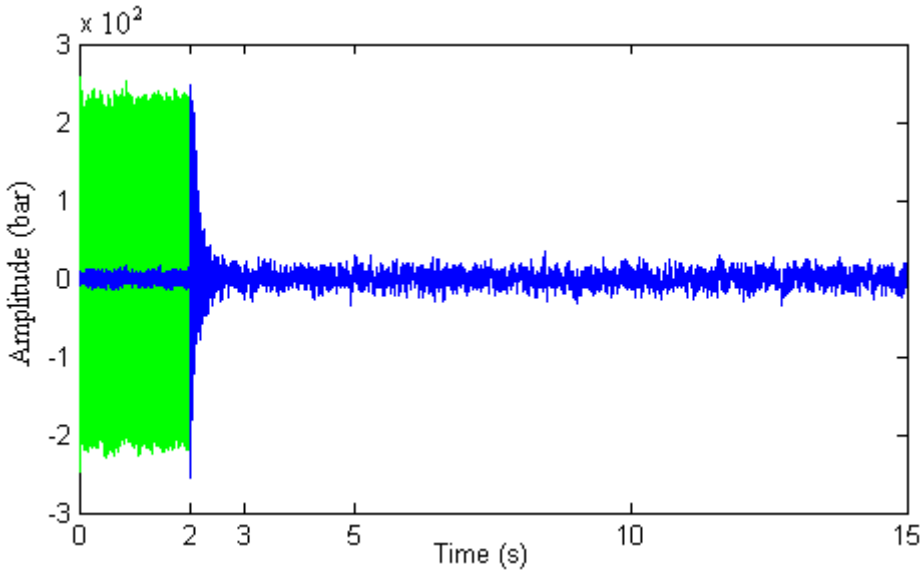

Figure 6.24 Multiple frequency cancellation result using Zhang's method

To summarize, as the reflection factor may change with variation of flow in the pipe, two different reflection factors can be applied in two stages. From results obtained using both the improved Bao's method and Zhang's method, accurate secondary path impulse response and good fluid-borne noise cancellation results are obtained using this strategy using big reflection change (k_P from 1 to 0.2), provided that there is enough length of identification of weighting functions. Additionally, in the second stage, as an adaptive process is needed for both secondary path identification and noise cancellation, which can affect the identification process, a smaller identification convergence factor needs to be applied at the beginning of the second stage. Because of the effect generated by the two-weight adaptive notch filter on the uncancelled white noise in the improved Bao's method, distorted secondary path estimation may occur and may make the system unstable with a large convergence factor for the two-weight adaptive notch filter. Additionally, a large convergence factor of two-weight adaptive filter can give a large effect on the secondary path impulse response at the beginning of second stage. In Zhang's method the secondary path estimation and the interference cancellation without white noise distortion are cross-updated, hence a large convergence factor of two-weight adaptive filter can also make the system unstable. A possible way to solve this problem is by using a relatively small identification convergence factor for a longer time; however, the convergence speed may decrease. During simulation it is found that if the reflection factor k_P is suddenly changed to a value between 0.1 and 0, the

system may become unstable because the phase difference between secondary path and its estimation may suddenly drift out of $\pm 90^{\circ}$. Furthermore, theoretically there are infinite frequency components in the pipe, but depending on computation ability only a finite number of frequencies can be attenuated. Therefore inaccurate secondary path estimation may be obtained with powerful uncancelled interferences in real experiment.

6.2.2 Second strategy

In the following part the second strategy for operating simulation and real experiment is presented using improved Bao's method and Zhang's method. In the first strategy accurate secondary path impulse response is obtained in the first stage. However, reflection factor k_P is changed from 1 to a small value, which means the dynamic characteristics of secondary path are changed and the impulse response needs to be updated by identification controller. Therefore another identification process, during which the whole system may become unstable, is needed. In the first strategy, changes in k_P beyond the range from 1 to 0.2 may cause instability. Another strategy without changes of reflection factor is presented. Primary fluid-borne noise along with the flow generated by the pump, interference cancellation controller and identification part are switched on without running the noise cancellation controller in the first stage. Then the noise cancellation controller is switched on and an estimated secondary path impulse response is applied for compensation synchronously in the second stage. As primary noise and flow generated by pump are injected into the pipe from the beginning of the first stage and the control flow is significantly smaller compared with them, reflection factor k_P can be assumed as a constant value during the whole process. Hence effects from reflection change can be eliminated. However, because primary noise exists with secondary path identification in the first stage, longer running time and length of identification weighting function are needed to obtain more accurate secondary path estimation. Additionally, a smaller reflection factor corresponds to a more complicated secondary path. The reflection factor in this strategy is set to 0.2 for both improved Bao's method and Zhang's method in simulation. Furthermore, because a short adaptive process is needed from control flow injection until noise is attenuated, a smaller identification convergence factor may be applied to ensure convergence at the beginning of the second stage.

Firstly, the improved Bao's method is simulated. Primary noise, which is 300 Hz with amplitude six times bigger than that of white noise, exists in the first stage. Consequently in order to obtain accurate secondary path impulse response longer running time and weighting function are needed. Convergence factors for two-weight adaptive filter and interference controller are the same as the used in the first strategy separately. The length of identification weighting function is 512. Then the noise cancellation controller is switched on and a relatively small value of identification convergence factor is applied. Accurate secondary path impulse response in the first stage is plotted in Figure 6.25 and compared with its theoretical value.

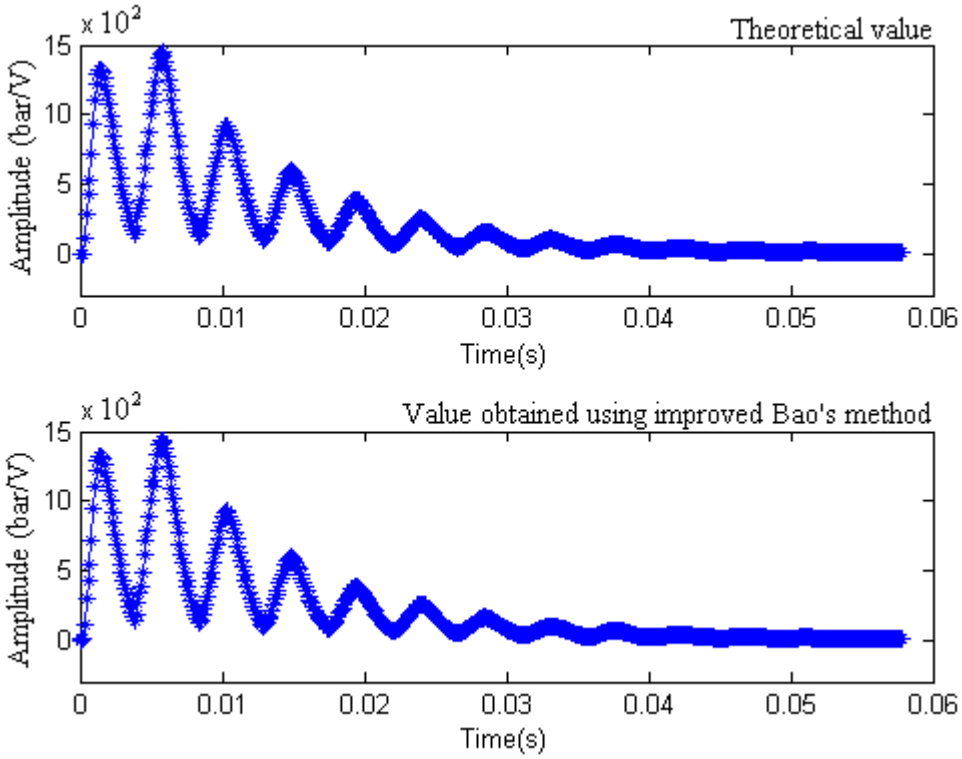

Figure 6.25 Comparison of 512-order estimated secondary path impulse response in the first stage with $k_P = 0.2$ under second strategy

The adaptive process of the 50th point on the secondary path impulse response is plotted as in Figure 6.26. 2×10^3 is used for the identification convergence factor in period 1. As in the second stage, the secondary path impulse response does not change 1×10^3 is used in second period for 1 s. To give a fast convergence speed, 2×10^3 is applied as the identification convergence factor in the third period.

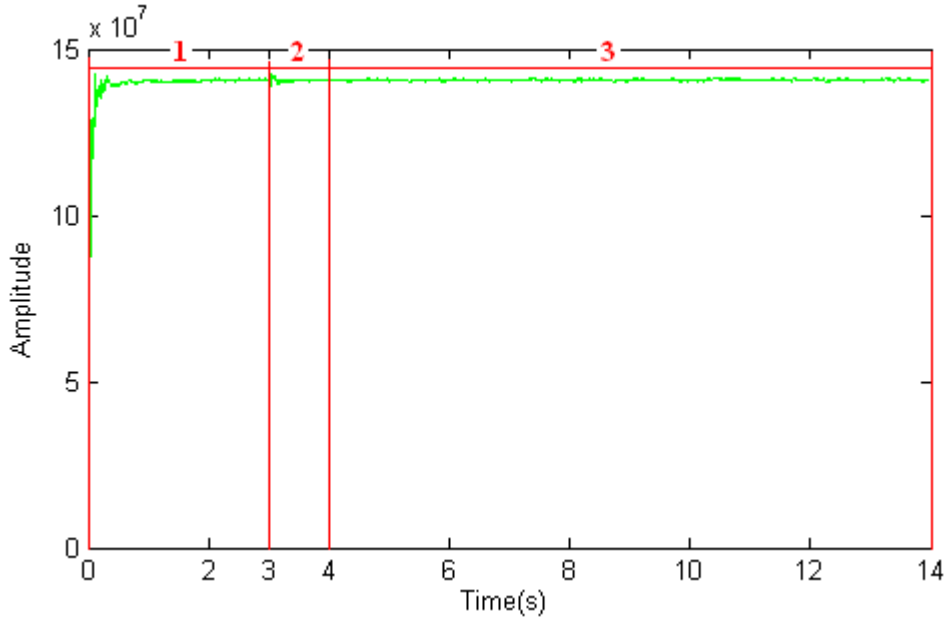

Figure 6.26 Adaptive process of the 50th point on estimated secondary path impulse response with $k_P = 0.2$ using improved Bao's method under second strategy

Residual fluid-borne noise signal during whole process is plotted in Figure 6.27.

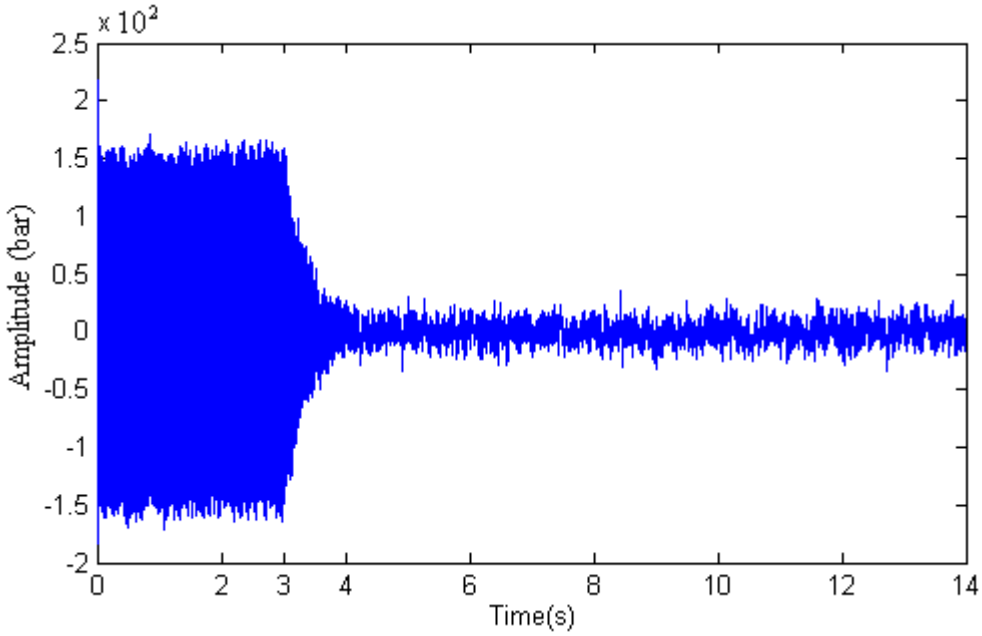

Figure 6.27 Single frequency cancellation result using improved Bao's method under second strategy

From this result, a good cancellation result is obtained. In the residual signal only auxiliary white noise, which is much smaller than the uncancelled primary fluid-borne noise, is left.

Furthermore, using the same process as that used in single frequency cancellation, multiple frequency noise cancellation is also simulated at 300 Hz, 600 Hz and 900 Hz with $k_P = 0.2$. The amplitude of the three summated signals is about eight times bigger than that of white noise. In the first stage because of the three different frequency signals, more running time is needed to obtain an accurate secondary path impulse response, which is nearly the same as the one in Figure 6.25.

The adaptive process of one point on impulse response is plotted in Figure 6.28.

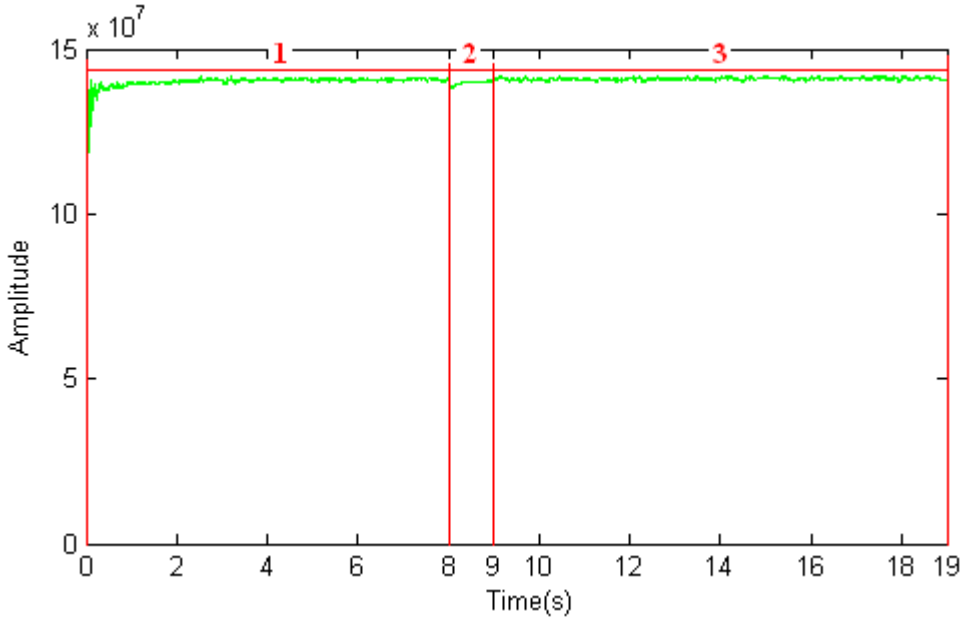

Figure 6.28 Adaptive process of the 50th point on estimated secondary path impulse response with $k_P = 0.2$ for multiple frequency using improved Bao's method under second strategy

As shown in period 1 in the above plot, longer simulation time is needed to obtain an accurate estimated impulse response. Additionally, during period 2 a smaller identification convergence factor of 2×10^{2}, compared with that used for single frequency cancellation, is applied because of more effect coming from three

cancellation processes. 2×10^3 is also used in the third period to give a fast convergence speed.

The noise cancellation result is plotted in Figure 6.29, only the auxiliary white noise is left.

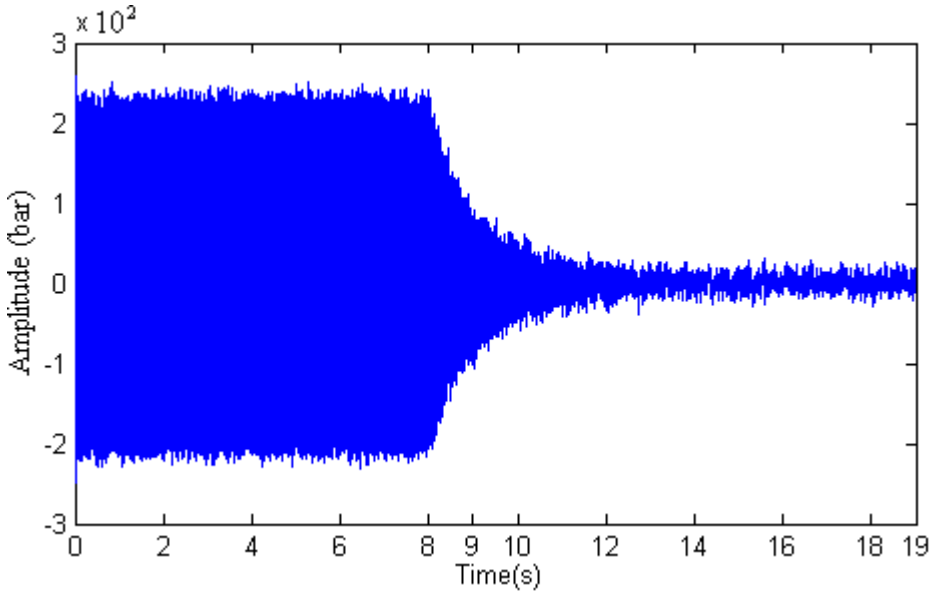

Figure 6.29 Multiple frequency cancellation result using improved Bao's method under second strategy

Simulation is also implemented using Zhang's method. The operation process is the same as that of single frequency noise cancellation using the improved Bao's method and a faster convergence factor of two-weight adaptive notch filter is used. The other parameters are the same as those used in the improved Bao's method. In the first stage, the primary noise and interference controller are switched on. At the beginning of this stage, the identification process can be affected. As the identification process and the accurate interference cancellation are cross-updated, more running time is needed for this stage to obtain an accurate secondary path impulse response, which is plotted in Figure 6.30. At the beginning of second stage, more running time is also needed because of cross-updated processes compared with the improved Bao's method.

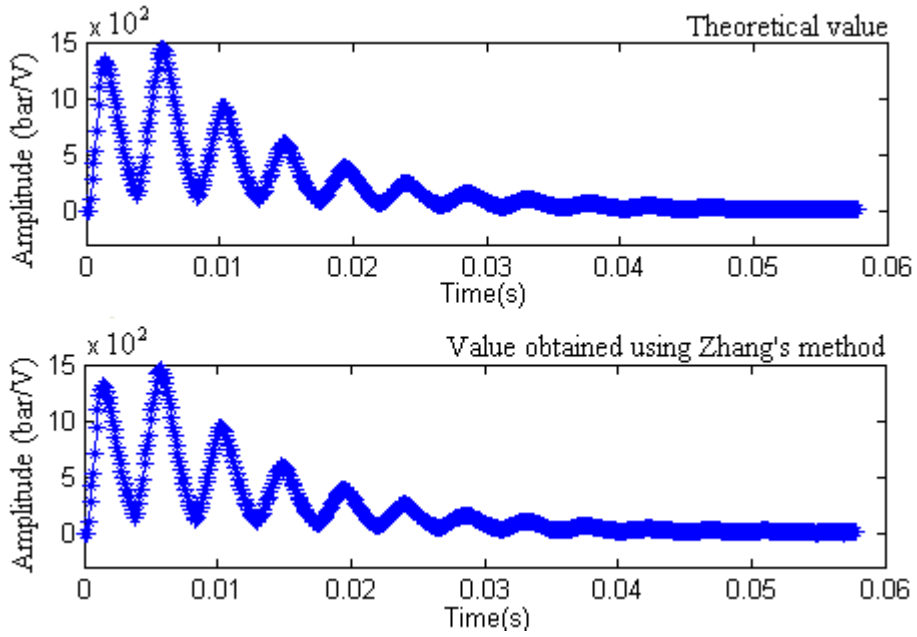

Figure 6.30 Comparison of 512-order estimated secondary path impulse response in the first stage with $k_P = 0.2$ using Zhang's method under second strategy

The adaptive process of the 50th point on estimated secondary path impulse response is shown in Figure 6.31.

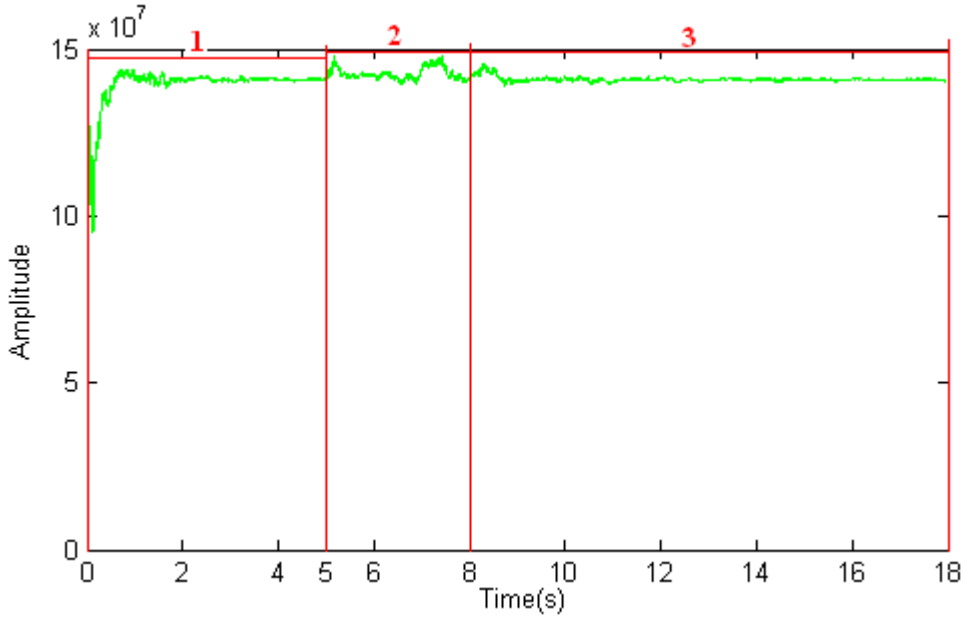

Figure 6.31 Adaptive process of the 50th point on estimated secondary path impulse response with $k_P = 0.2$ using Zhang's method under second strategy

As shown in the figure above, the first stage was running for 5 s, and 3 s is needed for the initial period in the second stage.

The cancellation result with fast convergence speed is plotted in Figure 6.32 compared with the uncancelled part in the first stage, which is the section from 0 s to 5 s.

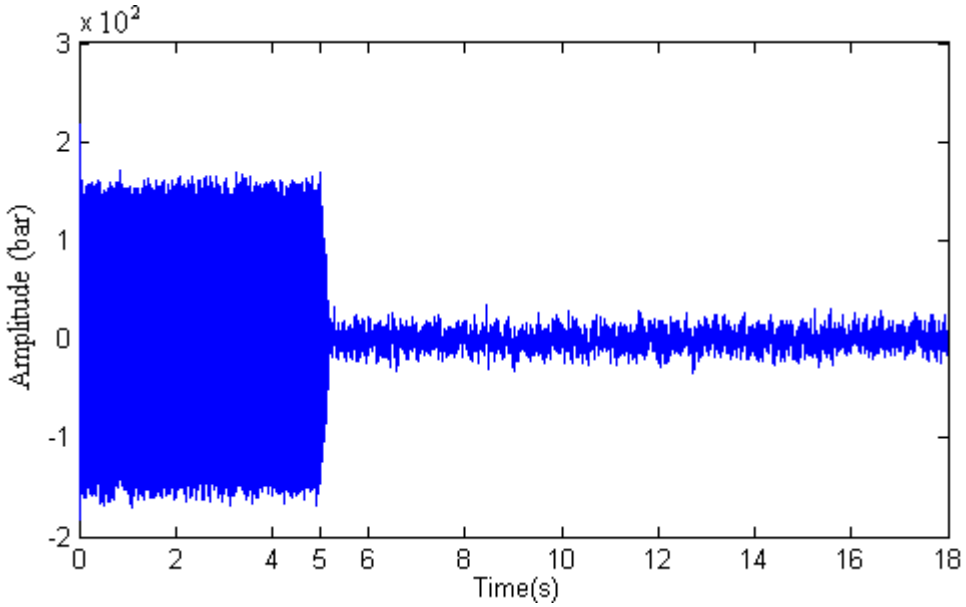

Figure 6.32 Single frequency cancellation result using Zhang's method under second strategy

Multiple frequency noise cancellation using 300 Hz, 600 Hz and 900 Hz is also implemented with 512 orders of secondary path impulse response, and the simulation process is the same as that of single frequency noise cancellation. As three different frequencies of noise cancellation are realized in this simulation, compared with single frequency cancellation process using Zhang's method, 10 s is needed for the first stage to obtain an accurate estimated secondary path impulse response, which is quite similar to that in Figure 6.30. For the same reason 2×10^{2} is used as the identification convergence factor at the beginning of second stage for 3 s rather than 1×10^{3}, which is applied in the single frequency cancellation, to keep the system stable. The whole process and other parameters are the same as those used for single frequency cancellation using Zhang's method. The adaptive process of 50^{th} point on estimated impulse response is plotted in Figure 6.33. Period 1 is the first stage; period 2 is the

beginning of second stage. In period 3, the identification convergence factor is 2×10^{3} to give a fast convergence speed.

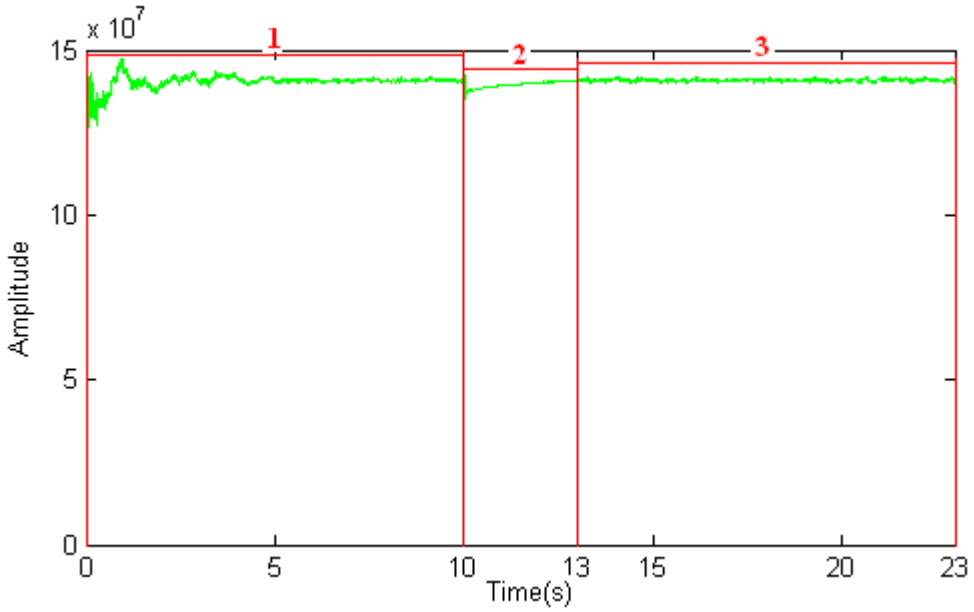

Figure 6.33 Adaptive process of the 50th point on estimated secondary path impulse response with $k_P = 0.2$ for multiple frequency using Zhang's method under second strategy

Noise cancellation result is plotted in Figure 6.34.

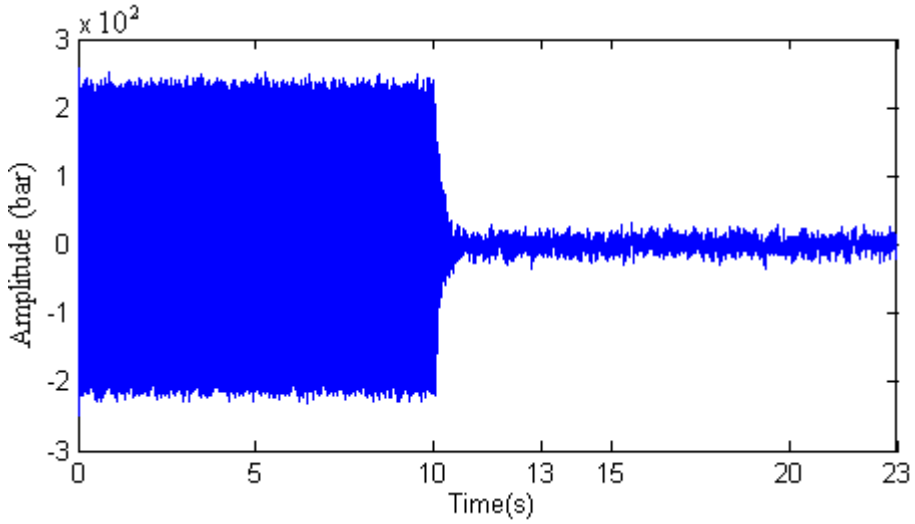

Figure 6.34 Multiple frequency cancellation result using Zhang's method under second strategy

To summarize, using this strategy a constant reflection factor is applied for both improved Bao's method and Zhang's method. Compared with the first strategy, because of the effect from interference cancellation a longer running time is needed to obtain accurate estimated secondary path impulse response in the first stage, especially for multiple frequency cancellation. This phenomenon is more serious for the cancellation using Zhang's method because of cross-updating of secondary path identification and accurate interference cancellation as described in section 6.1.4. Because the reflection factor can be seen as a constant value, the noise cancellation effect on the on-line identification becomes smaller. Hence a relatively big convergence factor can be applied for identification at the beginning of second stage.

Additionally, faster cancellation speed can be obtained using Zhang's method. However, the system may become unstable if the convergence factor of primary noise cancellation is too big because of large changes from primary noise and cross-updating in Zhang's method. Furthermore, as in first strategy, in a real experiment since many orders of fluid-borne noise frequency exist in the pipe, powerful components without attenuation may push the control system to instability.

In the next section another efficient on-line identification algorithm associated with a two-weight adaptive notch filter is also presented and evaluated during simulation with the pipe model.

6.3 Frequency domain on-line identification algorithms

As mentioned above, in time domain on-line identification algorithms auxiliary white noise, which is full of frequency components, is applied and a constant uniform convergence factor is used for all frequency components in each stage. In conjunction with an interference attenuation controller accurate secondary path estimation is obtained. In this section another algorithm is presented to obtain accurate impulse response estimation. Rather than using a constant value an adaptive function is applied for identification convergence factor on each frequency component. Realization of this process needs to be implemented in frequency domain. Identification part is shown in Figure 6.35, which can replace the dashed line part in Figure 6.1 [31, 37].

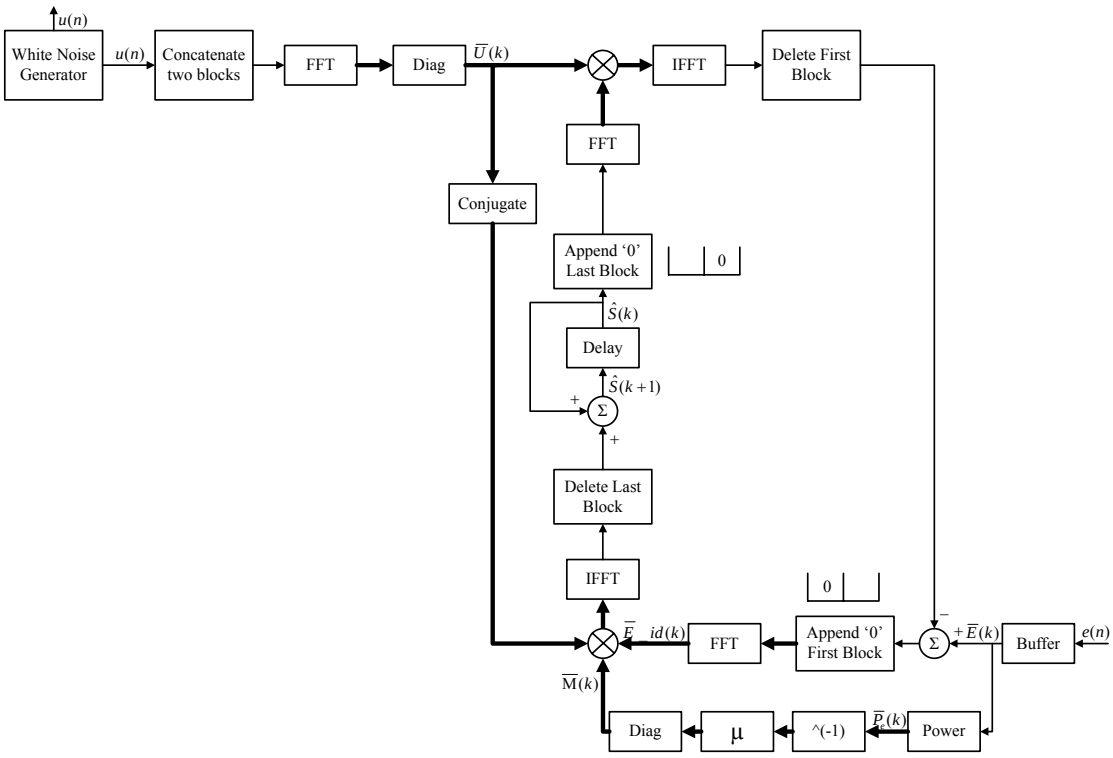

Figure 6.35 Frequency domain on-line identification part

In time domain, updating of identification weighting function can be written as:

$$\overline{w}(n+1) = \overline{w}(n) + \mu \cdot \overline{x}(n) \cdot e(n)$$

In this algorithm, rather than sample by sample the signals are processed block by block. The weighting function is not updated until the next block. Therefore the last term on the right side in the above equation becomes:

$$\mu \cdot \sum_{i=0}^{L-1} \overline{x}(kL+i)e(kL+i) = \mu \cdot \sum_{i=0}^{L-1} x_j(kL+i-j) \cdot e(kL+i) \qquad (6.1)$$

where $j = 0 \quad 1 \quad \cdots \quad M-1$

which is a cross correlation form between $x(kL+i)$ and $e(kL+i)$.

Control flow deduced in time domain is:

$$\overline{y}(n) = \overline{w}^T(n) \cdot \overline{x}(n)$$

In this block based algorithm it can be written as:

$$\bar{y}(kL+i) = \overline{w}^T(k)\bar{u}(kL+i) = \sum_{j=0}^{M-1} w_j(k)u(kL+i-j) \tag{6.2}$$

where $i = 0 \quad 1 \quad \cdots \quad L-1$

which is a convolution form between *w* and *u*.

Usually in practice *M* and *L*, which are the length of the weighting function and block, in equations (6.1) and (6.2), are equal to each other for simplicity of computation [27,31].

In order to increase the computation speed, fast convolution and fast cross correlation calculated using the "overlap-save" method are applied in frequency domain [38,39]. In Figure 6.35 the frequency domain calculation is denoted using a thick black line. Firstly the input white noise signal is buffered into two blocks, and then translated into frequency domain as diagonal of $2L \times 2L$ matrix:

$$\overline{U}(k) = diag\{FFT[\bar{u}(k-1) \quad \bar{u}(k)]\}$$

Updating of the weighting function can be realized using the following equation:

$$\hat{S}(k+1) = \hat{S}(k) + IFFT\{conj[\overline{U}(k)] \cdot \overline{\mathrm{M}}(k) \cdot \overline{E}\_id(k)\}_{last\_block}$$

where *k* denotes the number of the block, whose length is *L*, and $\overline{E}\_id(k)$ in the equation above is the block error signal used to obtain secondary path estimation:

$$\overline{E}\_id(k) = FFT\left\{\bar{E}(k) - IFFT\left[\overline{U}(k) \cdot FFT\begin{bmatrix}\hat{S}(k)\\ 0_{L\times 1}\end{bmatrix}\right]_{last\_block}\right\}$$

During this process, the appended zeros and discarded blocks are particular calculation method used in the over-lap saving algorithm, which is described in [38, 39].

Unlike time domain on-line identification methods, in which a constant value is used for identification convergence coefficient during the adaptive process, the convergence factor is an adaptive function of the estimated power residual noise signal $e(n)$ as shown in Figure 6.35. This factor is deduced in the frequency domain and different values assigned into individual frequency bins in order to increase convergence speed and eliminate the interference effect of residual primary noise. This equation can be presented as:

$$\overline{\mathrm{M}}(k) = diag\left[\mu \cdot \frac{1}{\overline{P}_e(k)} \right]$$

where μ is a constant value used to adjust convergence speed and $\overline{P}_e(k)$, which is the power estimation of the residual noise signal *e*, can be estimated using a first-order low pass filter:

$$\overline{P}_e(k+1) = \gamma \cdot \overline{P}_e(k) + (1-\gamma) \cdot \left| FFT\begin{bmatrix} 0_{L\times 1} \\ \overline{E}(k) \end{bmatrix} \right|^2$$

γ controls the amount of smoothing of $\overline{P}_e(k)$. The initial value of $\overline{P}_e(k)$ can be set to zero or small positive value in this case. By applying this adaptive convergence factor, updating at the interference frequency component becomes significantly smaller when large residual primary noise exists. Hence stability can be ensured with large interference.

Firstly similarly to the comparison between the improved Bao's method and Zhang's method at beginning of section 6.2.1, this frequency domain cancellation method is compared with the improved Bao's method and Zhang's method. A 300 Hz sine wave is applied as the primary noise, length of identification weighting function is 128 and the reflection factor $k_P = 0.6$. A big convergence factor for two-weight adaptive notch filter is used for these three methods. The operation process is under the first strategy. The estimated secondary path impulse responses obtained in the second stage are plotted in Figure 6.36 and compared with the theoretical value.

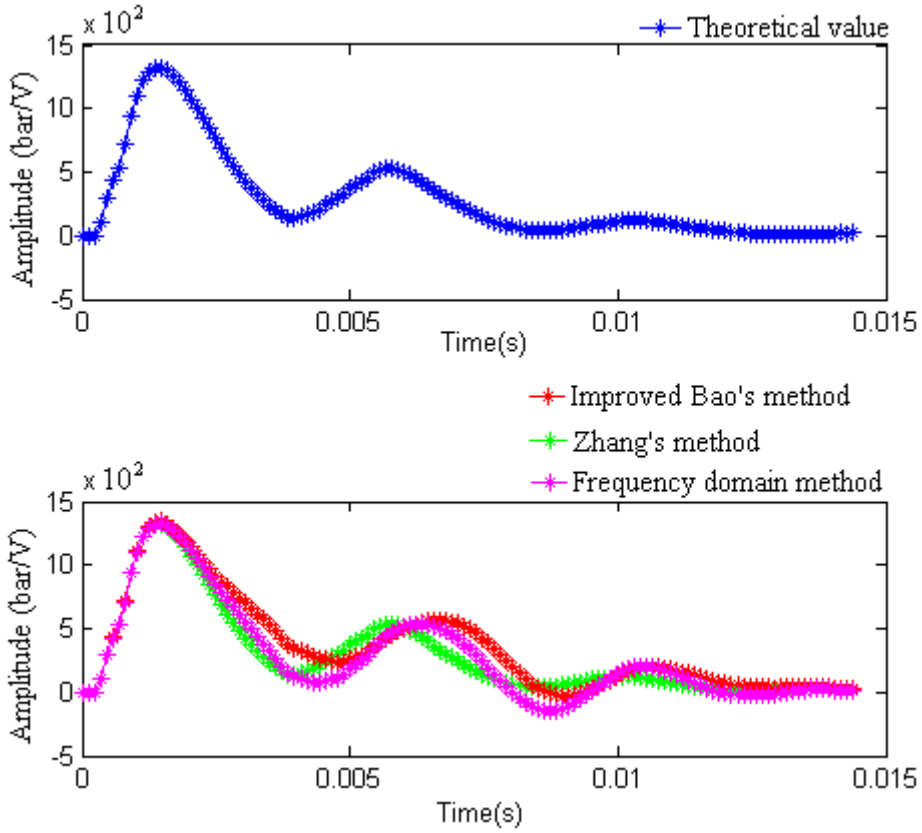

Figure 6.36 Comparison of 128-order secondary path impulse response with $k_P = 0.6$

Combining Figure 6.1 and Figure 6.35, the white noise in $e(n)$ cannot be eliminated and comes directly to the two-weight adaptive notch filter. The additional signal w_a, which is represented in section 6.2.1 exists and can distort the secondary path identification as shown in Figure 6.36. The system may become unstable under this effect. Additionally from the comparison in Figure 6.36 the distortion level of the secondary path impulse response obtained using the frequency domain method is better than the one obtained using the improved Bao's method. The possible reason may be that the signal w_a is filtered by an interference controller before being used for identification in the improved Bao's method.

Secondly as in real experiment the harmonic components of fluid-borne noise are infinite, however, only finite components can be cancelled according to the processor ability, hence comparison of cancellation ability is also simulated between Zhang's method and the frequency domain method with the effect of some uncancelled harmonic

components being included. In this simulation the primary noise is a 300 Hz sine wave, with amplitude six times bigger than that of the white noise. The uncancelled harmonic components are 600 Hz and 900 Hz sine waves, with amplitudes nine times smaller than that of primary noise. Reflection factor $k_P = 0.2$ and the same small convergence factors of the two-weight adaptive notch filter are selected for the two methods. For the frequency domain method, as the initial value of the error power cannot be considered a maximum limitation of 100 is set for the identification convergence factor. The estimated secondary path impulse responses are plotted in Figure 6.37 and compared with the theoretical value.

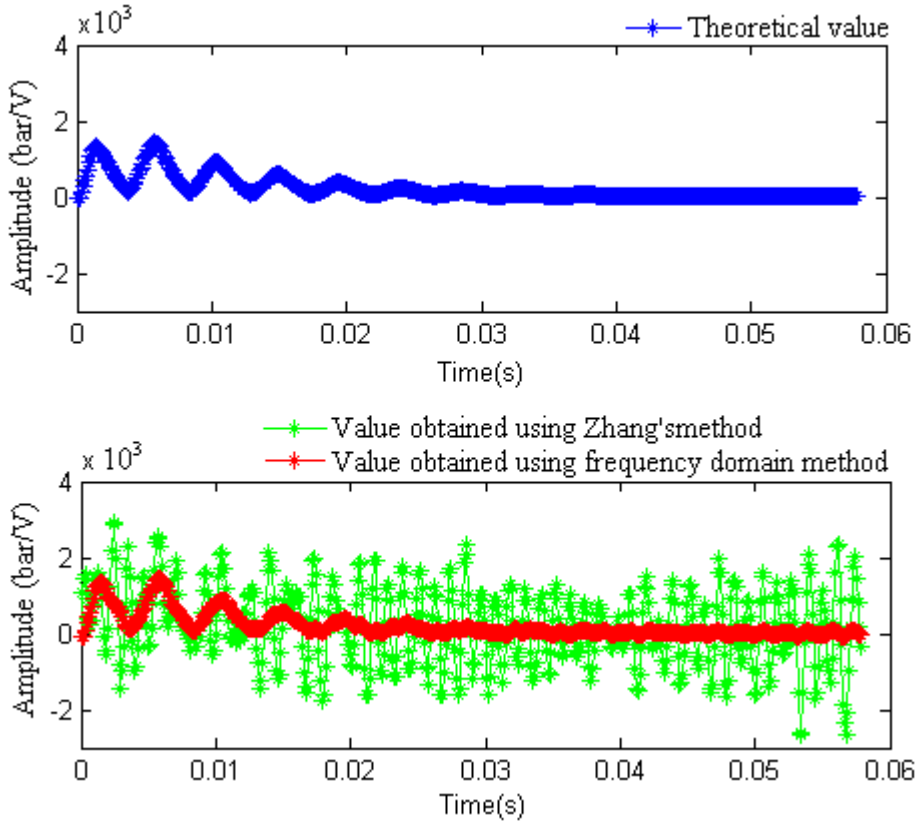

Figure 6.37 Comparison of 512-order secondary path impulse response using $k_P = 0.2$ with effect from uncancelled harmonics

For Zhang's method, the amplitudes of the uncancelled harmonic components are large relative to the white noise, and they affect the on-line secondary path identification. The distorted estimated impulse response is plotted as shown by the green line in Figure 6.37. Under the effect of the distorted identification, the system may become unstable. By decreasing the amplitudes of the uncancelled harmonic components a more accurate

identification result can be obtained and the system may be stable. Compared with Zhang's method, an accurate identification result is obtained using the frequency domain algorithm. The reason is that relatively small identification convergence factors are applied on the uncancelled frequency components, which is equivalent to the effect of using small amplitudes of the uncancelled components. The convergence factors on each frequency components are plotted in Figure 6.38.

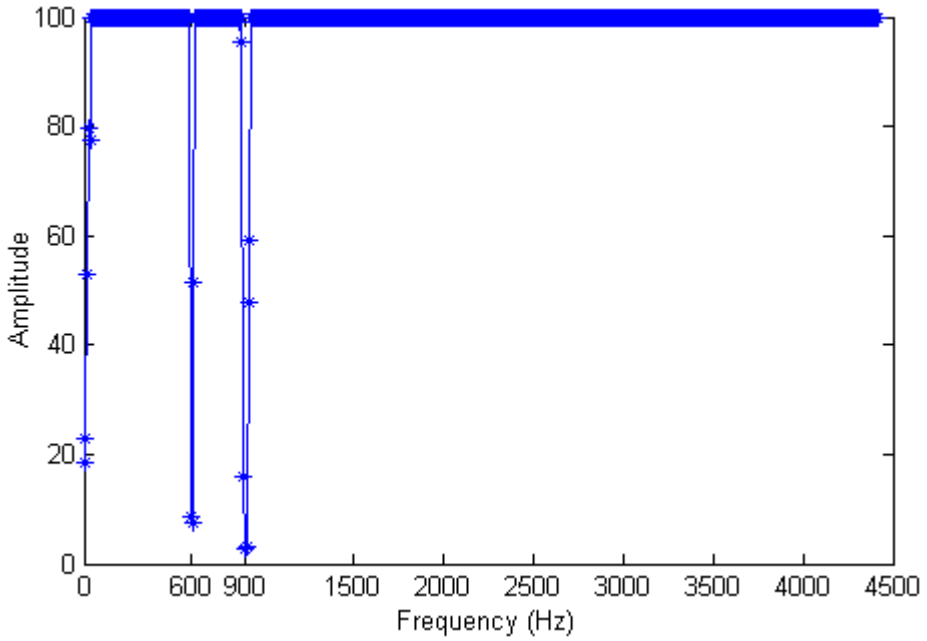

Figure 6.38 Convergence factor for each frequency component

From the plot above small convergence factors are applied for the uncancelled frequency components 600 Hz and 900 Hz.

Simulation was also implemented to cancel fluid-borne noise using the first strategy on this method associated with two-weight adaptive LMS notch filter. The length of the secondary path identification weighting function was 512. Primary noise is a 300 Hz sine wave, with amplitude six times bigger than that of the white noise. The same convergence factors are applied for two-weight adaptive notch filters with those used in Zhang's method. As the initial value of the error signal cannot be considered, a maximum limitation is set to ensure stability. The other advantage of this limitation is that a constant identification convergence factor can be used to obtain a accurate impulse response estimation because the power of the white noise is not constant.

During simulation in the first stage $k_P = 1$. The estimated secondary path impulse response and the convergence factor for each frequency bin are plotted in Figure 6.39.

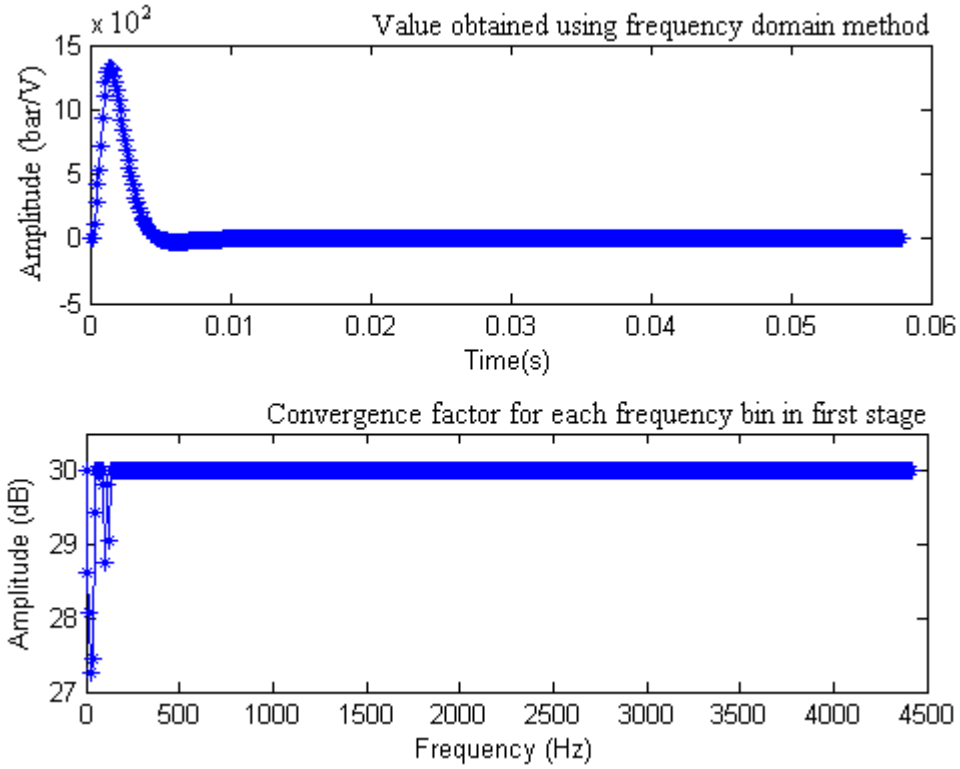

Figure 6.39 Estimated secondary path impulse response and convergence vector in the first stage

From the figure above some convergence factors at the low frequency components are smaller than the maximum limitation, because the corresponding frequency components have bigger power. An accurate impulse response estimation is also obtained.

In the second stage, the reflection factor is $k_P = 0.2$. In order to eliminate the residual primary noise effect, the adaptive convergence function can give small value according to the power of the residual noise. The plot of the convergence factors for each frequency component is plotted in Figure 6.40 when the primary noise comes into the system at the beginning of the second stage.

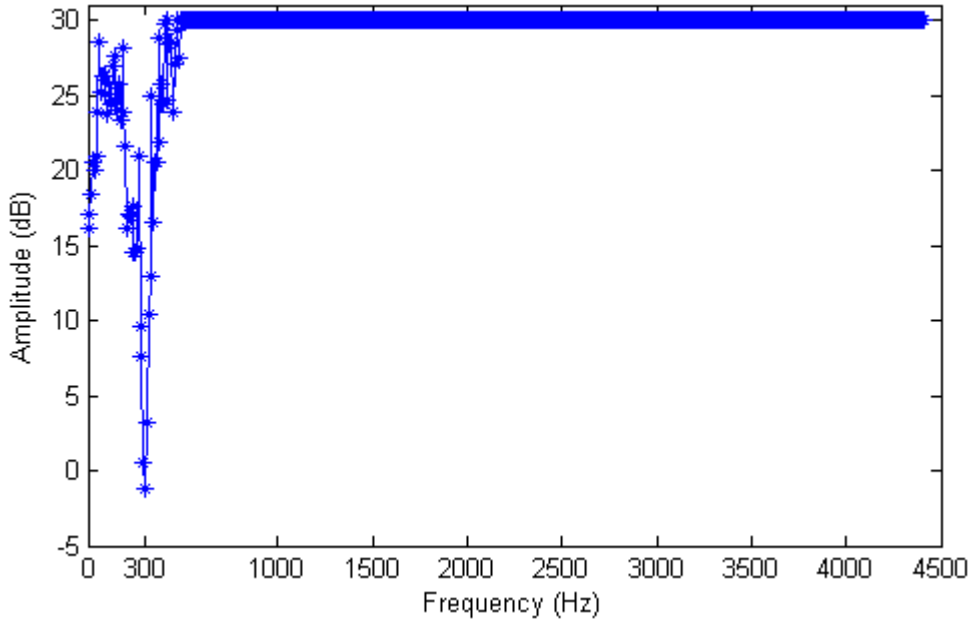

Figure 6.40 Identification convergence factor at the beginning of the second stage

However as seen from the figure above, firstly during simulation the fast Fourier transform calculation can introduce 'leakage' at the frequencies which are not the interference frequency. Secondly the peak value in the spectrum of frequency domain convergence function can drag the other nearby values up or down. These two effects can decrease the identification convergence speed on the corresponding frequency components. Additionally, the power of white noise accumulated by the buffer is not constant along the time in simulation, which can make the identification result oscillate around the optimum value. To solve this problem, the maximum limitation can be set to a small value; however, the whole convergence speed of identification may be decreased. As the decreasing process of primary noise may affect the on-line identification the convergence vector can be multiplied by a value smaller than 1 (0.5 is selected here) for a short period (period 2 in Figure 6.42). Then the identification convergence vector can be multiplied by 1 or a suitable bigger value to give a fast speed. Along with the cancellation process, residual primary noise becomes smaller and the convergence factor at 300 Hz becomes bigger to give a fast convergence speed in the second stage. The estimated secondary path impulse response in the second stage is plotted in Figure 6.41 compared with the theoretical value and the identification convergence vector is quite similar to the one in Figure 6.39.

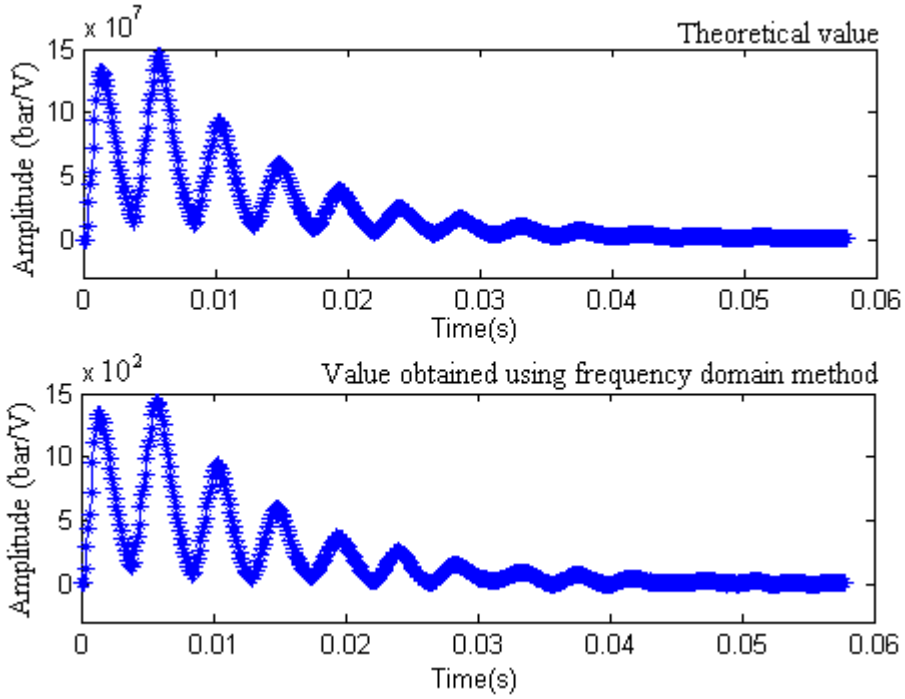

Figure 6.41 Comparison of 512-order estimated secondary path impulse response in the second stage with $k_P = 0.2$

The adaptive process of the 50th point on the estimated secondary path impulse response is plotted in Figure 6.42.

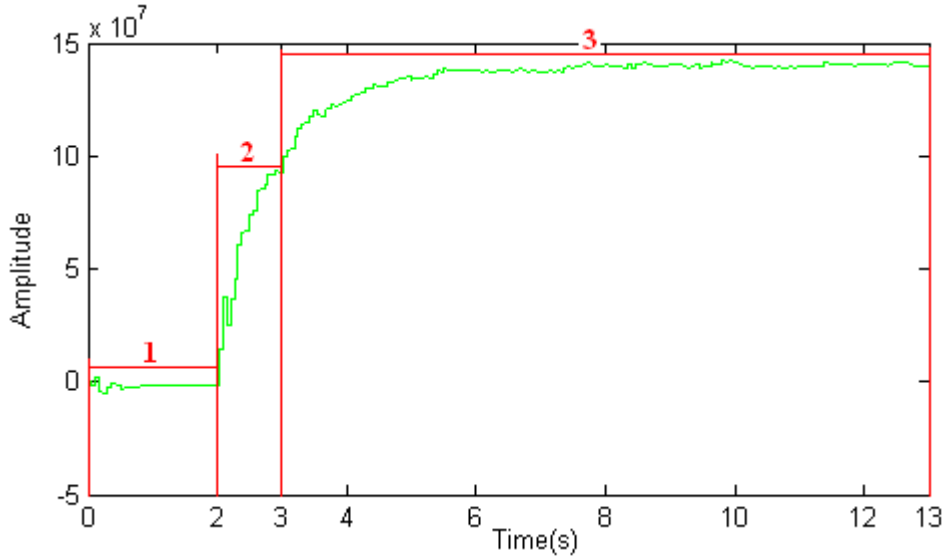

Figure 6.42 Adaptive process of the 50th point on estimated secondary path impulse response with k_P changing from 1 to 0.2 using frequency domain method

The cancellation result is plotted in Figure 6.43.

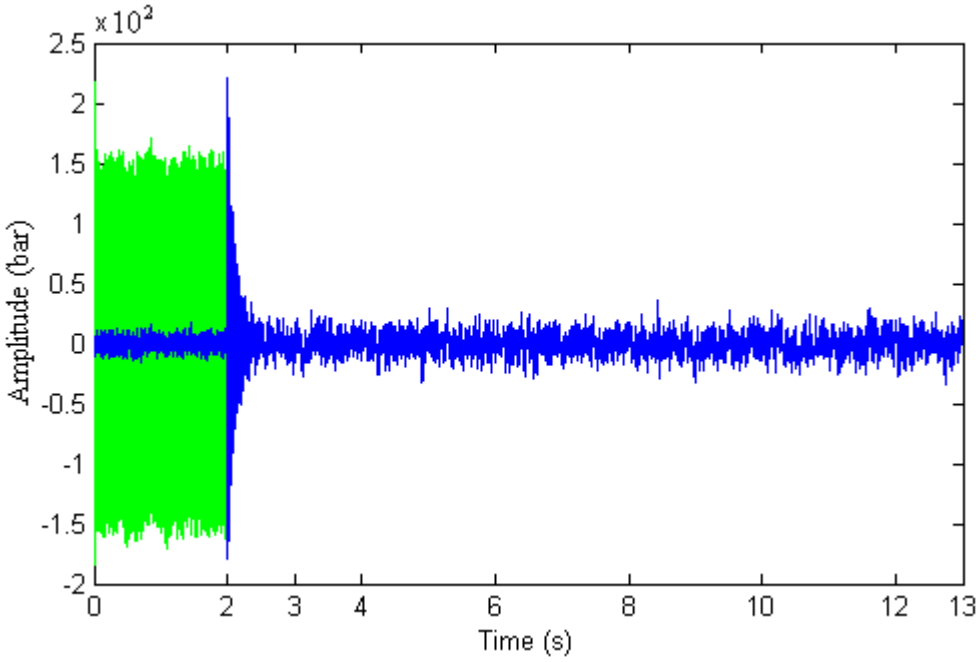

Figure 6.43 Single frequency cancellation result using frequency domain method

For multiple frequency fluid-borne noise cancellation simulation is implemented using primary noise with frequencies 300 Hz, 600 Hz and 900 Hz. The operation process and parameters applied are the same as those of single frequency noise cancellation. The estimated secondary path impulse response and the identification convergence vector in the first stage are quite similar to that in Figure 6.39.

The identification convergence vector used for each frequency component at the beginning of the second stage is plotted in Figure 6.44. As with single frequency cancellation, convergence factors at target frequencies are much smaller than the others when large residual noise exists at the beginning of the second stage.

As three frequency cancellations are operated, the greater decrease of the primary noise may give a large effect on the on-line identification at the beginning of second stage. Therefore, compared with the single frequency cancellation the identification convergence vector is multiplied by 0.1, which is smaller than the value 0.5 used for single frequency cancellation, at this period.

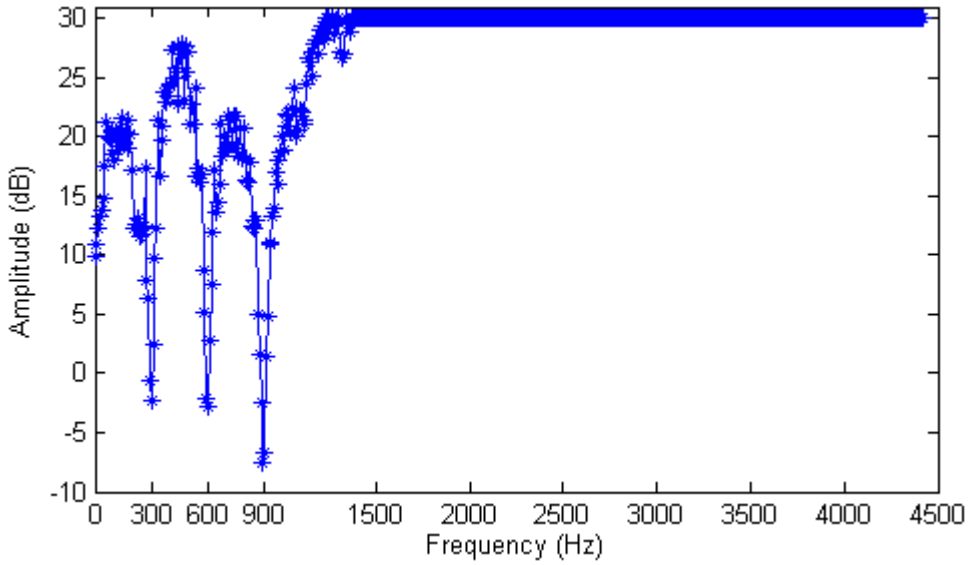

Figure 6.44 Identification convergence factor at the beginning of the second stage for multiple frequency

Then along with attenuation of primary fluid-borne noise, the convergence factors at target frequencies are increased until the maximum limitation value is achieved in the second stage. The accurate estimated secondary path impulse response can be represented using that shown in Figure 6.41.

The adaptive process of the 50^{th} point on the estimated impulse response is plotted in Figure 6.45 and the cancellation result is plotted in 6.46.

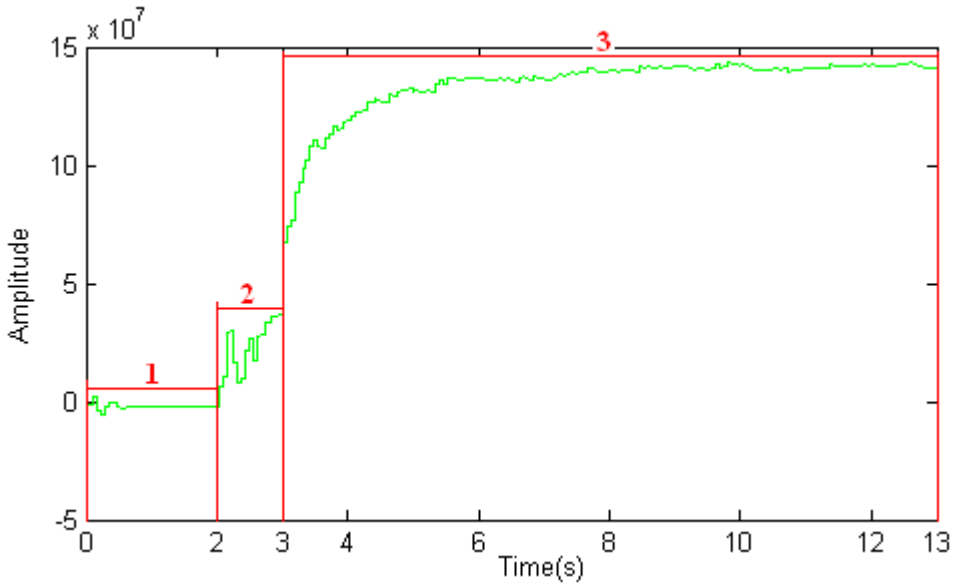

Figure 6.45 Adaptive process of the 50th point on estimated secondary path impulse response with k_p changing from 1 to 0.2 using frequency domain method for multiple frequency

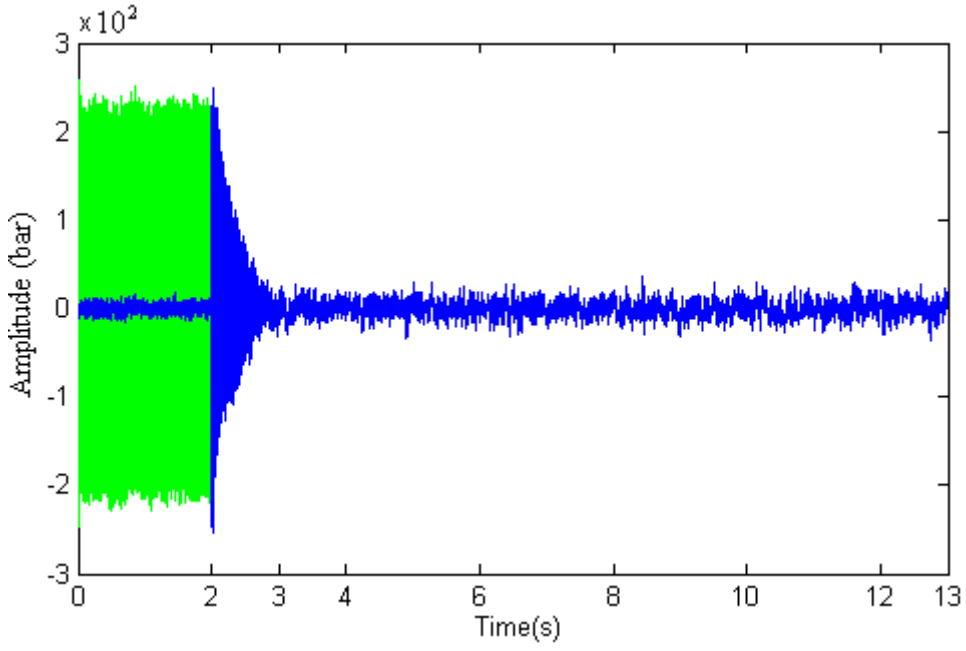

Figure 6.46 Multiple frequency cancellation result using frequency domain method

This frequency domain control algorithm is also simulated using the second strategy as applied for time domain methods. In the first stage the identification controller with primary noise, which is 300 Hz with amplitude six times bigger than that of white noise, is switched on. The length of identification weighting function is 512, and the reflection factor is $k_P = 0.2$. Compared with using this method under the first strategy, the identification convergence factor is multiplied by 0.5 and the value for maximum limitation is also half of the one used under the first strategy. The identification convergence vector is plotted in Figure 6.47.

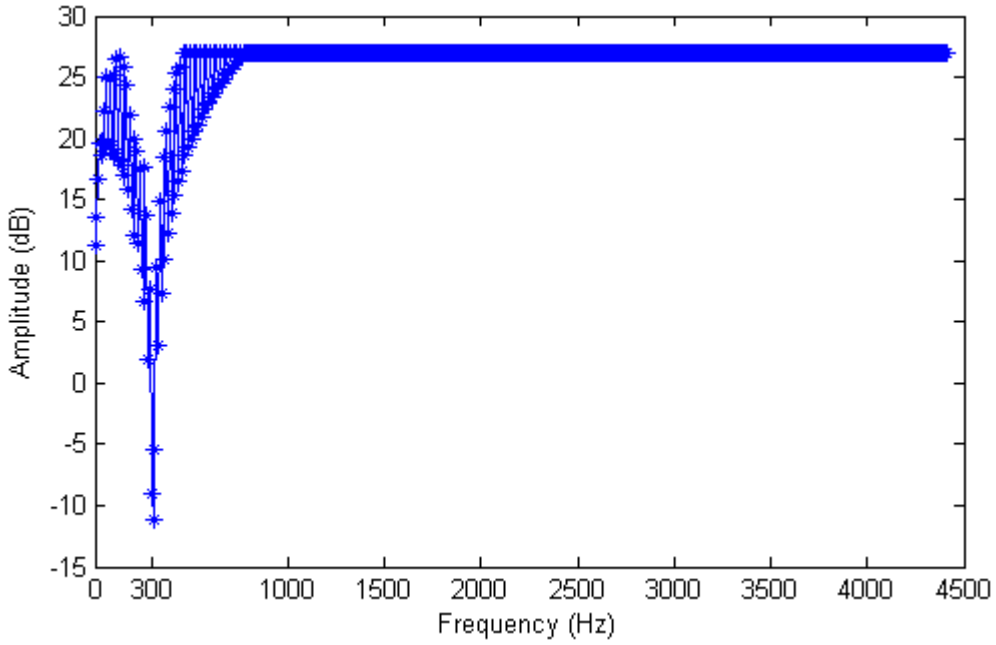

Figure 6.47 Identification convergence factor in the first stage under the second strategy

However, the interference effect from primary noise still has a large effect on the secondary path identification with a small convergence factor at that frequency. The distorted estimated impulse response plotted in Figure 6.48 (b) compared with the theoretical value in Figure 6.48 (a) can make the system unstable at the start of second stage. About 10 s is needed for the identification to converge as plotted in Figure 6.49 (a). A possible way to obtain the accurate impulse response is to multiply the identification convergence vector by a small value. In this simulation this factor is 0.05. Under this effect a more accurate estimated impulse response is obtained as shown in Figure 6.48 (c). Adaptive process of the 50th point on the impulse response is plotted in

Figure 6.49 (b). However, about 150 s is needed for running time, which means in the real experiment that the convergence time is too long. Hence the frequency domain cancellation algorithm is only realized using the first strategy.

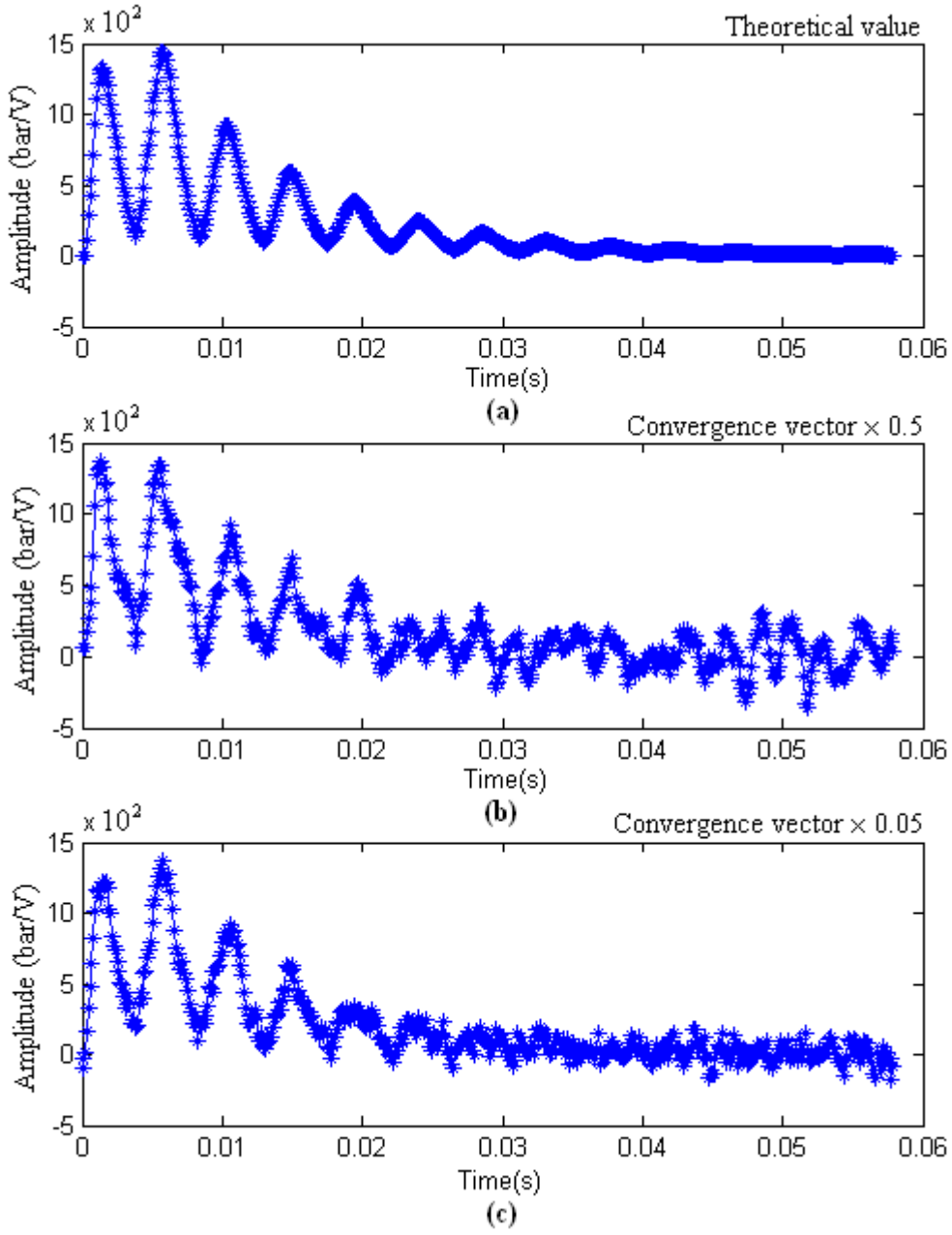

Figure 6.48 Comparison of 512-order estimated secondary path impulse response in the second stage using $k_P = 0.2$ with different convergence vectors. (a): theoretical value (b): convergence× 0.5 (c): convergence× 0.05

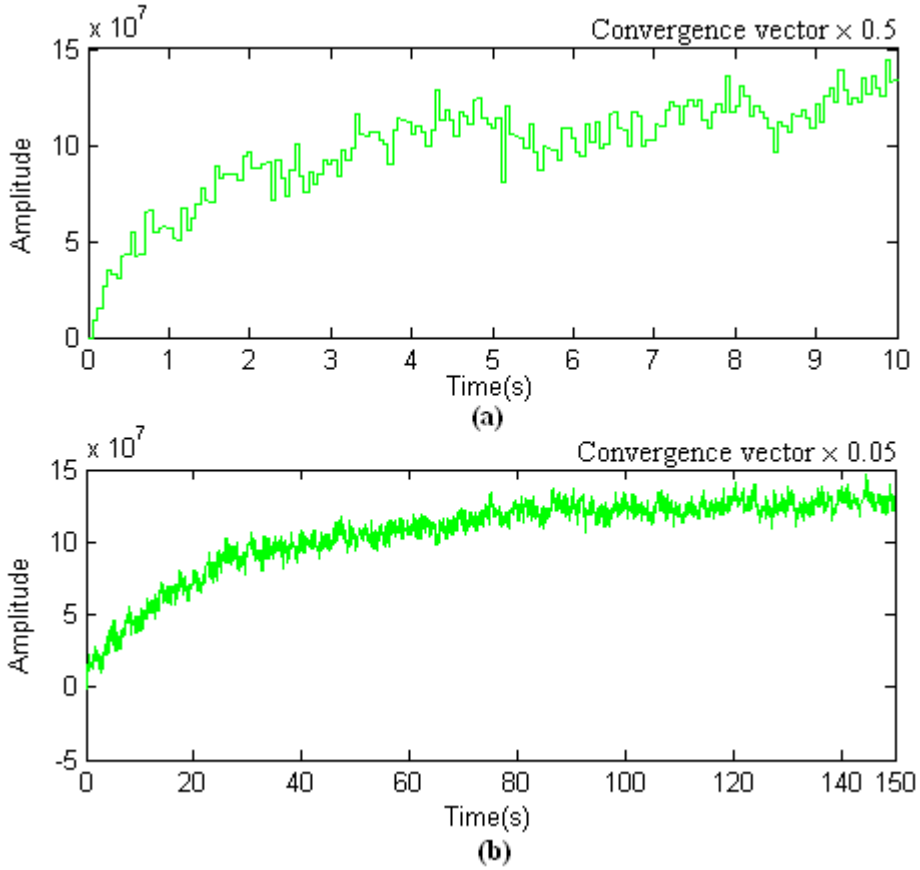

Figure 6.49 Adaptive process of the 50th point on estimated secondary path impulse response with $k_P = 0.2$ using frequency domain method for different convergence vectors. (a): convergence × 0.5 (b): convergence× 0.05

To summarize, from the control structure of frequency domain on-line algorithm and cancellation results above, an efficient and robust control effect is obtained using first control strategy. At the beginning of the second stage, because of the effect created by the decreasing primary noise, a smaller identification convergence vector is applied to ensure stability. Similar to the improved Bao's method the white noise in the error, which is used to update the two-weight adaptive notch filter, cannot be eliminated. However, as this white noise comes to the notch filter directly, distorted but better secondary path identification results can be obtained with the large convergence factor of the two-weight adaptive notch filter. Additionally, from the comparison with the time domain control method, accurate secondary path estimation can be obtained when the uncancelled harmonics of primary noise exist with large power. However, when using the second strategy, in the first stage small convergence factors corresponding to the

frequency components which have large power, can 'drag' the nearby components down. Hence, the convergence of the secondary path identification may require a very long time. A large identification convergence vector may give a fast speed but also a distorted identification result. Therefore, the frequency domain control method is only realized under the first strategy. It is also found that when the reflection factor suddenly changes from 1 to a small value, between 0 and 0.1 in this section, the phase difference between the secondary path and its estimation may move out of the range between $\pm 90^\circ$ and make the system unstable.

6.4 Variation of reflection factor

The first and second strategies are the different ways operated at the starting period of fluid-borne noise cancellation. The starting period includes the first stage, before the noise controller switched on, and the second stage, after switching on the noise controller. In real experiment a load valve is applied at the end of the hydraulic circuit as shown in Figure 5.1. In this section the effect from the variation of the load valve, which includes reflection factor change and primary noise power change, is considered and discussed during simulation.

The improved Bao's method for multiple frequency cancellation with this effect is simulated first. 300 Hz, 600 Hz and 900 Hz sine waves are applied as the primary fluid-borne noise. The amplitude of their summation is eight times bigger than that of white noise. The length of the identification weighting function is 512. The second strategy is used in this simulation. The reflection factor $k_P = 1$ is applied for both first and second stages. Then the reflection factor $k_P = 0.2$ is used when adjusting the load valve at the pipe end and the amplitude of the primary noise increases to twice that of the previous one with the same frequencies. Relatively small convergence factors for the two-weight adaptive filters are used to prevent system instability from big variation of primary noise and reflection. After a short period the increased fluid-borne noise is attenuated under the new working condition ($k_P = 0.2$) and the accurate secondary path identification result is quite similar to the one shown in Figure 6.25. The noise cancellation result is plotted in Figure 6.50 and the adaptive process of the 50^{th} point on the estimated impulse response is plotted in Figure 6.51.

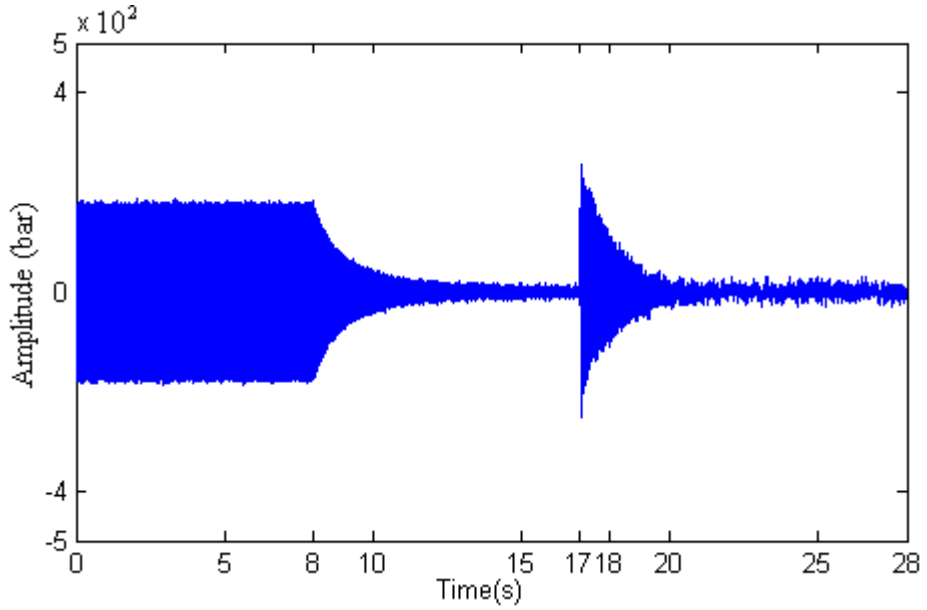

Figure 6.50 Multiple frequency cancellation result using improved Bao's method with effect from load valve variation

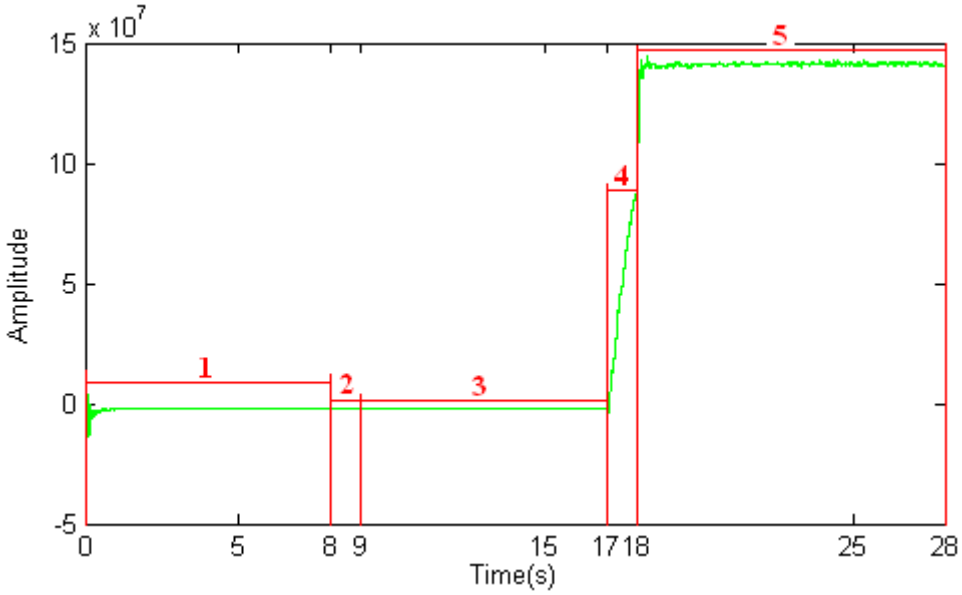

Figure 6.51 Adaptive process of the 50th point on estimated secondary path impulse response for multiple frequency using improved Bao's method with effect from load valve variation

From Figure 6.51, period 1 is the first stage with $k_P = 1$ and the identification convergence factor is 2×10^3; period 2 is the satrt of the second stage with $k_P = 1$ and the identification convergence factor is 1×10^2; in period 3 noise cancellation is

processed and the length of this period is not restricted. 1×10^2 is also used as the convergence factor. Then the reflection factor is changed to 0.2 and the amplitude of primary noise increases to twice the previous value at the beginning of period 4. The identification convergence factor is still 1×10^2. In order to give a fast convergence speed after the beginning stage 2×10^3 is used as identification convergence factor in period 5.

Secondly, with the load valve change, multiple frequency cancellation using Zhang's method under the second strategy is simulated. Compared with the improved Bao's method faster convergence factors are applied for the two-weight adaptive notch filters. The whole operation process and other parameters are the same as the improved Bao's method. The only difference is that longer running time is needed for periods 1, 2 and 4 as shown in the noise cancellation result plotted in Figure 6.52, and the adaptive process of the 50th point on the estimated impulse response is plotted in Figure 6.53. The accurate secondary path estimation is quite similar to the one shown in Figure 6.30.

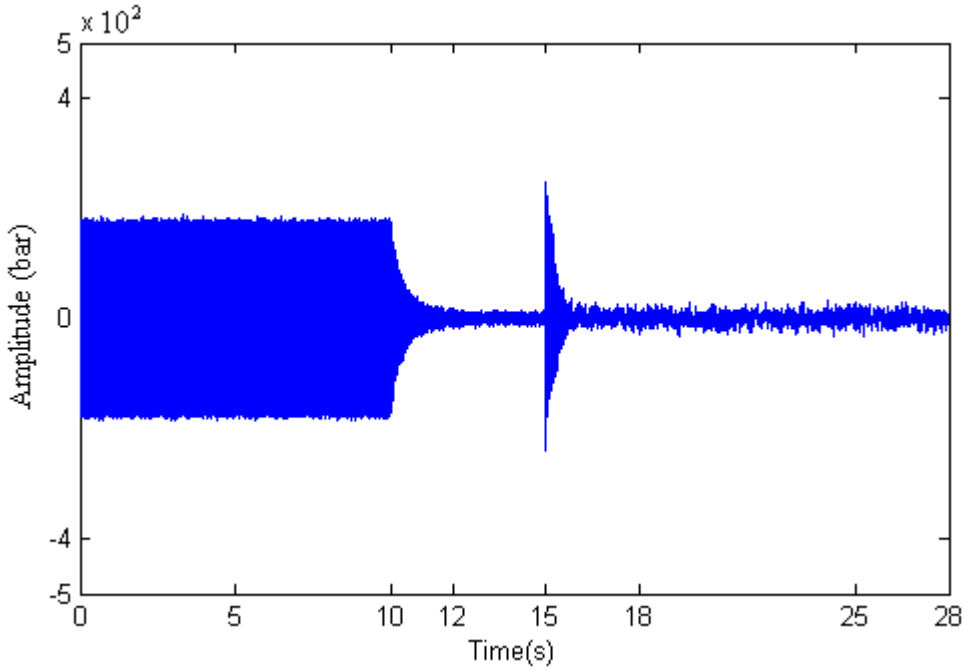

Figure 6.52 Multiple frequency cancellation result using Zhang's method with effect from load valve variation

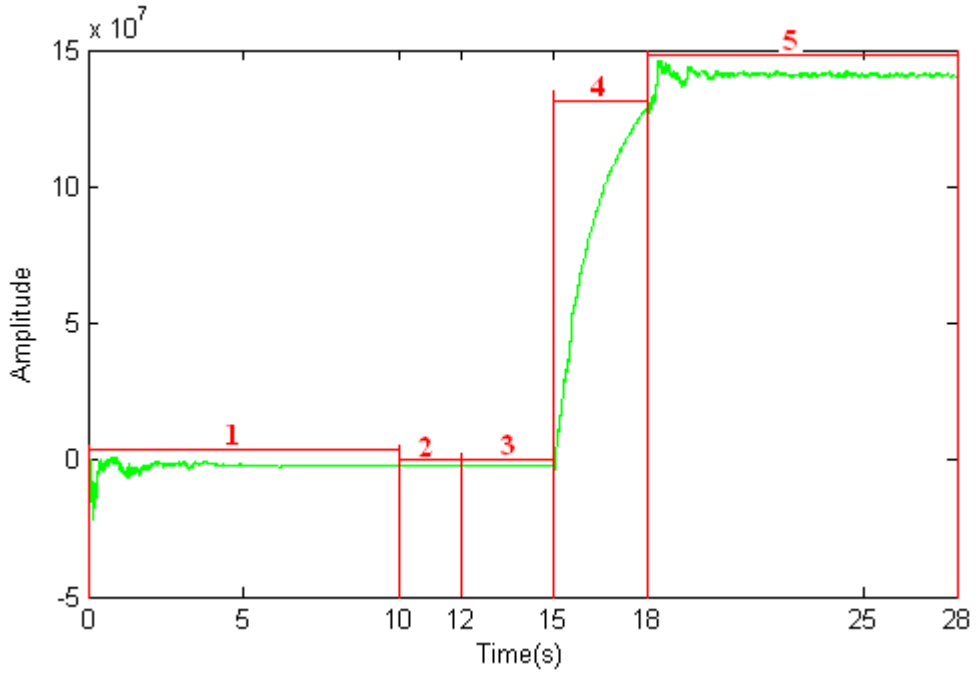

Figure 6.53 Adaptive process of the 50th point on estimated secondary path impulse response for multiple frequency using Zhang's method with effect from load valve variation

Finally with the effect from load valve variation the frequency domain control method is simulated under the first strategy. Variations of the primary noise and reflection factor are the same as those used in Zhang's method. Additionally the convergence factors of two-weight adaptive filters are also the same. Accurate estimation of the secondary path can be obtained, which can be represented using that in Figure 6.41. The noise cancellation result is plotted in Figure 6.54 and the adaptive process of the 50th point on the estimated impulse response is plotted in Figure 6.55.

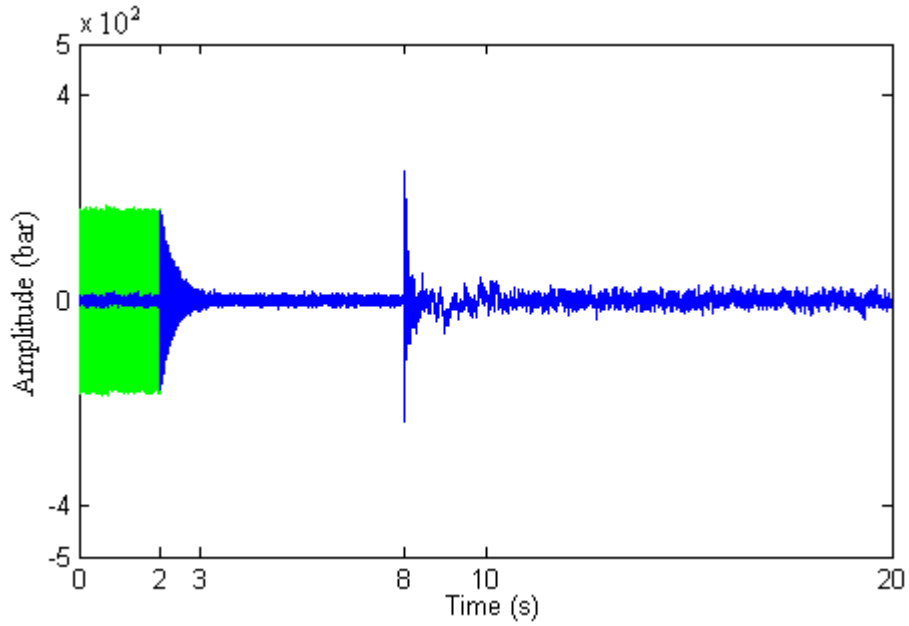

Figure 6.54 Multiple frequency cancellation result using the frequency domain method with effect from load valve variation

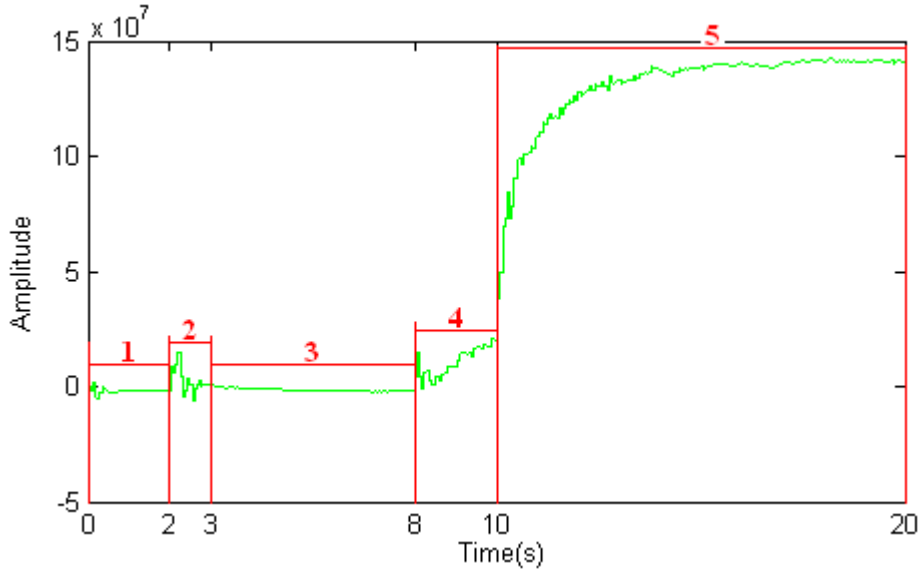

Figure 6.55 Adaptive process of the 50th point on estimated secondary path impulse response for multiple frequency using the frequency domain method with effect from load valve variation

In period 1, which is the first stage using the first strategy the identification convergence vector, which can be named as C_{id}, is applied. At the beginning of the second stage

denoted using period 2 in Figure 6.55, identification convergence vector is $C_{id} \times 0.02$ to ensure system stability. In this simulation in period 3 $C_{id} \times 0.02$ is still used. In this period a relatively large convergence can be applied to give a fast convergence speed, but this is not essential. During period 4 $C_{id} \times 0.02$ is not changed, as big effect from the cancellation process and reflection factor variation may distort the secondary path estimation to make the system unstable. In period 5 fast identification convergence speed can also be obtained by using C_{id}.

To summarize, by turning the load valve the reflection factor and power of primary noise may change in the hydraulic circuit. Simulation of fluid-borne noise cancellation is realized using the improved Bao's method, Zhang's method and the frequency domain method with this effect. Large reflection factor range, k_P from 1 to 0.2, is applied in the simulation. As the situations are the same after switching on the noise controller before turning the load valve, the first and second strategies can both be applied for this period. From the results obtained in this section, good cancellation results and accurate secondary path identifications can be obtained using all of the three control algorithms and fast convergence speed of two-weight adaptive notch filters can be reached using the Zhang's method and the frequency domain method. However, because a large change in primary noise and reflection factor change can affect on-line secondary path identification seriously, at the beginning period of turning the load valve a relatively small identification convergence factor is applied for a longer time in Zhang's method compared with the improved Bao's method because of 'cross-updating'. For the frequency domain method as the power of primary noise is suddenly twice as big when turning the load valve, smaller identification coefficient and long running time is needed for this period to ensure stability compared with the cancellation realized in section 6.3.

6.5 Conclusions

To conclude, in this chapter on-line identification algorithms, which are realized both in time domain and frequency domain, associated with two-weight adaptive LMS notch filter for narrowband fluid-borne noise cancellation are evaluated and simulated. Especially, Bao's method was improved to obtain a better secondary path estimation.

Two control process strategies are proposed and evaluated for simulation and real experiments. Good noise cancellation and secondary path identification results are obtained during simulation using these two strategies for both single frequency and multiple frequency primary noise.

A reflection factor k_P can be applied to represent the effect of adjusting the load valve. During simulation changes of reflection effect, which is from 1 to 0.2 in this chapter, from pipe end caused by flow variation are considered according to stable condition from phase difference between secondary path and its estimation in the model. However, a large change of load valve impedance can give a corresponding change in the reflection factor, which can make the phase shift between the secondary path and its estimation out of the stable range. Hence sudden and large load variety should be avoided to ensure system stability. During simulation at the beginning period when switching on the noise controller a large decrease process of primary noise may affect the on-line identification. A relatively small identification convergence factor or convergence vector can be applied in this period to make the system stable.

Three different on-line control methods are also compared. In the improved Bao's method, as the white noise is used to update the two-weight adaptive notch filter an extra unwanted signal exists in the anti-noise signal, which can affect the secondary path estimation, especially when the large convergence factor is applied on the two-weight adaptive filter. In Zhang's method the effect from the white noise can be eliminated to obtain accurate secondary path estimation when a large convergence factor is applied on the two-weight adaptive filter to get a fast response. However, because of cross-updating between the secondary path identification and the interference cancellation a longer running time is needed for the beginning period of second stage. In the frequency domain method, which is the most robust algorithm among the three, the white noise effect on the secondary path estimation is smaller but better compared with the improved Bao's method. Fast convergence speed of two-weight adaptive notch filters can also be obtained. As an adaptive identification convergence vector is applied when uncancelled harmonic components exist, an accurate secondary path estimation, which can not be reached using the time domain control algorithms, can be obtained. However, as signals need to be transformed between the time domain and frequency domain, more computational burden is added

on the processor. Additionally, comparing the primary noise cancellation results using different control methods, the effect of auxiliary white noise is quite small compared with the uncancelled primary noise.

CHAPTER 7

Experimental Research on Test Rig Using Artificial Noise Source

In this chapter the active noise cancellation methods with off-line and on-line system identification discussed in Chapter 5 and Chapter 6 to cancel narrowband noise are implemented on a simple hydraulic system with different working conditions. Two manipulation strategies are realized to implement the fluid-borne noise cancellation. A servo valve is applied as the fluid-borne noise source and another fast response servo valve is used as the actuator to generate the anti-noise. dSPACE® 1005 is applied as the signal processor with sampling frequency 3125 Hz. The purpose of this chapter is to test the feasibility of these control methods implemented on a simple hydraulic circuit.

7.1 Setting up of test rig

In this section a test rig is built up using a servo valve, which can generate fluid-borne noise artificially, as a noise source. Relative equipments, which are used on the test rig are also introduced.

7.1.1 Devices used on the rig

Firstly, the main devices used on this rig to realize a noise cancellation test are introduced. A servo valve is applied upstream to generate fluid-borne noise, and another is located downstream, which can give high response, to generate anti-noise. These two servo valves, which are named as noise servo valve and anti-noise servo valve, are not far from each other. Both of these two servo valves are mounted on different blocks to generate flow ripple as shown in Figure 7.1 and 7.2. A restrictor valve and a load valve are located at the two ends of the pipe to adjust working conditions. A pressure transducer applied near the noise servo valve downstream is only used to collect signal for identification of this valve. The amplifier used for the noise servo valve is ± 15 volt and for anti-noise servo valve is ± 30 volt.

dSPACE® 1005 is selected as signal processor in this experiment. Additionally, dSPACE® 2013 card is used as D/A converter and dSPACE® 2002 card is applied as A/D converter.

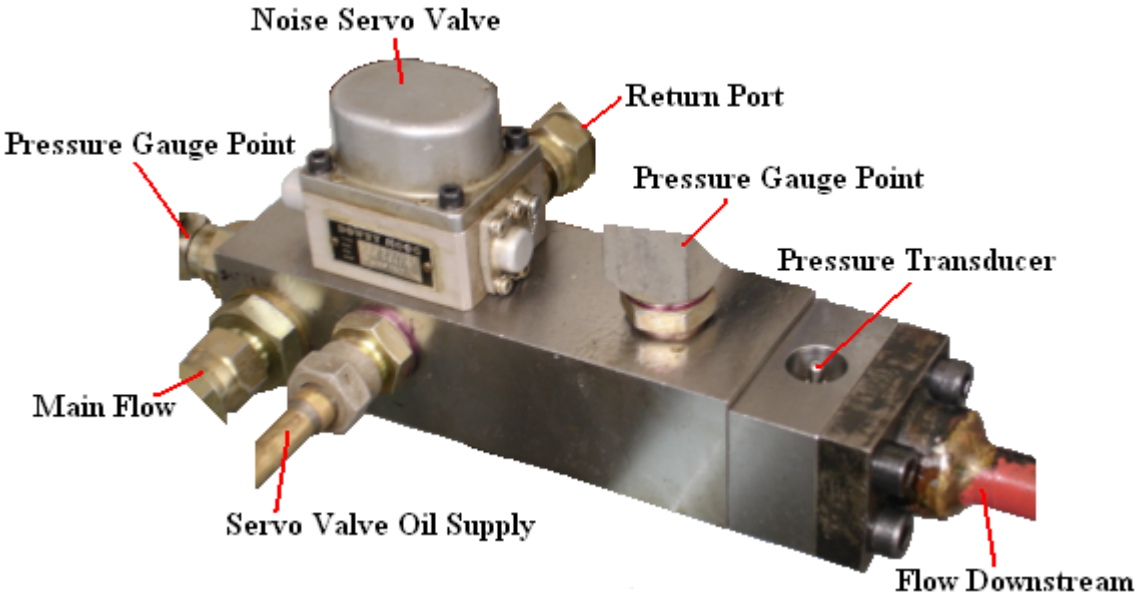

Figure 7.1 Fluid-borne noise source using a servo valve

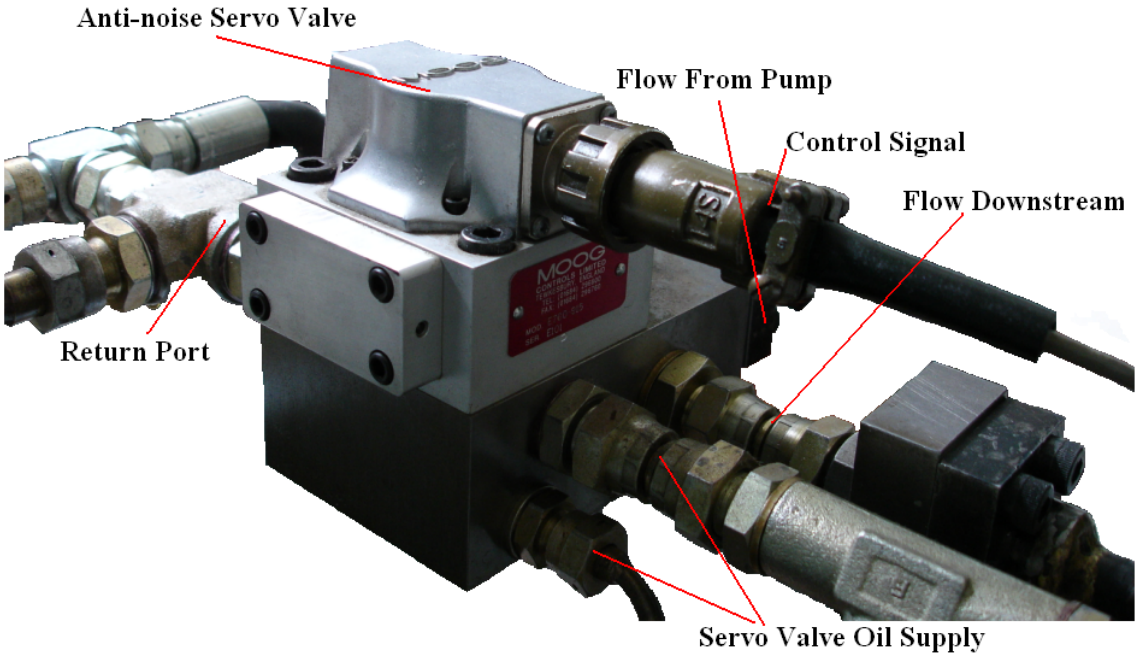

Figure 7.2 Anti-noise source using a fast response servo valve

7.1.2 Structure of test rig

The layout of this rig is shown in Figure 7.3.

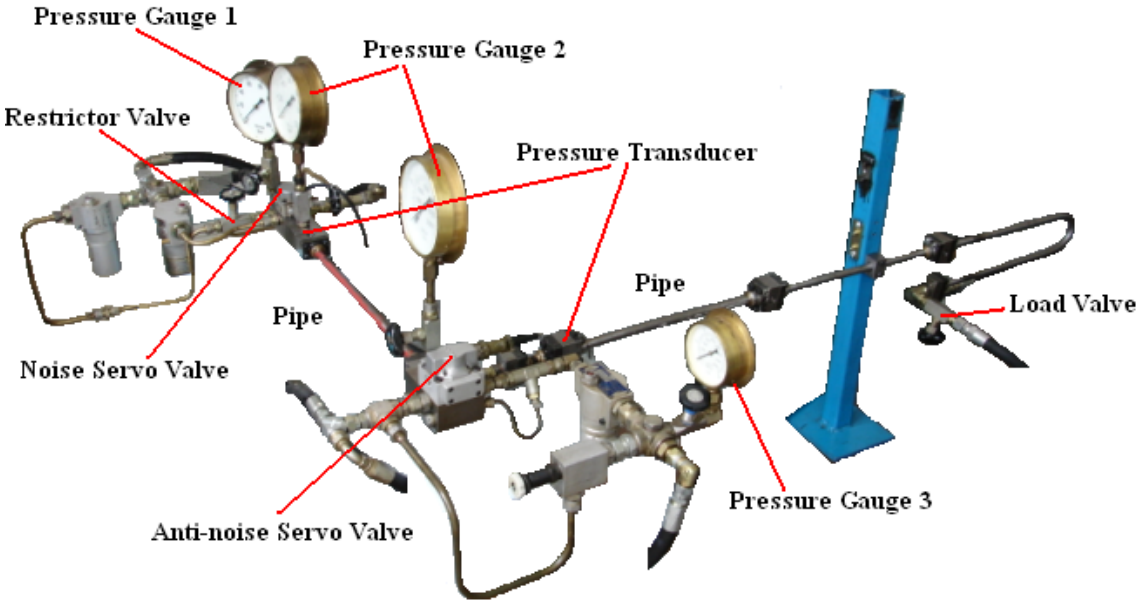

Figure 7.3 Test rig using a servo valve as fluid-borne noise source

A circuit diagram of this rig with control section is also shown in Figure 7.4.

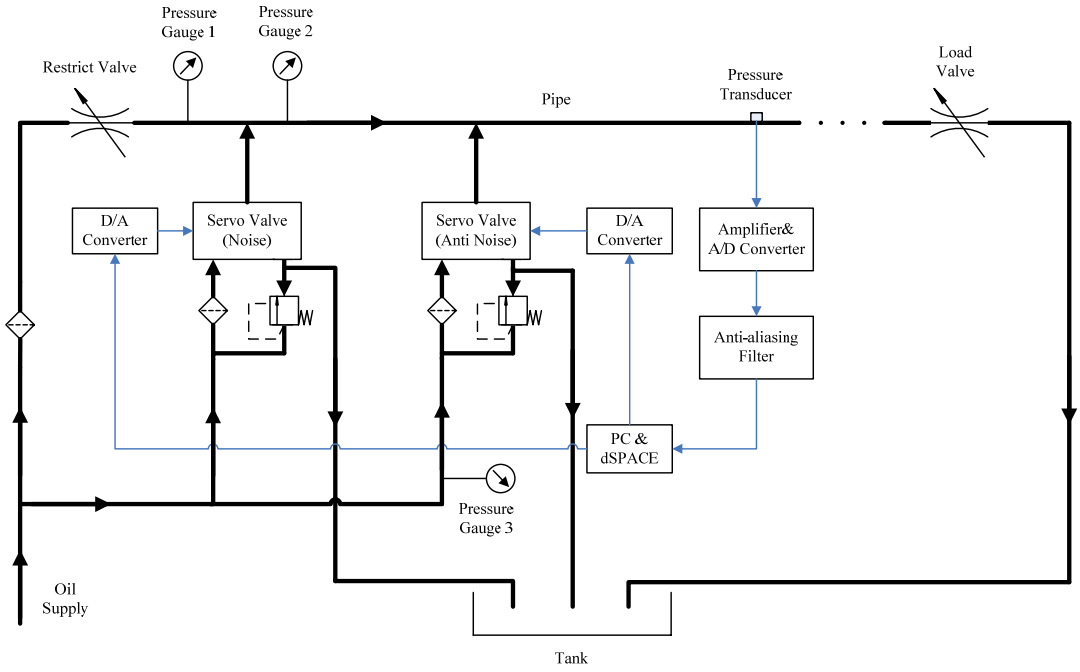

Figure 7.4 Circuit diagram of test rig using a servo valve as noise source

In this experiment the oil supply is from a ring main, and pressures at gauges 1 and 3 are the same when servo valves are switched off. Hence the restrictor valve is set closed to give a maximum reflection of the pressure ripple coming upstream. A pressure transducer is seated not far from the anti-noise servo valve downstream to pick up the residual noise signal. Pressure transducers applied in this experiment are high frequency response piezoelectric devices of type 6QP500 made by AVL. The pressure calibration is 0.49 pC/psi, which is about 7.1 pC/bar. The signal passes through a charge amplifier, which has the ratio 10 pC/V, to change the pressure to a voltage signal. Therefore the ratio of the pressure transducer and the amplifier is about 1.4 bar/V. Additionally, an anti-aliasing filter is used before processing signals. The noise servo valve is activated by dSPACE® with several orders of harmonic sine waves and the input signals used for cancellation are also supplied by dSPACE® with same order of harmonic components and have the same frequencies as those coming to the noise servo valve. However, in a real application using a pump as the fluid-borne noise source, the noise frequency cannot be obtained directly. This will be discussed in Chapter 8.

7.1.3 White noise with uniform power used in experiments

In this experiment, white noise signal with a zero mean and uniform power for broad frequency range is applied for secondary path identification. This signal is built up using the Fourier series summation:

$$x\_noise = A \cdot \sum_{i=1}^{f_{\max}} \cos\left(2 \cdot \pi \cdot f_i \cdot n \cdot \Delta t + \theta_i\right)$$

n is time index, i is integer, Δt is sampling time and $f_{\max}$ is the maximum frequency in this white noise, which should be smaller than Nyquist frequency. θ_i is the random phase shift for different frequencies. As summation of series of cosine waves are applied amplitude of this white noise is limited in a small range. Using this equation a synthetic zero mean white noise that has uniform power through the required frequency range is generated. This is plotted both in time domain and power spectrum in frequency domain in Figure 7.5.

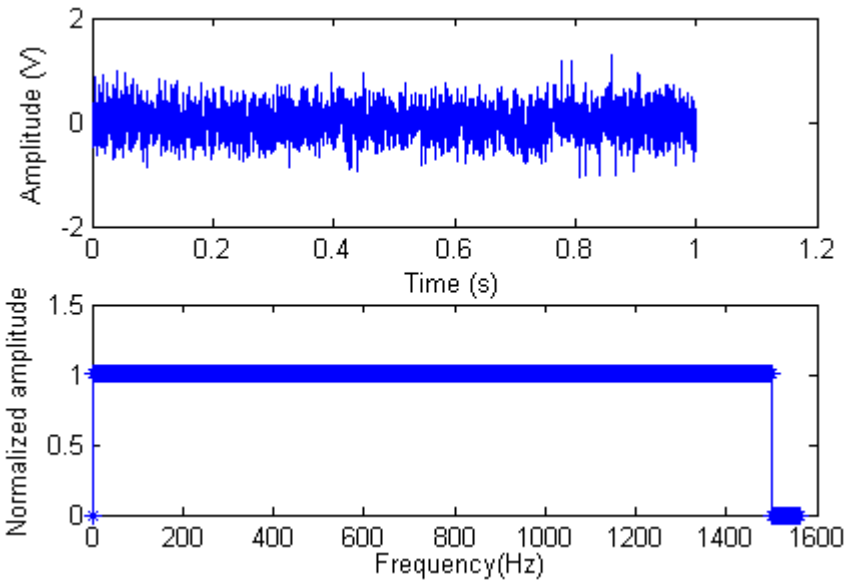

Figure 7.5 Synthetic zero mean white noise with uniform power within frequency 1 Hz to 1500 Hz

For simplicity the smallest frequency used is 1 Hz in the above plot and the length of this signal is from 0 s to 1 s. Frequency components are distributed from 1 Hz to 1500 Hz with uniform spacing.

7.2 Off-line cancellation methods applied on the test rig

As discussed in Chapter 5 the off-line identification algorithms associated with the two-weight adaptive notch filter are firstly realized on the test rig. Two different working conditions of 40 bar and 80 bar were applied, which can be read from pressure gauge 2 in Figure 7.4, by turning the load valve at the end of the pipe.

7.2.1 Background noise on test rig

In this experiment the oil supply from the ring main is 100 bar, and this can be shown using pressure gauge 3 in Figure 7.4. The ring main is driven using a powerful pump, which can give a maximum of 250 bar pressure and 80 L/min flow. Therefore a certain level of background noise at different working conditions exists from the ring main and this is plotted in Figure 7.6.

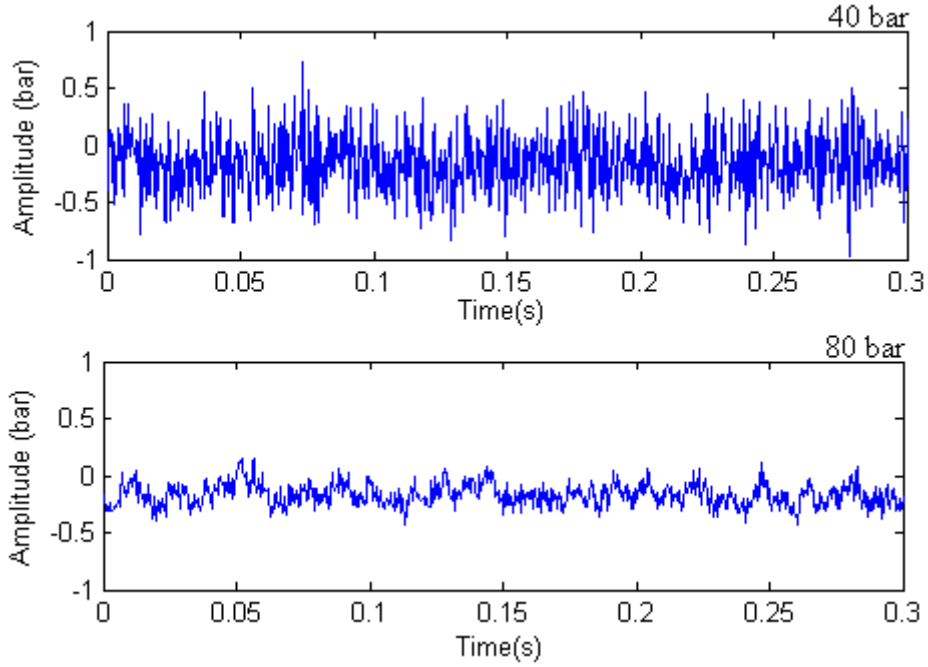

Figure 7.6 Background noise on the rig with different working pressures

From this result there is smaller background noise when the working pressure is higher.

7.2.2 Dynamic characteristics of a noise source servo valve

Firstly the ability of a noise servo valve was tested during system identification in different working conditions. The pressure transducer located downstream of the servo valve as shown in Figure 7.1 can be used to collect response from the noise servo valve. The transfer function of the noise servo valve can be obtained by calculating the ratio between output and input signals on this valve in the frequency domain, which can be named the frequency domain identification. The other method is to find out the impulse response of the noise servo valve LMS adaptive filter, which can be named as the impulse response identification. For accuracy the length of the weighting function in the LMS filter is 128. The comparison using these two identification methods is plotted in Figure 7.7 and Figure 7.8 at different working pressures. A Fourier transform has been applied to the impulse response.

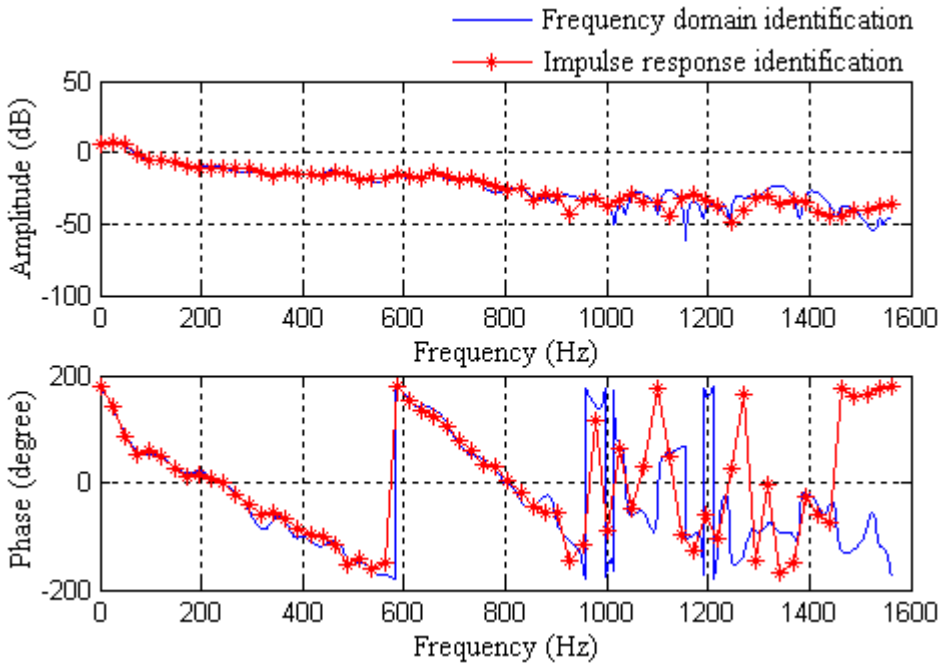

Figure 7.7 Comparison between frequency domain and offline impulse response identification at 40 bar

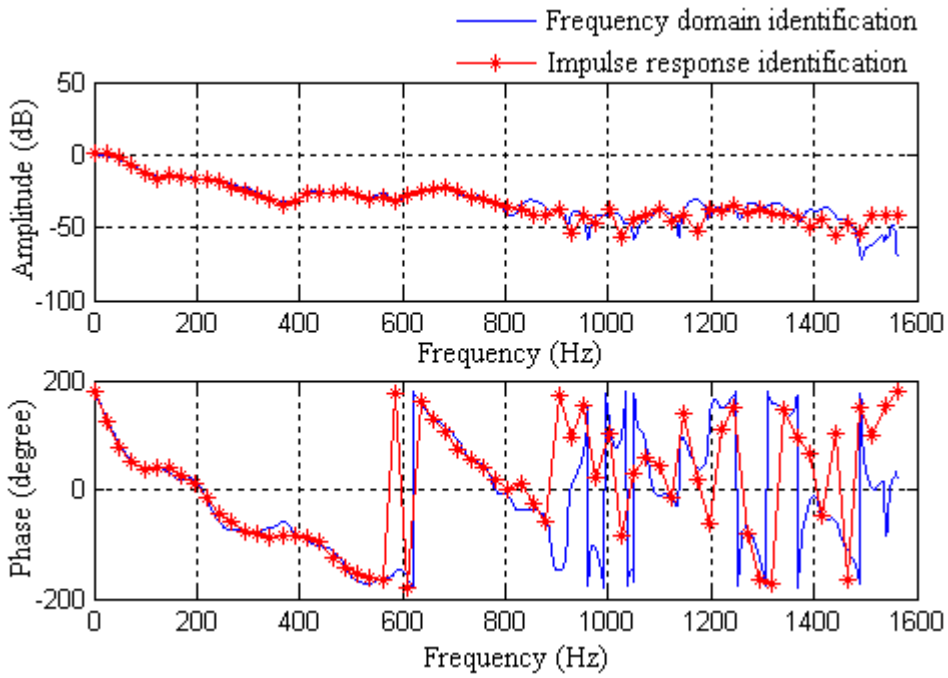

Figure 7.8 Comparison between frequency domain and offline impulse response identification at 80 bar

Good agreement of the secondary path impulse response is achieved at the low frequency range. The exciting white noise signal has uniform power for the frequency range from 1 Hz to 1500 Hz, but from these identification results the response from this noise servo valve is quite limited for high frequency range at both 40 bar and 80 bar. Additionally for high frequencies especially from 800 Hz to 1500 Hz distorted identification results are obtained because of background noise effect, which is much bigger than the small response from noise servo valve.

7.2.3 Dynamics characteristics of the secondary path

In order to find out the dynamic characteristics of the secondary path, which include amplifiers, A/D, D/A converters and anti-aliasing filter, its impulse response is obtained before realizing noise cancellation. Uniform power of white noise for frequency range from 1 Hz to 1500 Hz is 0.1 V^2. This exciting signal for system identification using an LMS filter is plotted in Figure 7.9. Compared with the plot in Figure 7.6, this is much higher so only a small effect from background noise can act on the secondary path estimation process. 64 order and 128 order weighting functions in LMS filter are applied separately for identification. The comparisons are plotted in Figures 7.10 and 7.11 for different working conditions.

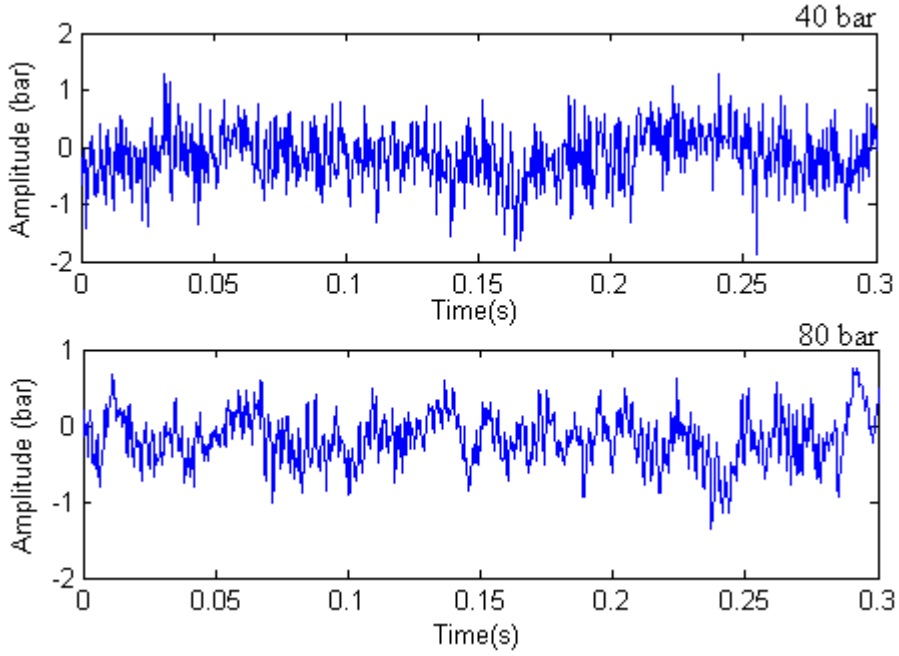

Figure 7.9 White noise used for secondary path estimation with power of 0.1 V^2 plus background noise

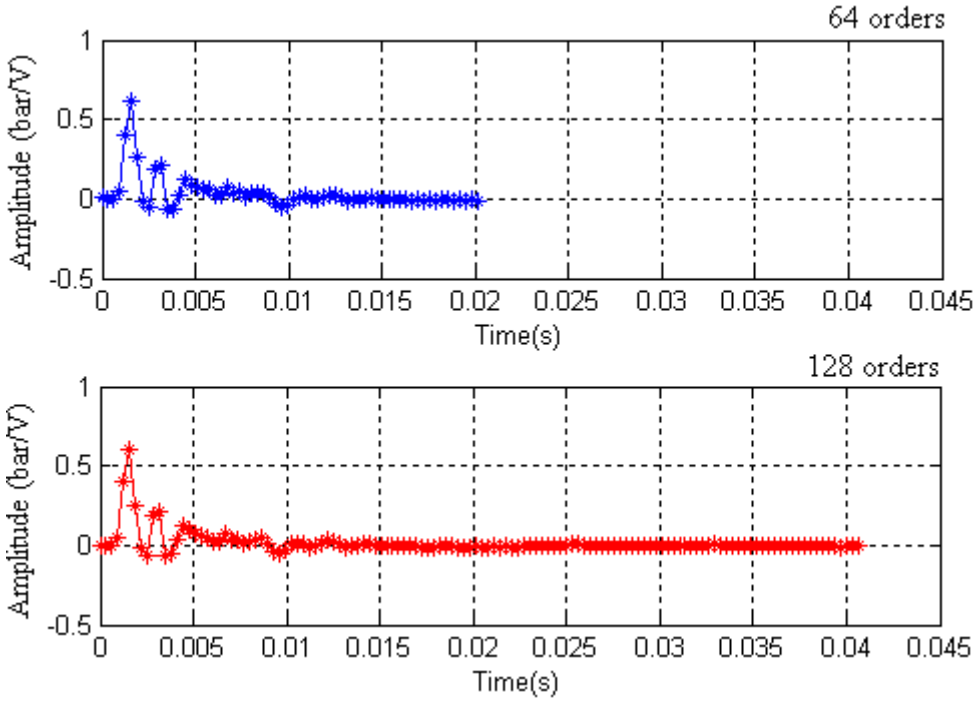

Figure 7.10 Secondary path impulse responses at 40 bar with different lengths

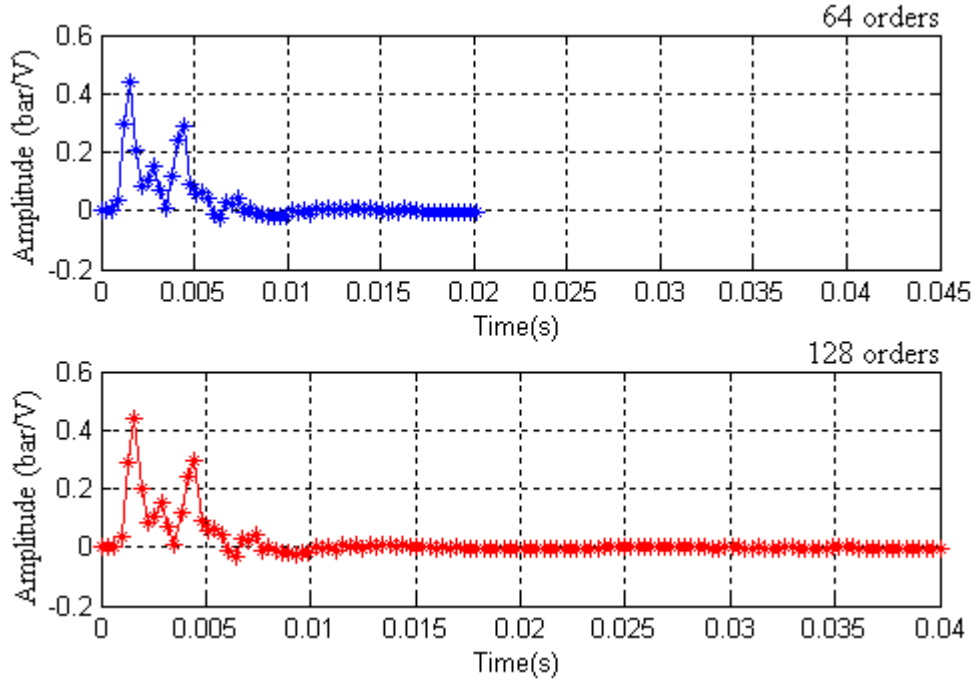

Figure 7.11 Secondary path impulse responses at 80 bar with different lengths

Similar accurate identifications are obtained with different orders of weighting function. With the same system sampling frequency a longer weighting function can obtain more

information of the dynamic response of the secondary path, especially for low frequency components. The importance of this difference will be plotted and discussed in Chapter 8.

In this experiment a 128 order weighting function is used for secondary path compensation. In order to describe the dynamic response for different frequency components amplitude and phase spectrum of the 128 order impulse response compared with the transfer function obtained using frequency domain identification method is plotted in Figure 7.12 and 7.13 for different working conditions. Accurate estimation results are obtained for the frequency range from 0 Hz to around 800 Hz. Additionally, compared with the identification results in Figure 7.7 and Figure 7.8 the high frequency section after 800 Hz is more accurate because of the stronger response from the anti-noise servo valve compared with background noise.

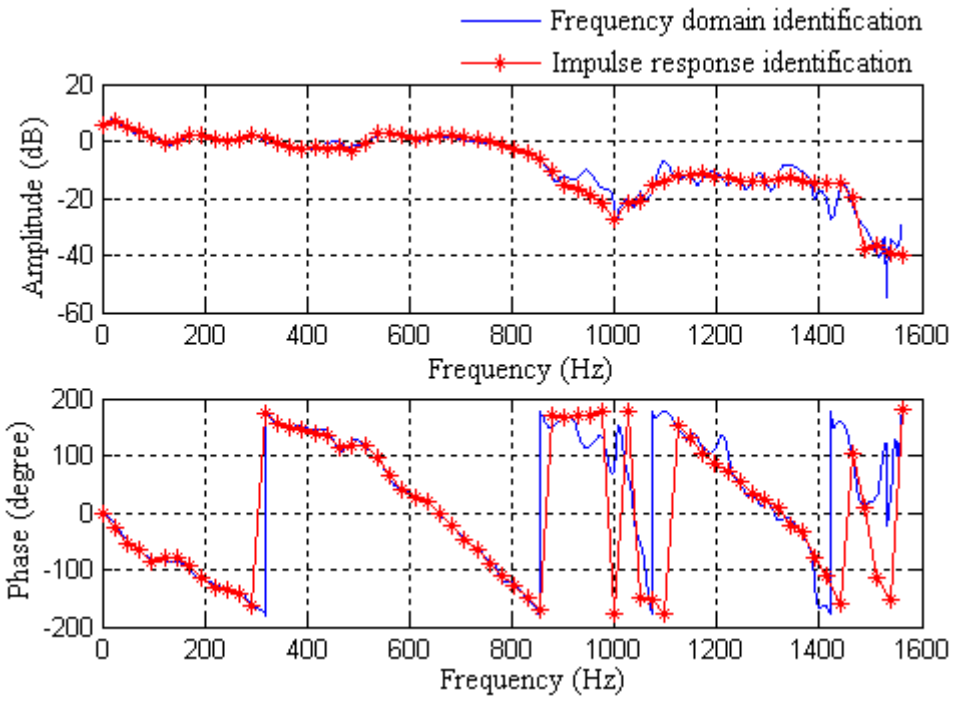

Figure 7.12 Comparison between frequency domain and off-line impulse response identification at 40 bar

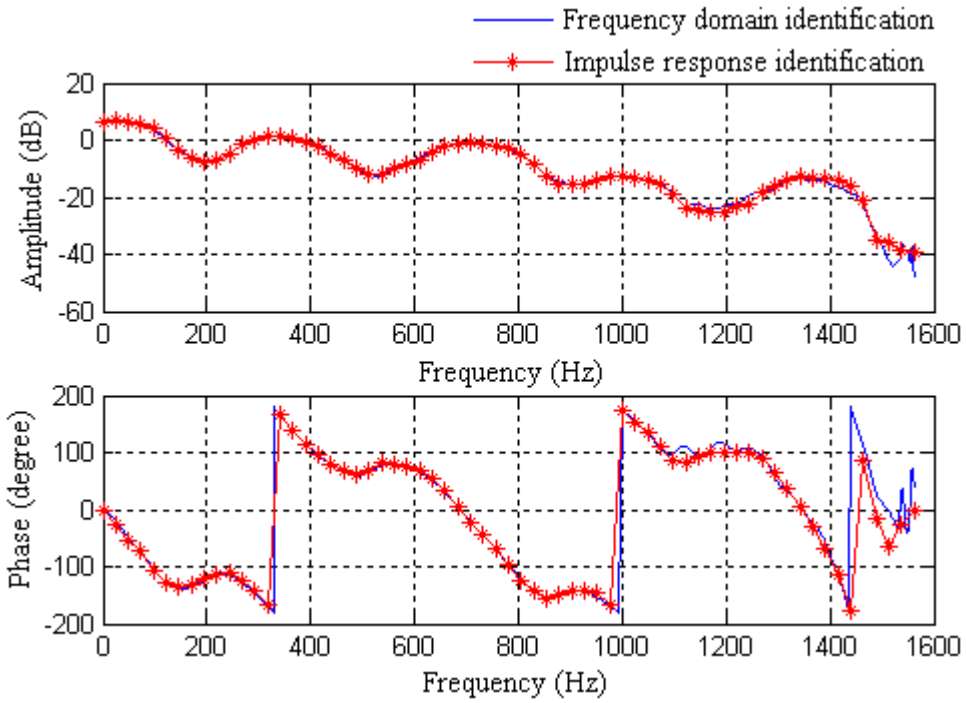

Figure 7.13 Comparison between frequency domain and off-line impulse response identification at 80 bar

7.2.4 Off-line delay unit compensation

From the secondary path identification spectrum obtained from 0 Hz to 800 Hz the relationship between frequency and phase shift can be roughly seen as linear and a 2π delay occurs near 800 Hz. As the sampling frequency for the control system is 3125 Hz, hence a delay of 4 samples can be used for secondary path compensation.

In this experiment, the noise servo cannot generate significant fluid-borne noise at high frequencies. Depending on this ability limitation, only 8 orders of harmonic components are applied with a fundamental frequency of 50 Hz as fluid-borne noise. Time domain of this signal is plotted in Figure 7.14 for different working conditions. It can be seen that the smaller flow from ring main can generate fluid-borne noise with less power.

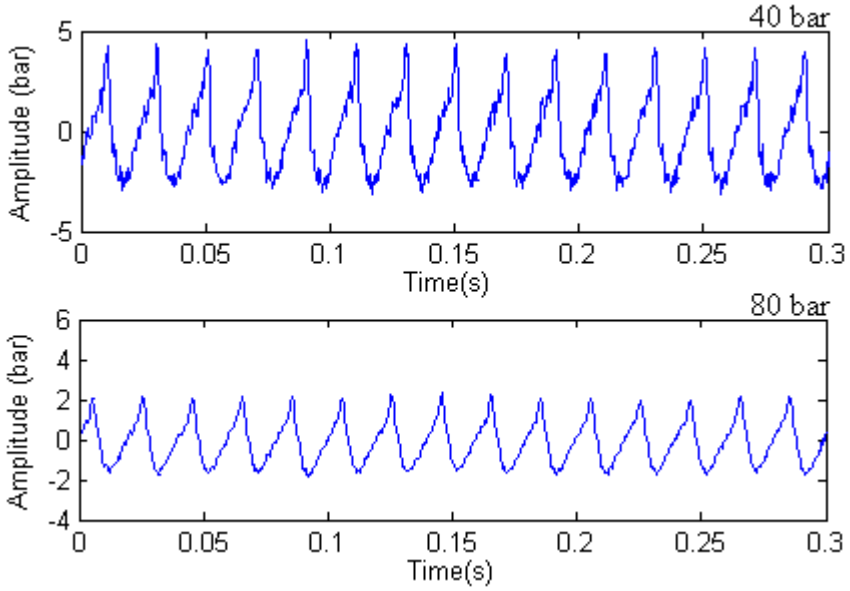

Figure 7.14 8 order harmonics fluid-borne noise on test rig plus background noise

Combined with the two-weight adaptive notch filter the off-line delay compensation control algorithm is realized on the test rig, and power spectrum cancellation results compared with the uncancelled signals are plotted in Figures 7.15 and 7.16 for different working pressures.

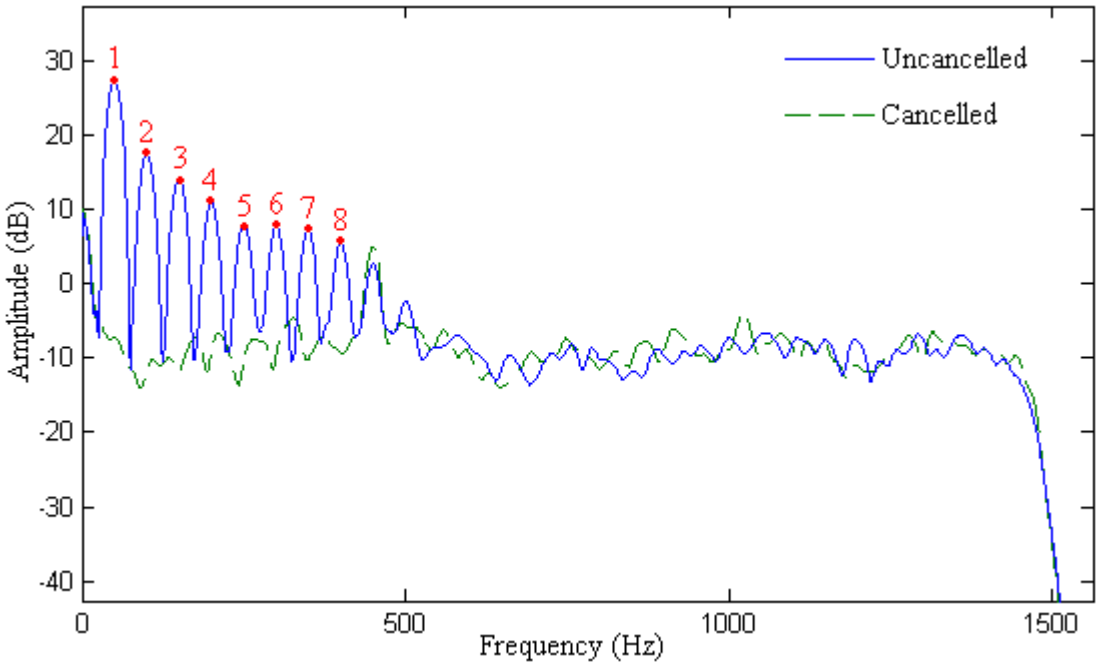

Figure 7.15 Measured frequency spectra with cancellation of 8 harmonics at 40 bar using delay unit off-line compensation

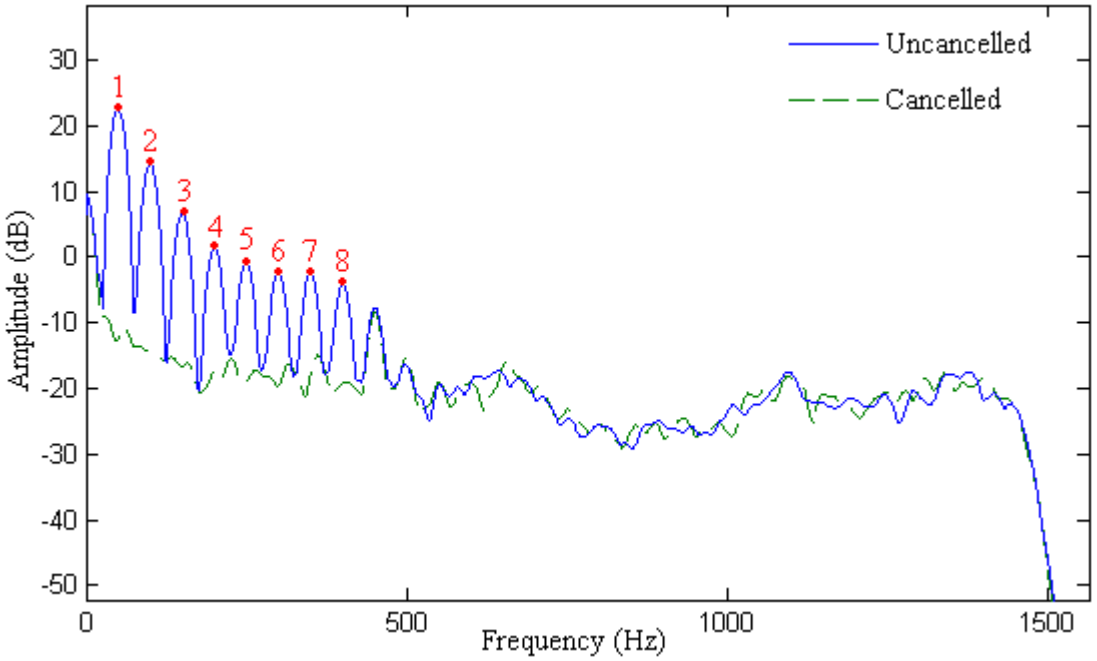

Figure 7.16 Measured frequency spectra with cancellation of 8 harmonics at 80 bar using delay unit off-line compensation

From these results the small power of the high frequency harmonic components, which is not generated by the control signal from the processor, exist on the uncancelled fluid-borne noise. These components are derived from the harmonic response of the noise servo valve. Typically, 20 dB to 30 dB fluid-borne noise is attenuated on the target frequency components for different working pressures. Limitation of this cancellation result may come from background noise from the ring main. Additionally, a slight increase of uncancelled frequency components is from the non-linear distorted response of the anti-noise servo valve.

7.2.5 Off-line compensation using secondary path estimation

Usually in a real application the secondary path effect cannot only be compensated by using a uniform delay unit for all frequency components. Therefore the secondary path effect can be compensated using the estimation of itself by system identification as discussed in Chapter 5. Under this effect different frequencies can be compensated by using a more accurate phase shift. By employing the impulse response obtained in Figure 7.12 and 7.13, similar cancellation results can be obtained as those plotted in Figures 7.15 and 7.16 for different working pressures. However, this off-line control algorithm cannot catch the variety of secondary change during the noise cancellation

process. The impulse response needs to be re-estimated to obtain accurate compensation when working conditions change.

7.3 On-line cancellation algorithms realized on test rig

In this section the on-line secondary path estimation algorithms, which are discussed in Chapter 6, to overcome the working condition variation during noise cancellation are implemented on the test rig. A higher power of auxiliary white noise can give more effect on noise cancellation performance and give more residual noise. In this experiment white noise power is 0.02 V^2 to give less effect and can obtain an impulse response with sufficient accuracy. The signal is plotted in Figure 7.17.

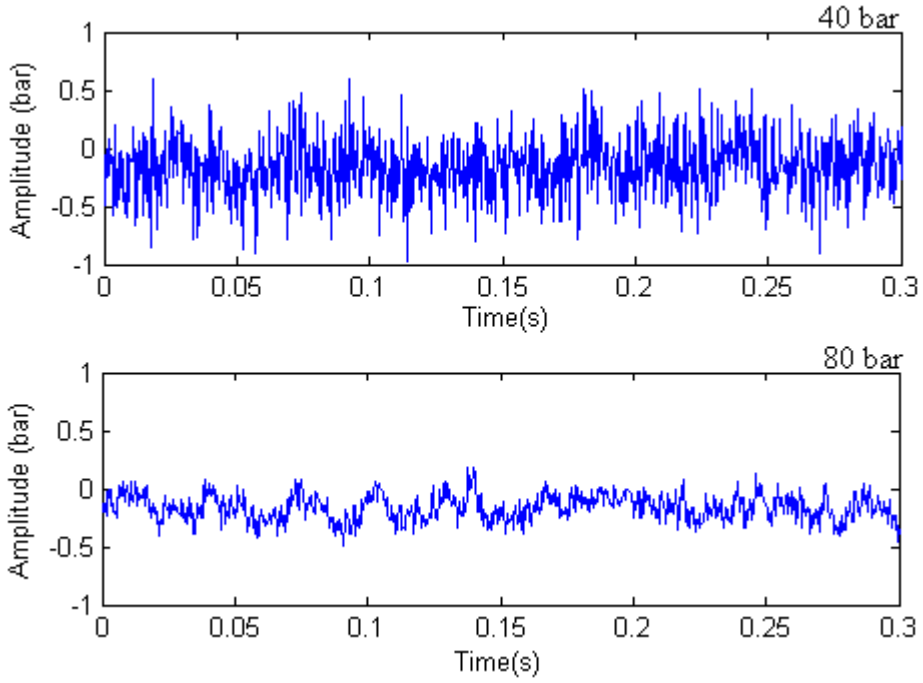

Figure 7.17 White noise used for secondary path estimation with power of 0.02 V^2 plus background noise

7.3.1 Experiment using improved Bao's algorithm

In this experiment in the first stage, which is the same as the off-line identification process, only the secondary path identification controller is switched on. A large identification convergence factor is applied in this stage. Then in second stage the noise servo valve, noise cancellation controller and interference controller are switched on when the secondary path estimation comes to a steady solution in the first stage. As

with the simulation process represented in Chapter 6 to ensure the stability of the system, a relatively small identification convergence factor is used in the second stage. Fluid-borne noise generated using a noise servo valve is the same as that used in off-line control methods. The obtained impulse responses in the first and second stages are compared both in time domain and frequency domain in Figure 7.18 when working pressure is 40 bar.

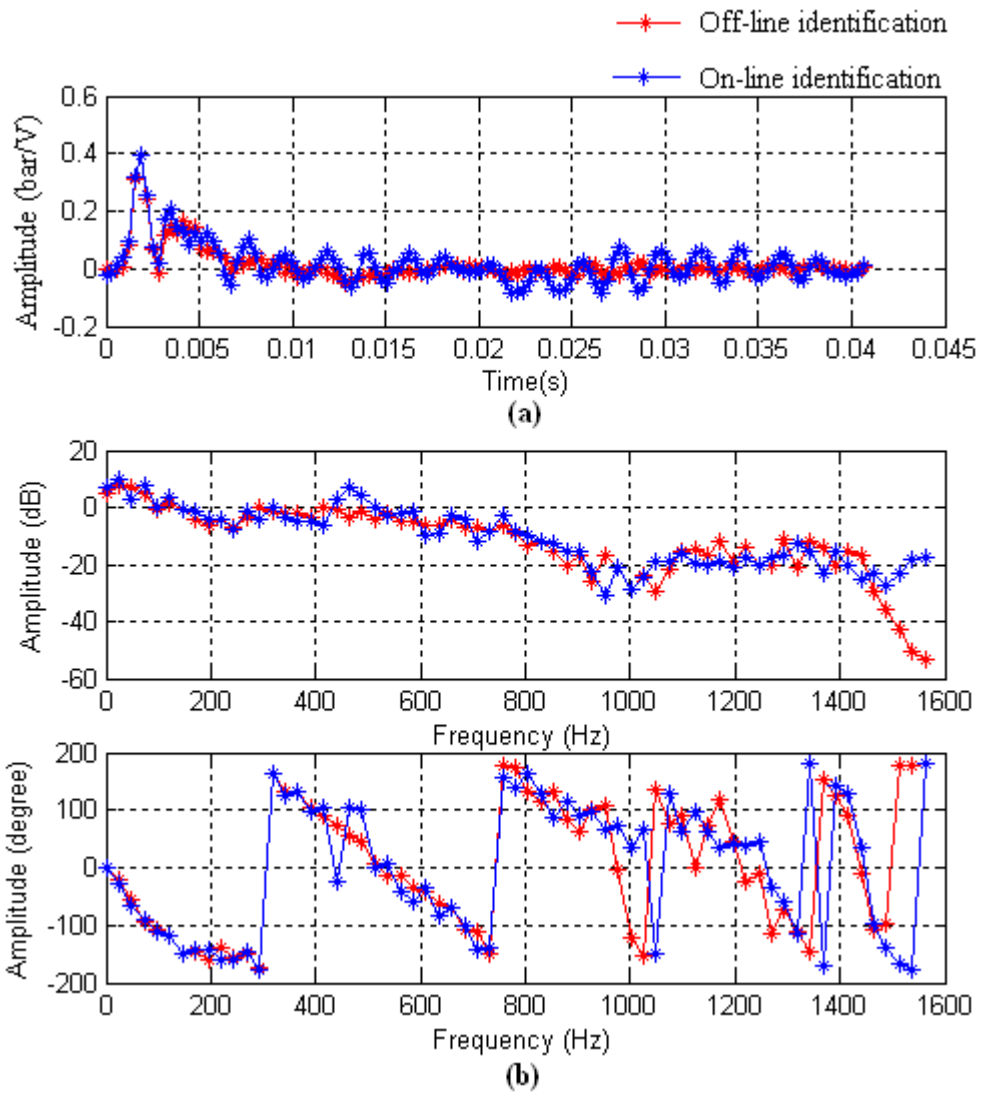

Figure 7.18 (a) Time domain impulse response comparison at 40 bar using the improved Bao's method

(b) Comparison of their amplitudes and phase shifts in the frequency domain

Using this on-line compensation the noise cancellation result is shown in Figure 7.19. Some high order harmonic components at 450 Hz, 500 Hz etc., which are not generated by the controller, exist on uncancelled fluid-borne noise. These components are the harmonics of the noise signal generated by the noise servo valve. As the secondary path impulse response in the second stage is obtained using an on-line identification method the uncancelled fluid-borne noise, with frequencies higher than the 8^{th} harmonic, can affect the identification result. As shown in Figure 7.18 a distortion occurs at frequencies 450 Hz and 500 Hz. The distortion of the secondary path estimation may also come from the extra signal w_a generated by the two-weight adaptive notch filters as discussed in section 6.2.1. As the uncancelled noise power is relatively small compared with the white noise the secondary path estimation with small distortion can still make the system stable, however, when uncancelled noise with large power exists the system may become unstable with the seriously distorted secondary path estimation.

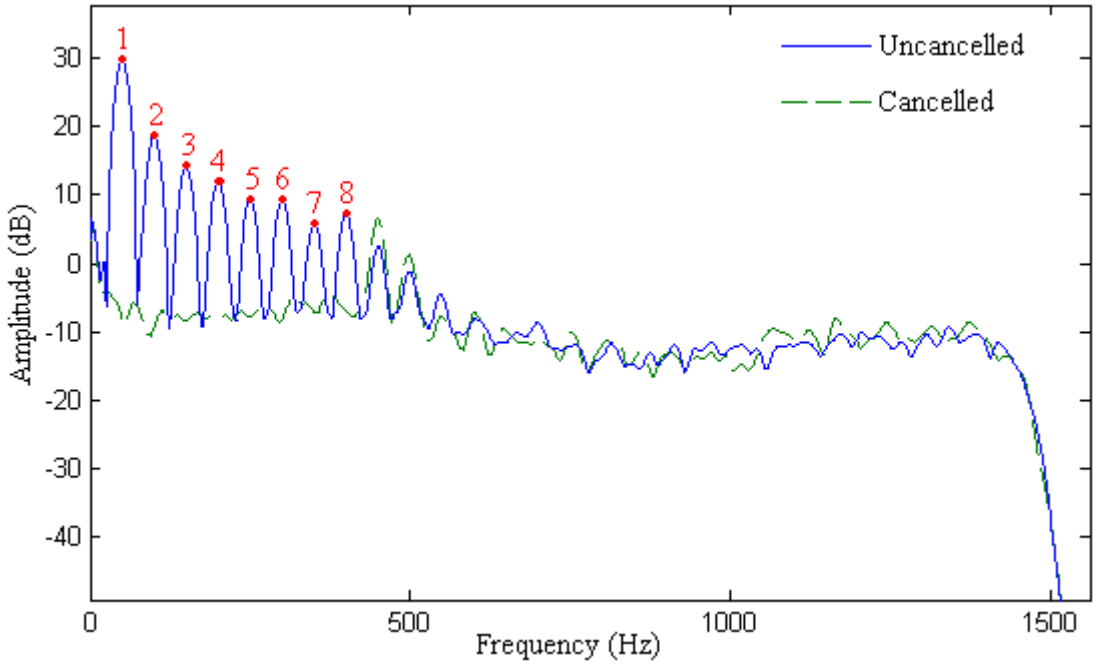

Figure 7.19 Measured frequency spectra with cancellation of 8 harmonics at 40 bar using improved Bao's method

Fluid-borne noise is reduced by about 20 to 30 dB at the cancellation frequencies using the improved Bao's method at 40 bar. Limitation of this cancellation result may not only come from background noise from ring main but also from the auxiliary white

noise for on-line identification. Additionally, a small increase of uncancelled frequency components is caused by the non-linear distorted response of the anti-noise servo valve.

Additionally, by turning the load valve at the end of the pipe, the pressure at the pressure gauge 2 is increased to 80 bar, and the reflection factor and the power of the fluid-borne noise is changed. As the relatively small identification convergence factor is still applied, the system is still stable after turning the load valve. A comparison of secondary path impulse responses obtained using an off-line identification method in the first stage and an on-line method in second stage at 80 bar is plotted in Figure 7.20.

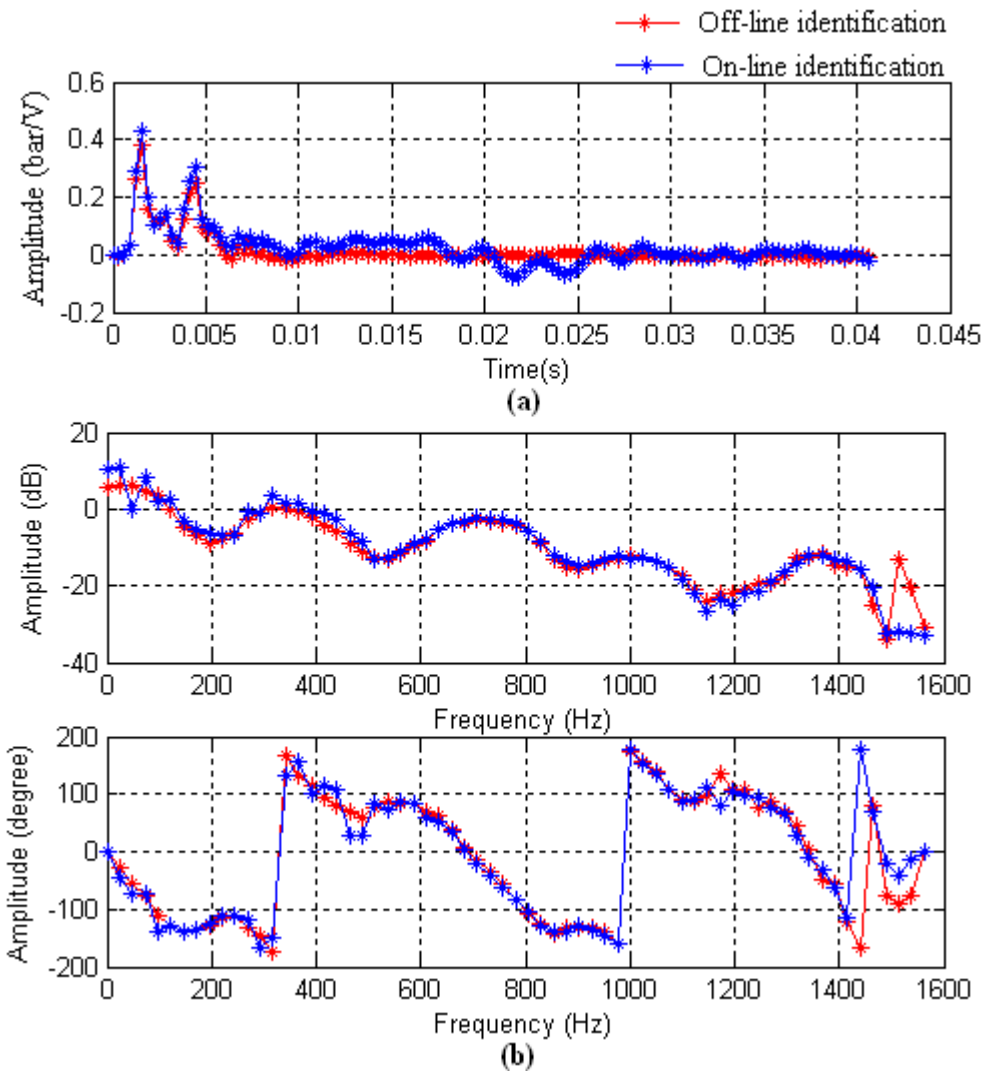

Figure 7.20 (a) Time domain impulse response comparison at 80 bar using the improved Bao's method

(b) Comparison of their amplitudes and phase shifts in the frequency domain

The convergence factors used for the two-weight adaptive notch filter are the same during the periods before and after turning on the load valve. The power spectrum of the cancellation result compared with the uncancelled signal is plotted in Figure 7.21. It is clear to see with decreasing the flow through the pipe, the fluid-borne noise becomes smaller. As the uncancelled harmonics noise caused by the noise servo valve still exists, its effect on the on-line secondary path estimation makes the impulse response result jump at around 450 Hz and 500 Hz as shown in Figure 7.20. Additionally, because the power of the extra signal generated by the two-weight adaptive filters and the background noise become smaller at this pressure, a more accurate secondary path estimation is obtained compared with the one in Figure 7.18.

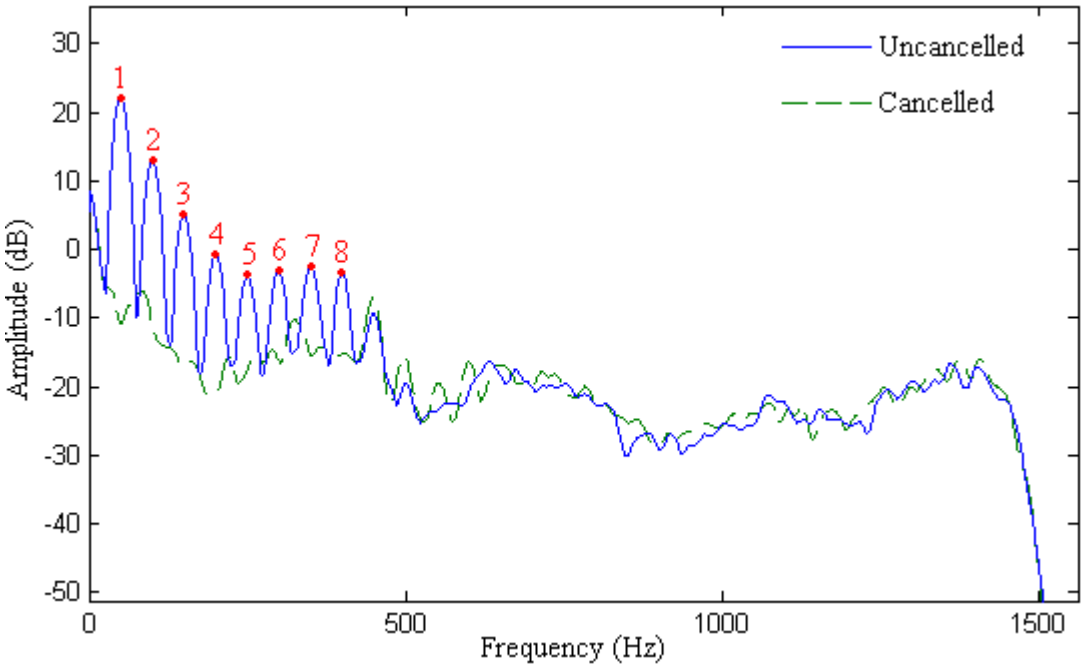

Figure 7.21 Measured frequency spectra with cancellation of 8 harmonics at 80 bar using the improved Bao's method

Cancellation reduces the fluid-borne noise by 20 dB to 30 dB on target frequency components. An increase due to the non-linear distorted response of the anti-noise servo valve still exists on uncancelled frequency components.

From the system estimation and noise cancellation results obtained in this section using the improved Bao's control method 20 dB to 30 dB of fluid-borne noise is attenuated with different working pressures. As there is nearly no flow difference between switching on and off the noise servo valve, reflection factors can be assumed the same

in these two stages and secondary path impulse responses are almost the same except for other effects. During the experiment a relatively small identification convergence factor is applied at the beginning of the second stage and the beginning period when turning the load valve to make the system stable. Because of high order harmonic components from the noise servo valve, which are not generated by the controller, distortion occurred on the secondary path impulse response at these frequencies, and when the power of the uncancelled harmonics is relatively large the secondary path estimation may be seriously distorted to make the system unstable. Additionally the distortion may also come from the extra white noise signal generated by the two-weight adaptive notch filter. Furthermore, the non-linear response of the anti-noise servo valve can bring a slight increase on the uncancelled frequency components. It is found that during the experiment the system may become unstable when the load valve at the end of the pipe is suddenly closed or nearly closed because the phase shift between the secondary path and its estimation is outside the range of $\pm 90^{\circ}$.

7.3.2 Experiment using Zhang's method

Similar with the improved Bao's control algorithm, Zhang's on-line control algorithm described in Chapter 6 is applied and experiments are implemented on the test rig with different working conditions. As discussed in Chapter 6, the extra white noise generated by two-weight adaptive notch filters is eliminated; hence faster convergence factors are applied for two-weight adaptive notch filters compared with the improved Bao's method. In the first stage only the secondary path identification controller is switched on and a large identification convergence factor is used. Then in the second stage the noise servo valve, noise cancellation controller and an interference controller are switched on when the impulse response in the first stage comes to a steady solution. A relatively small identification convergence factor is applied in the second stage to ensure stability. However, because of the 'cross-updating' in Zhang's method a longer operation time is needed with this relatively small value to obtain an accurate estimated impulse response compared with the improved Bao's method.

Estimated impulse responses in the first and second stages are compared in the time domain and frequency spectrum plotted in Figure 7.22 at 40 bar when the power of the uncancelled fluid-borne noise is relatively small. Compared with the result obtained

using the improved Bao's method in Figure 7.18, a more accurate secondary path estimation is obtained because the extra white noise generated by the two-weight adaptive notch filters is eliminated. However, as with the simulation represented in Chapter 6, more operation time is needed at the beginning of the second stage with a relatively small identification convergence factor because of the cross-update between the secondary path estimation and the accurate interference cancellation.

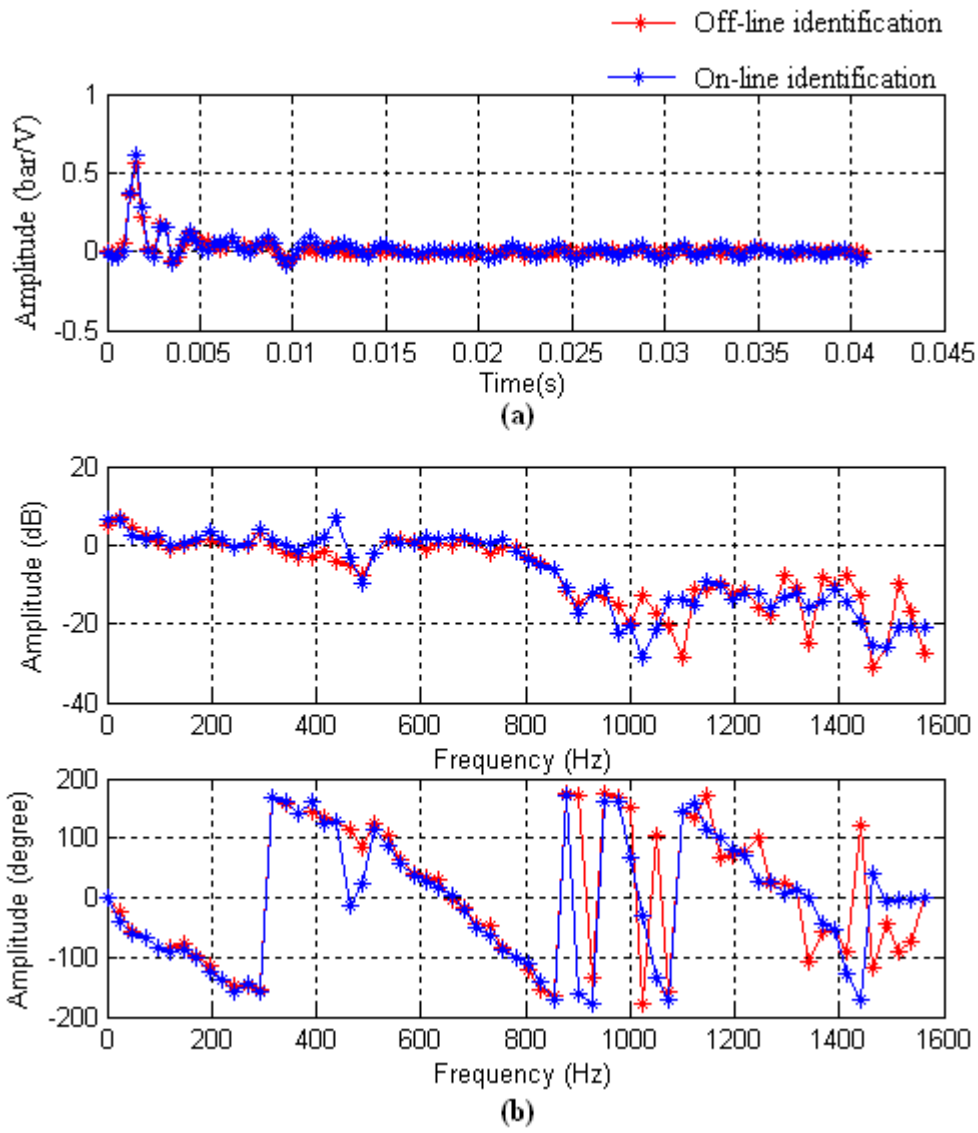

Figure 7.22 (a) Time domain impulse response comparison at 40 bar using Zhang's method

(b) Comparison of their amplitudes and phase shifts in the frequency domain

The power of the cancellation result is quite similar to that plotted in Figure 7.19. The uncancelled harmonic components also give a small distortion on the secondary path estimation at frequencies around 450 Hz and 500 Hz as shown in Figure 7.22.

As with the process in the improved Bao's method, an experiment is also realized at 80 bar by adjusting the load valve at the end of the pipe. Compared with the improved Bao's method, a longer operation time is needed at the beginning period with a relatively small identification convergence factor when adjusting the load valve, which is also because of the 'cross-updating' between the secondary path identification and the accurate interference cancellation. Compared with the one obtained at 40 bar, because of the smaller power of the background noise a more accurate secondary path impulse response estimation is obtained as shown in Figure 7.23 compared with the off-line result, which is obtained in the first stage.

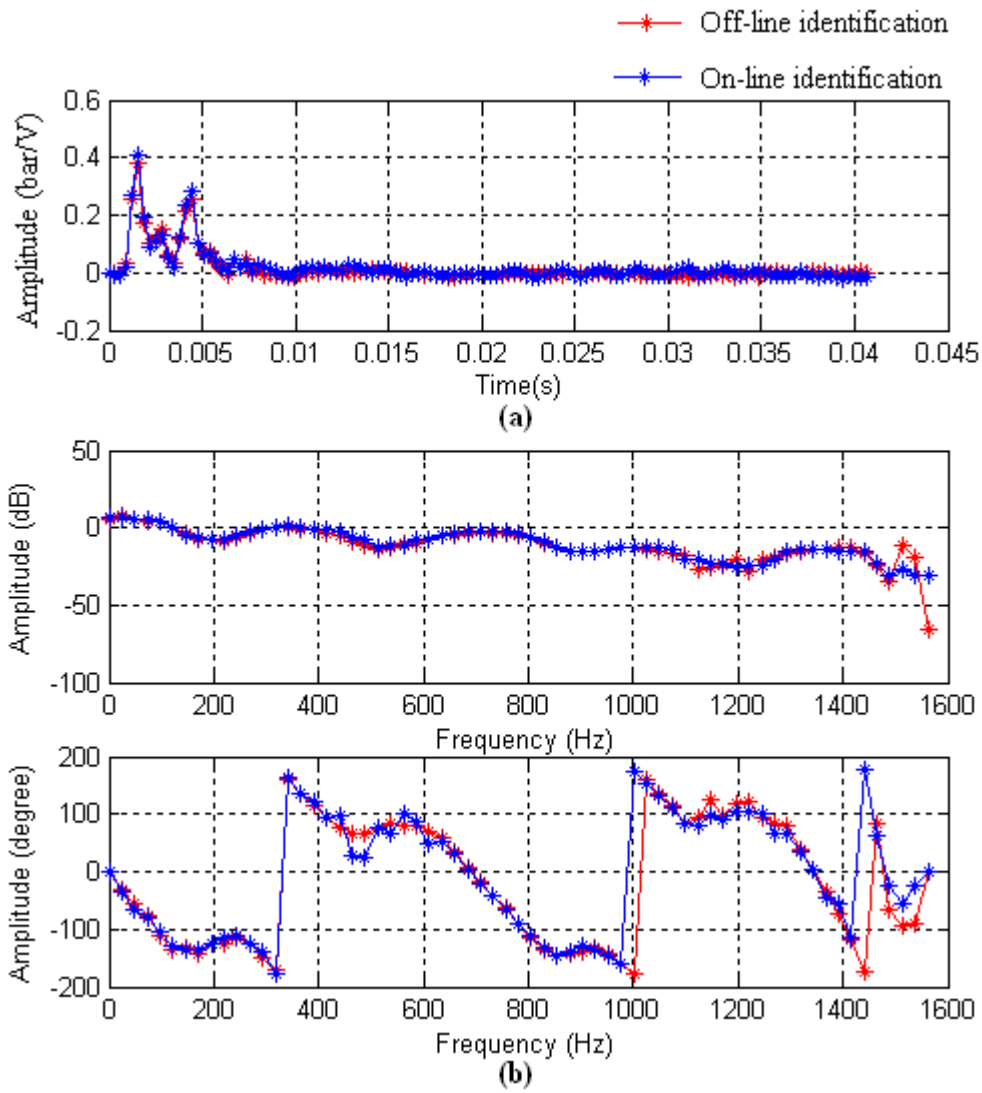

Figure 7.23 (a) Time domain impulse response comparison at 80 bar using Zhang's method

(b) Comparison of their amplitudes and phase shifts in the frequency domain

The cancellation result on the target harmonic components compared with the uncancelled signal is quite similar to the result plotted in Figure 7.21. The harmonic components with smaller power compared with that at 40 bar caused by the noise servo valve still existed after 8th harmonic. A small distortion on the secondary path impulse response occurs at the relative frequency around 450 Hz. 20 dB to 30 dB fluid-borne noise is attenuated on target frequencies in this experiment. A small increase is added on the uncancelled components because of the non-linear response of the anti-noise servo valve.

To summarize, accurate on-line secondary path estimation results are achieved using Zhang's method with different working conditions. 20 dB to 30 dB fluid-borne noise is cancelled using this method both at 40 bar and 80 bar. Harmonic components with relatively small power coming from the noise servo valve exist in the uncancelled noise and make small distortion on the secondary path identification at the relative frequencies. However, as with the improved Bao's method, the relatively large power of the uncancelled noise may make the system unstable. A slight increase on the uncancelled noise comes from the non-linear response of the anti-noise servo valve. During the experiment in the first stage a large identification convergence factor is applied. In the second stage a relatively small identification convergence factor is used to protect the system stability from the effect of primary noise decreasing. Compared with the improved Bao's method a longer operation time is needed with the relatively small identification convergence factor for both the beginning periods in the second stage and when changing the load valve because of the 'cross-updating' in Zhang's method. However, more accurate secondary path estimation result can be obtained. It is also found that when the pipe end is suddenly closed or nearly closed the system may become unstable because the phase difference between the secondary path and its estimation is out of the stable range.

7.3.3 Experiment using frequency domain method

In this section another on-line fluid-borne noise cancellation algorithm is implemented on the test rig with different working pressures. The convergence factors of the two-weight adaptive filters are the same as those used in Zhang's method. In this method an adaptive function is applied for the convergence coefficient in the secondary path identification controller as discussed in Chapter 6. This convergence function can give a small convergence value on the frequency components with large power. This function can avoid the effect of large interference from the powerful uncancelled residual noise to make identification system stable. As no interference controllers are used this controller has a more simple structure than the other on-line noise control methods. However, because signals are transformed between time domain and frequency domain twice in the controller more calculation burden is added on the processor.

Firstly experiment is realized at 40 bar using this algorithm. The control process divides into two stages, the same as those used in sections 7.3.1 and 7.3.2. In the first stage a large identification convergence vector is applied. Because the noise cancellation starts at the beginning of the second stage, the decrease of the primary noise may affect the secondary path estimation to make the system unstable. In the second stage a relatively small identification convergence vector is used. In Figure 7.24 the impulse responses of the secondary path are compared between off-line and on-line methods.

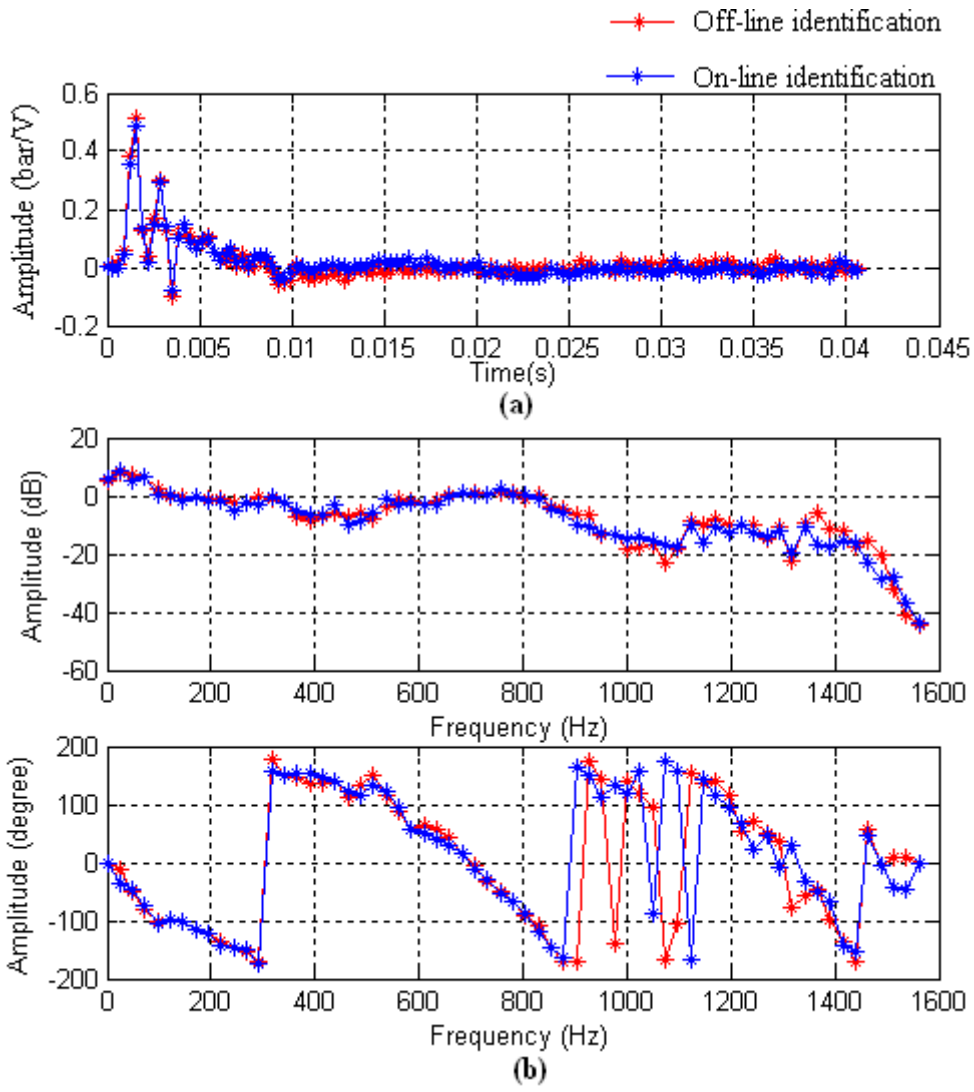

Figure 7.24 (a) Time domain impulse response comparison at 40 bar using the frequency domain method

(b) Comparison of their amplitudes and phase shifts in the frequency domain

Comparing the identification result using the improved Bao's and Zhang's control algorithms at this working pressure in Figures 7.18 and 7.22, although the extra white noise generated by the two-weight adaptive filter may affect the identification, a more accurate impulse response is obtained because a suitable convergence factor is provided for corresponding frequencies, which are not cancelled. The power of the fluid-borne noise cancellation compared with the uncancelled one is also quite similar to the plot in Figure 7.19. However, the effect from the 450 Hz, 500 Hz etc. components is almost eliminated by the adaptive convergence function in the identification controller.

Furthermore similar to the improved Bao's method, an experiment is also implemented at 80 bar by adjusting the load valve at the end of the pipe pressure. As discussed in the simulation using this method in Chapter 6 the relatively small identification vector is still applied to protect accurate secondary path identification from the variation of primary noise. After a period the accurate impulse response compared with the one obtained using off-line method is plotted in Figure 7.25.

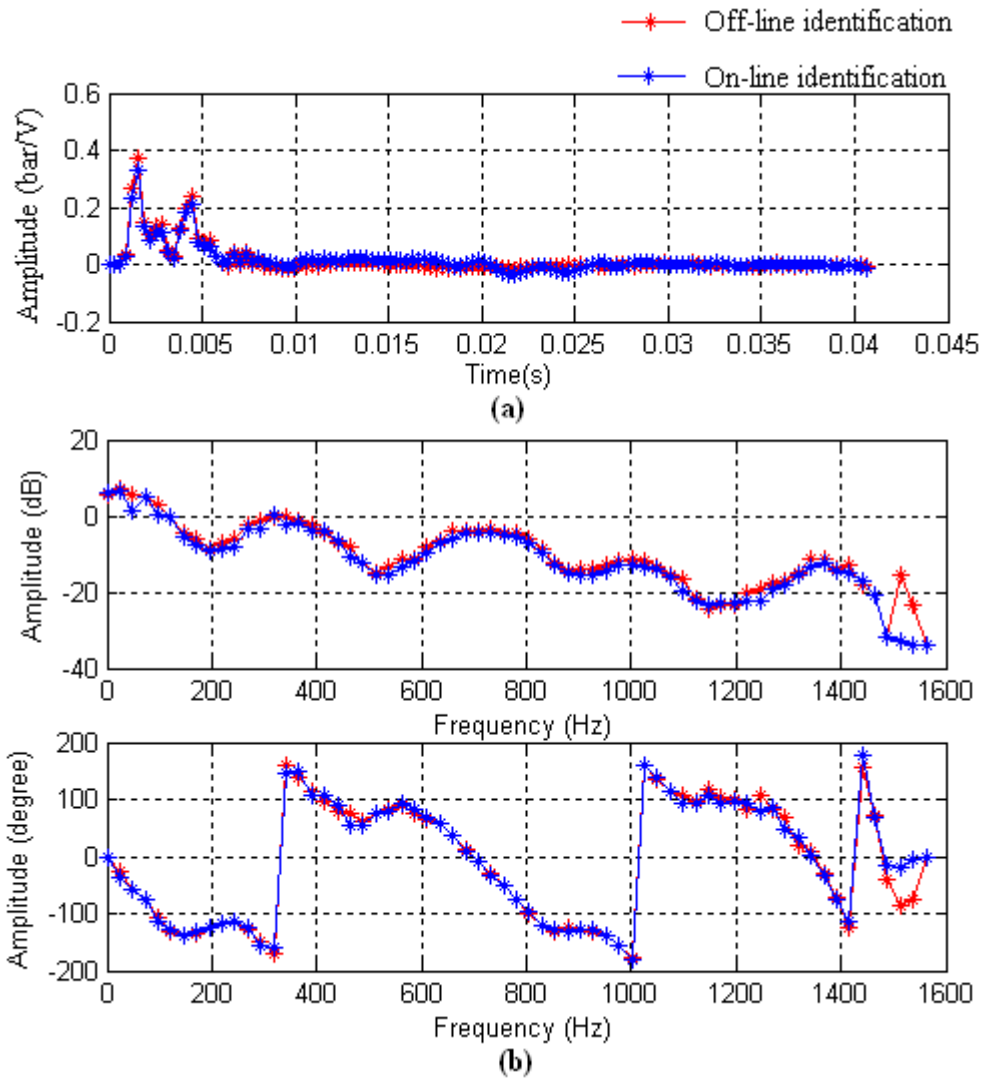

Figure 7.25 (a) Time domain impulse response comparison at 80 bar using the frequency domain method

(b) Comparison of their amplitudes and phase shifts in the frequency domain

During the whole process the convergence factors used for two-weight adaptive notch filters are not changed. Compared with the identification result obtained at 40 bar in Figure 7.24, a more accurate secondary path estimation is obtained because of smaller background noise effect at this pressure as plotted in Figure 7.17.

The noise cancellation result compared with the uncancelled one is similar to Figure 7.21.

To summarize, fluid-borne noise cancellation results obtained using this frequency domain on-line cancellation method and the experimental process are similar to those obtained and used in the improved Bao's method. As an adaptive convergence vector, which can give a suitable convergence factor to the corresponding frequency components, is applied the effect from the uncancelled noise components can be eliminated. Hence more accurate secondary path estimation can be obtained. However, as signals are transformed between time domain and frequency domain, more calculation time is needed for the processor for calculation. In the experiment the system may become unstable when the load valve is suddenly closed or nearly closed.

7.4 Conclusions

To conclude, in this chapter a test rig with simple hydraulic circuit is built up using a servo valve as the noise source to give an artificial fluid-borne noise and another one, which has fast response, as an anti-noise source. The purpose of it is to test the feasibility of different control methods implemented on a simple hydraulic system. Depending on the ability of the noise servo valve only 8 harmonics of fluid-borne noise is generated, which are used as the target frequencies to be cancelled.

Off-line identification methods associated with a two-weight adaptive notch filter described in Chapter 5 are tested on first the experimental rig. An accurate secondary path impulse response is obtained for different working conditions and 20 dB to 30 dB fluid-borne noise is cancelled on the target frequencies. Limitation of this cancellation result may come from the background noise generated by the ring main. Harmonic components from the noise servo valve, which are not generated from the controller, are added to the uncancelled noise. Non-linear response of the anti-noise servo valve also increases the uncancelled noise slightly. However, with the off-line identification method the secondary path impulse response needs to be re-estimated when the working conditions change.

On-line control algorithms discussed in Chapter 6 are then implemented on the test rig using the two proposed manipulation strategies. Using this kind of controller 20 dB to 30 dB of attenuation is achieved. Limitation of this cancellation result may not only come from the background noise from the ring main but also from the auxiliary white noise for on-line identification methods. A slight increase on uncancelled noise comes

from non-linear response of the anti-noise servo valve. During the experiment a relatively small identification convergence factor is used in the second stage and the beginning period when adjusting the load valve because the primary noise cancellation process can affect the secondary path estimation. Faster convergence speed is reached using the Zhang's method and the frequency domain method in the experiments. However, longer operation time is needed with the relatively small identification convergence factor for Zhang's method because of the 'cross-updating'. Harmonics from the noise servo valve exist in uncancelled noise and may affect the secondary path estimation. Additionally, for the improved Bao's method and the Zhang's method when the power of the uncancelled harmonic components is relatively large compared with the white noise, the secondary path estimation may seriously be distorted to make the system unstable. As an adaptive identification convergence vector is applied, the frequency domain method, which is the most efficient on-line control algorithm of the three, can obtain accurate secondary path estimation by eliminating the effect of the uncancelled harmonics.

During experiments it was found that when the load valve is suddenly closed or nearly closed the system may become unstable because of the phase shift between the secondary path and its estimation goes out of the stable range. From these tests the controllers and hardware applied on the rig are proved by the overall success of the experiments, and all these devices will be used during the tests in Chapter 8 with a real pump as a noise source.

CHAPTER 8

Experiment research using real pump

In this chapter a real pump is applied as the source of fluid-borne noise instead of the servo valve unit on the test rig. A new hydraulic circuit was built to suit this change. Experiments were implemented using both off-line and on-line (Zhang's method and frequency domain method) control algorithms, which are discussed in Chapters 5 and 6, to cancel narrowband fluid-borne noise in different working conditions and test results are analyzed. Two manipulation strategies are realized to implement the fluid-borne noise cancellation. dSPACE® model 1005 is used as a signal processor with sampling frequency 3125 Hz.

8.1 Test rig and frequency synchronization

The layout of the test rig with a real pump, as a fluid-borne noise source for experiments is shown in Figure 8.1. The pump is an axial piston type with three pistons. It runs at around 16.47 Hz (approximately 1000 rev/min) and can supply a maximum pressure of 56 bar and maximum flow rate of 12.2 L/min. The circuit diagram is shown in Figure 8.2.

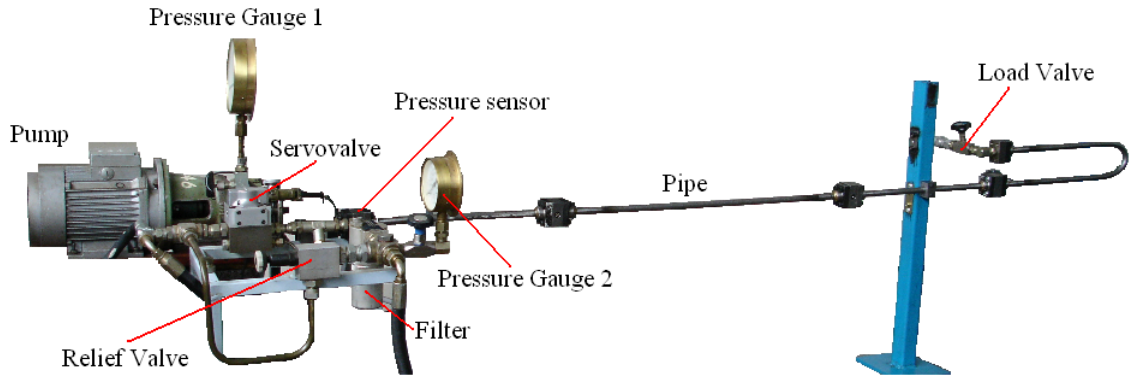

Figure 8.1 Test rig using a real pump as fluid-borne noise source

As a real pump is applied in the rig, its frequency when switching on cannot usually be obtained in advance. Therefore frequency synchronization is needed in order to obtain

reference signals for adaptive notch filter. As shown in Figure 8.2 one tooth is fixed on the shaft of pump and a tachometer is applied to generate one impulse, whose amplitude is 5 volt, every rotation. Then after amplifier and A/D converter, dSPACE® card 4001 can pick up this signal and change it to the value of frequency.

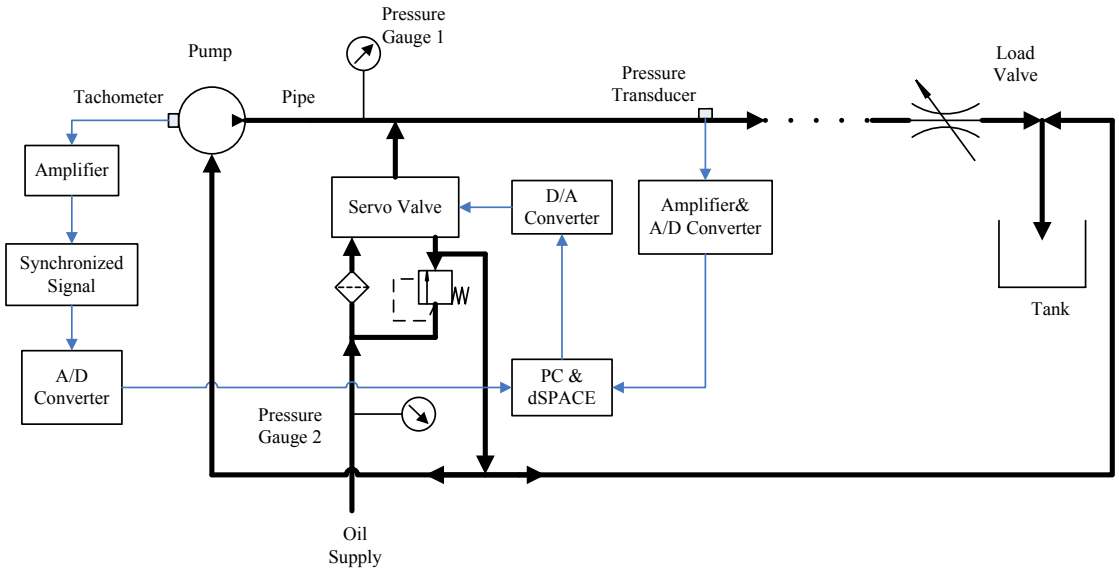

Figure 8.2 Sketch structure of test rig using a real pump as noise source

However, in real experiment the estimated frequency of the pump is not a fixed value and a small fluctuation occurs. Care must be taken to handle these frequencies correctly. Reference input signals are deduced using equations:

$$x_1(n) = \sin(\omega \cdot n \cdot \Delta t) \tag{8.1}$$

$$x_2(n) = \cos(\omega \cdot n \cdot \Delta t) \tag{8.2}$$

where ω is the frequency to be synchronized.

If a new frequency $\omega + \Delta\omega$ occurs at time $(n+1)\cdot\Delta t$, the bracket term at the right hand side of equations (8.1) and (8.2) can be written as:

$$(\omega + \Delta\omega)\cdot(n \cdot t + \Delta t) = \omega \cdot n \cdot \Delta t + (\omega + \Delta\omega)\Delta t + \Delta\omega \cdot n \cdot \Delta t \tag{8.3}$$

A sudden jump, which is caused by the last term in equation (8.3), occurs at the point when frequency changes is shown in Figure 8.3 (b) using the blue line. As a result a

sharp change happens in the reference input signals. In Figure 8.4 this effect is plotted using a sine wave when frequency changes from 20 rad/s to 30 rad/s at 0.5 s.

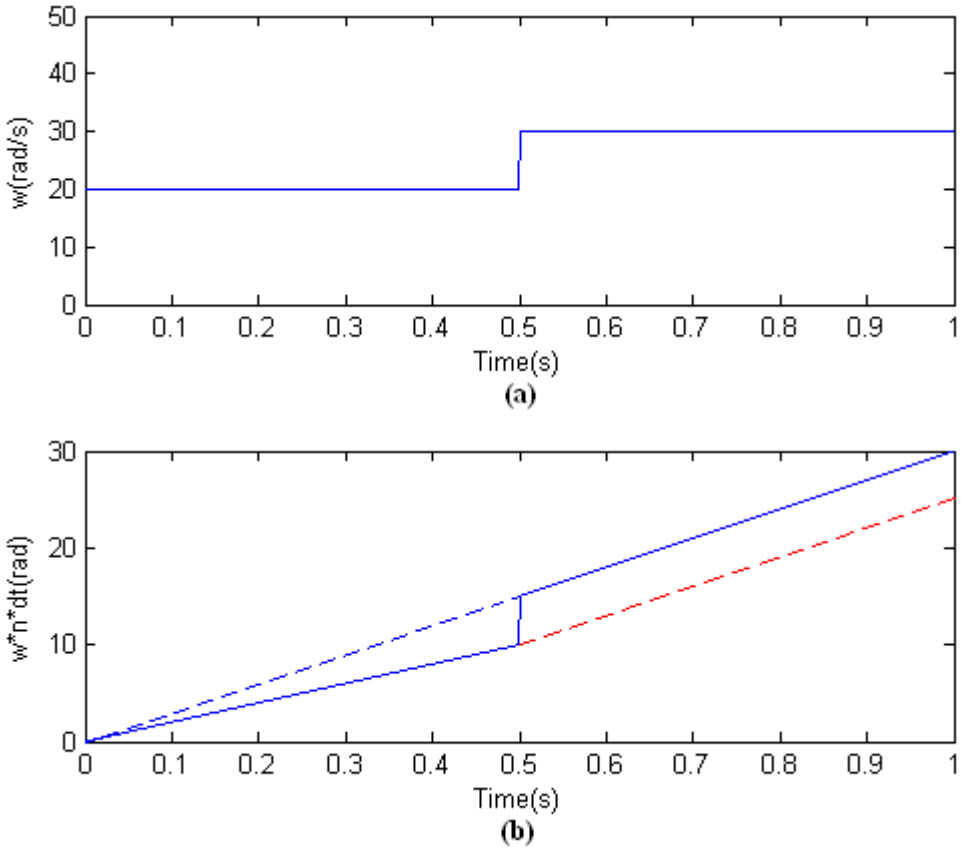

Figure 8.3 (a) Frequency changes with time
(b) Frequency multiplied by time changes with time

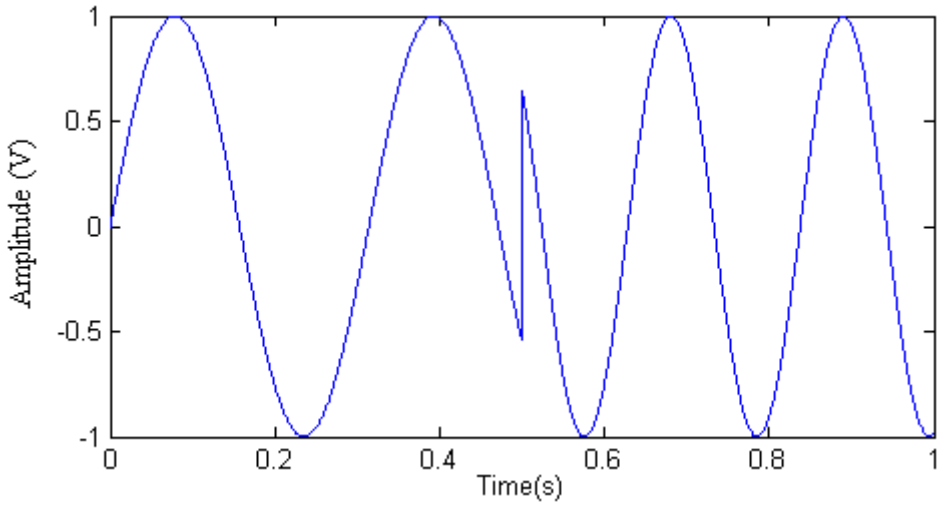

Figure 8.4 Frequency changing from 20 rad/s to 30 rad/s: effect on a sine wave

Under this effect the fluid-borne noise cancellation cannot be realized and the system may become unstable. To eliminate this effect the third term on the right hand side of equation (8.3) should be discarded. Assume at time n synchronized frequency is $\omega \cdot n \cdot \Delta t$ and at time n+1 it is $\omega \cdot n \cdot \Delta t + (\omega + \Delta\omega)\Delta t$ and $\omega' = \omega + \Delta\omega$ is the new frequency. Using this assumption the value of frequency multiplying time can be represented using the red dashed line in Figure 8.3. Hence reference input x_1 at time n is $\sin(\omega \cdot n \cdot \Delta t)$ and at time n+1 can be written as:

$$\sin(\omega \cdot n \cdot \Delta t + \omega' \cdot \Delta t)$$

$$= \sin(\omega \cdot n \cdot \Delta t) \cdot \cos(\omega' \cdot \Delta t) + \cos(\omega \cdot n \cdot \Delta t) \cdot \sin(\omega' \cdot \Delta t)$$

In this equation $\sin(\omega \cdot n \cdot \Delta t)$ and $\cos(\omega \cdot n \cdot \Delta t)$ are signals at time n, $\cos(\omega' \cdot \Delta t)$ and $\sin(\omega' \cdot \Delta t)$ are signals at time n+1. Let $S_n = \sin(\omega \cdot n \cdot \Delta t)$ and $C_n = \cos(\omega \cdot n \cdot \Delta t)$, the new values of reference input signals depend on their old values and are represented using following equations:

$$x_1(n+1) = S_{n+1} = S_n \cdot \cos(\omega' \cdot \Delta t) + C_n \cdot \sin(\omega' \cdot \Delta t)$$
$$x_2(n+1) = C_{n+1} = C_n \cdot \cos(\omega' \cdot \Delta t) - S_n \cdot \sin(\omega' \cdot \Delta t)$$

In Figure 8.5 the sine wave with frequency change from 20 rad/s to 30 rad/s at 0.5 s is plotted.

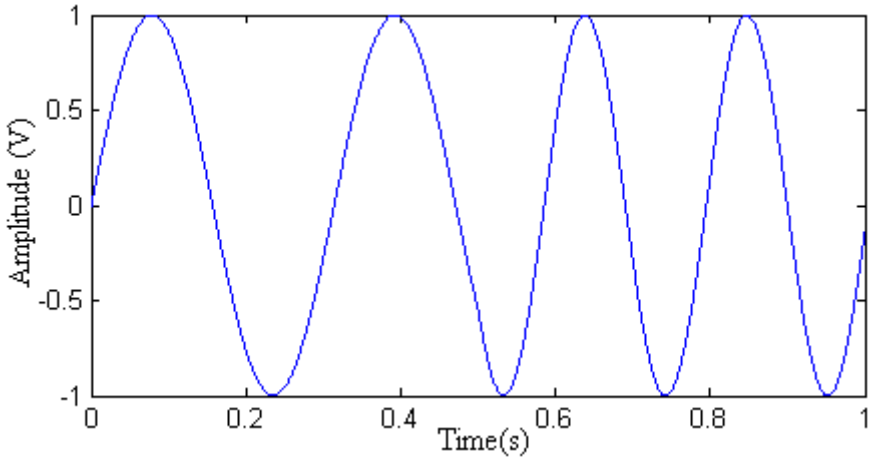

Figure 8.5 Frequency changing from 20 rad/s to 30 Hz without effect on a sine wave

Compared with Figure 8.4, the sudden change effect is eliminated using this reference signals generation method. Another equivalent method can also avoid the effect from the frequency sudden jump using the following equations:

$$x_1(n) = \sin(\theta_n \cdot n)$$
$$x_2(n) = \cos(\theta_n \cdot n)$$

where

$$\theta_{n+1} = \theta_n + \omega_n \cdot \Delta t$$

ω_n is the frequency at nth time step.

Furthermore, in order to smooth out fluctuations a first order low pass filter is applied:

$$f'(n+1) = \alpha \cdot f'(n) + (1-\alpha) \cdot f(n+1)$$

where f' is the frequency after filter and f is the obtained value from pump, *n* is the time index. Parameter α determines the amount of smoothing.

In the following sections fluid-borne noise cancellation with off-line and on-line control methods are implemented and results are discussed.

8.2 Noise cancellation using off-line control algorithms

Firstly off-line control methods, which use delay unit compensation and compensation from secondary path impulse response, are realized on this rig in this section. Three different working pressures 10 bar, 25 bar and 80 bar are set by turning the load valve in Figure 8.2 during experiments to obtain different loads and different levels of noise. Test results from different working conditions are also discussed.

8.2.1 Background noise on test rig

In this experiment pressure from the oil supply is 100 bar. As plotted in Figure 8.2 the oil supply to this hydraulic system is from a powerful pump, which can give 250 bar maximum pressure and 80 L/min maximum flow, in a ring main. Hence fluid-borne

noise generated by this pump can be transmitted to the rig and can be detected by a pressure sensor. As shown in Figure 8.6 background noise with different working pressures 10 bar, 25 bar and 80 bar are plotted in time domain.

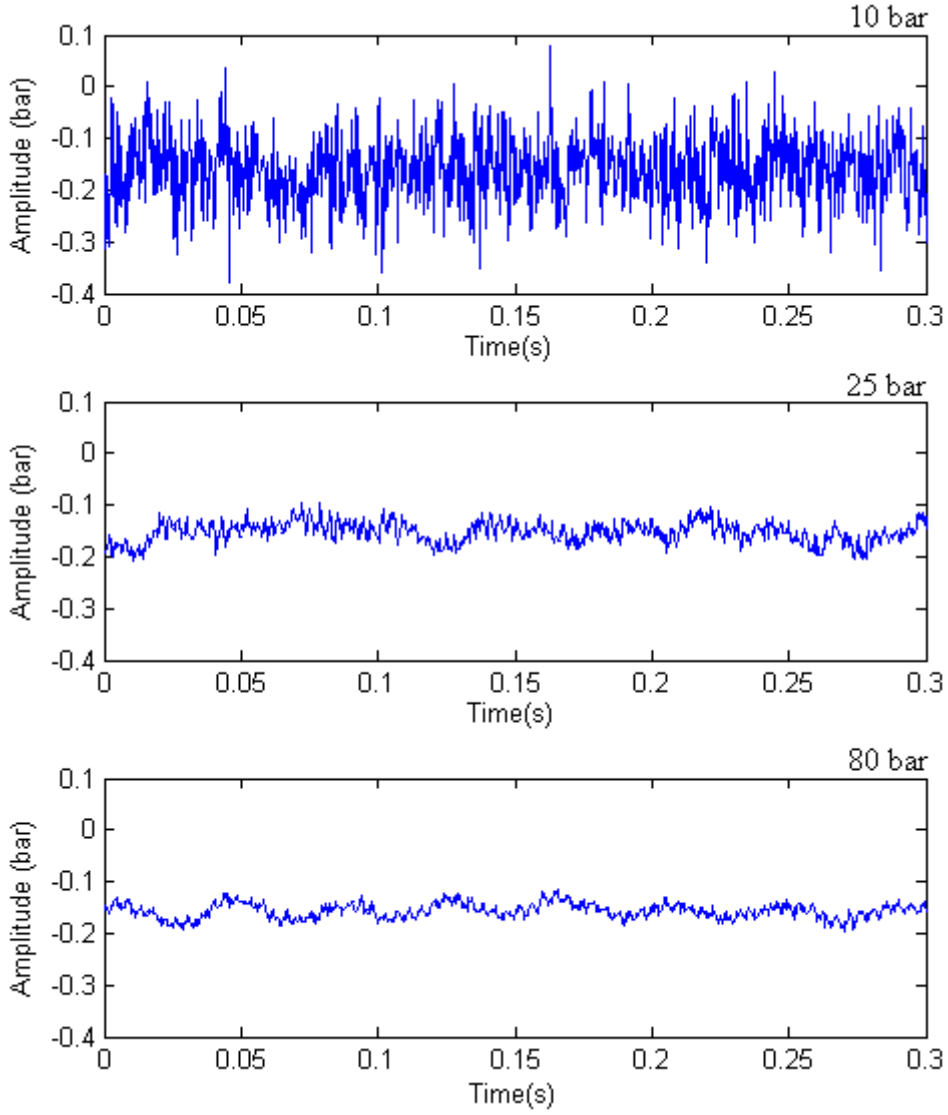

Figure 8.6 Background noise along the rig pipe for different pressures

As shown in the figure above, with an increase of pressure the background noise from the ring main becomes smaller, which means a smaller disturbance for both system identification and fluid-borne noise cancellation.

8.2.2 Dynamics characteristics of secondary path

Firstly, in order to check whether or not delay unit compensation can work for this rig secondary path dynamic impulse response is needed. In this experiment, the power of

white noise applied is 0.1 V^2 for pressures 10 bar, 25 bar and 80 bar as shown in Figure 8.7.

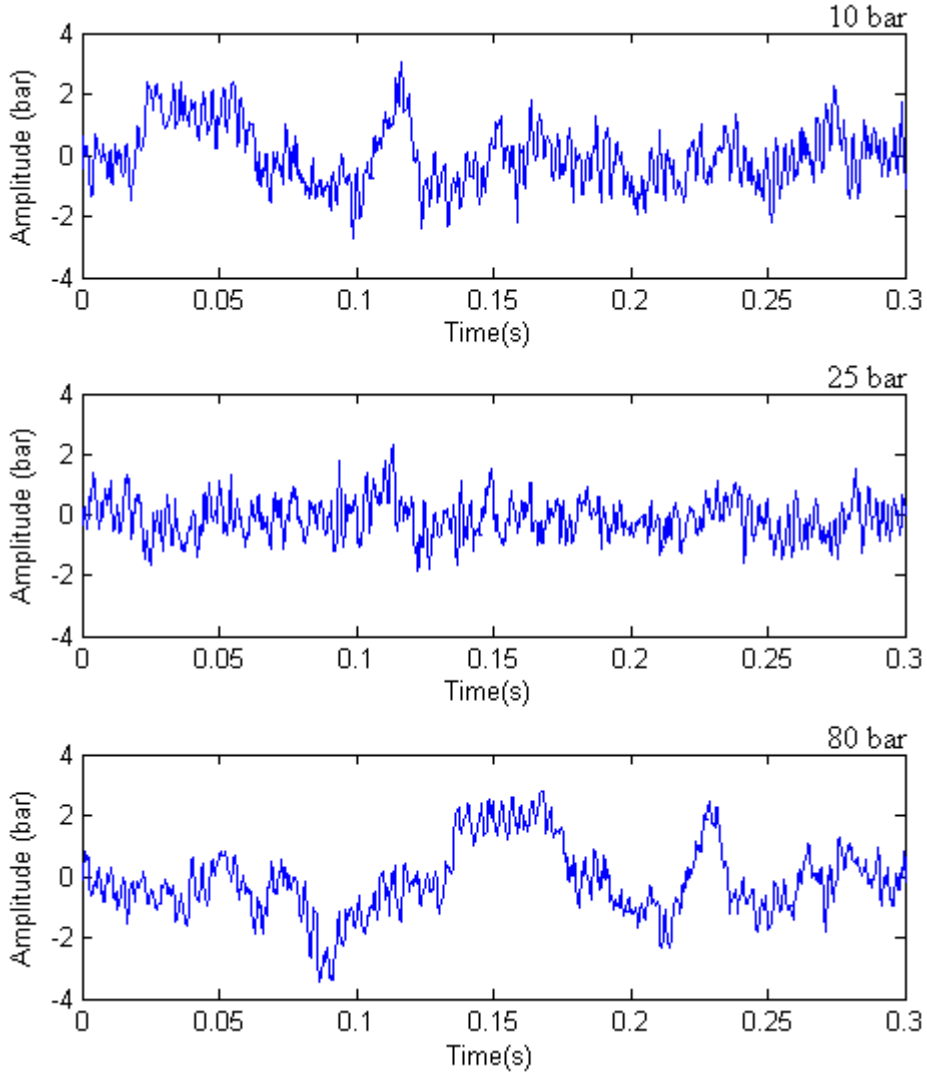

Figure 8.7 White noise used for secondary path estimation with power of 0.1 V^2 plus background noise

64 orders and 128 orders weighting functions are applied to obtain a secondary path impulse response estimation and compared in time domain with different working pressures (10 bar, 25 bar and 80 bar) as shown in Figure 8.8, 8.9 and 8.10. From comparison of impulse response with 64 orders and 128 orders in different pressure conditions weighting function with 64 orders tends to miss part of the secondary path estimation under a constant sampling frequency when the pressure increases.

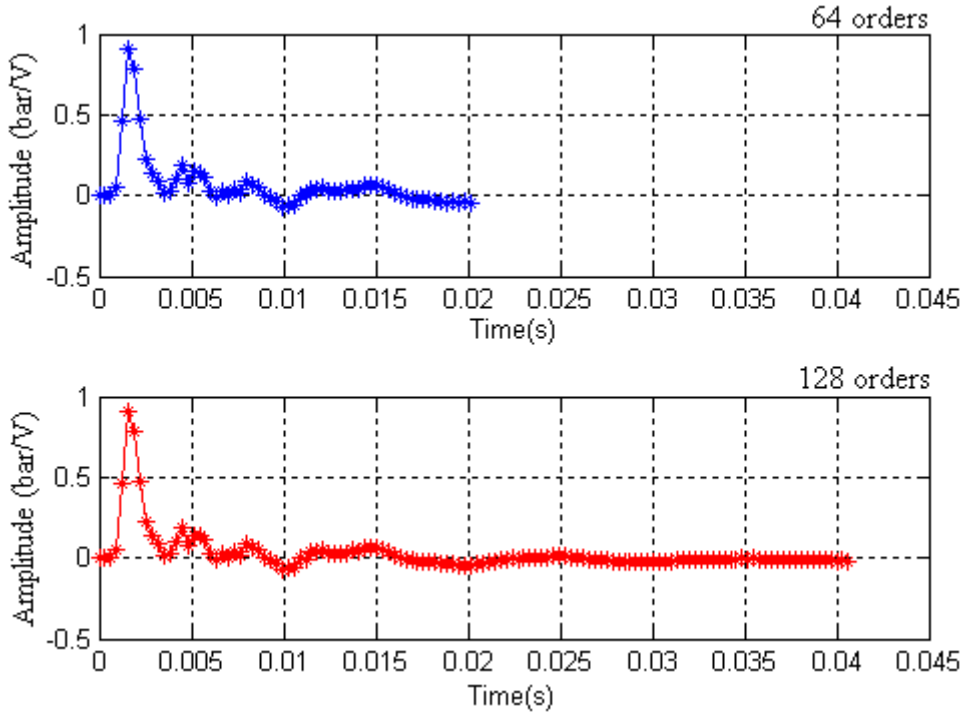

Figure 8.8 Secondary path impulse responses at 10 bar with different lengths

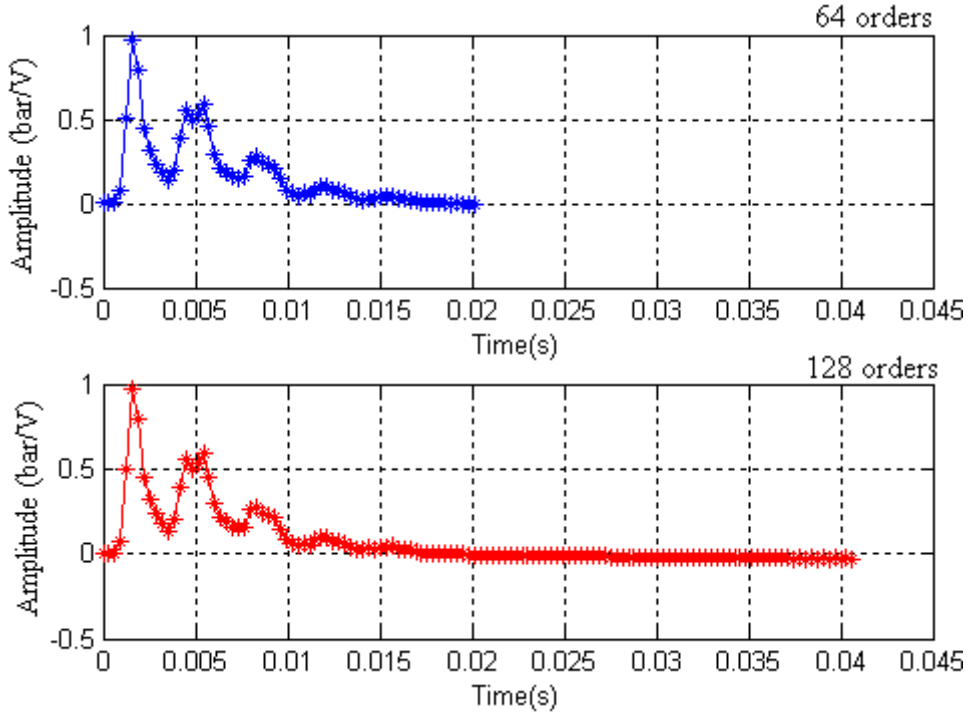

Figure 8.9 Secondary path impulse responses at 25 bar with different lengths

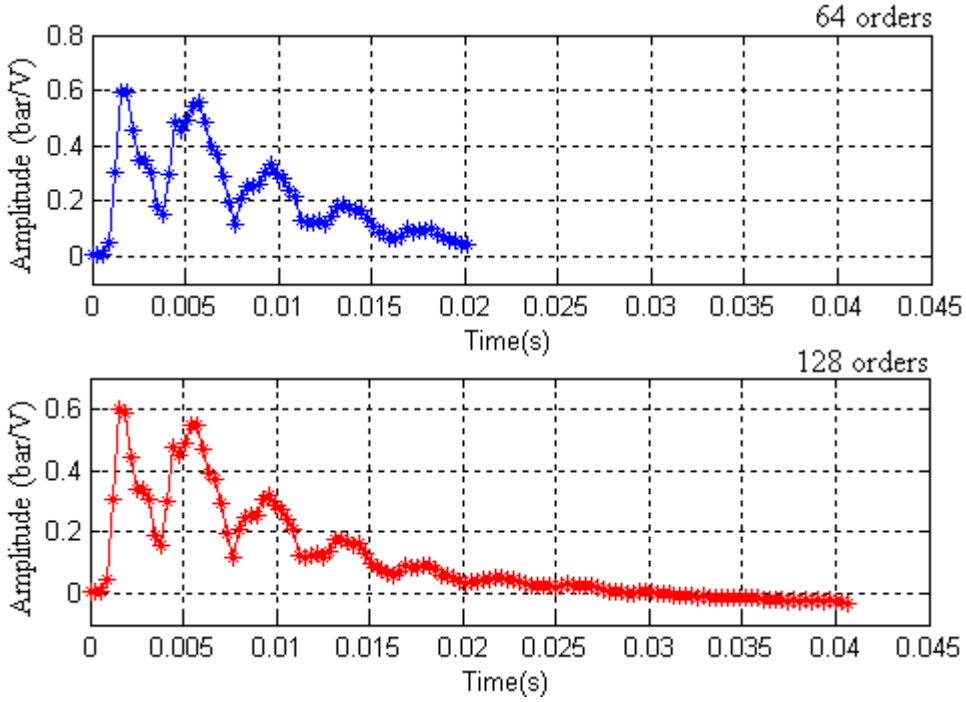

Figure 8.10 Secondary path impulse responses at 80 bar with different lengths

In order to check the secondary path phase shift for different frequencies its 128 orders impulse responses are plotted in the frequency domain and compared with the value obtained from the ratio between secondary path input and output in the frequency domain for these three different pressures as shown in Figures 8.11, 8.12 and 8.13. As white noise applied here for identification is from 1 Hz to 1500 Hz, accurate results can be obtained for this bandwidth.

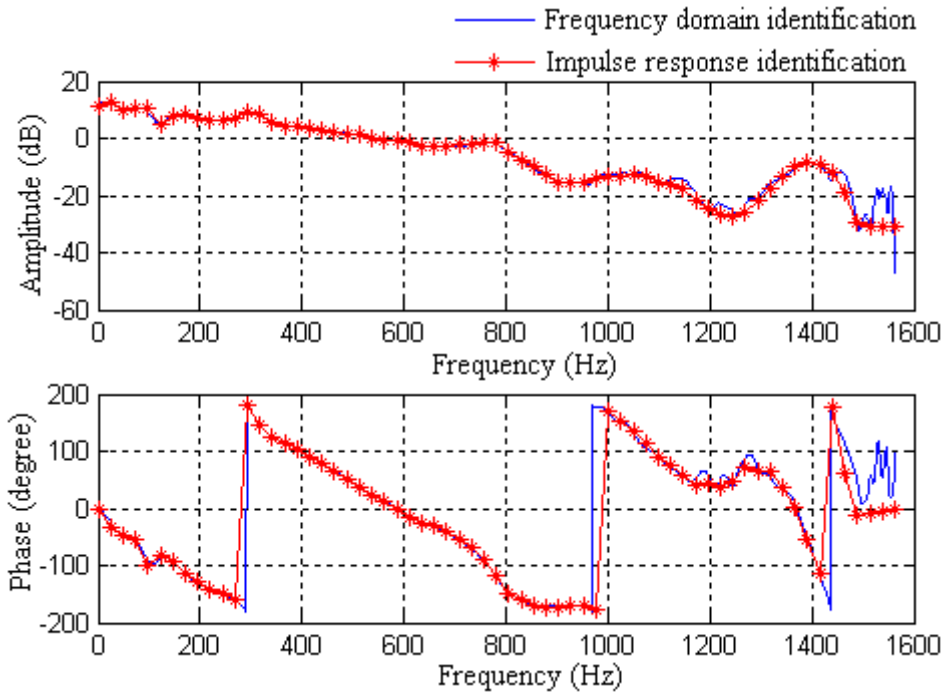

Figure 8.11 Comparison between Frequency domain and offline impulse response identification at 10 bar

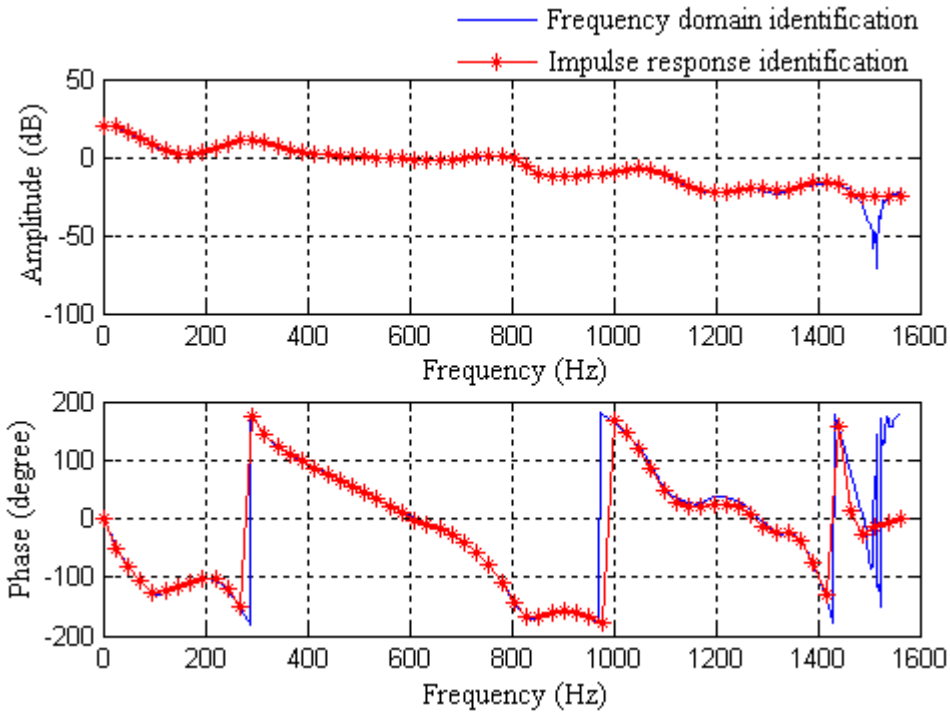

Figure 8.12 Comparison between Frequency domain and offline impulse response identification at 25 bar

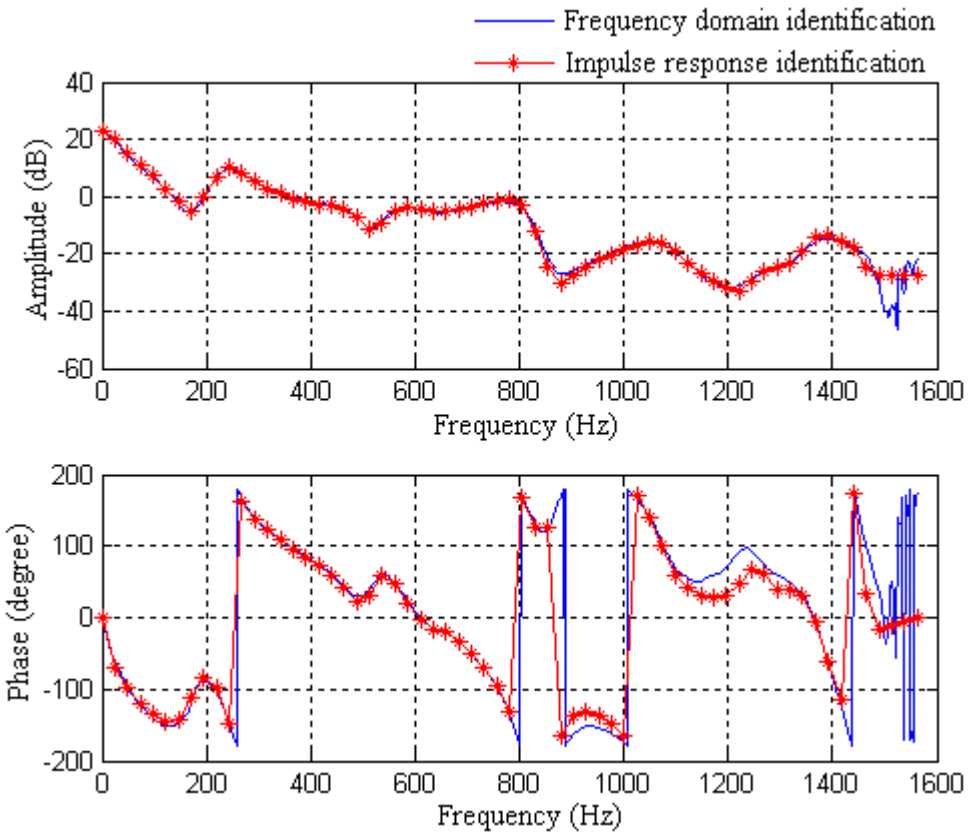

Figure 8.13 Comparison between Frequency domain and offline impulse response identification at 80 bar

Firstly, from these results in the frequency domain, the impulse response of secondary path estimation obtained using an off-line identification method is accurate enough for both amplitude and phase shift. Secondly, from the plots of phase from 0 to 800 Hz, the relationship between phase shift and frequency can be roughly seen as linear and the 2π delay occurred around 800 Hz. Since sampling frequency in this experiment is 3125 Hz, a delay of 4 samples can be used for delay unit to compensate the secondary path effect for most frequencies.

8.2.3 Delay unit compensation

Before implementing cancellation, the fluid-borne noise generated by the rig pump plus background noise with these different working pressures (10 bar, 25 bar and 80 bar) are as plotted in Figure 8.14.

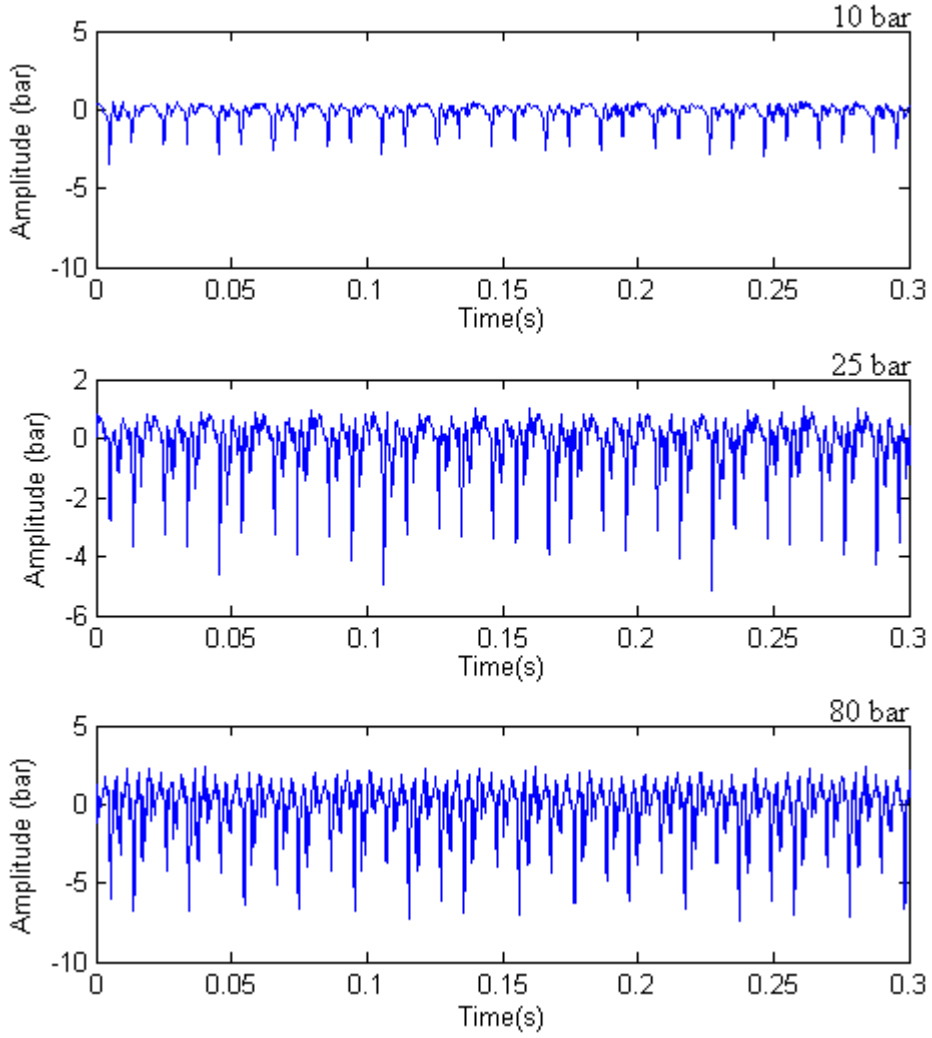

Figure 8.14 Fluid-borne noise from a rig pump plus background noise

Comparing fluid-borne noise in Figure 8.14 with background noise shown in Figure 8.6, with an increase of pressure background noise becomes smaller while fluid-borne noise increases, which means more effect come to system identification and noise cancellation performance with high pressure.

4 sample delays are applied in the delay unit for compensation with the two-weight adaptive notch filter, which is discussed in Chapter 5. As the rig pump has three axis pistons, hence fluid-borne noise harmonic frequencies are 3, 6, 9…etc. times of pump frequency. In this experiment according to the calculation ability of dSPACE® 1005, 15 harmonic frequencies are attempted to be cancelled with pressures of 10 bar, 25 bar and 80 bar. Cancellation results in frequency domain are shown in Figure 8.15, 8.16 and 8.17 compared with the uncancelled noise.

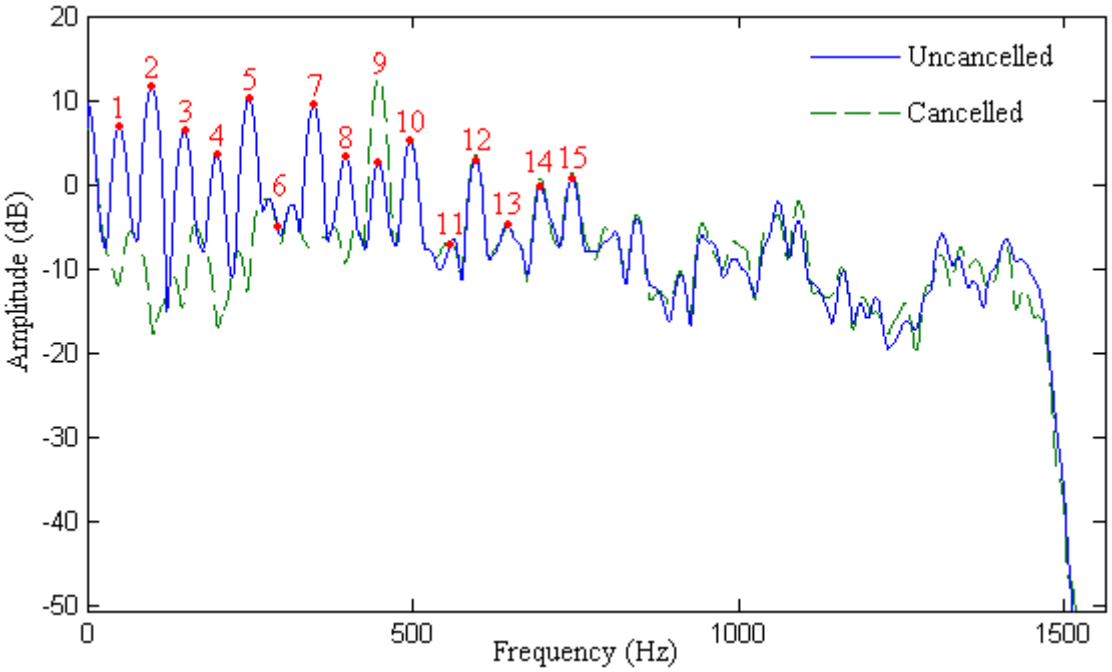

Figure 8.15 Measured frequency spectra with cancellation of 9 harmonics at 10 bar using delay unit off-line compensation

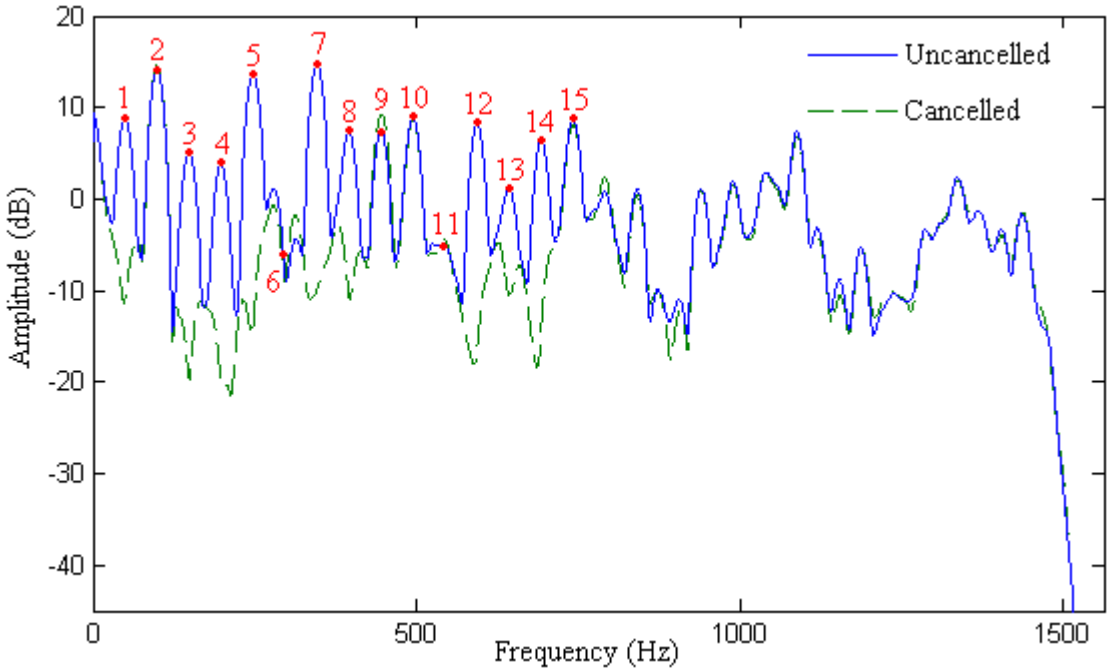

Figure 8.16 Measured frequency spectra with cancellation of 11 harmonics at 25 bar using delay unit off-line compensation

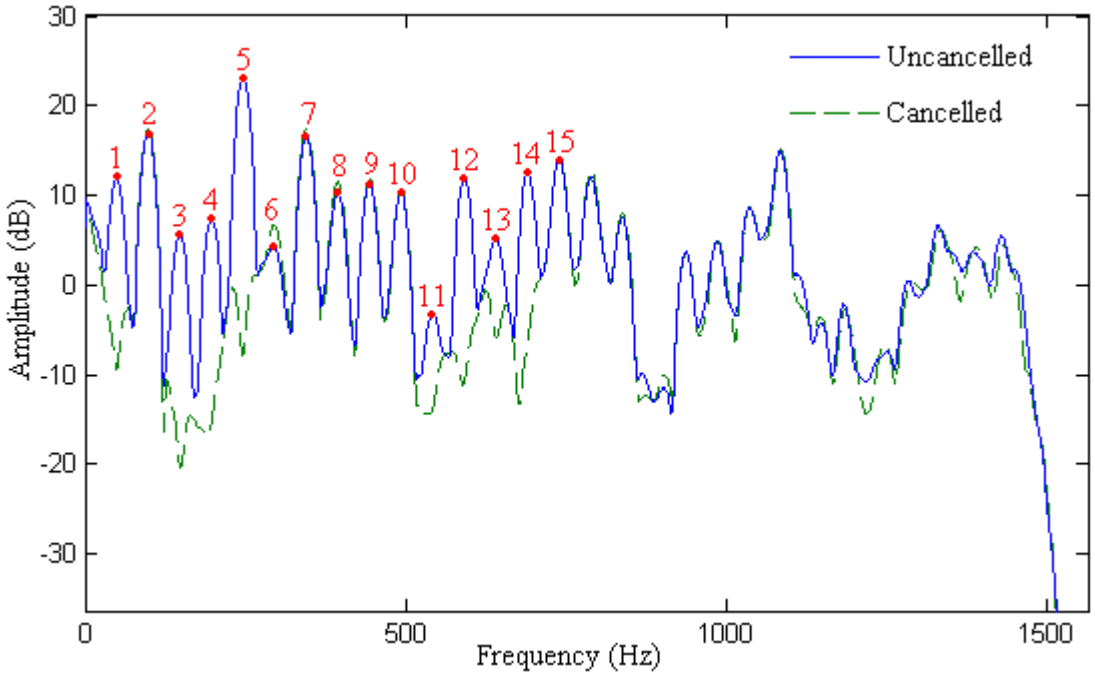

Figure 8.17 Measured frequency spectra with cancellation of 8 harmonics at 80 bar using delay unit off-line compensation

In real experiment the secondary path cannot only be seen as a delay unit especially for high pressure working conditions. Hence a uniform delay unit for all frequencies may not give correct compensation and may make the system unstable. In the experiment at 10 bar, Figure 8.15, it was necessary to disable the contribution for the 10^{th}, 11^{th}, 12^{th}, $13^{th,}$ 14^{th} and 15^{th} harmonics to avoid instability. The 9^{th} harmonic component increases and tends to make the system unstable, which is also caused by inaccurate compensation. For 25 bar, Figure 8.16, the controllers for the 2^{nd}, 10^{th}, 11^{th} and 15^{th} harmonics controller are disabled to avoid sudden instability and the 9^{th} component starts to be unstable. For pressure at 80 bar 1^{st}, 3^{rd}, 4^{th}, 5^{th}, 11^{th}, 12^{th}, 13^{th} and 14^{th} harmonic controllers are enabled to achieve good cancellation results. Overall for the cancelled components 20 to 30 dB fluid-borne noise is attenuated. Limitation of this result may come from the background noise from the ring main. Additionally slightly increase is added on the uncancelled harmonics because of non-linear response of anti-noise servo valve.

8.2.4 Compensation using secondary path estimation

In order to overcome this problem, the estimation of secondary path impulse response is applied for compensation as presented in Chapter 5. The 128 orders impulse response are obtained before realizing noise cancellation as plotted in Figures 8.8, 8.9 and 8.10 for pressure 10 bar, 25 bar and 80 bar. Fluid-borne noise cancellation results are plotted in Figure 8.18, 8.19 and 8.20 for the three different pressures.

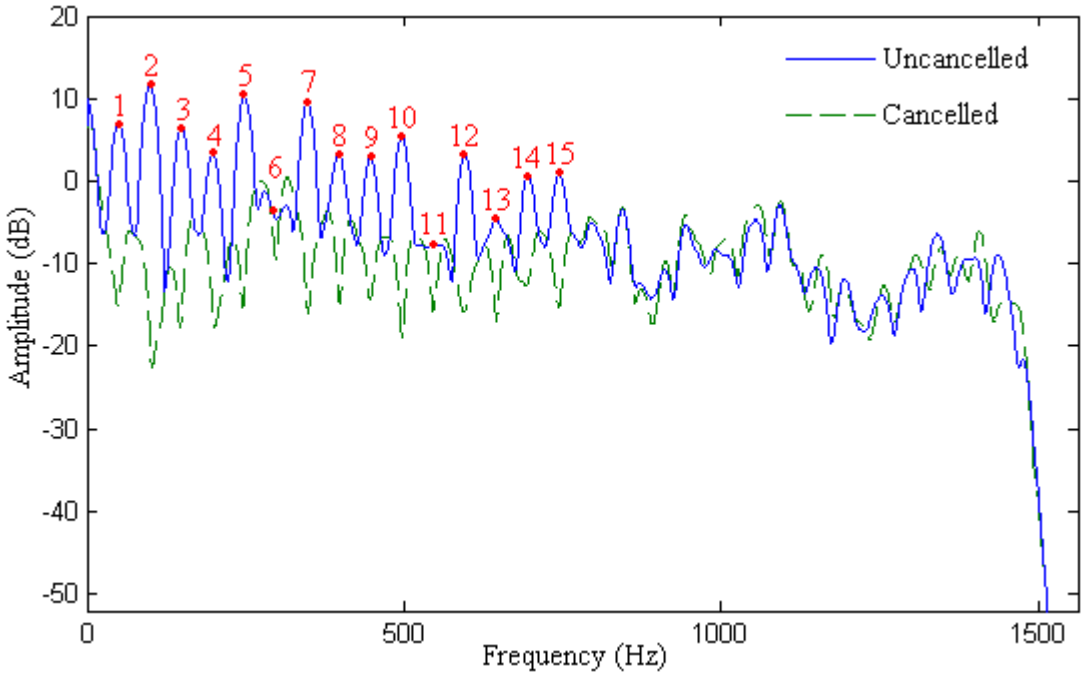

Figure 8.18 Measured frequency spectra with cancellation of 15 harmonics at 10 bar using off-line secondary path estimation, for compensation

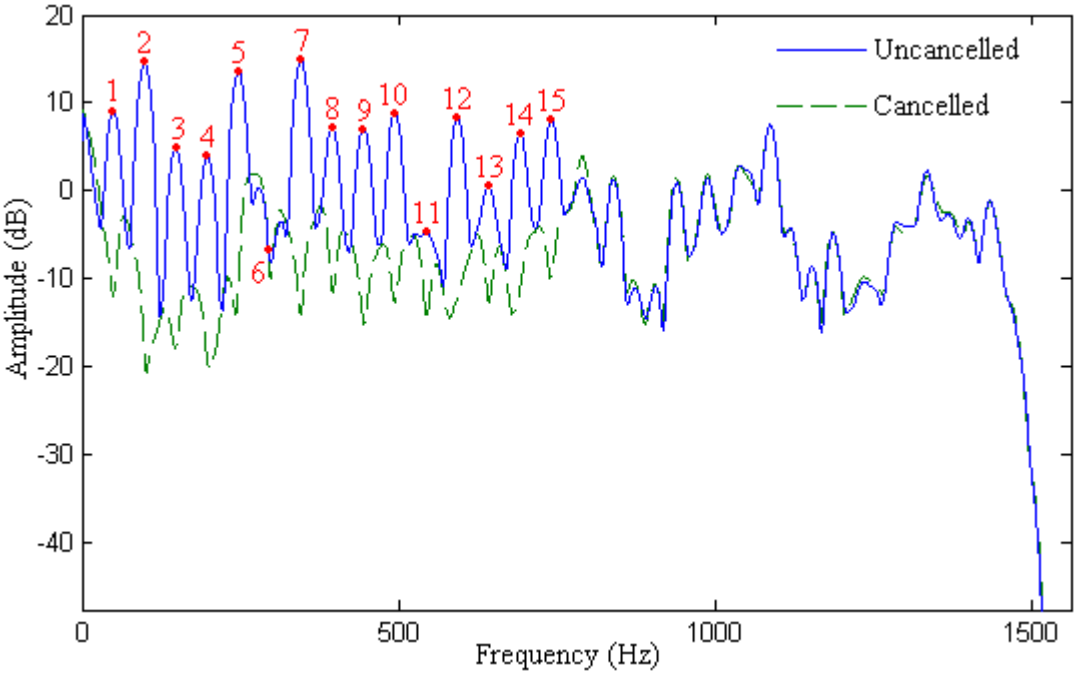

Figure 8.19 Measured frequency spectra with cancellation of 15 harmonics at 25 bar using off-line secondary path estimation, for compensation

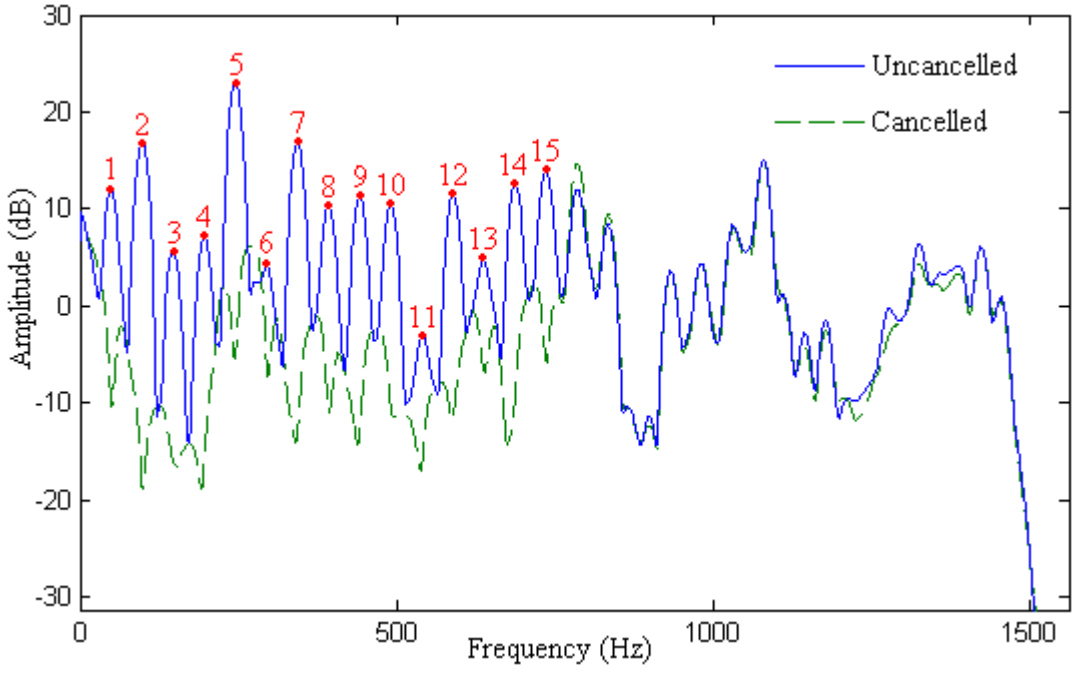

Figure 8.20 Measured frequency spectra with cancellation of 15 harmonics at 80 bar using off-line secondary path estimation, for compensation

For all different pressure conditions good cancellation results were obtained for the first 15 target frequencies. However, there was a slight increase in some higher frequency, uncancelled harmonic components, which may be due to non-linearity and distortion in the servo valve response. Using this cancellation method with off-line system identification algorithm at least 20 dB attenuation is achieved at target frequencies. However, in a real experiment the secondary path estimation is needed before implementing noise cancellation with any change of working conditions, which may sometimes have a large effect.

8.3 Control effect using on-line identification methods

To catch the variation of working conditions during noise cancellation, in this section on-line secondary path identification algorithms associated with two-weight adaptive notch filter as discussed in Chapter 6 are realized on the rig. The power of white noise applied here is 0.02 V^2, rather than 0.1 V^2 for the off-line method to give less effect on noise cancellation performance and residual noise. Figure 8.21 is the plot of this pressure ripple with the white noise input without pump running. However, compared with Figure 8.6 there is more influence from background noise on on-line secondary path identification with low working pressure.

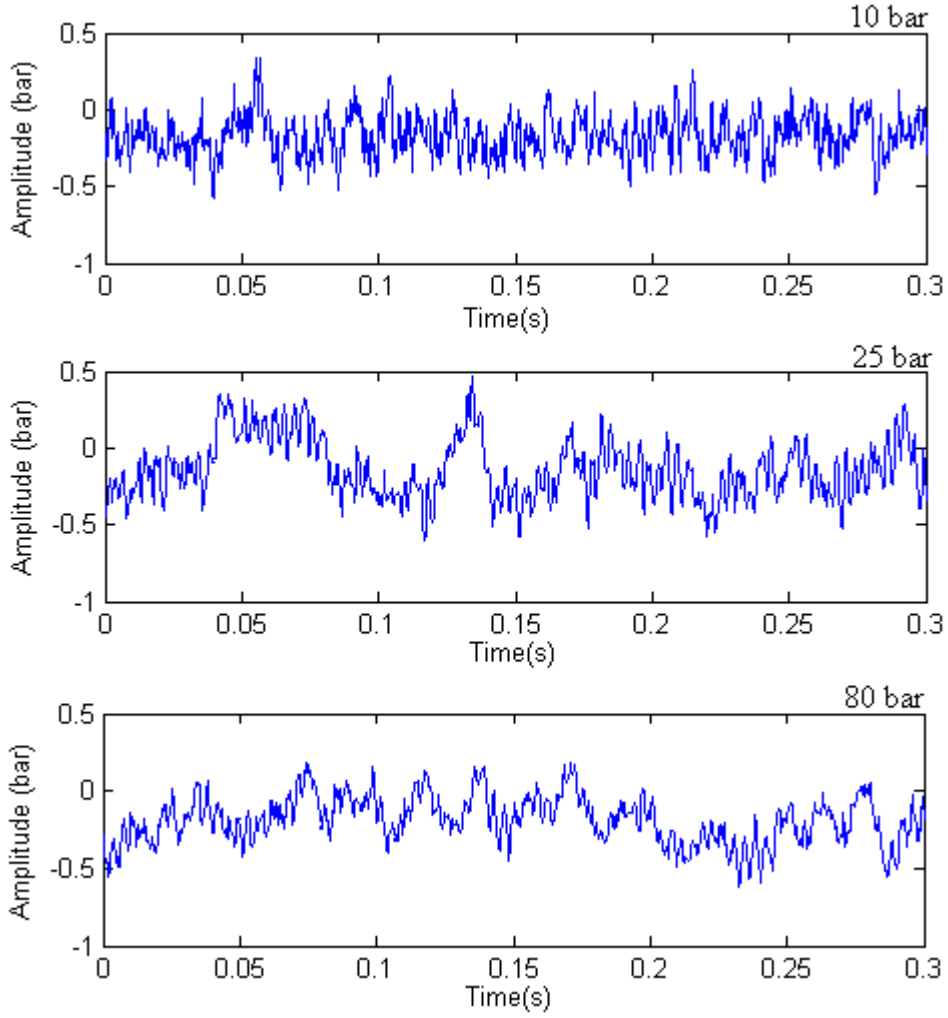

Figure 8.21 White noise used for secondary path estimation with power of 0.02 V^2 plus background noise

In this section for their good control performance as discussed in Chapter 6, Zhang's method using two strategies is implemented on the test rig in time domain, and then the frequency domain algorithm is also realized and the results discussed.

8.3.1 Test using Zhang's algorithm under first strategy

In this section Zhang's method, as evaluated in Chapter 6, is tested on this rig. First of all the first strategy is applied to cancel 15 harmonic components at different working conditions of at 10 bar, 25 bar and 80 bar by changing the load valve, which can cause the variation on reflection factor and primary noise power. In the first strategy identification controller and interference controller are switched on until the impulse response of the secondary path estimation is stable, which is named first stage. In this

stage a large identification convergence factor is applied to obtain a fast convergence speed. Then the pump and noise cancellation controller are running nearly at the same time and a relatively small identification convergence factor is used in the second stage. The estimated impulse response comparison between the off-line method in the first stage and the on-line algorithm in the second stage is plotted in Figure 8.22.

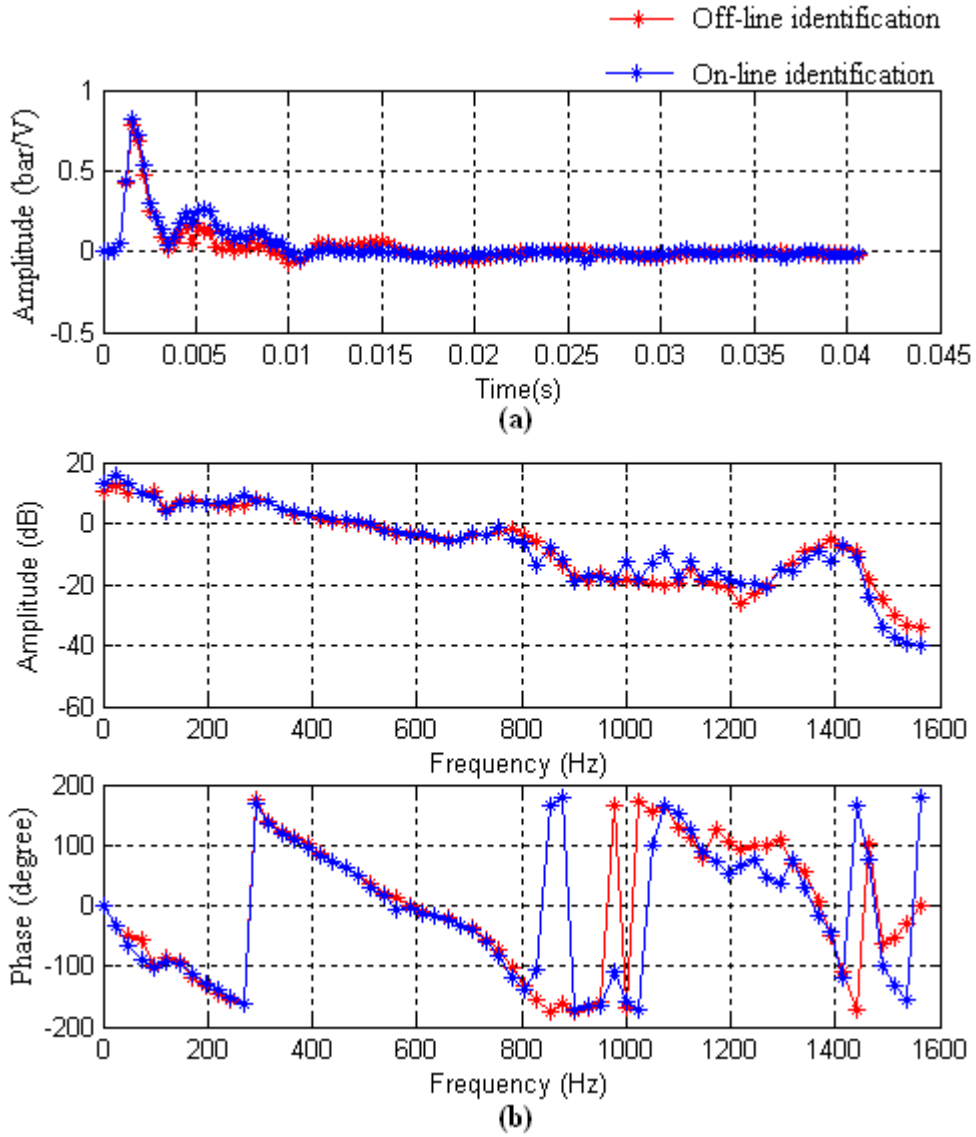

Figure 8.22 (a) Time domain impulse response comparison at 10 bar with Zhang's method

(b) Comparison of their amplitudes and phases in frequency domain

In this experiment, the maximum target frequency is $16.5 \times 3 \times 15 = 742.5$ Hz. In the second stage, the uncancelled high order harmonic components and the unwanted signal from the non-linear response of the anti-noise servo valve may affect the on-line

secondary path estimation as plotted using the blue line in Figure 8.22. The off-line identification, which is marked using a red line in the above figure, is smoother until 1500 Hz with the same bandwidth white noise. Furthermore although the reflection factor may change with more flow with the pump running, the impulse response estimations of the secondary path are nearly the same for both amplitude and phase spectrum until around 750 Hz with the rig pump switched off and on. This may be because the flow from the pump is small. Under compensation from secondary path estimation, the noise cancellation result is plotted in Figure 8.23.

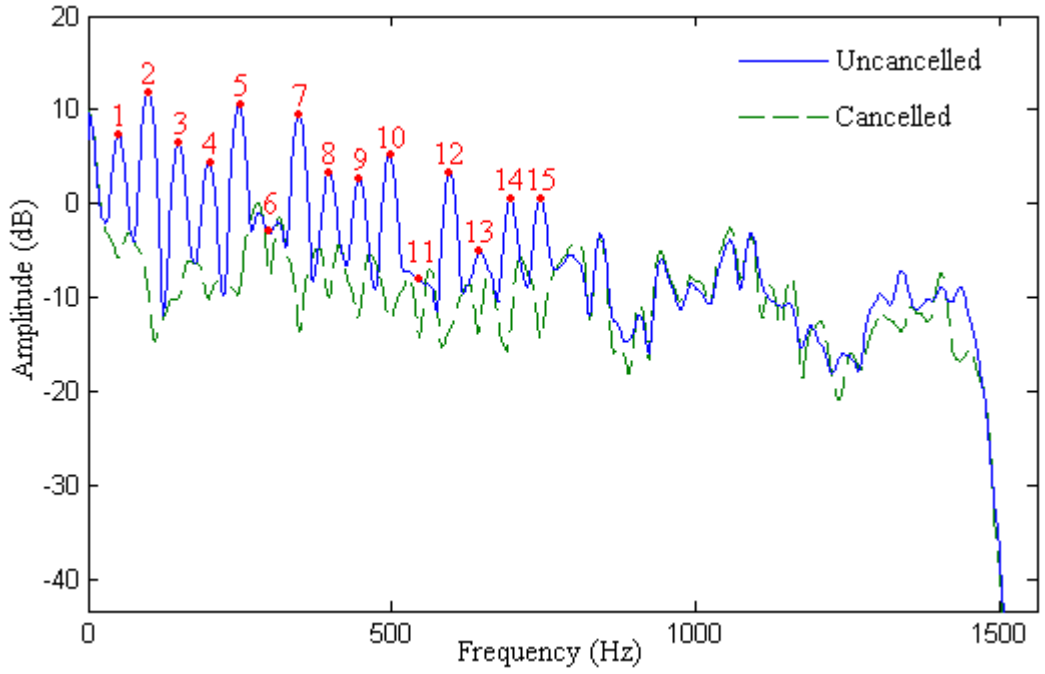

Figure 8.23 Measured frequency spectra with cancellation of 15 harmonics at 10 bar using Zhang's method under the first strategy

From this result, it can be seen that fluid-borne noise at target frequencies is reduced by typically 20 dB to insignificant levels when cancellation is applied. Limitation of this cancellation result may not only come from background noise from the ring main but also from the auxiliary white noise for on-line cancellation methods. At some harmonic components smaller cancellation occurs, for example at the 6^{th} harmonic, because of the small convergence factor. For the same reason as with the off-line cancellation method, the increase at uncancelled frequencies may come from non-linearity and distortion of the servo valve response.

The same experiment is implemented when working pressure is at 25 bar by turning the load valve without changing any control parameters. Not only the reflection factor is affected, but the power of primary noise also increases. The relatively small identification convergence factor is still used to ensure system stability as discussed during simulation in Chapter 6. Impulse response estimation is also plotted in time domain and frequency domain compared with the value obtained using the off-line method shown in Figure 8.24.

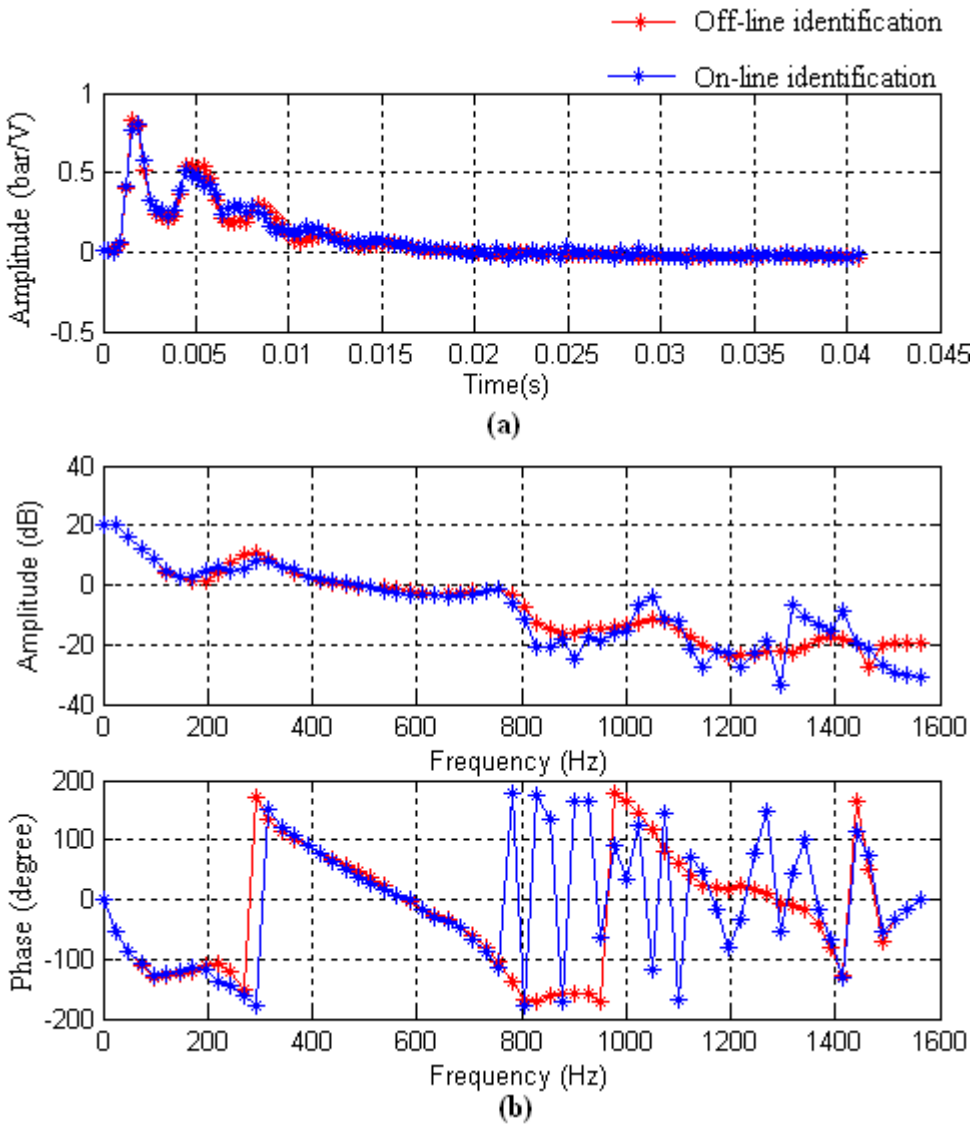

Figure 8.24 (a) Time domain impulse response comparison at 25 bar with Zhang's method

(b) Comparison of their amplitudes and phases in frequency domain

From this result the characteristics of the impulse responses obtained in the first and second stages are nearly the same during the cancellation range, from 0 Hz to 750 Hz. The reflection effect is also very small when the rig pump is running. However, the uncancelled frequency components give more effect for on-line identification at this pressure as plotted in Figure 8.24 using the blue line. The fluid-borne noise cancellation result for 15 harmonic components is plotted in Figure 8.25.

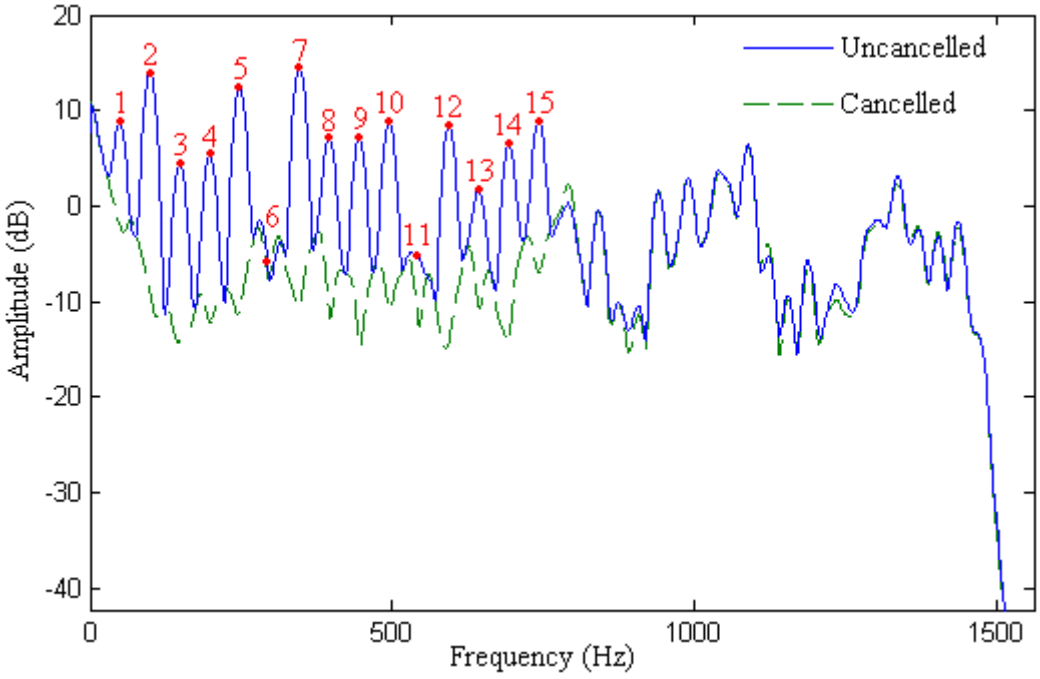

Figure 8.25 Measured frequency spectra with cancellation of 15 harmonics at 25 bar using Zhang's method under the first strategy

From experimental results the power of the fluid-borne noise increases at this pressure and secondary path estimation is still accurate enough for target frequencies to keep the system in the stable range.

Without changing any parameters, turning the load valve at the end of the pipe, the pressure increases to 80 bar. Comparison of secondary path estimation with off-line identification realized in the first stage and on-line identification obtained in the second stage is plotted in Figure 8.26 at 80 bar.

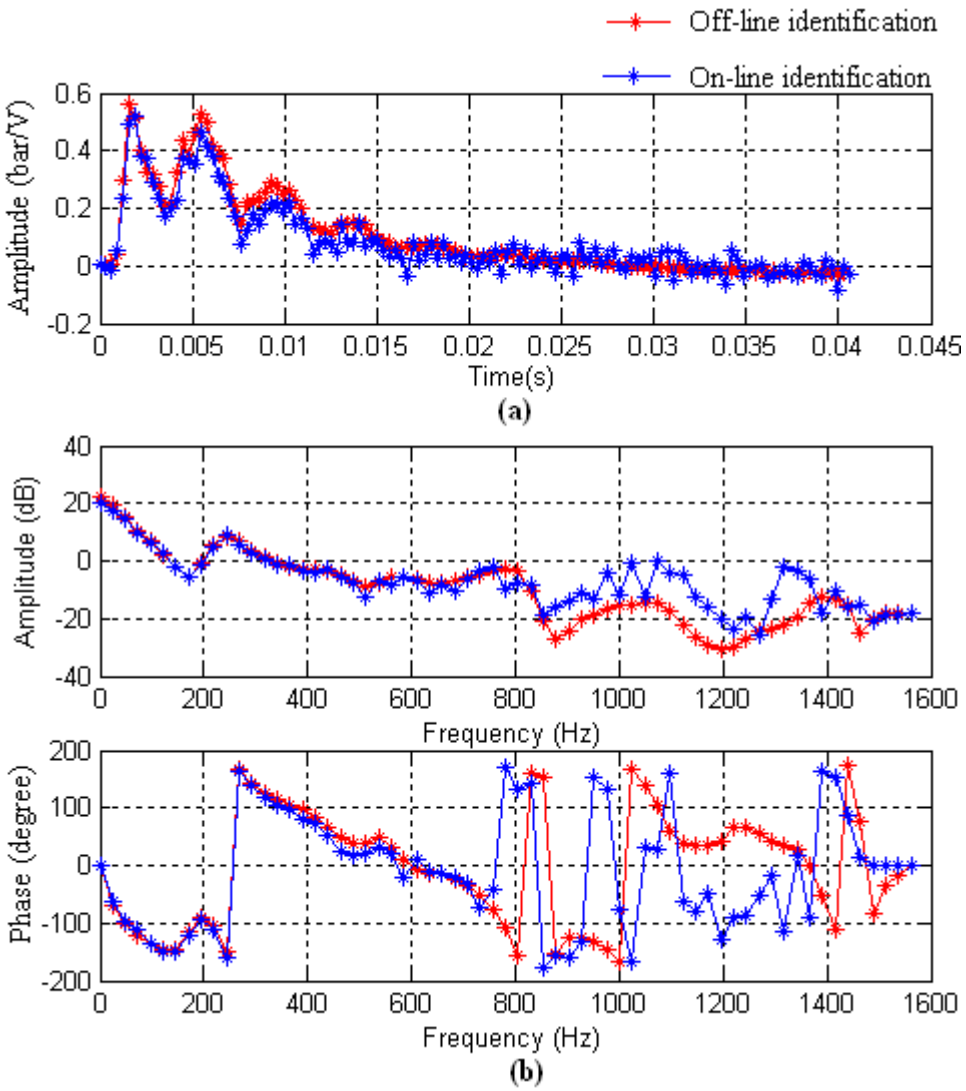

Figure 8.26 (a) Time domain impulse response comparison at 80 bar with Zhang's method

(b) Comparison of their amplitudes and phases in frequency domain

Compared with the results at pressure 10 bar and 25 bar, a significant effect from the uncancelled frequencies occurred on the on-line identification. However, a good impulse response for target frequencies is still reached for transient compensation. Under this effect an average of 20 dB cancellation is achieved and is plotted in Figure 8.27.

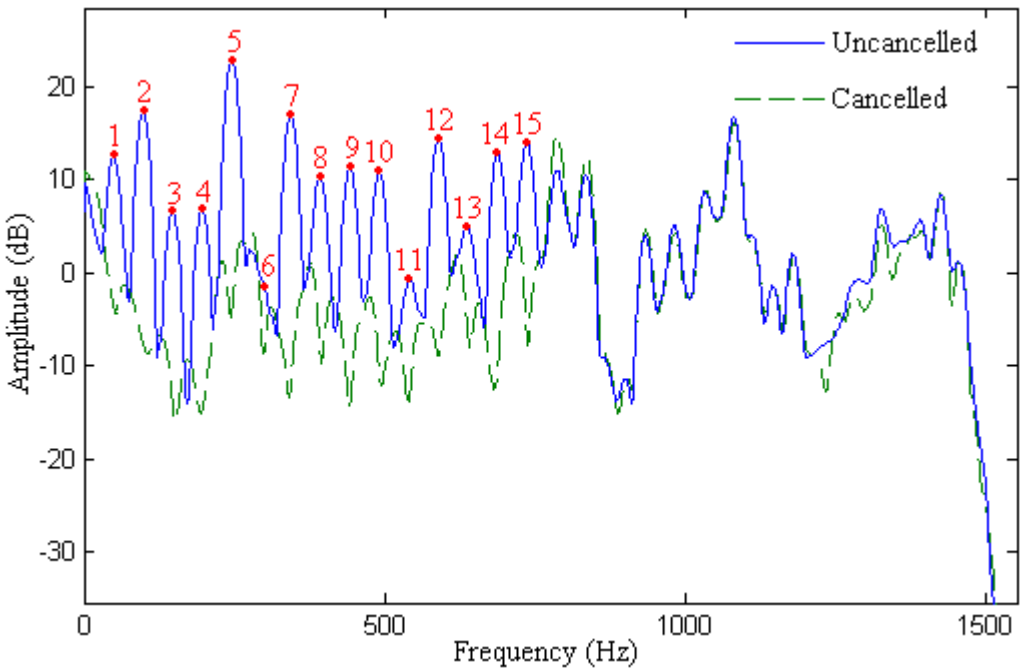

Figure 8.27 Measured frequency spectra with cancellation of 15 harmonics at 80 bar using Zhang's method under the first strategy

By discussing the identification and cancellation results above using this first strategy of Zhang's control algorithm, sufficiently accurate on-line secondary path identification is achieved for compensation and around 20 dB fluid-borne noise cancellation results are obtained with different working conditions at 10 bar, 25 bar and 80 bar. With a small change of reflection factor, secondary path estimation is accurate enough for compensation in the stable condition range, which is $-90^\circ < \Delta\varphi < +90^\circ$ mentioned in Chapter 5. The uncancelled harmonic components and the signal from the anti-noise servo valve non-linear response may affect the secondary path estimation, especially at the high pressure. A relatively small identification convergence factor is applied in the second stage, especially at the beginning, and the period when turning the load valve. It is also found that when the load valve is suddenly closed or nearly closed the system may become unstable because the phase shift between the secondary path and its estimation goes out of the stable range.

8.3.2 Test using Zhang's algorithm under second strategy

Zhang's method is also realized under the second strategy on the test rig. In the first stage the pump is running with the identification controller and interference cancellation

controller switched on. Then the fluid-borne noise cancellation controller is switched on when the impulse response comes to a steady value.

As in the first strategy, experiments are realized at three different working conditions at 10 bar, 25 bar and 80 bar to cancel 15 target harmonic components.

In the first stage, as the adaptive period is needed for the interference controller to eliminate primary noise effect for the secondary path estimation, compared with the first strategy a longer operation time is needed to obtain an accurate secondary path estimation. The estimated impulse response as shown using the red line in Figure 8.28 is accurate enough compared with the off-line identification result in Figure 8.22, which means that the interference controller can give a good effect on elimination of primary noise. Additionally, as secondary path estimation is processed with effect from the uncancelled high harmonic components, a certain level of fluctuation exists for these frequency components. In the second stage, similar to the simulation process, a relatively small identification convergence factor is also applied to protect system stability from the primary noise cancellation effect. The blue line is the estimated impulse response in the second stage with cancellation of primary fluid-borne noise. By comparing with the result obtained in the first stage only a slight difference, which may be caused by the non-linear response of the anti-noise servo valve, occurs between them in the target frequency range.

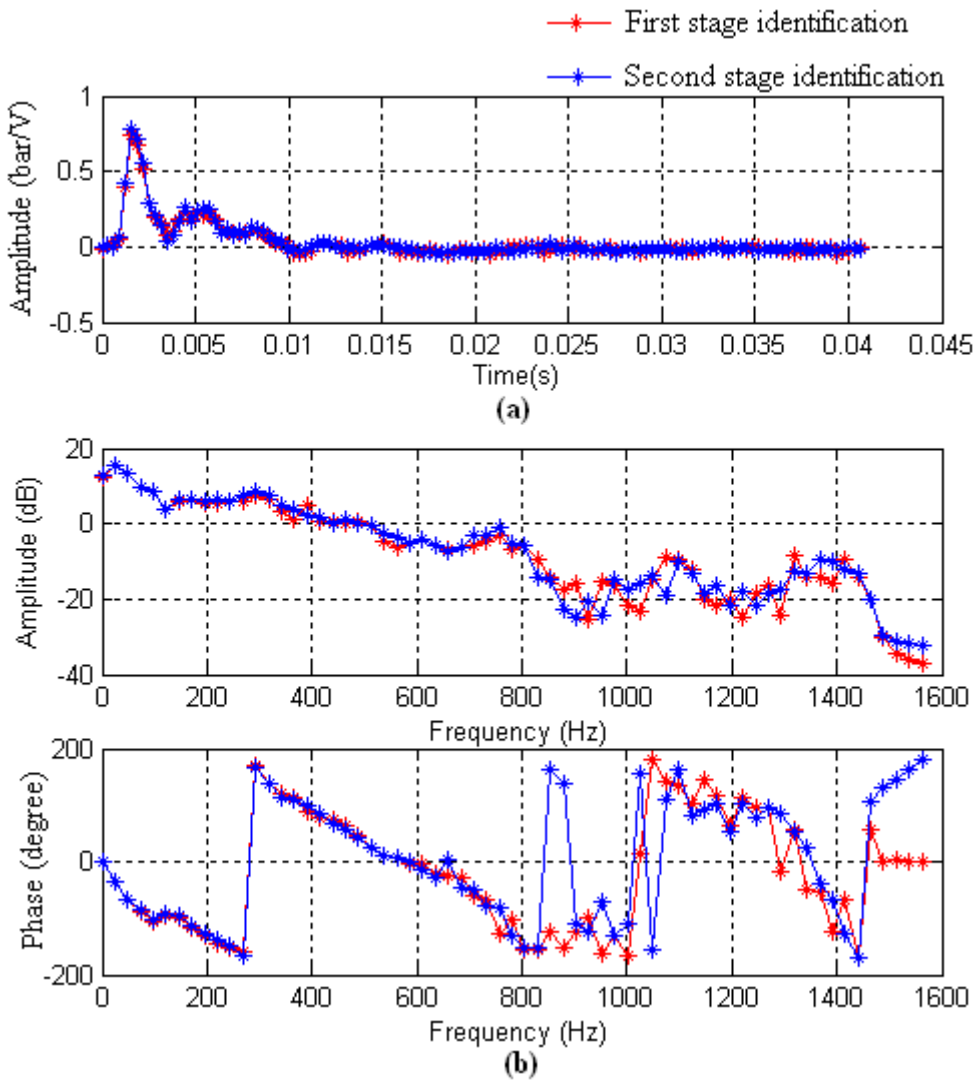

Figure 8.28 (a) Time domain impulse response comparison at 10 bar with Zhang's method

(b) Comparison of their amplitudes and phases in frequency domain

The cancellation result at this pressure is quite similar to the one in Figure 8.23. Insignificant fluid-borne noise is left at target frequencies.

By turning the load valve, the experiment at 25 bar is realized. All parameters for different controllers are not changed. Comparison of secondary path impulse response estimation in the first and second stages is plotted in Figure 8.29. Along with the power increase of fluid-borne noise at this pressure, more effect from the uncancelled frequencies especially the high order harmonic components is activated. However,

impulse responses for these two stages from 0 Hz to around 750 Hz only have a small difference with the contribution from the interference controller.

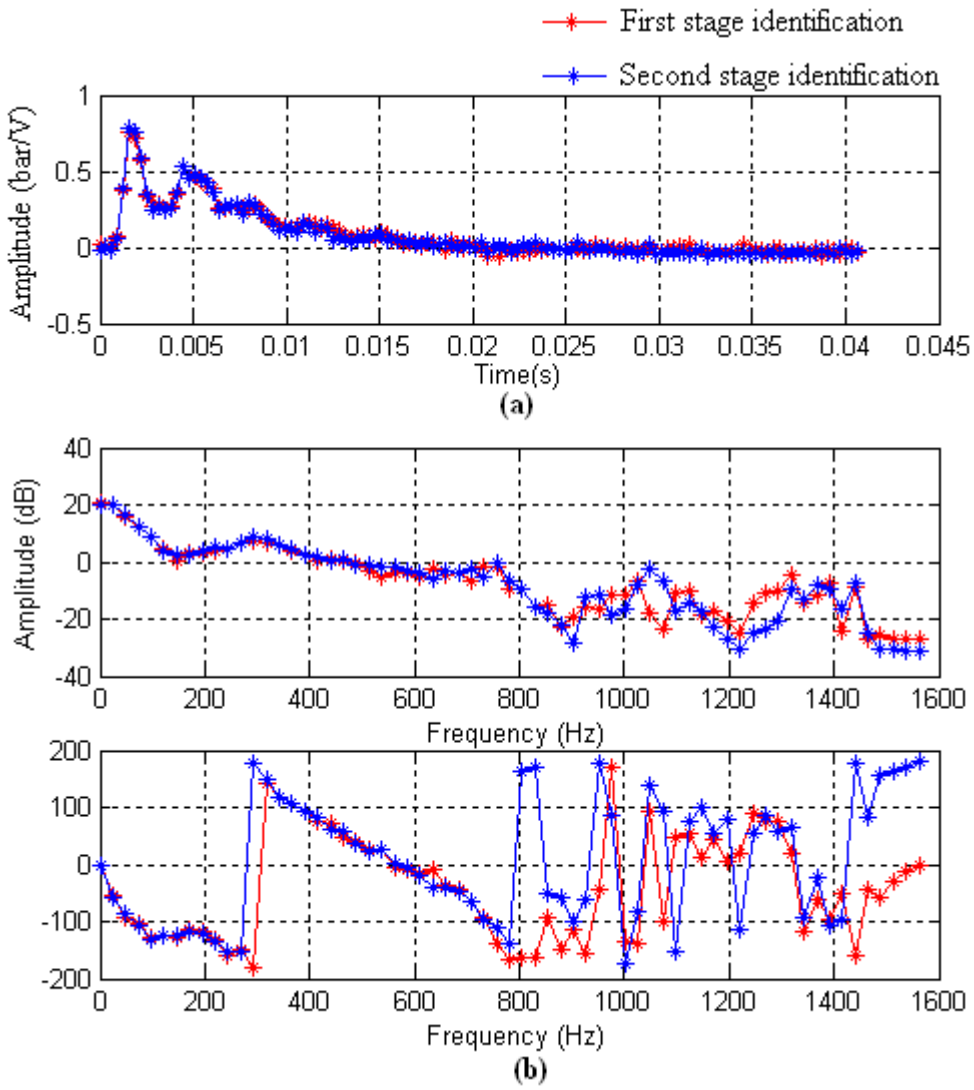

Figure 8.29 (a) Time domain impulse response comparison at 25 bar with Zhang's method

(b) Comparison of their amplitudes and phases in frequency domain

The noise cancellation result is similar to the one plotted in Figure 8.25.

Finally, turning the load valve, the experiment was performed at 80 bar. Firstly, the secondary path impulse response comparison is plotted in Figure 8.30 in both time domain and frequency domain. As there is an increase of fluid-borne noise from the

pump, the uncancelled frequency components, especially the uncancelled high harmonic components, give the biggest effect at this working pressure.

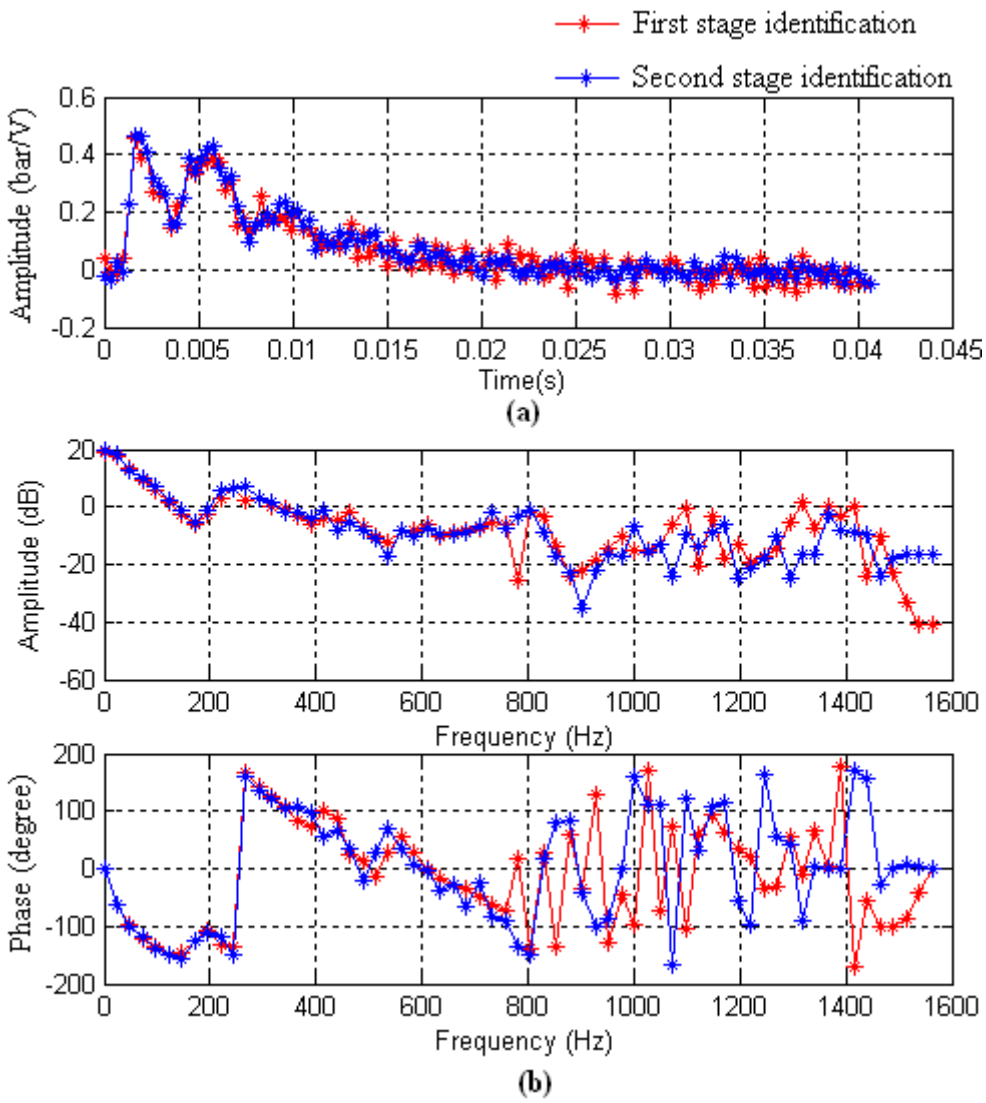

Figure 8.30 (a) Time domain impulse response comparison at 80 bar with Zhang's method

(b) Comparison of their amplitudes and phases in frequency domain

The noise cancellation result for target harmonic components is similar to the one plotted in Figure 8.27.

To summarize in this second strategy using Zhang's method, firstly the secondary path estimation in the first stage with the interference controller is accurate enough to compensate noise cancellation controller, however, the uncancelled harmonic

components and non-linear response from the anti-noise servo valve can affect the secondary path estimation, which increases with more power of fluid-borne noise. Furthermore longer operation time is needed in this stage compared with the first strategy. Secondly, the reflection factor difference between the pump on and off conditions is eliminated for all different working conditions. Finally, the system may become unstable when suddenly closing or nearly closing the load valve.

8.3.3 Test using frequency domain on-line algorithm

In this section the frequency domain on-line secondary path identification algorithm associated with the two-weight adaptive notch filter is implemented on the test rig. As described in Chapter 6 an adaptive function is applied for the secondary path estimation convergence factor realized in the frequency domain. This adaptive convergence function can give small convergence factor to frequency components where the power of fluid-borne noise is large, and a relatively large value when noise power is small. Hence comparing with Zhang's method, the interference controller is not needed in this algorithm. However, as signals are transformed between time domain and frequency domain twice by the controller, a high level of computation ability is required for the processor. In this experiment as more calculation burden is added on the processor only 9 harmonic components can be cancelled using dSPACE® 1005 depending on its ability at three different working conditions. As discussed during simulation in section 6.3 this method is realized only under the first strategy, in which only the identification controller running in the first stage and the pump with the noise controller switched on running in second stage.

Firstly a cancellation test was realized on the 1^{st} to 9^{th} harmonic components at 10 bar. Similar with Zhang's method in the first stage a large identification vector is applied. Compared with this, in the second stage a relatively small value is used, especially at the beginning period, because the primary noise cancellation process can affect the secondary path identification. The same convergence factors for the two-weight adaptive notch filters are applied with Zhang's method. The estimated impulse response comparison between off-line identification and on-line identification is plotted in Figure 8.31.

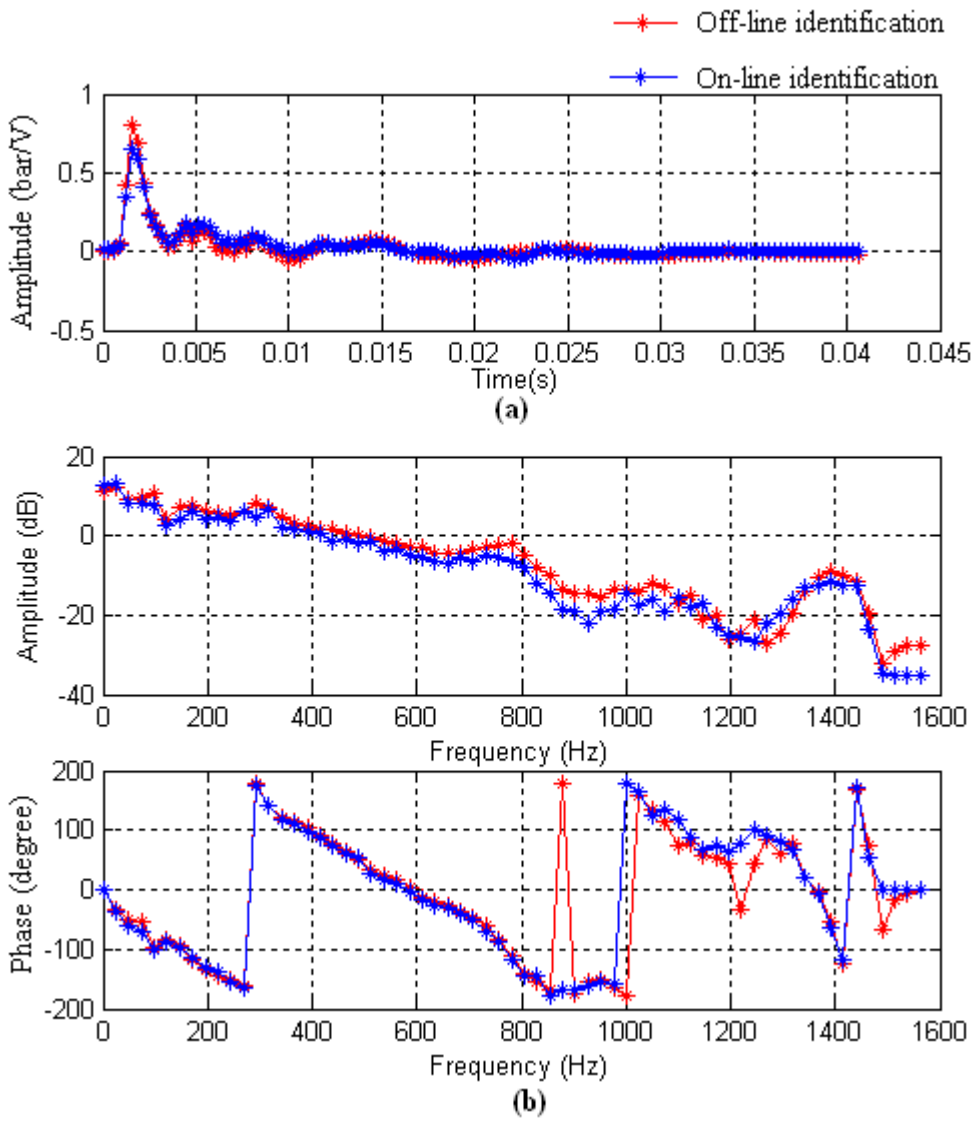

Figure 8.31 (a) Time domain impulse response comparison at 10 bar using frequency domain method to cancel 1 to 9 orders

(b) Comparison of their amplitudes and phases in frequency domain

Compared with Zhang's algorithm, estimated impulse response at the uncancelled frequency components, especially high order harmonics, is 'smoother' because the adaptive convergence function can eliminate the effect from all frequency components. Therefore a more accurate impulse response estimation can be obtained.

The noise cancellation result is plotted in Figure 8.32 for the 1st to 9th target frequencies. 10 dB to 20 dB attenuation level is achieved to reduce the noise to an insignificant level.

A small increase of uncancelled frequency components is caused by non-linear distorted response from the anti-noise servo valve.

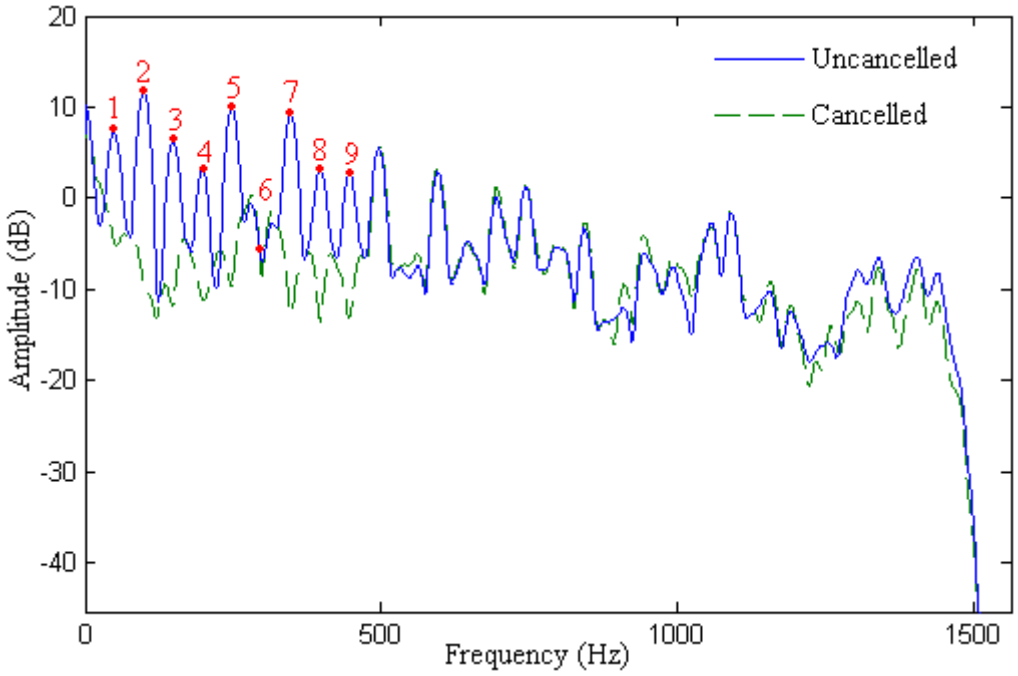

Figure 8.32 Measured frequency spectra with cancellation of 9 harmonics at 10 bar using frequency domain method to cancel 1 to 9 orders

Furthermore, cancellation was also realized on the 7^{th} to 15^{th} harmonics at 10 bar. Comparison of impulse response between the off-line and on-line methods is plotted in Figure 8.33. Because the secondary path identification effect from all the uncancelled harmonic components is eliminated, this estimated result is almost the same as the one in Figure 8.31.

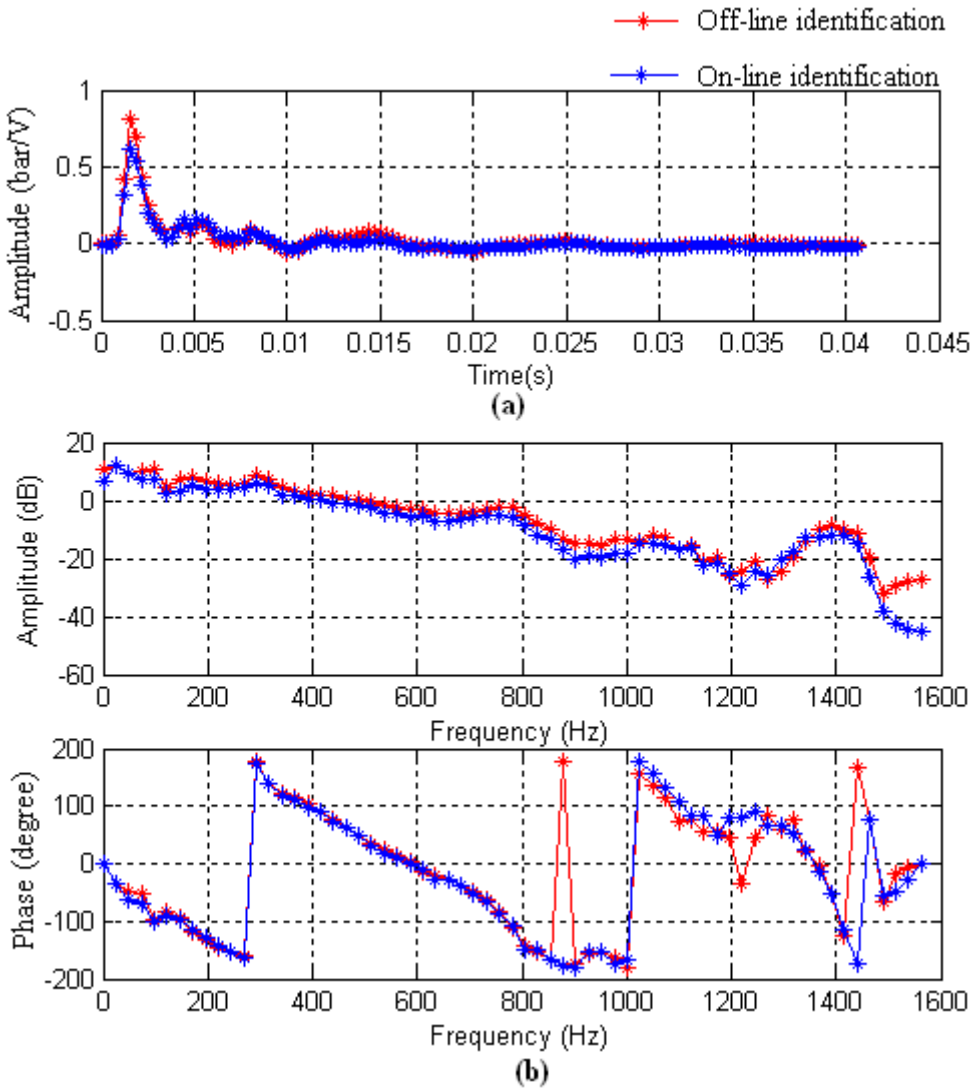

Figure 8.33 (a) Time domain impulse response comparison at 10 bar using frequency domain method to cancel 7 to 15 orders

(b) Comparison of their amplitudes and phases in frequency domain

The fluid-borne noise cancellation result for these target frequencies is plotted in Figure 8.34, and 10 dB to 20 dB attenuation level is achieved for these harmonic components.

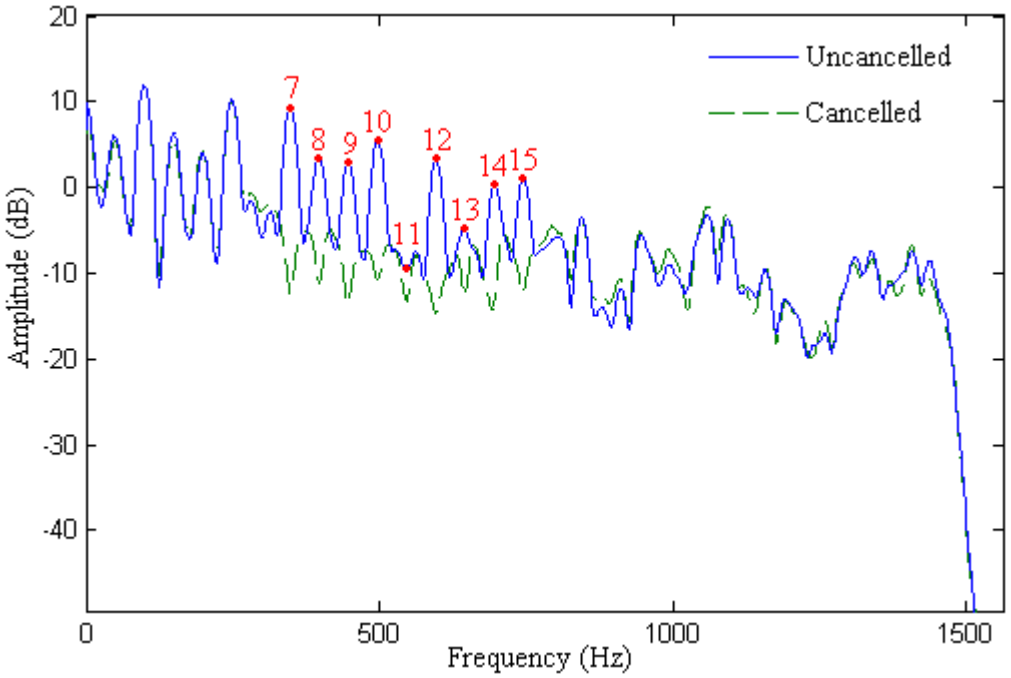

Figure 8.34 Measured frequency spectra with cancellation of 9 harmonics at 10 bar using the frequency domain method to cancel 7 to 15 orders

A test was then implemented at 25 bar by turning the load valve at the pipe end. As with the other on-line noise cancellation methods, a relatively small identification convergence vector was applied because the secondary path impulse may be affected by the adaptive process of noise cancellation.

An impulse response comparison between off-line and on-line methods is plotted in Figure 8.35. As adaptive coefficient function can give a suitable convergence factor for each frequency bin depending on the noise power at that frequency, a good identification result is obtained for all frequency components rather than only for target frequencies.

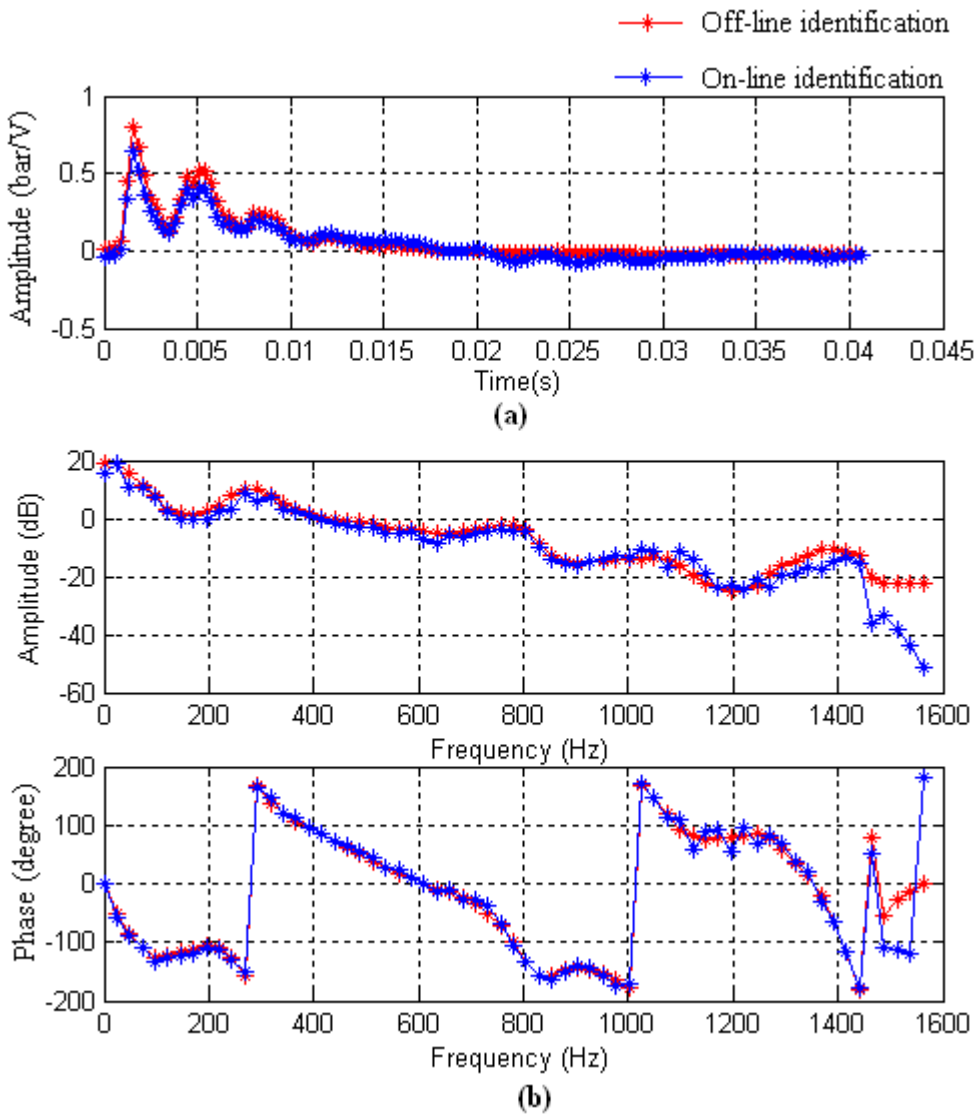

Figure 8.35 (a) Time domain impulse response comparison at 25 bar using the frequency domain method to cancel 1 to 9 orders

(b) Comparison of their amplitudes and phases in the frequency domain

The noise cancellation result is plotted in Figure 8.36, and 20 dB noise is attenuated on average for the target frequency components.

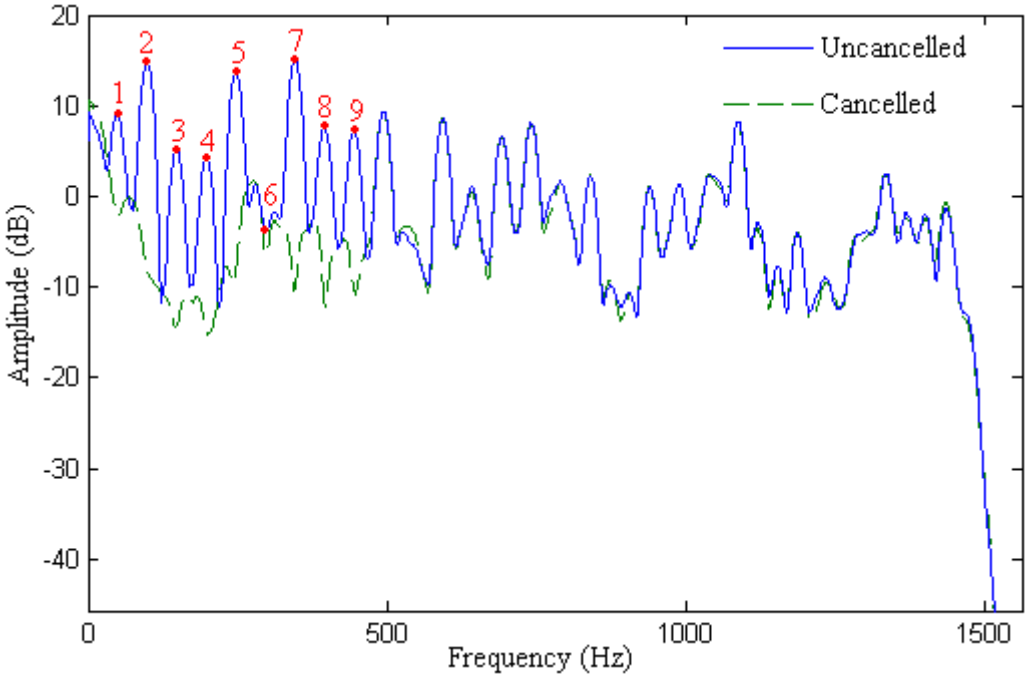

Figure 8.36 Measured frequency spectra with cancellation of 9 harmonics at 25 bar using the frequency domain method to cancel 1 to 9 orders

At this pressure a cancellation test was also realized on 7^{th} to 15^{th} target frequency components. The fluid-borne noise cancellation result is shown in Figure 8.37. On average 20 dB is attenuated on target frequency components.

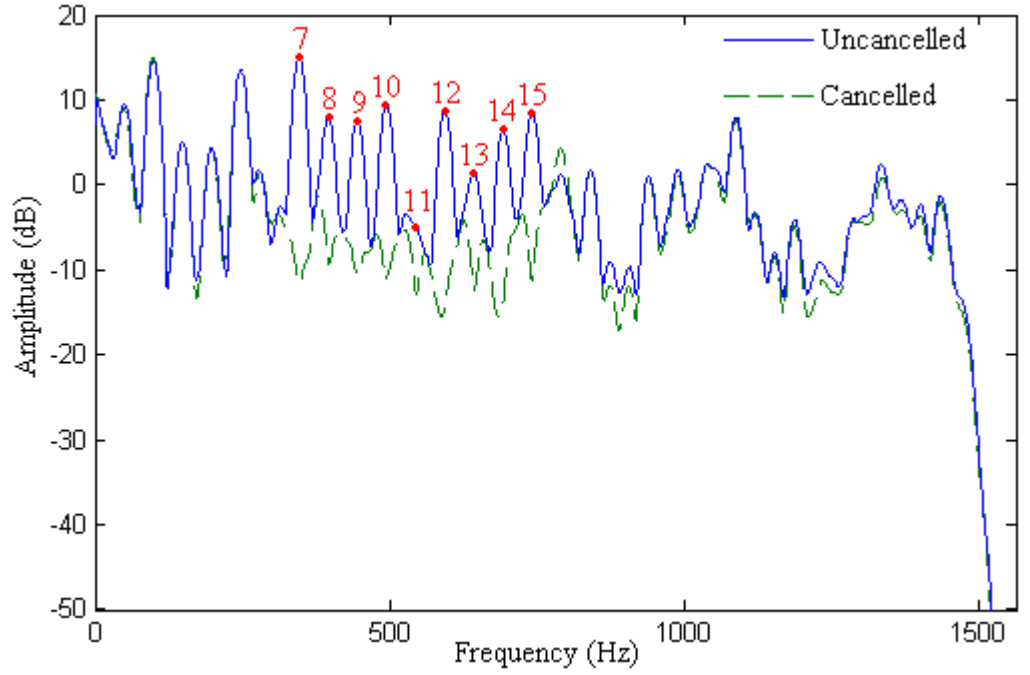

Figure 8.37 Measured frequency spectra with cancellation of 9 harmonics at 25 bar using the frequency domain method to cancel 7 to 15 orders

The secondary impulse response is similar to the one in Figure 8.35.

Finally, an experiment was completed at 80 bar by adjusting the load valve. Firstly cancellation is realized on 1st to 9th target frequencies. Although the power of the uncancelled frequency components increases with the pressure, accurate secondary path estimation, plotted in Figure 8.38, is obtained compared with Zhang's method because of the adaptive identification convergence vector. The noise cancellation result for these target frequencies is plotted in Figure 8.39, and 20 dB to 30 dB attenuation is achieved for most target components.

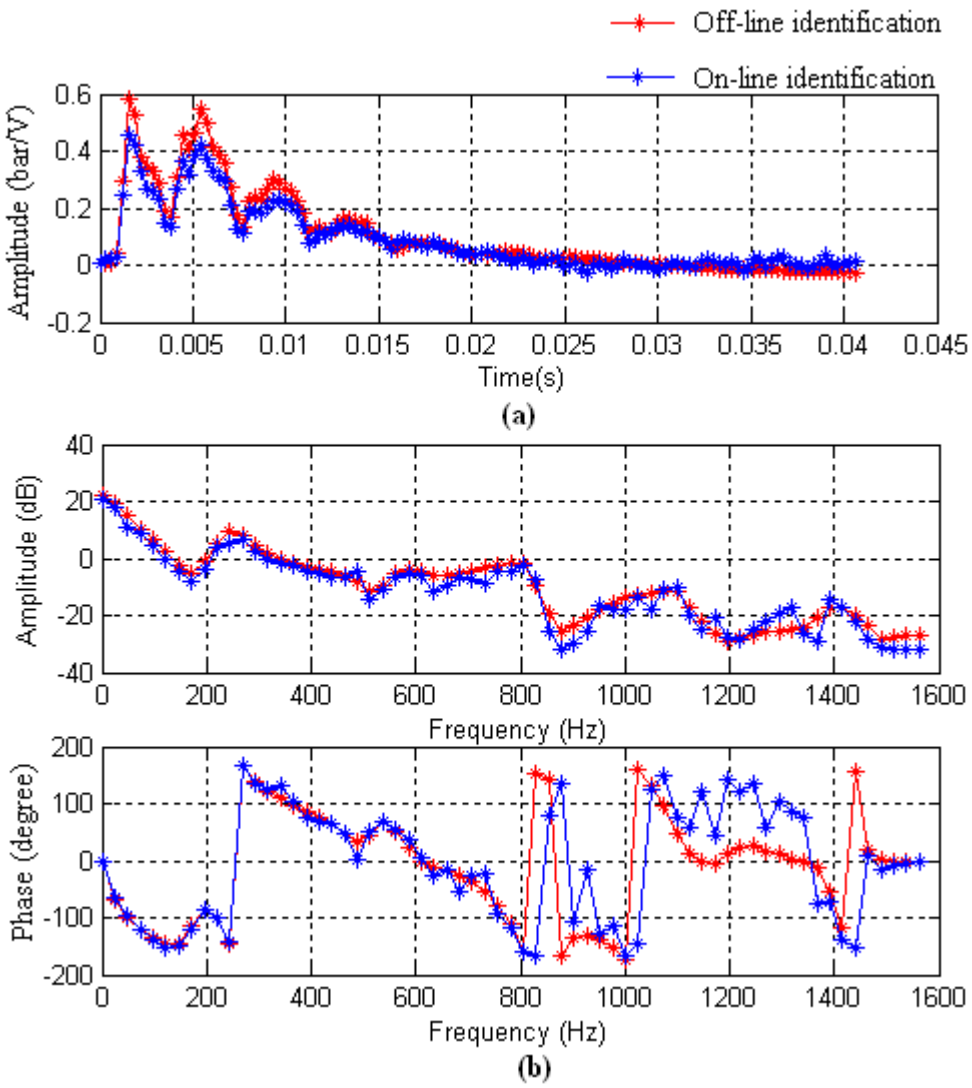

Figure 8.38 (a) Time domain impulse response comparison at 80 bar using frequency domain method to cancel 1 to 9 orders

(b) Comparison of their amplitudes and phases in frequency domain

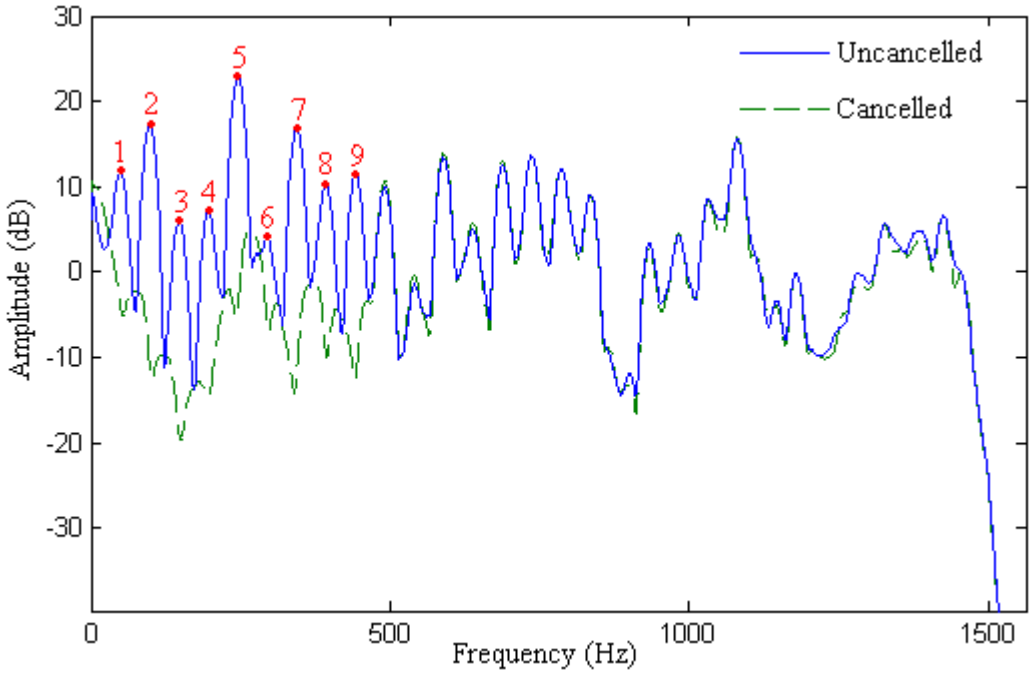

Figure 8.39 Measured frequency spectra with cancellation of 9 lower harmonics at 80 bar using frequency domain method to cancel 1 to 9 orders

Cancellation on 7th to 15th target frequency components was realized at this pressure, and this is plotted in Figure 8.40. The estimation result is similar to the one in Figure 8.38.

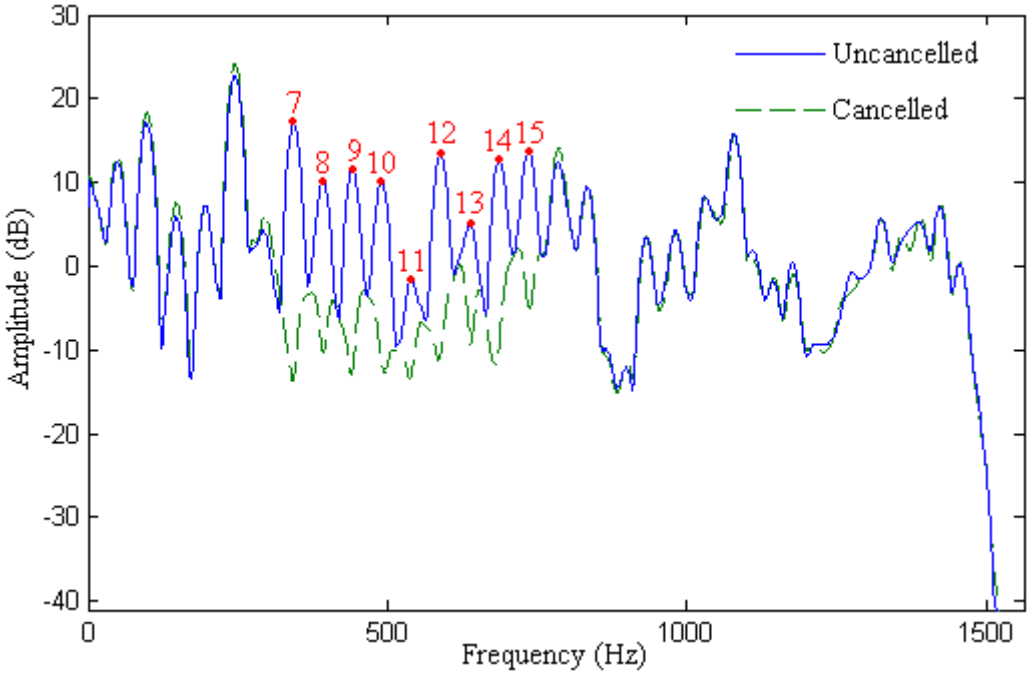

Figure 8.40 Measured frequency spectra with cancellation of 9 higher harmonics at 80 bar using frequency domain method to cancel 7 to 15 orders

From the experimental results obtained using this frequency domain on-line control method, accurate secondary path estimation can be obtained and good fluid-borne noise cancellation results are also achieved in different working conditions. As an adaptive convergence function is applied for on-line identification extra interference controllers are not needed to make the system simple, and better identification results for uncancelled frequency components can be obtained under this effect compared with other on-line identification algorithms. However, because data transformations between frequency domain and time domain are needed there is a bigger computation burden for the processor. Under this effect only 9 order harmonic components can be attenuated at the same time using dSPACE® 1005. In this experiment sudden changing of working conditions by turning the load valve may make the system become unstable.

8.4 Conclusions

To conclude, in this chapter based on the rig used in Chapter 7, a real pump with fixed running speed was applied instead of a servo valve as a fluid-borne noise source. The transient pump frequency is synchronized to generate reference input signals. Off-line and on-line (Zhang's method and frequency domain method) noise control algorithms with proposed manipulation strategies as discussed in Chapter 5 and Chapter 6 were implemented on the test rig. According to the calculation ability of dSPACE® 1005, 15 harmonics of fluid-borne noise were the targets to be cancelled. Typically, 20 dB fluid-borne noise was attenuated on the target frequency components with different working conditions. Limitation of this result might be caused by the background noise from the ring main. Additionally it might be also from the auxiliary white noise when using on-line identification methods. Because of the non-linear distorted response of the servo valve, a slight increase occurred on the uncancelled noise.

Additionally during the experiment using the on-line cancellation algorithms, at the beginning stage of the second stage and the beginning period when adjusting the load valve, a relatively small identification convergence factor or convergence vector was needed to protect the system stability from the adaptation effect caused by the primary noise cancellation. Particularly the operation time of the first stage in second strategy was longer than that used in the first strategy because the interference cancellation process can affect the secondary path identification. Additionally, when the load valve

is suddenly closed or nearly closed, the system may become unstable because the phase shift between the secondary path and its estimation moves out of the stable range.

Compared with Zhang's method, as the adaptive identification convergence vector can supply a suitable identification convergence factor to the corresponding frequency component to make the system stable, the frequency domain control method with a fast noise cancellation speed is a more robust algorithm. However, during the control process as the signals transform between time domain and frequency domain, a large computational burden is added on the processor. Hence, only 9 harmonics of the fluid-borne noise can be attenuated using the dSPACE® 1005.

One important point needs to be noted. In this project the anti-noise servo valve applied on the test rig is supplied by the pressure from the ring main. Hence the off-line secondary path identification can be realized without running the pump. However, in a hydraulic circuit in which the pressure and flow to activate the servo valve are only supplied by the pump, the secondary path impulse response cannot be estimated off-line, which means that the off-line noise control method and the first strategy for on-line control algorithms can not be realized. To solve this problem, a direct-acting actuator such as a piezoelectric actuator may work without a hydraulic supply.

CHAPTER 9

Conclusion and recommendation

In this chapter a summary is presented to conclude the work of the whole thesis. According to the limitations on control methods described in this thesis and devices applied on the test rig, recommendations of future work are proposed.

9.1 Conclusions

The purpose of this thesis is to research and develop efficient active control methods, which have simple and robust performance under different working conditions, to attenuate fluid-borne noise to an insignificant level in a simple hydraulic system.

The LMS adaptive control algorithm based on an FIR filter has been evaluated in detail. Based on this concept, two-weight LMS adaptive notch filter, which is applied in this thesis for fluid-borne noise cancellation, is investigated.

A model of the test rig system has been realized using the method of characteristics (MOC) to give an accurate description of pressure and flow ripple at any point along the pipe. Development of this rig model is investigated to introduce control flow, which is given by the actuator, into the pipe. This developed model is applied on Kojima's method, which is a forward attenuation algorithm of fluid-borne noise, to investigate the efficiency and accuracy of the model. Compared with the method using the adaptive LMS filters there are three main disadvantages to using Kojima's method:

1. As the frequency-dependent friction term is not included, Kojima's method is not accurate and is restricted by the structure of the hydraulic circuit.
2. Two pressure transducers are needed, which can increase the cost of the system.
3. The approximation of pressure gradient makes Kojima's method inherently unstable.
4. Very accurate positions of the two pressure transducers and control flow injecting point are needed to give good cancellation and make the system stable.

5. The transfer function of the anti-noise device needs to be known accurately.

Depending on the LMS adaptive control method, a filtered reference LMS filter (FXLMS), which can be applied in a wider bandwidth, is introduced. Using the off-line system identification algorithm the obtained actuator impulse response can be applied to compensate the actuator effect in the FXLMS method. Additionally, depending on the characteristic of secondary path, which includes the actuator, a simple delay unit can be employed for compensation. Associated with the two-weight LMS notch filter these off-line FXLMS control methods are implemented using the rig model. Applying the obtained accurate identification impulse response, fluid-borne noise is attenuated to an insignificant level. However, the transient dynamic response of the secondary path cannot be obtained during the noise cancellation process in different working conditions.

To overcome this problem the on-line control method, by which the secondary path is estimated synchronously with the noise cancellation process using an auxiliary white noise signal, was applied. No prior knowledge of the secondary path is needed. Three efficient control methods were realized:

1. Improved Bao's algorithm was realized in the time domain firstly with a controller to cancel interference from the uncancelled frequency components. At the same time another similar controller was also applied to compensate its distortion effect on white noise. However, the extra white noise generated by the two-weight adaptive notch filter can affect the on-line secondary path identification, especially with fast noise cancellation speed.
2. Zhang's on-line control method with one interference controller was implemented with the rig model. The extra white noise effect can be eliminated to give a faster noise cancellation speed compared with the improved Bao's method. However, as weighting functions for the on-line identification part and interference controller are cross-updated, more operating time may be needed for convergence.
3. An on-line control algorithm is realized in the frequency domain, in which a convergence function is used instead of a constant convergence factor. Faster noise cancellation speed can also be obtained using this method. Small convergence value is supplied by convergence function when noise power is large at relatively frequency component. Under this effect interference from residual noise with high

power is eliminated. The controller structure is more simple when applying this algorithm, however, there is more calculation burden for the processor with block data transforming between the time domain and the frequency domain.

Two strategies are suggested for on-line noise cancellation methods to make the system stable. From simulation results using these on-line control algorithms, accurate secondary path estimations are obtained with different length and different working conditions. Above 90 percent of fluid-borne noise can be attenuated for both single frequency and multiple frequency cases.

A test rig with a simple hydraulic circuit was built up to implement and evaluate the off-line and on-line control methods. Firstly a servo valve was used as a noise source to give artificial fluid-borne noise, and 8 orders of sine waves with specified harmonic frequencies were generated depending on the ability of the noise servo valve. Another fast-response servo valve was applied to generate anti-noise with same harmonic components. A load valve was applied at the end of the pipe to alter working conditions. From the experiment results, an impulse response of secondary path with enough accuracy was achieved and overall fluid-borne noise was attenuated by 20 dB to 30 dB to an insignificant level on target frequency components under different working conditions. Limitation of this cancellation result may come from the background noise generated by the ring main. Additionally, when using the on-line identification methods, limitation of the cancellation result may also come from the auxiliary white noise. It was found that when the load valve was suddenly closed or nearly closed the system may become unstable because the transient phase difference between the secondary path and its estimation moves out of the stable range. Furthermore, non-linear distorted response from the anti-noise servo valve may also give a slight increase on uncancelled frequency components.

These controllers were then tested on the same rig with a fixed speed real pump as a noise source. A tachometer was fixed on the pump shaft to pick up fundamental frequency of the fluid-borne noise synchronously. Off-line and on-line (Zhang's method and frequency domain method) control algorithms were evaluated using this test rig with two process strategies in different working conditions. Depending on the calculation ability of the processor, which was dSPACE® 1005 in this thesis, 15 harmonics of fluid-borne noise were the targets to be cancelled. Typically, around 20

dB fluid-borne noise was cancelled on target harmonics with accurate secondary path impulse response compensation. Limitation of this cancellation result may also come from background noise from the ring main and the auxiliary white noise. Instability of the system occurred when the load valve at the pipe end was suddenly closed or nearly closed. A slight increase was added to uncancelled frequency components because of the non-linear response of the anti-noise servo valve.

Additionally, in a real system for industrial application, the anti-noise servo valve used in this thesis may not be supplied by an extra ring main. The power in the closed-loop hydraulic circuit may only be supplied by the pump, which is also a noise source. Hence the dynamic characteristics of the secondary path cannot be obtained using the off-line method. A servo valve may not be a suitable anti-noise source. Other types of actuators with a fast response, which are not dependent on the hydraulic power supply, such as piezoelectric actuators, may be a suitable solution. Suddenly closing or nearly closing the load valve may make the system unstable and suitable parameters for different controllers may also be needed for different working conditions. Hence, in a real machine system the efficiency and robustness may be degraded for these reasons.

To summarize, the main problem of using the FXLMS noise cancellation method is that a relatively accurate secondary path estimation is needed for different working conditions. Other improvements of this control method, such as applying a feedback loop controller in parallel with the secondary path in the acoustic noise reduction of the headphone, may make the system stable when the working condition suddenly changes in a large range for the interested frequencies. Furthermore, other active noise control method without the secondary path identification, such as a kind of model reference adaptive control algorithm used in [18], may be another solution to solve the problem.

9.2 Recommendations for future work

Recommendations for future work are described in this section in three main parts:

1. Control algorithm

   White noise is applied on the on-line control algorithms described in the previous chapters. More powerful white noise compared with background noise and

fluid-borne noise to be cancelled can give more accurate secondary path estimation. However, bigger residual noise exists after cancellation from this auxiliary signal. Efficient control methods without extra effect on the system would compliment. As an on-line system identification is needed during cancellation intensive calculation is required for the processor. Hence more efficient control algorithms on computation are suggested in the future work. Additionally, control algorithms to track system dynamic response with sudden change of working condition in a large range are also recommended in the future work.

2. Anti-noise actuator

As shown in experimental results, a slight increase on uncancelled frequency components is caused by the non-linear response of the anti-noise servo valve. Furthermore limitation of this servo valve response ability makes the cancellation only for the low frequency range. Also servo valve is expensive, sensitive to contamination and inefficient because of the hydraulic power lost through the valve. Additionally, in a practical hydraulic circuit the pressure and flow used in the servo valve may only be supplied by the pump; hence the off-line secondary path estimation cannot be realized. For these reasons development of a suitable actuator is necessary.

3. Variety of experiment conditions

A small flow rate is provided by the pump used in the experiments. A significant change of reflection factor is not evident with the pump switched off and on. Additionally a fixed running speed is applied during the experiment. In future work the method could be applied to a higher pressure, higher flow rate, variable speed pump with a wider variety of loading conditions, including for example directional control valves.

REFERENCES

[1] Petrusewicz, S.A. and Longmore, D.K., "*Noise and vibration control for industrialists*", Elek Science, London, 1974.

[2] Peters, B., "*Noise control*", Pira International, 2000.

[3] Barron, R.F., "*Industrial noise control and acoustics*", Marcel Dekker Inc, 2003.

[4] Skaistis, S., "*Noise control of hydraulic machinery*", Marcel Dekker Inc, 1988.

[5] "*Hydraulic System Design, Section 14: Fluid-Borne Noise*", Centre for PTMC, University of Bath, November 2003, Module FP3-14.1-14.7.

[6] Johnston, D.N. "*Measurement and prediction of the fluid-borne noise characteristics of hydraulic components and systems*", Ph.D thesis, University of Bath, 1987.

[7] Beranek, L.L. and Vér, I.L., "*Noise and vibration control engineering principles and applications*", John Wiley & Son Inc, 1992.

[8] Tokhi, O. and Veres, S., "*Active sound and vibration control theory and applications*", The Institution of Electrical Engineerings, 2002.

[9] Nakaji, Y., Satoh, S., Kimura, T., Hamabe, T., Akatsu, Y. and Kawazoe, H., "*Development of an active control engine mount system*", Vehicle System Dynamics, 32, 1999, pp.185-198.

[10] Stevens, J.C. and Ahuja, K.K., "*Recent advances in active noise control*", American Institute of Aeronautics and Astronautics, Vol. 29, No. 7, 1991.

[11] Nelson, P.A. and Elliott, S.J., "*Active control of sound*", Academic Press Limited, 1992.

[12] Kou, S.M. and Morgan, D.R., "*Active noise control systems algorithms and DSP implementations*", John Wiley & Sons Inc, 1996.

[13] Yokota, S., Somada, H. and Yamaguchi, H., "*Study on an active accumulator (Active control of high-frequency pulsation of flow rate in hydraulic systems)*", JSME International Journal, Series B, Vol 39, No. 1, 1996.

[14] Jiao, Z., Chen, P., Hua, Q. and Wang, S., "*Adaptive vibration active control of fluid pressure pulsations*", Proceeding of IMechE, Vol.217, Part I, Journal of Control Engineering, 2003.

[15] Kojima, E. and Shinada, M., "*Development of an Active-Attenuator for Pressure pulsation in Liquid Piping Systems*", JSME International Journal, Series II, Vol. 34, No.4, 1991, pp. 466-473.

[16] Piper, G.E. and Calvert, T.E., "*Active fluid-borne noise control of a magnetic bearing pump*", NCA-Vol.21, Proceeding of the ASME Noise Control and Acoustics Division, ASME, 1995.

[17] Morgan, D.R. and Quinlan, D.A., "*Local silencing of room acoustic noise using broadband active noise control*", Applications of Signal Processing to Audio and Acoustics, 1993, Final program and paper summaries, 1993, IEEE workshop on 17-20, Oct. 1993, pp. 23-25.

[18] Hillis, A.J., Harrison, A.J.L. and Stoten, D.P., "*A comparison of two adaptive algorithms for the control of active engine mounts*", Journal of Sound and Vibration, Vol.286, Aug. 2003.

[19] Gan, W.S. and Kou, S.M., "*An integrated audio and active noise control headsets*", IEEE Transactions on Consumer Electronics, Vol.48, No.2, May 2002.

[20] Kuo, S.M., Mitra, S. and Gan, W., "*Active noise control system for headphone applications*", IEEE Transactions on Control System Technology, Vol.14, No.2, March 2006.

[21] Song, Y., Gong, Y. and Kuo, S.M., "*A robust hybrid feedback active noise cancellation headset*", IEEE Transactions on Speech and Audio Processing, Vol.13, No.4, July 2005.

[22] Eriksson, L.J. and Allie, M.C., "*Use of random noise for on-line transducer modeling in an adaptive active attenuation system*", Journal of Acoustic Society of America, Vol 85, pp.797-802, Feb. 1989.

[23] Kuo, S.M. and Vijayan, D., "*A secondary path modeling technique for active noise control systems*", IEEE Transactions on Speech and Audio Processing, Vol 5, No.4, July 1997.

[24] Zhang, M., Lan, H. and Ser, W., "*An improved secondary path modelling method for active noise control systems*", IEEE Signal Processing Letters, Vol.7, No.4, April 2000.

[25] Bao, C., Sas, P. and Brussel, H.V., "*Adaptive active control of noise in 3-D reverberant enclosures*", Journal of Sound and Vibration, Vol.161, pp.501-514, 1993.

[26] Zhang, M., Lan, H. and Ser, W., "*Cross-updated active noise control system with online secondary path modeling*", IEEE Transactions on Speech and Audio Processing, Vol 9, No.5, July 2001.

[27] Shynk, J.J., "*Frequency-domain and multirate adaptive filtering*", IEEE Magazine, Jan. 1992.

[28] Widrow, B. and Stearns, S.D., "*Adaptive signal processing*", Prentice-Hall Inc, 1985.

[29] Astrom, K.J. and Wittenmark, B., "*Adaptive control*", Addison-Wesley Publishing Company, 1995.

[30] Douglas, S.C. and Meng, T.H.Y., "*Stochastic gradient adaptation under general error criteria*", IEEE Transactions on Signal Processing, Vol.42, No.6, Jun.1994.

[31] Haykin, S., "*Adaptive filter theory*", Prentice-Hall Inc, 2002.

[32] Roberts, M.J., "*Signals and systems analysis using transform methods and MATLAB*", The McGraw-Hill Companies, 2003.

[33] Glover, J.Jr., "*Adaptive noise canceling to sinusoidal interferences*", IEEE Transactions on Acoustics, Speech and Signal Processing, Vol.ASSP-25, No.6, Dec. 1977.

[34] Johnston, D.N., "*Efficient Methods For Numerical Modelling Of Laminar Friction In Fluid Lines*", Transactions of ASME, Vol. 128, No.4, 2006, 829-634.

[35] D'Souza, A.F. and Oldenburger, R., "*Dynamic Response of Fluid Lines*", Journal of Basic Engineering, Transactions of ASME, Series D, Vol. 86, No.3, Sept. 1964, pp. 589-598.

[36] Taylor, S.E.M., Johnston, D.N. and Longmore, D.K., "*Modelling of transient flow in hydraulic pipelines*", Proc. IMechE Pt I, Vol.211, No.16, 1997, pp. 447-456.

[37] Hillis, A.J. "*Adaptive control of active engine mounts*", Ph.D thesis, University of Bristol, 2004.

[38] Ifeachor, E.C. and Jervis, B.W., "*Digital signal processing a practical approach*", Addison-Wesley Publishing Company Inc., 1993.

[39] Defatta, D.J., Lucas, J.G. and Hodgkiss, W.S., "*Digital signal processing a system design approach*", John Wiley & Sons, Inc., 1988.

APPENDICES

Appendix 1

Parameters used in the model for Chapter 4

c : Speed of sound in liquid	1324.356 m/s
L : Length of pipe model	4.5 m
r : Pipe internal radius	0.0127 m
n : Number of pipe model node	21, 41 and 81
ν : Fluid kinematic viscosity	39.67×10^{-6} m^2/s
ρ : Liquid density	870 kg/m^3
t : Simulation running time	2 s

Appendix 2

Conditions for equation (3.26) to get complex poles

Poles of equation (3.26) can be written as:

$$z = \frac{\left(2 - \mu \cdot A^2\right) \cdot \cos\omega_0 \pm \sqrt{\left(2 - \mu \cdot A^2\right)^2 \cdot \cos^2\omega_0 - 4 \cdot \left(1 - \mu \cdot A^2\right)}}{2}$$

To get complex poles

$$\left(2 - \mu \cdot A^2\right)^2 \cdot \cos^2\omega_0 - 4 \cdot \left(1 - \mu \cdot A^2\right) < 0$$

After rearranging:

$$\left(\mu \cdot A^2\right)^2 \cdot \cos^2\omega_0 + 4 \cdot \left(\mu \cdot A^2\right) \cdot \sin^2\omega_0 - 4 \cdot \sin^2\omega_0 < 0 \qquad \text{(A1)}$$

Two roots of equation

$$\beta^2 \cdot \cos^2\omega_0 + 4 \cdot \beta \cdot \sin^2\omega_0 - 4 \cdot \sin^2\omega_0 = 0$$

,where $\beta = \mu \cdot A^2 > 0$, can be obtained:

$$\beta_{1,2} = -2 \cdot \sin^2\omega_0 \pm 2 \cdot \sin\omega_0 \cdot \sqrt{1 + \cos^2\omega_0}$$

To research the quadratic curve, if equation (A1) is true the following condition should be satisfied.

$$0 < \beta < \frac{2 \cdot \sin\omega_0 \cdot \sqrt{1 + \cos^2\omega_0} - 2 \cdot \sin\omega_0}{\cos^2\omega_0}$$

Appendix 3

Deduction of two-weight notch filter using FXLMS adaptive algorithm

Figure A3.1 shows the signal flow for narrowband single frequency noise cancellation using FXLMS algorithm with two-weight notch filter, which is similar to the plot in [28].

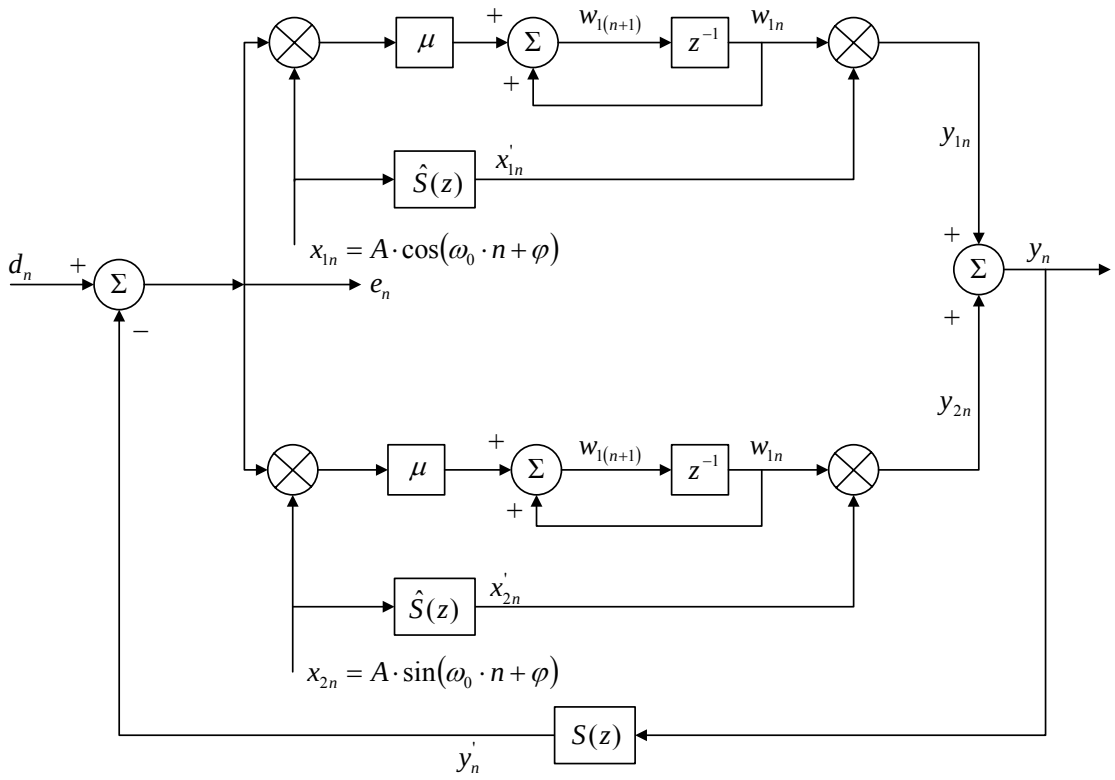

Figure A3.1 Signal flow of FXLMS adaptive algorithm using two-weight notch filter for narrowband single frequency noise cancellation

Deduced by Widrow in [28], the steady state transfer function of LMS adaptive algorithm using two-weight notch filter was obtained. Comparing with it，signals at point *L1* and *L2* can be written as:

$$x'_{1n} = A \cdot \hat{A}_S \cdot \cos(\omega_0 \cdot n + \varphi + \hat{\varphi}_S)$$

$$x'_{2n} = A \cdot \hat{A}_S \cdot \sin(\omega_0 \cdot n + \varphi + \hat{\varphi}_S)$$

Putting these two expressions rather than x_{1n} and x_{2n} into Widrow's deduction process, the ratio between *C* to *G* in time domain can be written as:

$$\frac{y_n}{e_n} = \mu \cdot A^2 \cdot \hat{A}_S \cdot u(n-1) \cdot \cos(n \cdot \omega_0 - \hat{\varphi}_S) \tag{A3.1}$$

where $u = \begin{cases} 0 & for \quad n < 0 \\ 1 & for \quad n \geq 0 \end{cases}$

Rearranging equation (A3.1):

$$\frac{y_n}{e_n} = \mu \cdot A^2 \cdot \hat{A}_S \cdot [\cos(n \cdot \omega_0) \cdot \cos\hat{\varphi}_S + \sin(n \cdot \omega_0) \cdot \sin\hat{\varphi}_S - \cos\hat{\varphi}_S] \tag{A3.2}$$

Take both sides of equation (A3.2) into z domain:

$$\frac{Y(z)}{E(z)} = \frac{z \cdot (z - \cos\omega_0) \cdot \cos\hat{\varphi}_S}{z^2 - 2 \cdot z \cdot \cos\omega_0 + 1} + \frac{z \cdot \sin\omega_0 \cdot \sin\hat{\varphi}_S}{z^2 - 2 \cdot z \cdot \cos\omega_0 + 1} - \cos\hat{\varphi}_S \tag{A3.3}$$

Rearranging equation (A3.3):

$$G(z) = \mu \cdot A^2 \cdot \hat{A}_S \cdot \left[\frac{z \cdot \cos(\omega_0 - \hat{\varphi}_S) - \cos\hat{\varphi}_S}{z^2 - 2 \cdot z \cdot \cos\omega_0 + 1} \right]$$

Then the closed loop transfer function from *A* to *G* can be written as:

$$H(z) = \frac{1}{1 + S(z) \cdot G(z)} \tag{A3.4}$$

In time domain A_S and φ_S can be used to represent amplitude and phase shift of $S(z)$. According to equation (A3.1), term $S(z) \cdot G(z)$ in time domain can be written as:

$$\mu \cdot A^2 \cdot \hat{A}_S \cdot A_S \cdot u(n-1) \cdot \cos(n \cdot \omega_0 - \hat{\varphi}_S + \varphi_S)$$

Therefore,

$$S(z)\cdot G(z) = a\cdot\left[\frac{z\cdot\cos(\omega_0-\Delta\varphi)-\cos\Delta\varphi}{z^2-2\cdot z\cdot\cos\omega_0+1}\right]$$

Hence,

$$H(z) = \frac{z^2-2\cdot z\cdot\cos\omega_0+1}{z^2-2\cdot\left(1-\frac{a}{2}\right)\cdot z\cdot\cos(\omega_0-\Delta\varphi)+(1-a\cdot\cos\Delta\varphi)}$$

Appendix 4

Parameters used in simulation for section 5.2, section 5.3

c : Speed of sound in liquid	1324.356 m/s
L : Length of pipe model	3 m
r : Pipe internal radius	0.0127 m
n : Number of pipe model node	21
ν : Fluid kinematic viscosity	$39.67\times10^{-6}\,\mathrm{m}^2/\mathrm{s}$
ρ : Liquid density	870 $\mathrm{kg/m}^3$
t : Simulation running time	2 s

Appendix 5

Parameters used in simulation for Chapter 6

c : Speed of sound in liquid	1324.356 m/s
L : Length of pipe model	3 m
r : Pipe internal radius	0.0127 m
n : Number of pipe model node	21
ν : Fluid kinematic viscosity	$39.67\times10^{-6}\,\mathrm{m}^2/\mathrm{s}$
ρ : Liquid density	870 $\mathrm{kg/m}^3$
t : Simulation running time	Variety